AIRCRAFT NAVIGATION AND SURVEILLANCE ANALYSIS FOR A SPHERICAL EARTH

Michael Geyer

Navigation

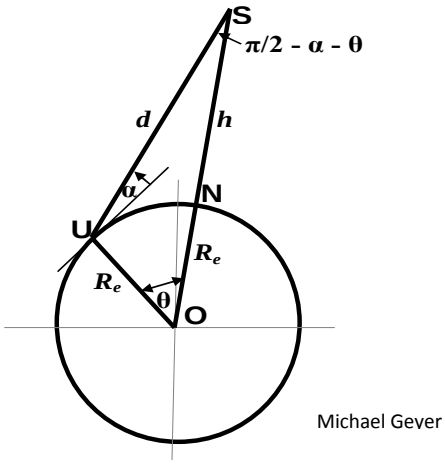

Vertical Plane Model

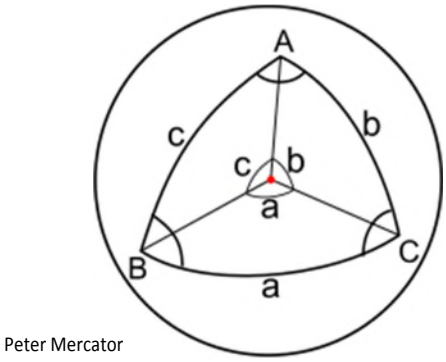

Spherical Surface Model

Surveillance

Project Memorandum — October 2014

DOT-VNTSC-FAA-15-01

Prepared for:
Federal Aviation Administration
Wake Turbulence Research Office

U.S. Department of Transportation
Research and Innovative Technology Administration
John A. Volpe National Transportation Systems Center

FOREWORD

This memorandum addresses a basic function of aircraft (as well as marine, missile and satellite) surveillance and navigation systems analyses — quantifying the geometric relationship of two or more locations relative to each other and to a spherical earth. Here, geometry simply means distances (ranges) and angles. Applications that fit well with the methods presented herein include (a) planning a vehicle's route; (b) determining the coverage region of a radar or radio navigation installation; or (c) calculating a vehicle's position from slant-ranges, spherical-ranges, slant- or spherical-range differences, azimuth/elevation angles and/or altitude.

The approach advocated is that, to simplify and clarify the analysis process, the three-dimensional problems inherent in navigation and surveillance analyses should, to the extent possible, be re-cast as the most appropriate set/sequence of sub-problems/formulations:

- **Vertical-Plane Formulation** (two-dimensional (2D) problem illustrated in top right panel on cover) — Considers the vertical plane containing two problem-specific locations and the center of the earth, and utilizes plane trigonometry as the primary analysis method; provides a closed-form solution.
- **Spherical-Surface Formulation** (2D problem illustrated in bottom left panel on cover) — Considers two or three problem-specific locations on the surface of a spherical earth; utilizes spherical trigonometry as the primary analysis method; provides a closed-form solution.
- **Three-Dimensional Vector Formulation** — Utilizes 3D Cartesian vector framework; best-suited to situations involving four or more problem-specific points and slant-range or slant-range difference measurements; provides a closed-form solution.
- **Linearized Least-Squares Iterative Formulation** — When warranted by the distances involved, the accuracy required, and/or the need to incorporate empirical data, the least-squares iterative method is employed based on an ellipsoidal earth model.

These techniques are applied to a series of increasing complex situations, starting with those having two problem-specific points, then extending to those involving three or more problem-specific points (e.g., two or more sensor stations and an aircraft). Closed-form (non-iterative) solutions are presented for determining an aircraft's position based on virtually every possible combination of ranges, pseudoranges, azimuth or elevation angles and altitude measurements.

The Gauss-Newton Linearized Least-Squares (LLS) iterative methodology is employed to address the most complex situations. These include any combination of the following circumstances: more measurements than unknown variables, measurement equations are too complex to be analytically inverted (including those for an ellipsoidal-shaped earth), or empirical data is utilized in the solution. Also, the capability of the LLS methodology to provide an estimate of the accuracy of any solution to the measurement equations is presented.

TABLE OF CONTENTS

FOREWORD I

1. INTRODUCTION 1

1.1 Overview of Methodologies and Their Applications 1
1.1.1 Overview of Methodologies 1
1.1.2 Overview of Application of Methodologies 2

1.2 Vertical Plane Formulation 3

1.3 Spherical Surface Formulation 3

1.4 Applicability and Limitations of Analysis 5

1.5 Outline of this Document 6

2. MATHEMATICS AND PHYSICS BASICS 8

2.1 Exact and Approximate Solutions to Common Equations 8
2.1.1 The Law of Sines for Plane Triangles 8
2.1.2 The Law of Cosines for Plane Triangles 8
2.1.3 Solution of a Quadratic Equation 9
2.1.4 Computing Inverse Trigonometric Functions 9
2.1.5 Expansions of arcsin, arccos and arctan for Small Angles 11
2.1.6 Secant Method for Root Finding 12
2.1.7 Surface Area on a Sphere 13

2.2 Shape of the Earth 13
2.2.1 WGS-84 Ellipsoid Parameters 13
2.2.2 Radii of Curvature in the Meridian and the Prime Vertical 14
2.2.3 Methods for Addressing an Ellipsoidal Earth 16

2.3 Accounting for User Altitude 17
2.3.1 Accounting for Known User Altitude 17
2.3.2 Conditions for Unblocked Line-of-Sight 17

3. TWO-POINT / VERTICAL-PLANE PROBLEM FORMULATION 20

3.1 Mathematical Problem and Solution Taxonomy 20
3.1.1 Mathematical Formulation 20
3.1.2 Taxonomy of Solution Approaches 20
3.1.3 Detailed Geometry 21

3.2 Computing Geocentric Angle 22
3.2.1 Altitude and Elevation Angle Known – Basic Method 22
3.2.2 Altitude and Elevation Angle Known – Alternative Method 23
3.2.3 Altitude and Slant Range Known 23
3.2.4 Elevation Angle and Slant Range Known 24

3.3 Computing Elevation Angle 24
3.3.1 Altitude and Geocentric Angle Known 24
3.3.2 Altitude and Slant Range Known 25
3.3.3 Geocentric Angle and Slant Range Known 25

3.4 Computing Slant Range 25
3.4.1 Altitude and Geocentric Angle Known 25
3.4.2 Altitude and Elevation Angle Known 26

3.4.3 Geocentric Angle and Elevation Angle Known 26
3.5 Computing Altitude 27
3.5.1 Slant Range and Geocentric Angle Known 27
3.5.2 Slant Range and Elevation Angle Known 27
3.5.3 Elevation Angle and Geocentric Angle Known 27
3.6 Example Applications 28
3.6.1 Example 1: En Route Radar Coverage 28
3.6.2 Example 2: Aircraft Precision Approach Procedure 32
3.6.3 Example 3: Satellite Visibility of/from Earth 34

4. TWO-POINT / SPHERICAL-SURFACE PROBLEM FORMULATION 35
4.1 Basics of Spherical Trigonometry 35
4.1.1 Basic Definitions 35
4.1.2 Application to Navigation and Surveillance 35
4.1.3 Applicability to Two-2D Problem Formulation 36
4.1.4 General Characteristics of Spherical Triangles 36
4.1.5 Resources on the Web 37
4.1.6 Key Formulas 37
4.1.7 Taxonomy of Mathematical Spherical Triangle Problems 39
4.1.8 Taxonomy of Navigation Spherical Surface Problems 40
4.2 The Indirect Problem of Geodesy 41
4.2.1 Computing the Geocentric Angle 41
4.2.2 Computing the Azimuth Angles of the Connecting Arc 43
4.3 The Direct Problem of Geodesy 44
4.3.1 Computing the Satellite Latitude 44
4.3.2 Computing the Satellite Longitude 44
4.3.3 Computing the Azimuth of the Connecting Path at the Satellite 45
4.3.4 Applications 45
4.4 A Modified Direct Problem: Path Azimuth at Satellite Known 46
4.4.1 Computing the Satellite Longitude 46
4.4.2 Computing the Satellite Latitude 46
4.4.3 Computing the Azimuth of the Connecting Arc at the User 46
4.4.4 Application 47
4.5 A Modified Direct Problem: Satellite Longitude Known 47
4.5.1 Computing the Satellite Latitude 47
4.5.2 Computing the Geocentric Angle 48
4.5.3 Computing the Azimuth of the Connecting Arc at the Satellite 48
4.6 A Modified Direct Problem: Satellite Latitude Known 48
4.6.1 Computing the Azimuth of the Connecting Arc at the Satellite 48
4.6.2 Computing the Satellite Longitude 49
4.6.3 Computing the Geocentric Angle 49
4.7 Latitude Extremes of a Great Circle 50
4.8 Example Applications 51
4.8.1 Example 1, Continued: En Route Radar Coverage 52
4.8.2 Example 2, Continued: Aircraft Precision Approach Procedure 54
4.8.3 Example 3, Continued: Satellite Visibility of/from Earth 54
4.8.4 Example 4: Great Circle Flight Route 55
4.8.5 Example 5: Radar Display Coordinate Transformations 58
4.8.6 Example 6: Single-Station VOR / DME RNAV Fix 60

4.8.7 Example 7: Path-Length Ellipticity Error for Selected Airport Pairs 61

5. TWO-POINT / 3D-VECTOR PROBLEM FORMULATION 64

5.1 Vector and Coordinate Frame Definitions 64
5.1.1 Earth-Centered Earth-Fixed (ECEF) Coordinate Frame 64
5.1.2 Local-Level Coordinate Frame at User's Position 65
5.1.3 User and Satellite Positions in User's Local-Level Frame 66

5.2 The Indirect Problem of Geodesy 67
5.2.1 Geocentric Angle from Latitudes and Longitudes, by Vector Dot Product 67
5.2.2 Geocentric Angle from Latitudes and Longitudes, by Vector Cross Product 68
5.2.3 Path Azimuth Angles, from Latitudes and Longitudes 68

5.3 Corollaries of the Indirect Problem Solution 69
5.3.1 Intermediate Points between **U** and **S**: Dividing the Chord 69
5.3.2 Intermediate Points between **U** and **S**: Dividing the Arc 70
5.3.3 Latitude Extremes of a Great Circle 70
5.3.4 Locus of Points on a Great Circle 71

5.4 Computing Satellite Elevation Angle and Slant Range 72
5.4.1 Solution for Elevation Angle from Altitude and Geocentric Angle 72
5.4.2 Solution for Slant Range from Altitude and Geocentric Angle 72

5.5 The Direct Problem of Geodesy 73

6. AIRCRAFT POSITION FROM TWO RANGE AND/OR AZIMUTH MEASUREMENTS (TRIGONOMETRIC FORMULATIONS) 75

6.1 General Considerations 75
6.1.1 Problems Addressed 75
6.1.2 Geometric Concerns 76
6.1.3 Rationale for Two-Station Area Navigation (RNAV) 77
6.1.4 Chapter Overview 78

6.2 Relationship between a Point and a Great Circle 78
6.2.1 Problem Statement 78
6.2.2 Problem Solution 79

6.3 Position Solution for Two Azimuth Measurements 80
6.3.1 Step 1: Solve the Navigation Spherical Triangle **PUS** 80
6.3.2 Step 2: Determine if the Problem is Well-Posed 80
6.3.3 Step 3: Solve the Mathematical Spherical Triangle **USA** 80
6.3.4 Step 4: Find the Coordinates/Path Azimuths for **A** 81
6.3.5 Remarks 82

6.4 Position Solution for Two Slant Range Measurements 83
6.4.1 Step 0: Convert Slant-Ranges to Spherical-Ranges/Geocentric Angles 83
6.4.2 Step 1: Solve the Navigation Spherical Triangle **PUS** 83
6.4.3 Step 2: Determine if the Problem is Well-Posed 83
6.4.4 Step 3: Solve the Mathematical Spherical Triangle **USA** 84
6.4.5 Step 4: Find the Coordinates/Path Azimuths for **A** 84
6.4.6 Remarks 84

6.5 Position Solution for a Slant Range and an Azimuth Measurement 85
6.5.1 Step 0: Convert Slant-Range to Spherical-Range/Geocentric Angle 85
6.5.2 Step 1: Solve the Navigation Spherical Triangle **PDV** 85
6.5.3 Step 2: Determine if the Problem is Well-Posed 85
6.5.4 Step 3: Solve the Mathematical Spherical Triangle **DVA** 86

6.5.5 Step 4: Find the Coordinates/Path Azimuths for **X** 87
6.5.6 Remarks 88
6.6 Crosscheck of Continuous Descent Approach Altitude 88
6.6.1 Application Context 88
6.6.2 Altitude vs. DME Information for the Pilot 89
6.6.3 "ILS DME" Scenario 90
6.6.4 "Airport DME" Scenario 91
6.6.5 Remarks 94

7. AIRCRAFT POSITION FROM PSEUDORANGE MEASUREMENTS 96
7.1 Overview of Pseudoranges 96
7.1.1 Concept 96
7.1.2 Pseudorange Lines-of-Position (LOPs) and Fix Geometry 97
7.1.3 Algorithm Taxonomy 97
7.2 Solution for Pseudo Slant-Ranges/Cartesian Coordinates (Bancroft) 98
7.2.1 Background / Problem Formulation 98
7.2.2 Problem Solution 100
7.2.3 Remarks 101
7.3 Solution for Slant-Ranges/Cartesian Coordinates (Bancroft Extensions) 103
7.3.1 Background / Motivation 103
7.3.2 Three Slant-Range Measurements 104
7.3.3 Two Slant-Ranges and an Altitude Measurement 105
7.4 Solution for Three Pseudo Slant-Ranges and an Altitude Measurement 106
7.4.1 Introduction 106
7.4.2 Problem Formulation 106
7.4.3 Problem Solution 107
7.4.4 Remarks 108
7.5 Solution for Two Pairs of Pseudo Slant-Ranges and Altitude 108
7.5.1 Introduction 108
7.5.2 Problem Formulation 108
7.5.3 Problem Solution 110
7.5.4 Remarks 113
7.6 Solution for Three Pseudo Slant-Range Stations in Flatland (Fang) 113
7.6.1 Problem Statement 113
7.6.2 General Solution 114
7.6.3 Solution Cases 115
7.6.4 Remarks 118
7.7 Solution for Three Pseudo Spherical-Range Stations (Razin) 121
7.7.1 Problem Formulation 121
7.7.2 Problem Solution 121
7.7.3 Types of Solutions 123
7.7.4 Remarks 124
7.8 Solution for Two Pairs of Stations Measuring Pseudo Spherical-Ranges 125
7.8.1 Problem Formulation 125
7.8.2 Problem Solution 126
7.8.3 Remarks 128
7.9 Example Applications 128
7.9.1 Example 8: Slant-Range Measurement System in Flatland 128
7.9.2 Example 9: Three Pseudo Slant-Range Stations in Flatland 132

7.9.3 Example 10: Three Pseudo Spherical-Range Stations 133
7.9.4 Example 11: Two Pairs of Pseudo Spherical-Range Stations 134
7.9.5 Example 12: Wide Area Multilateration (WAM) 136

8. LINEARIZED LEAST-SQUARES (LLS) METHOD (GAUSS-NEWTON) 139
8.1 General LLS Method 139
8.1.1 Background / Context 139
8.1.2 Linearized Least Squares Problem and Solution 139
8.1.3 Solution Properties 143
8.1.4 Advantages of the LLS Technique 144
8.1.5 Remarks 145
8.2 Solution Employing Cartesian Coordinates 147
8.2.1 Introduction 147
8.2.2 Measurement Equations 148
8.2.3 Solution Process 149
8.2.4 Altitude Constraint 150
8.2.5 Dilution of Precision (DoP) 152
8.2.6 Remarks 152
8.3 Solution Employing Spherical Coordinates (Latitude/Longitude/Altitude) 153
8.3.1 Introduction / Rationale 153
8.3.2 Measurement Equations 154
8.3.3 Dilution of Precision (DoP) 157
8.3.4 Remarks 157
8.4 Example Applications 158
8.4.1 Example 8 Continued: Slant-Range Measurement Systems in Flatland 158
8.4.2 Example 9 Continued: Pseudo Slant-Range Measurement Systems in Flatland 159
8.4.3 Interpretation: Pseudo vs. Real Slant-Range Systems 161
8.4.4 Example 10 Continued: Three Pseudo Spherical-Range Stations 162
8.4.5 Example 11 Continued: Two Pairs of Pseudo Spherical-Range Stations 166
8.4.6 Example 12 Continued: Wide Area Multilateration (WAM) 168

9. APPENDIX: RELATED SPECIALIZED TOPICS 9-1
9.1 Aircraft Altitude and Air Data Systems 9-1
9.1.1 Meanings of “Altitude” 9-1
9.1.2 Aircraft Pitot-Static System 9-2
9.1.3 Barometric Altimeter Temperature Sensitivity 9-3
9.1.4 Vertical Speed Indicator Temperature Sensitivity 9-3
9.2 VNAV Constant Descent Angle Trajectory 9-4
9.2.1 Derivation of Equations 9-4
9.2.2 Typical Vertical Profiles 9-5
9.2.3 Remarks 9-5
9.3 Ellipsoidal Earth Model and ECEF Coordinate Frame 9-6
9.4 Rhumb Line Navigation 9-9
9.4.1 Background 9-9
9.4.2 Solution of the Indirect Problem 9-10
9.4.3 Solution of the Direct Problem 9-11

10. REFERENCES 10-1

LIST OF FIGURES

Figure 1 Vertical Plane Containing Points **U**, **O**, **N** and **S** 3
- **Figure 2** Spherical Surface Containing Points **U** and **S** 4

Figure 3 Principal Values of arcsin and arccos Functions 10
Figure 4 Ellipsoidal Earth's Radii of Curvature, Normalized to the Semi-Major Axis 15
Figure 5 Problem Geometry for LOS Tangent to the Earth's Surface 18
Figure 6 Detailed Geometry for Vertical Plane Formulation 21
Figure 7 Aircraft Minimum Visible HAT vs. Range for Three Radar Antenna HAT Values 30
Figure 8 Aircraft Minimum Visible Altitude vs. Horizontal Range from Radar in Vertical Plane Containing Radar and Aircraft 31
Figure 9 Approach Plate: RNAV (GPS) for MCI Runway 19L 33
Figure 10 Fraction of Earth Visible vs. Satellite Altitude 34
Figure 11 Example Spherical Triangle 35
Figure 12 "Navigation" Spherical Triangle 36
Figure 13 Illustrating the Taxonomy of Spherical Triangle Problems 40
Figure 14 Indirect Problem of Geodesy 41
Figure 15 Sine, cosine and versine, and the unit circle 42
Figure 16 Direct Problem of Geodesy 44
Figure 17 Aircraft Altitude Visibility Contours for the North Truro, MA, Radar System 53
Figure 18 WAAS Satellite Visibility Contours for 5 deg Mask Angle 56
Figure 19 Mercator-like Depiction of Latitude/Longitude Coordinates for Great Circle and Rhumb Line Paths Connecting BOS and NRT 57
Figure 20 Polar View of BOS-NRT Great Circle and Rhumb Line Routes 58
Figure 21 Effect of Displaying a Target's Slant Range 59
Figure 22 Slant-Range Correction Error for Tangent Plane Terminal Radar Display 60
Figure 23 Histogram of Ellipticity Errors for Spherical-Earth Length of 91 Selected Paths 63
Figure 24 Vector Technique Coordinate Frames of Interest 65
Figure 25 Possible Geometric Relationships involving an Aircraft and Two Ground Stations 77
Figure 26 Vessel **V** and Intended Great Circle Path **US** 79
Figure 27 Portion of LOC IAP to KOWD Runway 35 89
Figure 28 Relationship between Aircraft **A**, Runway **R** and DME **D** 92
Figure 29 Hyperbolic System Two-Dimensional Geometry 97
Figure 30 Solution Regions for Three Pseudo Slant-Range Stations in Flatland 118
Figure 31 Types of Solutions for Three Pseudo Slant-Range Stations 119
Figure 32 Classic Hyperbola 120
Figure 33 Pseudo Spherical-Range Scenario Involving Stations **M**, **X** and **Y** and Aircraft **A** 121
Figure 34 Pseudo Spherical-Range Measurement Scenario Involving Two Station Pairs and Aircraft 125

Figure 35 Two Slant-Range Stations and Aircraft in Flatland 130
Figure 36 Three Pseudo Slant-Range Stations in Flatland and Two Aircraft Tracks 132
Figure 37 Position Solutions for Triad of Stations from the Northeast U.S. Loran-C Chain ... 133
Figure 38 Two Pairs of Loran-C Stations and Seven Airport Locations 135
Figure 39 Example 11: Sensitivity of Law-of-Sines Difference to Trial Values of $\boldsymbol{\beta_X}$ 136
Figure 40 Three-Station WAM System and Example Flight Track 137
Figure 41 HDoP Contours for Slant-Range Measurement Systems in Flatland 159
Figure 42 HDoP Contours for Wye Configuration Using All Stations 160
Figure 43 HDoP Contours for Pseudo Slant-Range Measurement Systems in Flatland 160
Figure 44 Service Area with HDOP ≤ Max. HDOP for Five System Concepts 161
Figure 45 LOPs for Slant-Rang and Pseudo Slant-Range Systems 162
Figure 46 HDOP Contours for a Triad of Pseudo Spherical-Range Stations 163
Figure 47 HDoP Contours for Two Pairs of Pseudo Spherical-Range Stations 167
Figure 48 HDoP Contours for Three Pairs of Pseudo Spherical-Range Stations 168
Figure 49 Different Notions of Altitude 9-1
Figure 50 Basic Aircraft Pitot-Static System 9-2
Figure 51 Effect of Non-Standard MSL Temperature on Barometric Altimeter Indication 9-3
Figure 52 Aircraft Elevation vs. Distance along Ground, for Three Guidance Schemes 9-6
Figure 53 Ellipsoidal Earth Model for a Plane through the Spin Axis 9-7

LIST OF TABLES

Table 1 Topic Locations by Problem Geometry 6
Table 2 Geocentric Angle θ and Its Cosine and Tangent Functions, near $\theta = 0$ 10
Table 3 Comparison of Newton's and Secant Methods for Finding the Square Root of 2 13
Table 4 Specified and Computed Fix Altitudes for MCI Runway 19L LPV Approach 33
Table 5 Taxonomy of Navigation Spherical Surface Problems 40
Table 6 Computed Fix Coordinates for MCI Runway 19L LPV Approach 54
Table 7 CONUS Airports Used in Ellipticity Error Analysis 62
Table 8 International Airports Used in Ellipticity Error Analysis 62
Table 9 Sources for Range-Type Algorithms and Example Applications 98
Table 10 Roots for Aircraft Transmission Time, in NM, for Example 12 138
Table 11 Example of Ellipticity Errors for Razin's Algorithm 164
Table 12 Gauss-Newton Residual Error for Spherical-Range Difference Measurements 165
Table 13 Gauss-Newton Residual Error for WAM Slant-Range Difference Measurements ... 169
Table 14 Effect of Uncompensated Airport Temperature on VNAV Glide Path Angle 9-4

1. INTRODUCTION

1.1 Overview of Methodologies and Their Applications

This memorandum addresses a fundamental function in surveillance and navigation analysis — quantifying the geometry of two or more locations relative to each other and to a spherical earth. Here, "geometry" refers to: (a) points (idealized locations); (b) paths between points; and (c) distances and angles that quantify paths. Points represent locations of either vehicles or navigation/surveillance sensors. Paths constitute trajectories followed by vehicles or sensor signals. Distances are the lengths of paths/trajectories that are either straight lines or follow the earth's surface. Angles between paths may be measured on a plane or a spherical surface.

1.1.1 Overview of Methodologies

The approach that may first come to mind when addressing such a situation is to treat it as a three-dimensional problem and employ vector analysis. However, the approach recommended herein is that, to simplify and clarify the analysis process, three-dimensional problems should be re-cast, whenever possible, as two separate two-dimensional problems:

- **Vertical Plane Formulation** (Section 1.2 and Chapter 3)* — This formulation considers the vertical plane containing two problem-specific locations and the center of the earth. Problem-specific locations are unconstrained vertically, except that at least one altitude must be known. Plane trigonometry is the natural analysis tool when altitudes, elevation angles and slant-ranges are involved. Conversely, latitude and longitude coordinates are not utilized, which is a limitation.
- **Spherical Surface Formulation** (Section 1.3, Chapter 4) — This formulation — which is sometimes called great-circle navigation — considers two or more problem-specific locations on the surface of a spherical earth. Spherical trigonometry is the natural analysis tool when the earth's curvature must be considered. Latitudes and longitudes, as well as spherical ranges (distances along the earth's surface) and azimuth angles with respect to north or between two paths, are inherent to this formulation. A limitation is that altitudes cannot be accounted for.

These two-dimensional analyses can generally be performed in the above sequence, with the result that the limitations of each are overcome. This formulation is preferable to one-3D vector formulation because it provides better insight into the solution — which reduces computational errors and improves the analyst's understanding of the results.

For historical and practical reasons†, in this document when there are two problem-specific locations of interest, they are often labeled **U** (for user) and **S** (for satellite). However, these are

* Document organizational terminology: 1. Chapter; 1.1 Section; 1.1.1 Subsection.

† Historical: these notes were begun about 20 years ago, for a project involving satellites. Practical: the Microsoft Word equation editor does not have a global change capability.

only labels, and have no relevance to application of the analysis. Generally, for surveillance applications, one location will be associated with a sensor and the other will be associated with a vehicle— e.g., a ground-based radar and an aircraft. For navigation applications, the two locations may be those of a sensor and a vehicle or the beginning and ending points of a travel segment — e.g., an aircraft and a runway threshold.

Chapter 5 is devoted to the 3D-vector solution approach, which is largely an alternative to the two-2D approach outlined above that is better suited to some problems. Typically, these involve: (1) three or more problem-specific points that must be considered simultaneously (rather than sequentially, which allow one vertical plane to be considered at one time); and (2) only slant-range-type measurements are involved (true slant-ranges, slant-range differences and/or altitude). Conversely, the vector methodology does not handle spherical ranges or azimuth angles as well as the spherical surface formulation.

1.1.2 Overview of Application of Methodologies

Chapters 6 and 7 apply the analysis methodologies described in Chapter 3-5 to situations involving three or more problem-specific points (e.g., two, three or four sensors and an aircraft). Chapter 6 addresses sensors that measure slant- or spherical-range and azimuth angles. These problems are addressed using a sequence of vertical planes combined with the spherical surface formulation.

Chapter 7 addresses sensor systems that measure slant- or spherical range differences. When addressed algebraically, these problems require consideration of all measurements simultaneously; thus, the vector methodology is employed. Some two-dimensional special cases have geometry based solutions which do not require the vector approach.

The situations addressed in Chapters 3 through 7 share important characteristics including: (1) there are the same number of measurements as unknown quantities, and (2) a spherical earth model is used. These enable closed-form solutions to be found. Closed-form solutions are valuable for system planning, as they can be analyzed without collecting measurements. Moreover, they are often sufficiently accurate that they can be used operationally.

Chapter 8 departs from both of the conditions listed immediately above and addresses problems that may involve more measurements than unknown variables and which do not necessarily have invertible measurement equations. This relaxation of assumptions enables addressing situations involving, e.g., redundant measurements, non-ideal sensors and/or an ellipsoidal earth. The “cost” of this generality is that the solution methodology is numerical and iterative, rather than a set of closed-form expressions.

1.2 Vertical Plane Formulation

Figure 1 depicts a vertical-plane involving: an earth-based user **U**; a satellite **S** above a spherical earth; the satellite nadir (or sub-point) **N**; and the center of the earth **O**. Points **U** and **S** (or **N**) are problem-specific; **O** is not. All four locations are in the plane of the paper. Points **O**, **N** and **S** form a straight line. These points have no special relationship with the earth's spin axis. Since a "snapshot" analysis is involved, no assumptions are made regarding the satellite's trajectory.

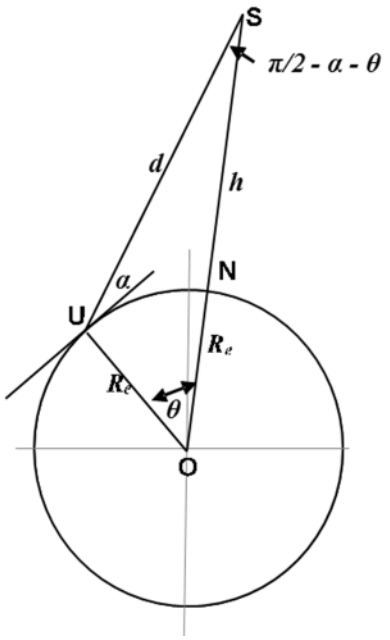

Figure 1 Vertical Plane Containing Points **U**, **O**, **N** and **S**

In Figure 1, three linear distances are of interest:

- R_e Earth radius (length of **OU** and **ON**)
- h Satellite altitude above the earth (length of **NS**)
- d User-satellite slant range (length of **US**).

And two angles are of interest:

- α Satellite elevation angle relative to the user's horizon (may be positive or negative)
- θ Geocentric angle between the user and satellite nadir (is always positive).

The earth radius R_e is always assumed to be known.

There are four variables associated with this formulation: h, d, α and θ. Any two must be known, and the remaining two can be found. Thus, there are six possible groupings. Subsection 2.3.1 shows how to relax the restriction of **U** being on the earth's surface, to its having a known altitude. Chapter 3 details the full set of 12 possible equations for this formulation.

Of these four variables, the geocentric angle θ (which is equivalent to distance along the earth's surface, or spherical-range) is also a variable in the spherical surface formulation. It serves as the link for relating the two formulations — i.e., for transferring a solution to the vertical plane formulation into the spherical surface formulation (Subsection 4.1.3 elaborates on this topic). The other three variables (h, d and α) are related to the altitude of **S** above the earth's surface and have no role in the spherical surface formulation.

1.3 Spherical Surface Formulation

The spherical surface formulation is an application of spherical trigonometry. This formulation is almost perfectly matched to marine surface navigation, and was developed by the ancients partly for that purpose. It can be used for many aviation navigation and surveillance situations by

combining it with the vertical plane formulation.

The left-hand side of Figure 2 depicts the earth's familiar latitude/longitude grid. The right-hand side shows two problem-specific points **U** and **S** on the earth's surface and the seven variables involved in a two-location problem on a sphere:

- the latitude/longitude, respectively, of **U** (L_U, λ_U) and of **S** (L_S, λ_S)
- the geocentric angle θ between **U** and **S**; and
- the azimuth angles $\psi_{S/U}$ and $\psi_{U/S}$ of the great circle arc connecting **U** and **S**.

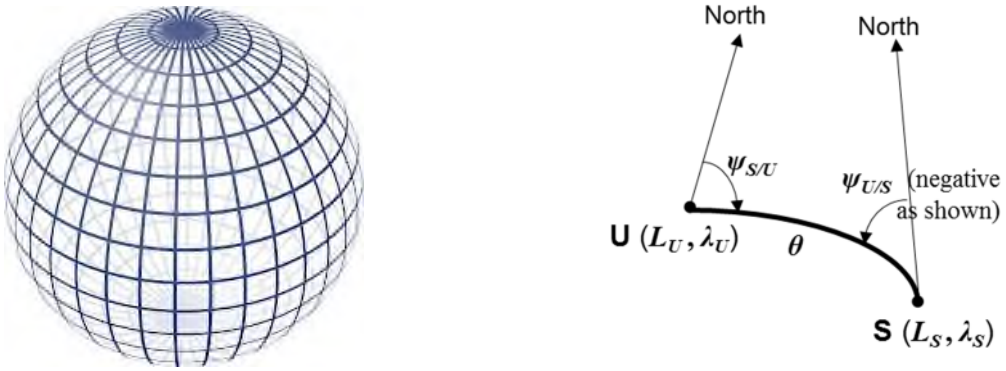

Figure 2 Spherical Surface Containing Points **U** and **S**

Generally, four of these seven variables must be known; from those, the other three can be computed. Even this simple problem involves 35 possible groupings of known / unknown variables. By taking advantage of symmetries, these can be reduced to 16 unique, solvable mathematical problems (Subsection 4.1.8) —still a significant number. Thus, in contrast with the exhaustive approach taken vertical plane formulation, a more selective approach is adopted for the spherical-earth formulation. Attention is limited to the variable groupings of highest interest, and a roadmap is provided for the remaining cases.

"Geodesy is the science concerned with the exact positioning of points on the surface of the Earth" (Ref. 1). In geodesy, analyses involving two groupings of known/unknown variables occur so frequently that they have been named:

- **Direct** (or *first*) problem[‡] of geodesy: (a) Given the coordinates (L_U, λ_U) of **U**, the geocentric angle θ between **U** and **S**, and azimuth angle $\psi_{S/U}$ of a great circle path starting at **U** and ending at **S**; (b) Find the coordinates (L_S, λ_S) of the end point **S** and the path azimuth angle at the end point $\psi_{U/S}$.
- **Indirect** (or *second*, or *inverse*) problem of geodesy: (a) Given the coordinates, (L_U, λ_U) and (L_S, λ_S), of two points **U** and **S**, (b) Find the geocentric angle θ connecting **U** and **S**, and the azimuth angles (relative to north), $\psi_{U/S}$ and $\psi_{S/U}$, of the path at each end.

[‡] Note the academic/mathematical use of the word "problem" in the narrow sense of specific groupings of known and unknown variables. This document also uses "problem" in the broader sense of a situation to be analyzed.

In both Chapter 4 (spherical surface formulation) and Chapter 5 (vector formulation), solution equations are provided for the direct and indirect problems of geodesy, and variations thereon that have relevant applications. Many of the three-point problems addressed in Chapter 6 use the Direct or Indirect problem as step in the solution algorithm.

1.4 Applicability and Limitations of Analysis

With a few exceptions, the methodology presented herein generally reflects conditions and assumptions appropriate to aircraft navigation and surveillance, including:

- **Earth Curvature Must Be Considered** — With the exception of aircraft on the surface of an airport, the curvature of the earth is a fundamental aspect of aircraft navigation and surveillance analysis.
- **Three-Dimensions Frequently Must Be Considered** — Some essential operations, such as aircraft approach, require that lateral/longitudinal position and altitude all be considered, necessitating a three-dimensional analysis methodology.
- **Horizontal Position and Altitude Decoupled at Long Ranges** — Generally, scenarios requiring simultaneous consideration of three dimensions involve aircraft-sensor ranges of less than 250 miles, the maximum "visible" distance of aircraft at 40,000 feet of altitude.
- **Altitude Measurement Always Available** — Aircraft of interest provide barometric altimeter information that can be adjusted to provide elevation above sea level.

The analysis also embodies the following assumptions/limitations:

- **Static Scenarios** — Scenarios analyzed are "snapshots" — i.e., motion of an aircraft or other vehicle is not explicitly involved. Sequence of locations are considered, but the notions of velocity or time as mechanisms for relating those locations are not utilized.
- **Great Circle Vehicle Paths** — Vehicle trajectories are always great circles. That is, they lie in a vertical plane that contains the center of the earth.
- **Geometrically Simple Radio Wave Propagation Paths**— Radio waves between transmitters and receivers lie in a vertical plane that contains the center of the earth. Two path geometries are considered: (a) line-of-sight, or Euclidean straight lines; and (b) following the curvature of the earth.
- **Terrain/Obstacles Ignored** — Except for the earth itself, obstacles such as hills/ mountains or man-made structures that could block the signal path between two locations (e.g., a sensor and a vehicle) are not addressed.

One might ask: Why focus on a spherical earth model, when an ellipsoidal model is more accurate? The rationale is:

- **Insight/Confidence** — When the number of measurements is equal to the number of unknown quantities, a spherical earth-model usually has a closed-form solution that is understandable geometrically. Conversely, an ellipsoidal model never has a closed form solution; the analyst must initialize, utilize and trust a numerical solution.

- **Error Often Insignificant** — While an ellipsoidal model more accurately describes the earth's shape, quantitatively the earth is "99.7% round". The so-called ellipticity error resulting from employing the spherical-earth approximation is often acceptably small (Subsections 2.2.2, 4.8.7, 8.4.4 and 8.4.6).

Engineering analyses methods have been characterized thusly: "There are exact solutions to approximate problems, and approximate solutions to exact problems. But there are no exact solutions to exact problems".[§] The techniques described herein, with the exception of Chapter 8, are exact solutions to approximate problems. They enable use of closed-form solutions that are valuable in multiple engineering activities. The spherical-earth approximation is often made in authoritative documents that address similar applications (e.g., Refs. 1, 2 and 3). When an ellipsoidal-earth model is required and iterative numerical technique must be employed, the spherical-earth solution provides an excellent initial value for the iteration process.

1.5 Outline of this Document

Chapter 1 (this one) describes the basic problems to be addressed, and outlines the approach recommended for their solution. Chapter 2 is mathematical in nature, and is included to make this document more self-contained.

Chapters 3 through 8 are synopsized in Section 1.1. Table 1 is a high-level roadmap of location of the topics addressed.

Table 1 Topic Locations by Problem Geometry

Dimension / Shape	Two Dimensions	Three Dimensions
Spherical Earth	▪ Plane Trigonometry (vertical plane) – Chapter 3 ▪ Spherical Trigonometry (spherical surface) – Chapter 4	▪ Vector Analysis – Chapter 5; Section 7.2 ▪ Plane & Spherical Trigonometry – Chapters 6 & 7 ▪ Linear Least Squares – Chapter 8
Ellipsoidal Earth	▪ Vincenty's Algorithm – Subsection 2.2.3 ▪ Linear Least Squares – Chapter 8	▪ Vector Analysis – Chapter 5; Section 7.2 ▪ Linear Least Squares – Chapter 8

To illustrate application of the analysis techniques described herein, example applications are presented at the ends of several chapters that address:

- Air Traffic Control (ATC) radar coverage (Example 1)
- Precision approach procedure design (Example 2)
- Satellite visibility of/from the Earth (Example 3)
- Great-circle flight route between Boston and Tokyo (Example 4)
- ATC radar display coordinate transformations (Example 5)
- Single VOR/DME station RNAV fix (Example 6)

[§] Conveyed by Prof. Donald Catlin (Univ. of Mass. Amherst, Mathematics Dept.), who attributed it to Prof. Lotfi Zadeh (Univ. of Calif. Berkley, Electrical Engineering Dept.).

- Ground path ellipticity error for selected airport pairs (Example 7)
- Systems that utilize measurements of slant-ranges or their difference in two dimensions (Examples 8 and 9)
- Systems that utilize measurements of spherical-range differences — a single Loran chain involving three stations (Example 10); and two chains involving four stations (Example 11)
- A Wide Area Multilateration (WAM) system using slant-range differences and altitude measurements (Example 12).

Relevant, specialized topics are presented in an Appendix (Chapter 9).

2. MATHEMATICS AND PHYSICS BASICS

2.1 Exact and Approximate Solutions to Common Equations

2.1.1 The Law of Sines for Plane Triangles

For future reference, the law of sines applied to the plane triangle **UOS** in Figure 1 yields

$$\frac{\sin(\theta)}{d} = \frac{\sin\left(\frac{\pi}{2} + \alpha\right)}{R_e + h} = \frac{\sin\left(\frac{\pi}{2} - \alpha - \theta\right)}{R_e} \qquad \text{Eq 1}$$

Eq 1 reduces to

$$\frac{\sin(\theta)}{d} = \frac{\cos(\alpha)}{R_e + h} = \frac{\cos(\alpha + \theta)}{R_e} \qquad \text{Eq 2}$$

In Eq 2, the left-center equality,

$$(R_e + h)\sin(\theta) = d\cos(\alpha) \qquad \text{Eq 3}$$

relates all five quantities of interest in a simple way.

The left-right equality in Eq 2 is equivalent to

$$R_e \sin(\theta) = d\cos(\alpha + \theta) \qquad \text{Eq 4}$$

This expression relates one side variable, ***d***, and the two angle variables, ***α*** and ***θ***.

Similarly, the center-right equality in Eq 1 is equivalent to

$$R_e \cos(\alpha) = (R_e + h)\cos(\alpha + \theta) \qquad \text{Eq 5}$$

This expression relates one side variable, ***h***, and the two angle variables, ***α*** and ***θ***.

2.1.2 The Law of Cosines for Plane Triangles

For future reference, the law of cosines is applied to the plane triangle **UOS** in Figure 1. When the angle at **O** is used, the result is

$$d^2 = R_e^2 + (R_e + h)^2 - 2R_e(R_e + h)\cos(\theta) \qquad \text{Eq 6}$$

When the law of cosines is applied using the angle at **U**, the result is

$$(R_e + h)^2 = R_e^2 + d^2 - 2R_e d\cos\left(\frac{\pi}{2} + \alpha\right) \qquad \text{Eq 7}$$

Each of these equations relates the two side variables, ***d*** and ***h***, and one angle variable. Eq 6 involves θ and Eq 7 involves α.

2.1.3 Solution of a Quadratic Equation

In some instances, a quadratic equation similar to the following must be solved

$$Ax^2 + Bx + C = 0 \qquad \text{Eq 8}$$

The algebraic solution is

$$x = \frac{-B \pm \sqrt{B^2 - 4AC}}{2A} \qquad \text{Eq 9}$$

We cannot have imaginary roots, so $B^2 > 4AC$. In many instances, (a) the positive root is sought (since lengths cannot be negative), and (b) $B^2 > |4AC|$. For these situations:

$$x = \frac{-B + \sqrt{B^2 - 4AC}}{2A}$$

$$x = \frac{B}{2A}\left(\frac{1}{2}D - \frac{1}{8}D^2 + \frac{1}{16}D^3 - \frac{5}{128}D^4 + \frac{7}{256}D^5 - \frac{21}{1024}D^6 \pm \text{etc.}\right) \quad , \quad D = \frac{-4AC}{B^2} \qquad \text{Eq 10}$$

$$x \to -\frac{C}{B} \quad \text{as} \quad \frac{4AC}{B^2} \to 0$$

2.1.4 Computing Inverse Trigonometric Functions

Intrinsic to navigation analysis is the calculation of angles using an inverse trigonometric function. In performing such calculations, two concerns should be borne in mind: (1) numerical ill-conditioning and (2) ambiguous solutions. These conditions generally do not arise simultaneously. Numerical ill-conditioning occurs near sine or cosine function values of ±1, which correspond to unique angles. Ambiguous solutions generally arise when the approximate value of the angle is not known. The equations provided in the following chapters attempt to address these concerns, but every situation may not be anticipated.

Concerning numerical ill-conditioning: Both the sine and cosine functions have angular arguments for which the function's (a) value is near ±1, and (b) derivative is zero — see Figure **3**. Changes in the angular arguments result in significantly smaller changes in the trigonometric function value, which may be subject to truncation or roundoff. Accurately computing the angular argument from the trigonometric function often requires increased precision.

Table 2 below illustrates this concern for the geocentric angle computed from the arc cosine function. If five decimal digits are used for angles and trigonometric functions, the minimum detectable cosine function change corresponds to distances between 10 NM and 30 NM. A remedy is to employ the sine or tangent function rather than the cosine function. Unlike the cosine function, the sine and tangent functions (a) increase monotonically from a zero value for a zero angle, and (b) have a positive derivative value near zero angle. In Table 2, the last column indicates that for distances up to approximately 70 NM, the tangent function has a minimum of a two decimal place numerical advantage over the cosine function. The same behavior occurs for the sine function near π/2.

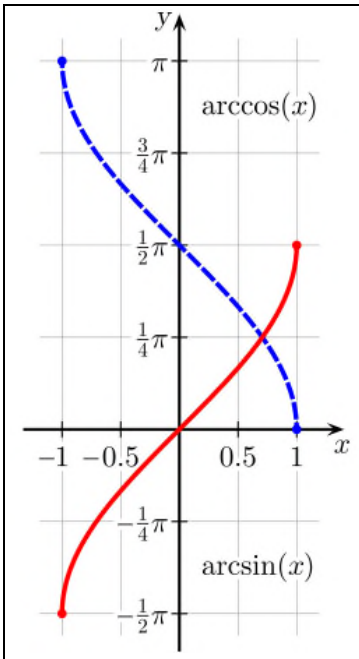

Figure 3 Principal Values of arcsin and arccos Functions

Table 2 Geocentric Angle θ and Its Cosine and Tangent Functions, near $\theta = 0$

θ (rad)	θ (deg)	Re*θ (NM)	cos(θ)	1-cos(θ)	tan(θ)	tan(θ) / 1-cos(θ)
0.00000	0.000	0.000	1.00000	0.00000	0.00000	—
0.00001	0.001	0.034	1.00000	0.00000	0.00001	2.0E+05
0.00003	0.002	0.103	1.00000	0.00000	0.00003	6.7E+04
0.00010	0.006	0.344	1.00000	0.00000	0.00010	2.0E+04
0.00030	0.017	1.031	1.00000	0.00000	0.00030	6.7E+03
0.00100	0.057	3.438	1.00000	0.00000	0.00100	2.0E+03
0.00300	0.172	10.313	1.00000	0.00000	0.00300	6.7E+02
0.01000	0.573	34.378	0.99995	0.00005	0.01000	2.0E+02
0.03000	1.719	103.134	0.99955	0.00045	0.03001	6.7E+01
0.10000	5.730	343.780	0.99500	0.00500	0.10033	2.0E+01

A method for recasting an ill-conditioned equation for cos(θ), which dates to the middle of the first millennium, is shown in Eq 11 below.

$$\textit{Given} \quad \cos(\theta) = f(\textit{other variables}) \quad \text{where} \quad f \approx 1$$

$$\textit{Invoke} \quad \cos(\theta) \equiv 1 - 2\sin^2\left(\frac{\theta}{2}\right) \qquad \text{Eq 11}$$

$$\textit{Thus} \quad \sin\left(\frac{\theta}{2}\right) = \frac{1}{\sqrt{2}}\sqrt{1-f}$$

To be effective, the quantity under the radical in Eq 11 must be further manipulated to eliminate

the subtraction of nearly equal quantities. For example, a common situation is finding one side, say $\boldsymbol{\theta_A}$, of a right spherical triangle, given the hypotenuse $\boldsymbol{\theta_C}$ and the other side $\boldsymbol{\theta_B}$.

$$\begin{aligned}\theta_A &= \arccos\left[\frac{\cos(\theta_C)}{\cos(\theta_B)}\right] \\ &= 2\arcsin\left(\sqrt{\frac{\sin\left(\frac{1}{2}(\theta_C+\theta_B)\right)\sin\left(\frac{1}{2}(\theta_C-\theta_B)\right)}{\cos(\theta_B)}}\right)\end{aligned} \qquad \text{Eq 12}$$

Concerning ambiguous solutions: Trigonometric functions are periodic, so inverse trigonometric functions can result in multiple angles. To address this issue: (a) when making a computation, take account of the expected range of values for the angle involved — e.g., elevation angle $\boldsymbol{\alpha}$ varies between $\pm\boldsymbol{\pi/2}$, so the arc sine or arc tangent functions are preferable to the arc cosine; (b) utilize half-angle formulas when possible, since they double the range of angles that can be computed uniquely; and (c) when possible, use a four-quadrant (two argument) arc tangent function.

2.1.5 Expansions of arcsin, arccos and arctan for Small Angles

In the analysis that follows, a common situation is the need to compute the inverse of a trigonometric function for an argument such that the resulting angle will be close to 0 — e.g., $\boldsymbol{\theta}$ = arcsin($\boldsymbol{x}$), $\boldsymbol{\theta}$ = arccos(**1** - $\boldsymbol{x}$) or $\boldsymbol{\theta}$ = arctan($\boldsymbol{x}$), where $\boldsymbol{x}$ is close to 0.

First, it is well known (Ref. 4) that

$$\arcsin(x) = x + \frac{1}{6}x^3 + \frac{3}{40}x^5 + \frac{5}{112}x^7 + \text{etc.} \qquad \text{Eq 13}$$

A Taylor series expansion of arccos(**1** - $\boldsymbol{x}$) is not available, due to its lacking a derivative at $\boldsymbol{x}$ = **0**. However, more general power series (often called Frobenius) expansions are available; thus, utilizing Eq 11 and Eq 13:

$$\arccos(1-x) = 2\arcsin\left(\sqrt{\frac{x}{2}}\right) = \sqrt{2}x^{1/2} + \frac{\sqrt{2}}{12}x^{3/2} + \frac{3\sqrt{2}}{160}x^{5/2} + \frac{5\sqrt{2}}{896}x^{7/2} + \text{etc.} \qquad \text{Eq 14}$$

Lastly, from Ref. 4:

$$\arctan(x) = x - \frac{1}{3}x^3 + \frac{1}{5}x^5 - \frac{1}{7}x^7 + \text{etc.} \qquad \text{Eq 15}$$

2.1.6 Secant Method for Root Finding

When finding an unknown quantity, one certainly prefers to have an expression (or sequence of expressions) whereby the unknown is a dependent variable and the known quantities are independent variables. (Developing such equations is the focus of this document.) However, situations inevitably arise whereby the available expressions contain the unknown quantity as an independent variable. If the expression(s) involved are too complicated to be manipulated into the desired form ("inverted"), recourse is often made to a numerical root-finding technique.

The most widely-known root-finding technique is "Newton's" or the "Newton-Raphson" method (Ref. 5). Newton's method performs well for most functions, but has the significant disadvantage that it requires a derivative with respect to the variable being sought. Often the derivative is difficult/tedious to compute analytically and to program in a computer. Thus, in applied work, interest is frequently limited to derivative-free root-finding techniques. Such techniques were first investigated by the ancients, including the Babylonians and Egyptians.

There are several alternative root-finder (or "solver") algorithms available. Implementations of some are found in mathematical software packages. The Secant method is among the simplest and oldest algorithms. Assuming that we seek a value of x that satisfies $f(x) = 0$, the Secant method of solution for x is

$$x_{n+1} = x_n - f(x_n)\frac{x_n - x_{n-1}}{f(x_n) - f(x_{n-1})} = x_n - \frac{x_n - x_{n-1}}{1 - \frac{f(x_{n-1})}{f(x_n)}} \qquad \text{Eq 16}$$

The secant method is a finite difference version of Newton's method; in effect, it uses the previous two points to estimate the function's derivative.

After initialization, both Newton's method and the Secant method converge in one step if the function f is linear. In general, convergence is governed by the behavior of the first and second derivatives of f. Functions that have a constant or continuously increasing (or decreasing) derivative are most amenable to a root finder. Many surveillance and navigation problems fit this description. Functions that have a derivative of zero or an inflection point (second derivative is zero) at or near the root being sought can flummox a root finder. For functions that are amenable to a root finder, Newton's method convergence is order 2 (i.e., the error for iteration n is proportional to the square of the error for iteration $n-1$), while the Secant method convergence is order 1.6.

An example involving a "root-finder friendly" function is determining the square root of 2 — i.e., $f(x) = x^2 - 2$. Table 3 shows the results of applying Newton's method and the Secant method, beginning from the same points.

Table 3 Comparison of Newton's and Secant Methods for Finding the Square Root of 2

Iteration, *n*	Newton's Method		Secant Method	
	Variable, x_n	Function, $f(x_n)$	Variable, x_n	Function, $f(x_n)$
1	1.0000000000	-1.0000000000	1.0000000000	-1.0000000000
2	1.5000000000	0.2500000000	1.5000000000	0.2500000000
3	1.4166666667	0.0069444444	1.4000000000	-0.0400000000
4	1.4142156863	0.0000060073	1.4137931034	-0.0011890606
5	1.4142135624	0.0000000000	1.4142156863	0.0000060073
6	—	—	1.4142135621	-0.0000000009
7	—	—	1.4142135624	0.0000000000

2.1.7 Surface Area on a Sphere

The surface area of the sphere with radius $\boldsymbol{R_e}$ is $4\pi\ (\boldsymbol{R_e})^2$. The surface area enclosed by a circle on the surface of that sphere is

$$A = 2\pi(R_e)^2[1-\cos(\theta)] \qquad \text{Eq 17}$$

Here $\boldsymbol{\theta}$ is the half-angle of the cone, with apex at the center of the sphere, whose intersection with the surface forms the circle under discussion. Using Figure 1, the cone would be formed by rotating sector **ONU** about line **ON**.

2.2 Shape of the Earth

2.2.1 WGS-84 Ellipsoid Parameters

While use of a spherical earth model is basic to much of the analysis herein, the most-accepted model for the shape of the earth is an oblate spheroid (ellipse rotated about its minor axis). The term 'ellipticity error' is used for differences between distances or angles found using a spherical earth model and the same quantities found using an ellipsoidal model.

The World Geodetic Survey 1984 (WGS-84) model parameter are the ellipsoid's semi-major axis, $\boldsymbol{a}$, and the flattening $\boldsymbol{f}$. Their numerical values are

- $\boldsymbol{a} \equiv 6{,}378{,}137$ m (WGS-84)
- $\boldsymbol{f} \equiv 1 / 298.257{,}223{,}563$ (WGS-84)

Flattening of the ellipsoid is defined by Eq 18, where $\boldsymbol{b}$ is the semi-minor axis.

$$f = \frac{a-b}{a} \qquad \text{Eq 18}$$

In computations, the square of the eccentricity $\boldsymbol{e^2}$ is frequently used in lieu of the flattening.

$$e^2 = \frac{a^2-b^2}{a^2} = 2f - f^2 = f(2-f) \qquad \text{Eq 19}$$

Although the earth's shape is not a sphere — it is nearly so. A useful "rule of thumb" is that the ellipticity error in the computed length of a path is 0.3%. The basis of this estimate is that the earth's flattening is approximately 0.003353, or 0.34%. Subsection 4.8.7 contains examples of the ellipticity error in computing the ranges between selected airports.

In the U.S., the foot is the most common unit of distance. As a result of the International Yard and Pound Agreement of July 1959, the international foot is defined to be exactly 0.3048 meter. Thus

- a = 20,925,646.3 ft (WGS-84)
- $b = (1 - f)\, a$ = 6,356,752.3 m = 20,855,486.6 ft (WGS-84)
- e^2 = 0.006,694,379,990,14 (WGS-84)

In marine and aviation applications, the nautical mile (NM) is often used as the unit of distance. The international nautical mile was defined by the First International Extraordinary Hydrographic Conference in Monaco (1929) as exactly 1,852 meters. This definition was adopted by the United States in 1954. The international nautical mile definition, combined with the definition for the foot cited above, result in there being 6,076.1155 feet in one nautical mile.

2.2.2 Radii of Curvature in the Meridian and the Prime Vertical

To approximate the ellipsoidal earth at a location on its surface by a sphere, two radii of curvature (RoCs) are commonly defined — the RoC in the meridian (north-south orientation), R_{ns}, and the RoC in the prime vertical (east-west orientation), R_{ew} (Ref. 6). These RoCs lie in orthogonal planes that include the normal (perpendicular line) to the surface of the ellipse. Their values are a function of the geodetic latitude L of the location involved — see Appendix (Section 9.3). Their analytic expressions are shown in Eq 20 and they are plotted in Figure 4.

$$R_{ns}(L) = \frac{a\,(1-e^2)}{[1-e^2\sin^2(L)]^{3/2}} = \frac{a^2 b^2}{[a^2\cos^2(L)+b^2\sin^2(L)]^{3/2}}$$

$$R_{ew}(L) = \frac{a}{[1-e^2\sin^2(L)]^{1/2}} = \frac{a^2}{[a^2\cos^2(L)+b^2\sin^2(L)]^{1/2}} \qquad \text{Eq 20}$$

The R_{ns} RoC in Eq 20 can vary more widely than the rule of thumb for ellipticity error. Figure 4 below shows that while R_{ew} does change by about 0.34% between the Equator and a Pole, R_{ns} changes by slightly over 1%. Excursions of the radius of curvature from a reasonable average value will usually be greater, on a percentage basis, than the ellipticity error in a path length.

The RoC in an arbitrary vertical plane that includes the normal to the ellipse and makes azimuth angle ψ with north is given by (Ref. 6)

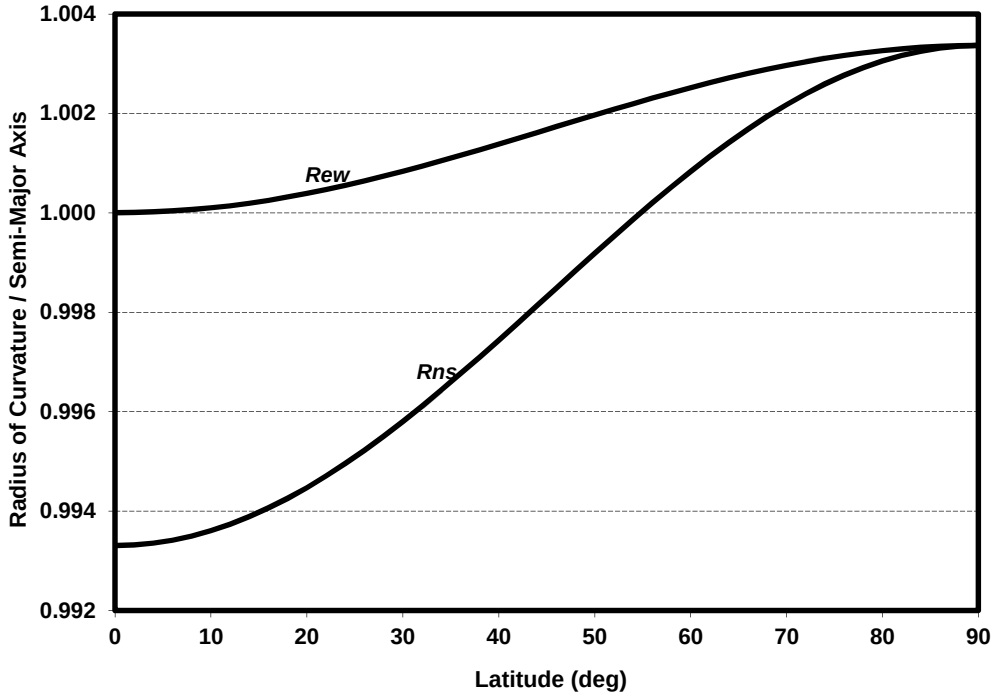

Figure 4 Ellipsoidal Earth's Radii of Curvature, Normalized to the Semi-Major Axis

$$R_{\psi} = \frac{1}{\frac{\cos^2(\psi)}{R_{ns}} + \frac{\sin^2(\psi)}{R_{ew}}} \qquad \text{Eq 21}$$

The average of $\boldsymbol{R_{\psi}}$ over $0 \le \boldsymbol{\psi} \le 2\pi$ (at a given latitude) is the Gaussian radius of curvature $\boldsymbol{R_G}$

$$R_G = \sqrt{R_{ns} R_{ew}} = \frac{a(1-f)}{1-e^2 \sin^2(L)} \qquad \text{Eq 22}$$

In some applications, a global approximation to $\boldsymbol{R_e}$ (independent of latitude) may be sufficient — e.g., the arithmetic mean of the three semi-axes of the ellipsoid

$$R_{e,arithmean} = \frac{1}{3}(a + a + b) = \left(1 - \frac{1}{3} f\right) a \qquad \text{Eq 23}$$

Thus

- $\boldsymbol{R_{e,\ arith\ mean}}$ = 6,371,008.8 m = 20,902,259.7 ft (WGS-84)

When analyzing procedures for the FAA and other U.S. Government agencies with an aviation mission, the value of $\boldsymbol{R_e}$ to be used is defined in Ref. 2:

- $\boldsymbol{R_e}$ = 20,890,537 ft (U.S. TERPS)

An earth-centered, earth-fixed (ECEF) Cartesian coordinate frame for an ellipsoidal model of the earth is defined in the Appendix (Section 9.3).

2.2.3 Methods for Addressing an Ellipsoidal Earth

During approximately the past half-century, there has been a resurgence of interest in ellipsoidal earth models. Reasons for this interest include: (1) wide availability of machine-based computational capabilities, (2) deployment of accurate long-range radionavigation systems, and (3) development of long-range, unmanned weapons systems. Much of the recent work derives from two volumes by Helmert[**] which were published in the 1880s (Ref. 7) and translated into English (Ref. 8) in the 1960s.

Andoyer-Lambert Formula — The Andoyer-Lambert formula (approximation) results from expansion of the geodesic (shortest) arc length between two points on a reference ellipsoid to first-order in the flattening (Ref. 9). This approximation was widely used in conjunction with both the Loran-C (Ref. 10) and Omega (Ref. 11) radionavigation systems. Accuracy for the Andoyer-Lambert formula is 10 m for distances up to 6,000 miles (Ref. 10).

Vincenty's Method — During the early 1970s, Vincenty[††] revisited the issue of geodesics on an ellipsoid, and programmed a version of earlier algorithms (including Helmert's) on a calculator. To accommodate the computing technology at that time, Vincenty's primary concern was minimizing the program's memory consumption. Accordingly, he developed iterative algorithms for both the direct and indirect problems of geodesy (Ref. 12).

Due to its ease of coding, Vincenty's algorithms are now the most widely used method for computing geodesics on an ellipsoidal earth. Their accuracy is quoted as less than one millimeter, which has been independently validated by comparison with numerical integration of the differential equations governing geodesic arcs on an ellipsoid (Ref. 13).

Sodano's Method — In a series of papers published between 1958 and 1968, Sodano[‡‡] described non-iterative approximate solutions to the direct and indirect problems of geodesy based on expansion of the arc length between two points to higher orders in the eccentricity (Refs. 14, 15 and 16). Quoting Ref. 14: "The accuracy of geodetic distances computed through the e^2, e^4, e^6 order for very long geodesics is within a few meters, centimeters and tenth of millimeters respectively. Azimuths are good to tenth, thousandths and hundreds thousandths of a second. Further improvement of results occurs for shorter lines".

[**] Friedrich Robert Helmert (July 31, 1843 – June 15, 1917) was born in Freiberg, Kingdom of Saxony (now Germany). According to Wikipedia, his texts "laid the foundations of modern geodesy".

[††] Thaddeus Vincenty worked at the U.S. Defense Mapping Agency Aerospace Center, Geodetic Survey Squadron, Warren Air Force Base, in Wyoming.

[‡‡] Emanuel Sodano worked at the U.S. Army Map Service and the Army Geodesy, Intelligence and Mapping Research and Development Agency.

2.3 Accounting for User Altitude

The equations developed in Chapters 3 generally assume that the user's location **U** is on the earth's surface. The primary exception are the examples, which do take account of the user's elevation above the earth's surface. Subsection 2.3.1 shows how to modify the equations in Chapter 3 to account of a non-zero, known user elevation/altitude, and Subsection 2.3.2 shows how to select the user altitude to ensure an unblocked line-of-sight to a satellite at a given distance or altitude. Background/tutorial information on different meanings of 'altitude' is provided the Appendix, Subsection 9.1.1.

2.3.1 Accounting for Known User Altitude

In most situations of interest, there is no concern about the line-of-sight (LOS) between the User **U** (generally a sensor) and the Satellite (or aircraft) **S** being blocked by the earth's curvature. This is the situation depicted in Figure 1. A method for determining the minimum elevation angle for which there is no LOS blockage is shown in Subsection 2.3.2.

When the user altitude $\boldsymbol{h_U}$ is known and the LOS between **U** and **S** is unblocked, the equations presented in Chapters 3 and thereafter can be used with these simple substitutions to account for a non-zero user altitude:

- $\boldsymbol{R_e} \rightarrow \boldsymbol{R_e} + \boldsymbol{h_U}$, and
- $\boldsymbol{h} \rightarrow \boldsymbol{h_S} - \boldsymbol{h_U}$ (where $\boldsymbol{h_S}$ is the satellite's altitude).

2.3.2 Conditions for Unblocked Line-of-Sight

Conditions for which the LOS between two points is unblocked by the earth can be determined using Figure 5, which shows the LOS connecting the User **U** and Satellite **S** having a point of tangency **T** with the earth's surface.

Below, Eq 24 (which utilizes Eq 14) applies to a situation where the user altitude $\boldsymbol{h_U}$ and satellite altitude $\boldsymbol{h_S}$ are known and the geocentric angle $\boldsymbol{\theta}$ is unknown. Altitudes $\boldsymbol{h_U}$ and $\boldsymbol{h_S}$ can be traded off — i.e., one can be increased and the other decreased — without changing $\boldsymbol{\theta}$.

$$\theta_U = \arccos\left(\frac{R_e}{R_e + h_U}\right) = 2\arcsin\left(\sqrt{\frac{h_U}{2(R_e + h_U)}}\right)$$

$$\theta_S = \arccos\left(\frac{R_e}{R_e + h_S}\right) = 2\arcsin\left(\sqrt{\frac{h_S}{2(R_e + h_S)}}\right) \qquad \text{Eq 24}$$

$$\theta = \theta_U + \theta_S$$

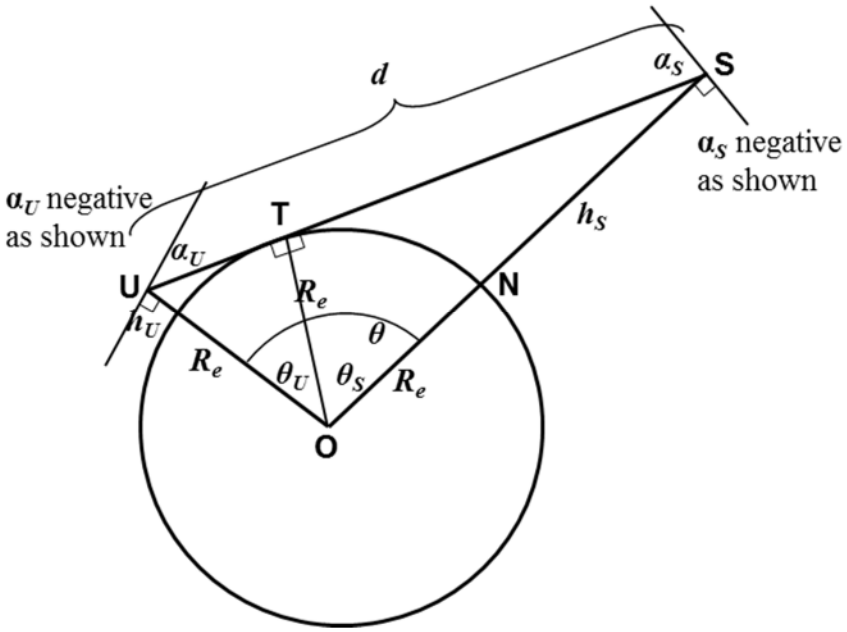

Figure 5 Problem Geometry for LOS Tangent to the Earth's Surface

When $\boldsymbol{\theta_U}$, $\boldsymbol{\theta_S}$, $\boldsymbol{h_U}$ and $\boldsymbol{h_S}$ are known, the variables $\boldsymbol{d}$, $\boldsymbol{\alpha_U}$ and $\boldsymbol{\alpha_S}$, can be found from

$$d = R_e \tan(\theta_U) + R_e \tan(\theta_S)$$

$$\alpha_U = -\arccos\left(\frac{R_e}{R_e + h_U}\right) = -2\arcsin\left(\sqrt{\frac{h_U}{2(R_e + h_U)}}\right) \qquad \text{Eq 25}$$

$$\alpha_S = -\arccos\left(\frac{R_e}{R_e + h_S}\right) = -2\arcsin\left(\sqrt{\frac{h_S}{2(R_e + h_S)}}\right)$$

While Eq 24 and Eq 25 reflect the common situation where the elevations/altitudes for both points (typically, the sensor and aircraft) are fixed, the known and unknown quantities vary with the application. A different situation is the siting an ATC radar, where $\boldsymbol{h_S}$ (minimum required coverage altitude) and $\boldsymbol{\theta} = \boldsymbol{\theta_U} + \boldsymbol{\theta_S}$ (distance between the location where the radar is to be installed and the outer boundary of the coverage region) are known. Then $\boldsymbol{h_U}$ is found using Eq 26, and $\boldsymbol{d}$, $\boldsymbol{\alpha_U}$ and $\boldsymbol{\alpha_S}$, can be found from Eq 25.

$$\theta_S = \arccos\left(\frac{R_e}{R_e + h_S}\right) = 2\arcsin\left(\sqrt{\frac{h_S}{2(R_e + h_S)}}\right)$$

$$\theta_U = \theta - \theta_S \qquad \text{Eq 26}$$

$$h_U = \left(\frac{1}{\cos(\theta_U)} - 1\right)R_e = \frac{2\sin^2\left(\frac{1}{2}\theta_U\right)}{\cos(\theta_U)}R_e = \left(\frac{1}{2}(\theta_U)^2 + \frac{5}{24}(\theta_U)^4 + \text{etc.}\right)R_e$$

In addition to the above geometric considerations, the analyst should be aware that radar signal propagation paths, such as **US** in Figure 5, are subject to bending caused by changes in atmospheric density with altitude. A simple, commonly used method for modeling this phenomenon is discussed in Subsection 3.6.1.

3. TWO-POINT / VERTICAL-PLANE PROBLEM FORMULATION

3.1 Mathematical Problem and Solution Taxonomy

3.1.1 Mathematical Formulation

In mathematical terms, the basic objective of this chapter is to analyze the plane triangle **UOS** in Figure 1. As a plane triangle, it is fully described by its three sides and three interior angles (or quantities having a one-to-one relationship with these six quantities). However, since the interior angles of a plane triangle (quantified in radians) must sum to π, interest can be limited to two interior angles (or their one-to-one equivalents). Thus, any three of the five quantities $\boldsymbol{R_e}$, $\boldsymbol{h}$, $\boldsymbol{d}$, $\boldsymbol{\alpha}$, and $\boldsymbol{\theta}$ can be selected independently (noting that at least one quantity will be a side), and the other two quantities will be uniquely determined. In this analysis,

- The angle having its vertex at the satellite **S** has a secondary role and is treated as a dependent variable.
- The earth's radius $\boldsymbol{R_e}$ is assumed to be a known parameter, rather than a variable.

Consequently, one purpose of this memorandum is to provide solutions for two of the four variables ($\boldsymbol{h}$, $\boldsymbol{d}$, $\boldsymbol{\alpha}$, $\boldsymbol{\theta}$) as a function of any two of the remaining variables (and the known parameter $\boldsymbol{R_e}$). Each group of three variables is related by one equation (provided in the next section) — thus a total of four equations mathematically define the geometric problem illustrated by Figure 1. Two equations (Eq 4 and Eq 5) are derived from the law of sines and involve two angle variables and one side variable. Two other equations (Eq 6 and Eq 7) are derived from the law of cosines and involve two side variables and one angle variable.

The equations in this chapter can be easily modified to account for the user having a known, non-zero altitude above the surface of the earth using the method described in Subsection 2.3.1.

3.1.2 Taxonomy of Solution Approaches

The preceding formulation — calculating one variable as a function of any two (of three possible) other variables — results in a total of 12 solutions. These solutions can be broken down into the following taxonomy, in approximate increasing order of complexity

- 2 angle variables and 1 distance variable involved; the distance variable is unknown — solution is based on the law of sines, and the most computationally complex operation is division — 2 cases
- 2 angle variables and 1 distance variable involved; an angle variable is the unknown — solution is based on the law of sines, and the most computationally complex operation is an inverse trigonometric function — 4 cases
- 1 angle variable and 2 distance variables involved; the angle variable is the unknown — solution is based on law of cosines, and the most computationally complex operation is an inverse trigonometric function — 2 cases

- 1 angle variable and 2 distance variables involved; the side opposite the angle is the unknown — solution is based on law of cosines, and the most computationally complex operation is a square root — 2 cases
- 1 angle variable and 2 distance variables involved; the distance variable adjacent to the angle is the unknown — solution is based on law of cosines, and the most computationally complex operation is solving a quadratic equation — 2 cases.

There are (usually more cumbersome) alternatives to the solution approaches outlined above. The first case addressed below, finding $\boldsymbol{\theta}$ from $\boldsymbol{h}$ and $\boldsymbol{\alpha}$, is an example.

3.1.3 Detailed Geometry

Figure 6 below is a more detailed depiction of the vertical-plane problem geometry shown in Figure 1. For each of the vertices of triangle **OUS** a line is constructed that intersects the opposite side (or an extension thereof) in a right angle. (These are the same lines that are created in some proofs of the law of sines and law of cosines.) These intersection points are labeled **A**, **B** and **C**. Because triangle **OUS** is oblique, intersections points **B** and **C** are outside the perimeter of **OUS**. Each of the constructed lines results in the creation of two right triangles with the right angle at **A**, **B** or **C** (for example, line **OC** creates right triangles **OCU** and **OCS**). Figure 6 also introduces the chord **UN**, which is an example of the role of half-angles. Color-coded distances (violet) and angles (blue) associated with these new lines and points are also shown.

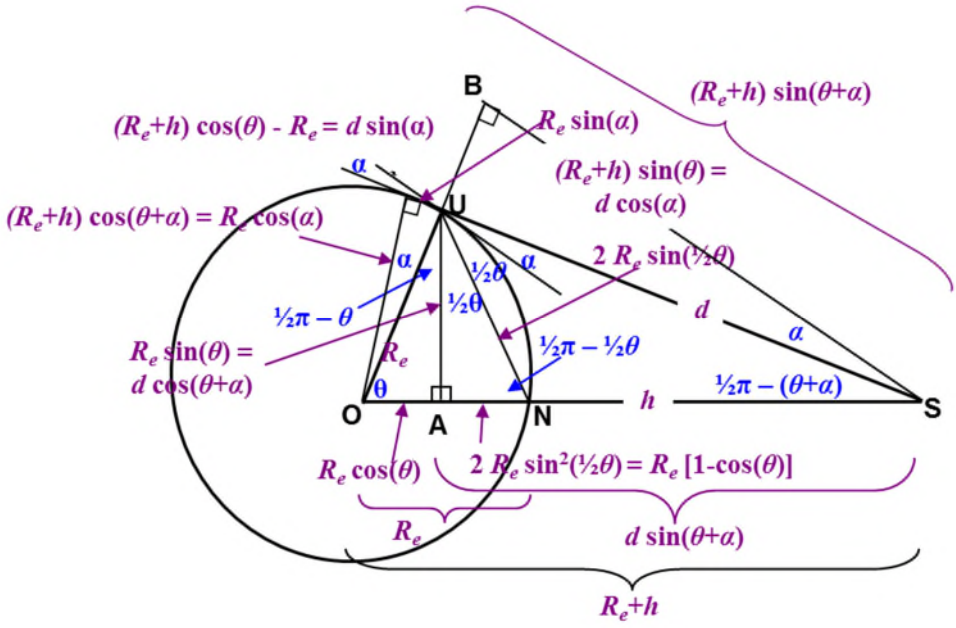

Figure 6 Detailed Geometry for Vertical Plane Formulation

3.2 Computing Geocentric Angle

3.2.1 Altitude and Elevation Angle Known – Basic Method

Manipulating Eq 5 yields

$$\theta = -\alpha + \arccos\left(\frac{R_e}{R_e + h}\cos(\alpha)\right)$$
$$= -\alpha + 2\arcsin\left(\sqrt{\frac{R_e \sin^2\left(\frac{1}{2}\alpha\right) + \frac{1}{2}h}{R_e + h}}\right) \qquad \text{Eq 27}$$

Referring to Figure 6, the first line in Eq 27 can also be derived from the right triangle **AUS**, where the length of the adjacent side is $R_e \sin(\theta)$ and the length of the hypotenuse is $(R_e+h)\sin(\theta) / \cos(\alpha)$.

The expressions on the right-hand sides of two lines in Eq 27 are analytically equivalent; however, the second is numerically better-conditioned when θ is small.

Using Eq 14, the first line in Eq 27 can be approximated by

$$\theta = -\alpha + \sqrt{2}\left(\frac{R_e}{2(R_e+h)}\alpha^2 + \frac{h}{R_e+h} - \frac{1}{24}\alpha^4\right)^{1/2} + \frac{\sqrt{2}}{12}\left(\frac{R_e}{2(R_e+h)}\alpha^2 + \frac{h}{R_e+h}\right)^{3/2} \qquad \text{Eq 28}$$
$$\text{to} \quad O(\alpha^3) \quad \text{and} \quad O\left(\left(\frac{h}{R_e}\right)^{3/2}\right)$$

When $\alpha = 0$ (satellite/aircraft is on user's horizon), θ achieves its maximum value for a visible target, which is given by

$$\theta_{\max vis} = \arccos\left(\frac{R_e}{R_e + h}\right) = 2\arcsin\left(\sqrt{\frac{\frac{1}{2}h}{R_e + h}}\right) \quad \text{for} \quad \alpha = 0 \qquad \text{Eq 29}$$

Since the interior angles of a planar triangle sum to π, it follows from Figure 1 that

$$\angle USO = \arcsin\left(\frac{R_e}{R_e + h}\cos(\alpha)\right) \qquad \text{Eq 30}$$

In the satellite field, it is sometimes said that angle USO accounts for the parallax caused by the satellite not being infinitely distant from the earth. The limiting values for angle USO are:

$$\angle USO \to 0, \qquad h >> R_e$$
$$\angle USO \to \frac{\pi}{2} - \alpha, \qquad h << R_e \qquad \text{Eq 31}$$

3.2.2 Altitude and Elevation Angle Known – Alternative Method

An alternative expression for the geocentric angle can be found by starting with Eq 7 (which involves ***d***, ***h*** and ***α***), then using Eq 4 to introduce ***θ*** and eliminate ***d***. The result is

$$\left[\frac{R_e + h}{\cos(\alpha)}\right]^2 \sin^2(\theta) + \left[2R_e(R_e + h)\tan(\alpha)\right]\sin(\theta) - \left[h^2 + 2R_e h\right] = 0 \qquad \text{Eq 32}$$

This is a quadratic equation in sin(***θ***). Its solution is given by

$$\theta = \arcsin(x)$$
$$x = \frac{-B + \sqrt{B^2 - 4AC}}{2A}$$
$$A = \left[\frac{R_e + h}{\cos(\alpha)}\right]^2 \qquad \text{Eq 33}$$
$$B = 2R_e(R_e + h)\tan(\alpha)$$
$$C = -h(h + 2R_e)$$

3.2.3 Altitude and Slant Range Known

From Eq 6, the geocentric angle is given by

$$\theta = \arccos\left(1 - \frac{1}{2}\frac{d-h}{R_e}\frac{d+h}{R_e+h}\right) = 2\arcsin\left(\frac{1}{2}\sqrt{\frac{d-h}{R_e}\frac{d+h}{R_e+h}}\right)$$
$$\approx \frac{d}{R_e}\sqrt{1-\left(\frac{h}{d}\right)^2} \approx \frac{d}{R_e}\left(1 - \frac{1}{2}\left(\frac{h}{d}\right)^2\right) \approx \frac{d}{R_e} \quad \text{for} \quad h << d << R_e \qquad \text{Eq 34}$$

Using Figure 6, the first expression on the right-hand side of the first line of Eq 34 can also be derived by applying Pythagoras's theorem to right triangle **UAS**. The second expression on the first line is numerically better-conditioned when ***θ*** is small, and is preferred in such situations.

A common application of Eq 34 is converting a slant-range ***d*** (which is usually easier to measure) to a geocentric ***θ*** (which is generally more useful in geodetic navigation and surveillance calculations). This conversion is termed the 'slant-range correction' in radar applications. When it is necessary to account for both the altitude h_U of the user **U** and the altitude h_S of the satellite **S**, Eq 34 is modified using the technique described in Subsection 2.3.1, and becomes:

$$\theta = 2 \arcsin\left(\frac{1}{2}\sqrt{\frac{d - (h_S - h_U)}{R_e + h_U}\,\frac{d + (h_S - h_U)}{R_e + h_S}}\right) \qquad \text{Eq 35}$$

3.2.4 Elevation Angle and Slant Range Known

Eq 4 can be written

$$R_e \sin(\theta) = d\cos(\alpha)\cos(\theta) - d\sin(\alpha)\sin(\theta) \qquad \text{Eq 36}$$

Thus

$$\begin{aligned}\theta &= \arctan\left(\frac{d\cos(\alpha)}{R_e + d\sin(\alpha)}\right) \\ &= \frac{\pi}{2} - \arctan\left(\tan(\alpha) + \frac{R_e}{d\cos(\alpha)}\right)\end{aligned} \qquad \text{Eq 37}$$

The right-hand side of the first line in Eq 37 can also be derived from right triangle **OBS** in Figure 6. The second line is simply an alternative form, as the arc tangent function is not ill-conditioned for any value of its argument.

3.3 Computing Elevation Angle

3.3.1 Altitude and Geocentric Angle Known

Manipulating Eq 5 yields

$$\begin{aligned}\tan(\alpha) &= \frac{(R_e + h)\cos(\theta) - R_e}{(R_e + h)\sin(\theta)} = \frac{h\cos(\theta) - 2R_e \sin^2\left(\frac{1}{2}\theta\right)}{(R_e + h)\sin(\theta)} \\ &= \frac{h}{R_e + h}\cot(\theta) - \frac{R_e}{R_e + h}\tan\left(\frac{1}{2}\theta\right)\end{aligned} \qquad \text{Eq 38}$$

The first expression on the right-hand side of Eq 38 can also be derived from right triangle **UBS** in Figure **6**.

Special / limiting cases of Eq 38 are

$$\begin{aligned}&\alpha = -\frac{1}{2}\theta \quad \text{for} \quad h = 0 \\ &\alpha \to \frac{h}{R_e + h}\frac{1}{\theta} - \frac{R_e}{R_e + h}\frac{\theta}{2} \quad \text{as} \quad \theta \to 0\end{aligned} \qquad \text{Eq 39}$$

$$h = \left(\frac{1}{\cos(\theta)} - 1 \right) R_e = \tan(\theta) \tan\left(\frac{1}{2}\theta \right) R_e \quad \text{for} \quad \alpha = 0$$

The first line in Eq 39 describes how the satellite/aircraft elevation angle decreases as the satellite/aircraft moves away from the user along the surface of the earth. The last line gives the altitude of the satellite/aircraft, as a function of distance, when the satellite/aircraft is on the horizon (ignoring refraction due to the earth's atmosphere).

3.3.2 Altitude and Slant Range Known

Manipulating Eq 7 yields

$$\begin{aligned} \sin(\alpha) &= \frac{h^2 + 2\,h\,R_e - d^2}{2\,d\,R_e} \\ &= \frac{1}{d}\left(h - \frac{(d - h)(d + h)}{2\,R_e} \right) \end{aligned} \qquad \text{Eq 40}$$

Using Figure 6, the first line of Eq 40 can also be derived by applying Pythagoras's theorem to the right triangle **OBS**, with the length of the sides being $\boldsymbol{R_e + h}$ (hypotenuse), $\boldsymbol{R_e + d}\sin(\boldsymbol{\alpha})$ and $\boldsymbol{d}\cos(\boldsymbol{\alpha})$. In the second line, the term in large parentheses is the perpendicular height of the satellite above the tangent plane at the user's location. It is interpreted as the altitude of the satellite minus a term which corrects for the curvature of the earth.

3.3.3 Geocentric Angle and Slant Range Known

Manipulating Eq 4 yields

$$\alpha = -\theta + \arccos\left(\frac{R_e}{d} \sin(\theta) \right) \qquad \text{Eq 41}$$

Eq 41 can also be derived from right triangle **AUS** in Figure 6.

3.4 Computing Slant Range

3.4.1 Altitude and Geocentric Angle Known

From Eq 6, it follows that

$$d = \sqrt{h^2 + 2R_e(R_e + h)(1 - \cos(\theta))}$$
$$= 2R_e\sqrt{\left(1 + \frac{h}{R_e}\right)\sin^2\left(\frac{1}{2}\theta\right) + \left(\frac{h}{2R_e}\right)^2} \qquad \text{Eq 42}$$

The first line in Eq 42 can also be derived by applying Pythagoras's theorem to right triangle **AUS** in Figure 6. The second line is analytically equivalent to the first, but numerically better-conditioned when θ is small, and thus is preferred in such situations.

As partial validation of Eq 42, when h and θ are set to zero separately, d is found to be equal to, respectively, the length of the chord connecting **U** and **S**, $2R_e\sin(\frac{1}{2}\theta)$, and the altitude, h. The partial derivatives of d with respect to θ and h do not exist.

3.4.2 Altitude and Elevation Angle Known

Eq 7 can be written

$$d^2 + 2R_e d\sin(\alpha) - (h^2 + 2R_e h) = 0 \qquad \text{Eq 43}$$

Its solution is

$$d = -R_e\sin(\alpha) + \sqrt{(R_e)^2\sin^2(\alpha) + 2hR_e + h^2} \qquad \text{Eq 44}$$

Referring to Figure 6, Eq 44 can be interpreted as length(**CS**)-length(**CU**), where length(**CS**) is found by Pythagoras's theorem applied to right triangle **OCS**.

The minimum and maximum values for the slant range d (requiring the satellite is visible) are

$$d_{\min} = h \quad \text{for} \quad \alpha = \frac{1}{2}\pi$$
$$d_{\max\ vis} = \sqrt{h^2 + 2R_e h} \quad \text{for} \quad \alpha = 0 \qquad \text{Eq 45}$$

As the satellite altitude approaches zero, the slant range converges as follows

$$d \to \frac{h}{\sin(\alpha)} \quad \text{as} \quad h \to 0 \qquad \text{Eq 46}$$

3.4.3 Geocentric Angle and Elevation Angle Known

Eq 5 can be written

$$d = R_e\frac{\sin(\theta)}{\cos(\alpha + \theta)} \qquad \text{Eq 47}$$

Eq 47 is a manipulation of the two expressions for the length of **AU** in Figure 6. This equation is not ill-conditioned for any values of θ and α.

3.5 Computing Altitude

3.5.1 Slant Range and Geocentric Angle Known

Eq 6 can be written as a quadratic equation in R_e+h. Its solution is

$$\begin{aligned} h &= -R_e\left(1-\cos(\theta)\right)+\sqrt{d^2-{R_e}^2\left(1-\cos^2(\theta)\right)} \\ &= -2R_e\sin^2\left(\frac{1}{2}\theta\right)+\sqrt{d^2-{R_e}^2\sin^2(\theta)} \end{aligned} \qquad \text{Eq 48}$$

Referring to Figure 6, the first line in Eq 48 can be interpreted as length(**AS**)-length(**AN**), where length(**AS**) is found by Pythagoras's theorem applied to right triangle **AUS**. The right-hand sides of the two lines are analytically equivalent. However, the right-hand side of the second line is numerically better-conditioned when θ is small, and is preferred in such situations.

3.5.2 Slant Range and Elevation Angle Known

Rearranging Eq 7 yields

$$\begin{aligned} h &= -R_e+\sqrt{{R_e}^2+d^2+2R_e\,d\sin(\alpha)} \\ &= R_e\left(\frac{x}{2}-\frac{x^2}{8}+\frac{x^3}{16}-\frac{5x^4}{128}+\frac{7x^5}{256}\pm\text{etc.}\right) \quad \text{when} \quad x=\frac{2d\sin(\alpha)}{R_e}+\frac{d^2}{{R_e}^2}<1 \end{aligned} \qquad \text{Eq 49}$$

Referring to Figure 6, the first line in Eq 49 can be interpreted as length(**OS**)-length(**ON**), where length(**OS**) is found by Pythagoras's theorem applied to right triangle **OBS**.

As the satellite slant range approaches zero, the altitude converges as follows

$$h\to d\sin(\alpha) \qquad \text{as} \qquad d\to 0 \qquad \text{Eq 50}$$

3.5.3 Elevation Angle and Geocentric Angle Known

Manipulating Eq 5 yields

$$\begin{aligned} h &= \left(\frac{\cos(\alpha)}{\cos(\alpha+\theta)}-1\right)R_e=\frac{\sin\left(\alpha+\frac{1}{2}\theta\right)\sin\left(\frac{1}{2}\theta\right)}{\cos(\alpha+\theta)}2R_e \\ &\approx \left(\alpha+\tfrac{1}{2}\theta\right)\theta R_e \qquad \alpha<<1 \;\;\&\;\; \theta<<1 \end{aligned} \qquad \text{Eq 51}$$

Eq 51 can also be derived by manipulating the two expressions for the length of **OC** in Figure 6.

Setting $\alpha = 0$ in Eq 51 yields and expression (Eq 52) for the "height of the user's horizon". Sometimes Eq 52 is replaced by a modified version that attempts to account for refraction due to variations in atmospheric density. This topic is partially addressed in the following section.

$$h_{horiz} = \left(\frac{1}{\cos(\theta)} - 1 \right) R_e = \tan(\theta)\tan(\tfrac{1}{2}\theta) R_e \quad \text{for} \quad \alpha = 0$$
$$= \left(\frac{1}{2}\theta^2 + \frac{5}{24}\theta^4 + \frac{61}{720}\theta^6 + \text{etc.} \right) R_e \qquad \text{Eq 52}$$

3.6 Example Applications

Three example applications are presented in this section, with the intent of providing a sense of how the mathematical equations presented earlier in this chapter relate to real problems. The examples are intended to illustrate that it is necessary to understand the application in order to utilize the equations properly and to interpret the results. Also, these examples suggest that, while providing useful information, the equations in this chapter cannot answer some relevant question. For that reason, the same examples are re-visited at the end of Chapter 4.

3.6.1 Example 1: En Route Radar Coverage

Application Context — A frequent surveillance engineering task is predicting a radar installation's "coverage". There are two common formulations: Calculate either the minimum visible aircraft (a) Elevation MSL or HAT, for a known ground range (geocentric angle) from the radar; or (b) Ground range (geocentric angle) from the radar, for a known elevation MSL or HAT.

For either case, the issues to be considered, and the approach taken herein, are:

- **Terrain Effects** — As stated in Chapter 1, blockage of electromagnetic waves by hills/mountains/structures is not addressed herein. These effects would be included in a more thorough analysis, and are particularly important in mountainous areas. However, terrain effects are handled numerically, rather than by an analytic model, and are thus outside the scope of this memorandum. The earth surrounding the radar is assumed to be smooth, although not necessarily at sea level.
- **Propagation Model** — As stated in Chapter 1, real sensors may not have the straight line propagation paths. Relevant to radars: electromagnetic waves behave according to Snell's Law and refract towards the vertical as the atmospheric density increases with decreased altitude. Refraction effects are most pronounced for long, predominantly horizontal paths within the earth's atmosphere (such as occur for an en route radar). A widely used model that approximates the effects of refraction and is compatible with the equations developed earlier in this chapter is the "four-thirds earth" model (Refs. 17 and 18). According to Ref. 17: "The 4/3 Earth radius rule of thumb is an average for the Earth's atmosphere assuming it is reasonably homogenized, absent of temperature inversion layers or unusual meteorological conditions." Ref. 18 is an in-depth treatment of radar signal refraction.

- **Radar Antenna Height** — Three values are used for the height of the radar antenna phase center above the surrounding terrain, h_U: 50 ft, representative of the antenna height for a radar mounted on a tower; 500 ft, representative of the antenna height for a radar on a hill top; and 5,000 ft, representative of the antenna height for a radar on a mountain top.

Based on these considerations, the two known/independent variables are taken to be:

(1) The satellite/aircraft elevation angle α (provided it is equal to or greater than the minimum value for the associated antenna height h_U); and

(2) Either

(a) The geocentric angle θ between the radar and a target aircraft (so the unknown/dependent variable is the aircraft altitude h_S above the terrain) — governed by Eq 51; or

(b) The aircraft altitude h_S (so the unknown/dependent variable is the geocentric angle θ) — governed by Eq 27.

Associating **U** with the radar antenna location (because its elevation is known) and **S** with possible aircraft locations, the resulting equations are shown in Eq 53 below. Substitutions are made for the four-thirds earth model and to account for a non-zero user altitude (Subsection 2.3.1). Also included is the equation for the geocentric angle θ_U between the radar and the location **T** where the signal path (for elevation angle α_{min}) is tangent to the earth (Figure 5).

$$(a)\quad h_S = h_U + \left(\frac{\cos(\alpha)}{\cos\left(\alpha + \frac{3}{4}\theta\right)} - 1 \right)\left(\tfrac{4}{3}R_e + h_U\right) \quad \text{for} \quad \alpha \geq \alpha_{min}$$

$$(b)\quad \theta = -\frac{4}{3}\alpha + \frac{8}{3}\arcsin\left(\sqrt{\frac{\left(\tfrac{4}{3}R_e + h_U\right)\sin^2\left(\tfrac{1}{2}\alpha\right) + \tfrac{1}{2}\left(h_S - h_U\right)}{\tfrac{4}{3}R_e + h_S}} \right) \quad \text{for} \quad \alpha \geq \alpha_{min} \qquad \text{Eq 53}$$

$$\alpha_{min} = -\arccos\left(\frac{\tfrac{4}{3}R_e}{\tfrac{4}{3}R_e + h_U} \right) = -2\arcsin\left(\sqrt{\frac{h_U}{2\left(\tfrac{4}{3}R_e + h_U\right)}} \right)$$

$$\theta_U = -\frac{4}{3}\alpha_{min}$$

The results of exercising Eq 53 for case (a), when the geocentric angle is known, are shown in Figure 7. The maximum range depicted, 250 NM, is the specified value for current en route ATC radars (e.g., ARSR-4 and ATCBI-6). Curves are shown that correspond to the three radar HAT values at the theoretical minimum elevation angle for which targets are visible (blue) and for 1 deg larger than the minimum elevation angle (violet). Aircraft whose range/HAT combinations are above a given curve are visible to the radar; otherwise they are said to be "below the radar horizon". If curves for the visibility of aircraft relative to mean sea level (altitude MSL) are needed, the elevation of the terrain is added to the HAT values in Figure 7.

Sensitivity to radar antenna HAT — Increasing the height of the radar's antenna significantly decreases the minimum HAT at which aircraft are visible. In this example, raising the antenna HAT from 50 to 5,000 feet decreases the visible aircraft HAT by almost 21,000 feet — i.e., the ratio is greater than 4:1. This leverage can be appreciated by examining Figure 5. Line **US** acts like a lever arm with its fulcrum at **T**. Raising **U** lowers **S**, and since **T** is generally closer to **U** than **S**, the change in the elevation of **S** is greater than it is in **U**.

Sensitivity to antenna elevation angle — Increasing the elevation angle of a radar antenna above the minimum required to avoid blockage of the signal by the earth has a significant coverage penalty. At the radar's maximum range, a 1 degree increase in elevation angle corresponds to an increase in the minimum HAT at which targets are visible of approximately

$$\Delta\boldsymbol{\alpha} \bullet \boldsymbol{d} = (1 \text{ deg})(\pi \text{ rad}/180 \text{ deg})(250 \text{ NM})(6{,}076 \text{ ft/NM}) = 26{,}511 \text{ feet} \qquad \text{Eq 54}$$

The resulting decrease in airspace under surveillance is more than is gained by raising the radar HAT to 5,000 feet. Thus, aligning (often called "bore sighting") the antenna is an important aspect of a radar installation.

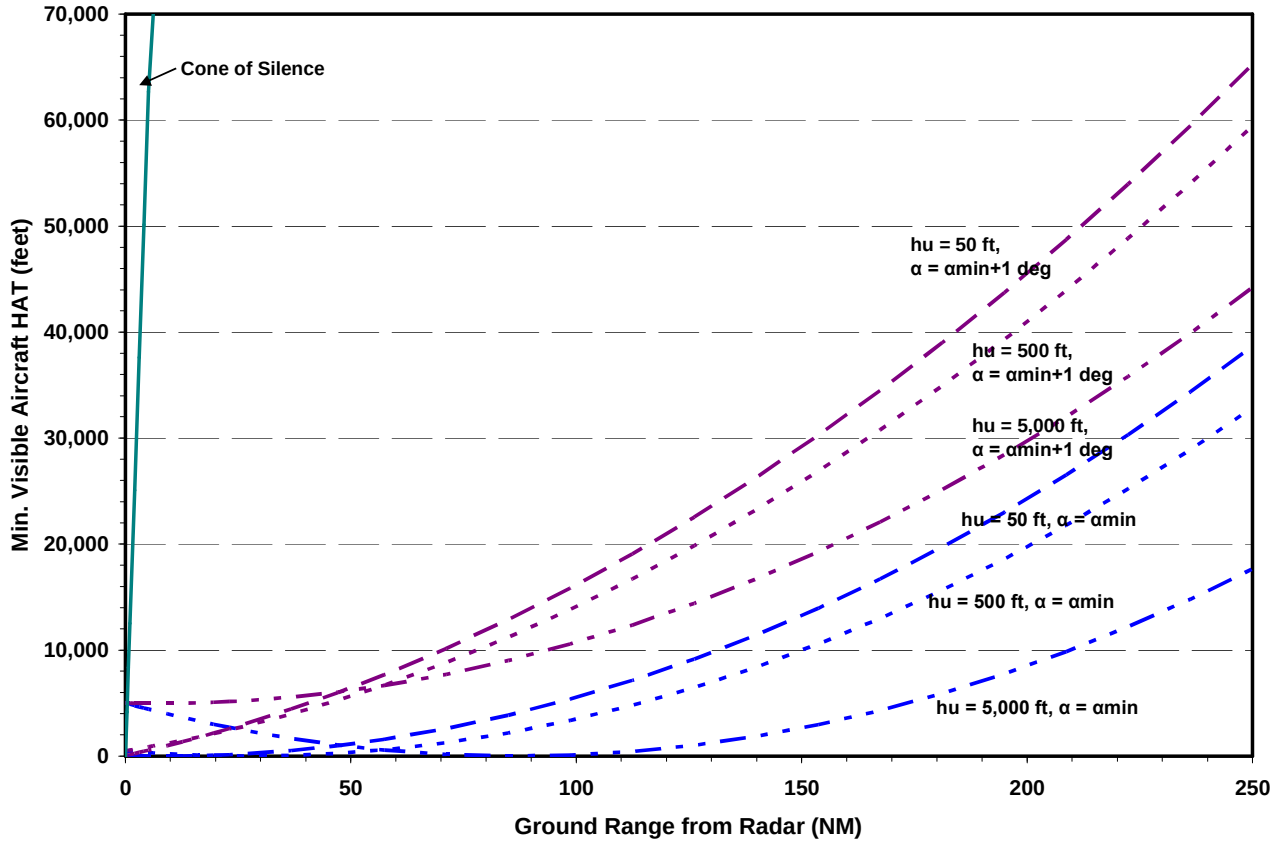

Figure 7 Aircraft Minimum Visible HAT vs. Range for Three Radar Antenna HAT Values

Cone of Silence — "Visibility" is necessary for an aircraft to be detected by a radar. But it is not sufficient. Energy transmitted by the radar must reach the aircraft; then, energy scattered

(primary radar) or transmitted (secondary radar) by the aircraft must return to the radar at a detectable level. When a radar performs well for most targets (the case here) and a target is visible, the determining factor for detectability is the antenna pattern. ATC radar antennas are designed to have their gain concentrated near the horizon, where most aircraft are. Conversely, ATC radars are not designed to detect aircraft almost directly above them (the "cone of silence").

A "rule of thumb" for detecting a target by an ATC radar is that the target range be at least twice its height above the radar antenna — e.g., an aircraft at 10,000 ft above the antenna would not be detected when less than 20,000 ft or 3.3 NM from the radar (Ref. 19). Figure 7 includes the predicted cone of silence for an ATC radar antenna on the surface; larger antenna HAT values will result in slightly smaller cones of silence. Generally, the cone of silence is an issue to be aware of, but is not a major concern.

Targets "Below" the Radar — While the cone of silence is a concern for aircraft nearly above a radar, when a radar antenna is installed significantly higher than the local terrain level, a similar issue arises for aircraft close to but at lower altitudes than the antenna. Figure 8 depicts the vertical plane (analogous to Figure 1) containing the radar antenna and the signal paths (for a

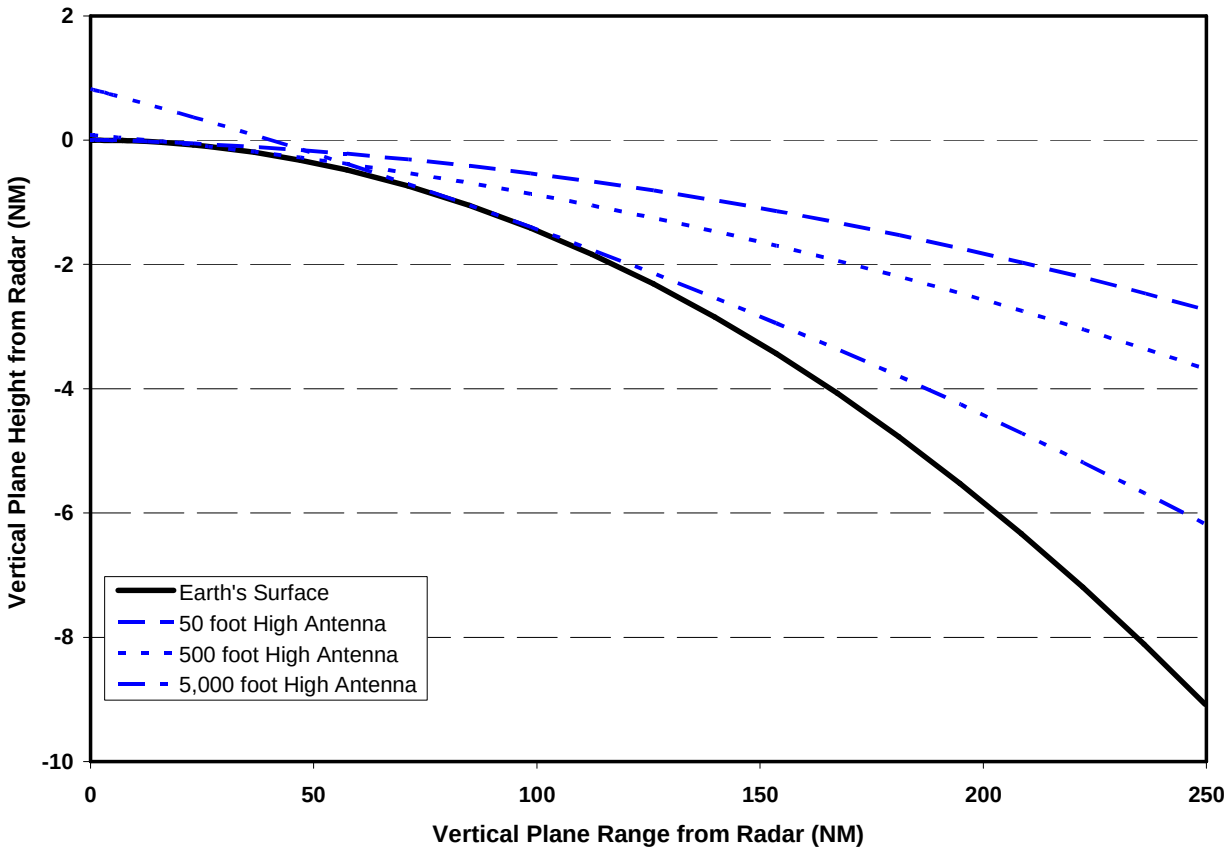

Figure 8 Aircraft Minimum Visible Altitude vs. Horizontal Range from Radar in Vertical Plane Containing Radar and Aircraft

4/3rds earth model) that are unblocked by the earth for antenna heights of 50 ft, 500 ft and 5,000 ft above the earth. (Data for these curves are the same as data for Figure 7.) The points of tangency **T** with the earth's surface for these signal paths are 8.7, 27.5 and 86.9 NM from the radar **U**. Aircraft located between **U** and **T** and vertically below the paths shown are visible to the radar (i.e., the propagation paths between those aircraft and the antenna are unblocked). Whether the radar can detect them is mainly an issue of the antenna vertical pattern. Some radars are designed with a "look down" mode to detect such aircraft. Figure 7 and Figure 8 may understate coverage for such targets.

Earth Model — For either the standard-size or 4/3rds earth model, the minimum visible aircraft altitudes are small at short ranges, and model differences are not important. However, the minimum visible altitudes for the individual models, and their differences, are substantial at longer ranges. For example, at a ground range of 250 NM, the predicted visible aircraft HAT for a 4/3rds earth model is less than that for a normal-size earth by between 13.4 kft (for a radar antenna HAT of 50 ft) and 9.4 kft (for a radar antenna HAT of 5,000 ft).

3.6.2 Example 2: Aircraft Precision Approach Procedure

Design of a Precision Instrument Approach Procedure (IAP) is a straightforward application of the analyses in this chapter. The RNAV (GPS) LPV approach to Kansas City International Airport (MCI) runway 19L is selected as an example. The approach plate is shown as Figure 9.

The first consideration is that, since the navigation fixes on the approach plate quantify vertical height in terms of altitude MSL, the same quantity must be used for procedure design. Second, the user location **U** is chosen as the point where aircraft crosses the runway threshold. The elevation above MSL of **U** is the sum of the elevation of the runway threshold (THRE = 978 ft) and the threshold crossing height (TCH = 59 ft); thus, $\boldsymbol{h_U}$ = 1,037 ft.

In terms of the four variables defined in Subsection 3.1.1, the elevation angle $\boldsymbol{\alpha}$ is set equal to the specified glide path angle — i.e., $\boldsymbol{\alpha}$ = 3.00 deg — and constitutes one independent variable. The second independent variable describes movement along the approach route. Either $\boldsymbol{\theta}$ or $\boldsymbol{h_S}$ could be used; in this example, $\boldsymbol{\theta}$ is selected because it has fewer drawbacks. While its published precision (0.1 NM) is less than desired, the limits of its precision are known. Conversely, only lower bounds for $\boldsymbol{h_S}$ are specified on the approach plate; the amount that each is below the glide path angle is not known. (However, a positive, and one reason for selecting this example is that there are six positions along the approach where the minimum altitude MSL is stated.)

For this set of variables — $\boldsymbol{\alpha}$ and $\boldsymbol{\theta}$ known, and $\boldsymbol{h}$ unknown — Subsection 3.5.3 provides the solution (Eq 51). After substituting for a non-zero user altitude $\boldsymbol{h_U}$ (Eq 35), the result is Eq 55. Evaluating this equation (using the TERPS value for $\boldsymbol{R_e}$ in Subsection 2.2.2) yields Table 4.

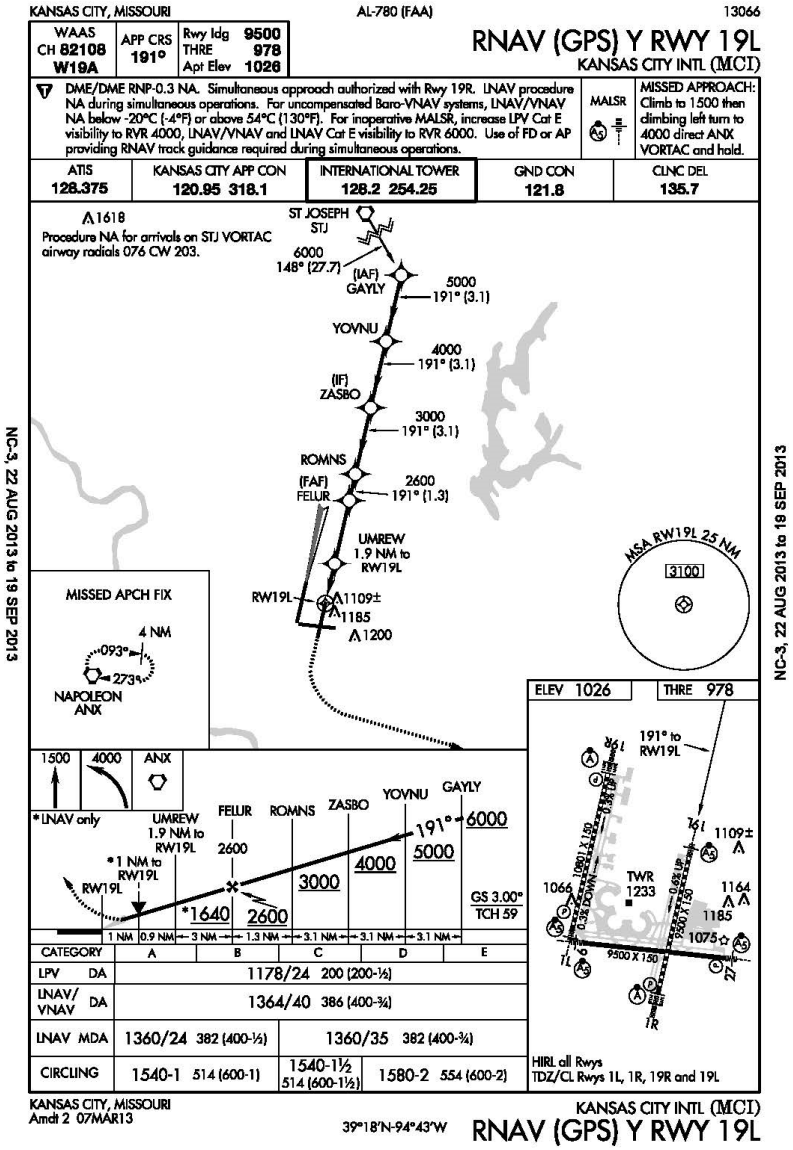

Figure 9 Approach Plate: RNAV (GPS) for MCI Runway 19L

$$h_S = h_U + \left(\frac{\cos(\alpha)}{\cos(\alpha + \theta)} - 1 \right)(R_e + h_U) \qquad \text{Eq 55}$$

Table 4 Specified and Computed Fix Altitudes for MCI Runway 19L LPV Approach

Fix Name	UMREW	FELUR	REMNS	ZASBO	YOVNU	GAYLY
Dist. from Threshold, NM (Figure 9)	1.9	4.9	6.2	9.3	12.4	15.5
Min. Altitude, ft MSL (Figure 9)	1,640	2,600	3,000	4,000	5,000	6,000
Glide Path Altitude, ft MSL (Eq 55)	1,645	2,619	3,046	4,075	5,122	6,187

Because the computed values in the last row of Table 4 are slightly larger than the published minimum altitudes on the row above, it is reasonable to conclude that the IAP design process described in the subsection closely replicates FAA process.

3.6.3 Example 3: Satellite Visibility of/from Earth

A question that is readily addressed using the equations in this chapter is: What fraction of the earth's surface can see (and be seen by) a satellite at altitude ***h***? Clearly, ***h*** is one independent variable in such an analysis. The other independent variable is taken to be the minimum elevation angle α (often called the mask angle in this context) at which the satellite provides a usable signal. The quality of signals received at low elevation angles can be degraded due to multipath and attenuation by the atmosphere; and terrain blockage is an issue at low elevation angles. The dependent variable is taken to be θ, the geocentric angle between the satellite nadir **N** and the user **U**. For this set of variables, Subsection 3.2.1 provides the solution approach.

An issue is whether to use a normal-size or 4/3 earth model. Normal-size is selected, because (unlike radar signals) satellite signals are outside of the earth's atmosphere over most of their propagation path. The earth's atmosphere extends to an altitude of approximately 5 NM, while satellite altitudes are at least several hundred nautical miles.

The basic equation to be evaluated is thus taken from Eq 27. As a way of visualizing the impact of satellite altitude on visibility, a modified version of Eq 17 is used. The results of exercising these equations are shown in Figure 10.

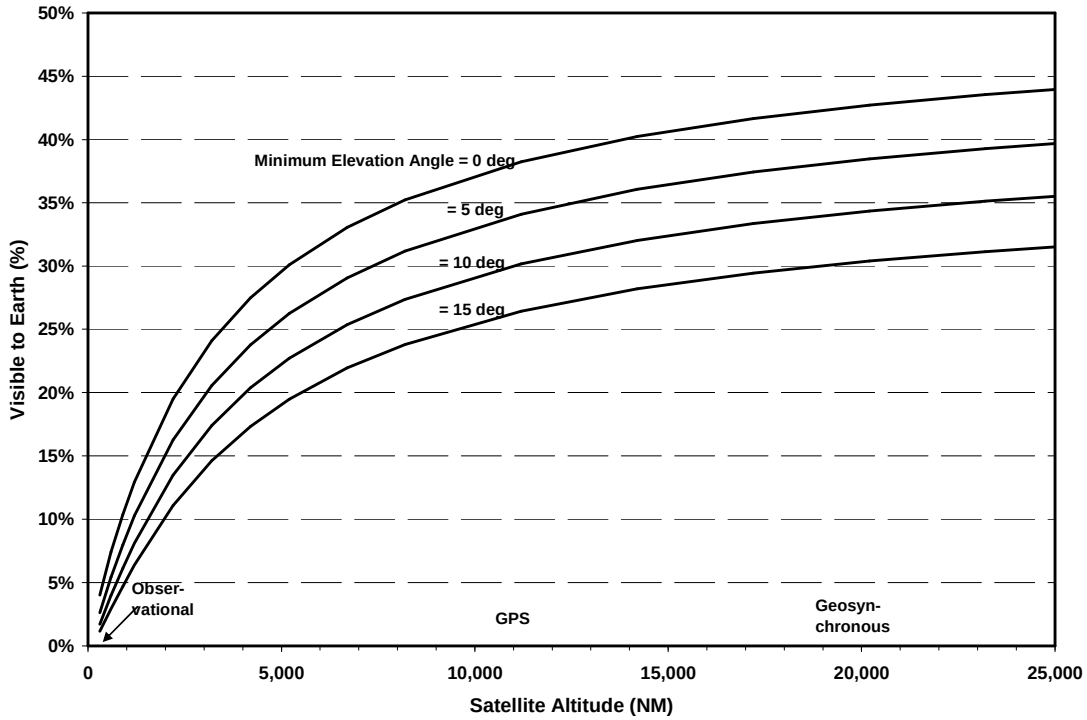

Figure 10 Fraction of Earth Visible vs. Satellite Altitude

4. TWO-POINT / SPHERICAL-SURFACE PROBLEM FORMULATION

4.1 Basics of Spherical Trigonometry

4.1.1 Basic Definitions

Spherical trigonometry deals with relationships among the sides and angles of spherical triangles. Spherical triangles are defined by three vertices (points **A**, **B** and **C** in Figure 11) on the surface of a sphere and three arcs of great circles (**a**, **b** and **c** in Figure 11), termed sides, connecting the vertices. The angles at the vertices are ***A***, ***B*** and ***C***, and the lengths of the sides are quantified by their corresponding geocentric angles (***a***, ***b*** and ***c***). In this memorandum, the sphere always represents the earth.

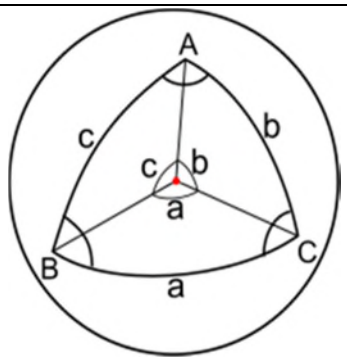

Figure 11 Example Spherical Triangle

Spherical trigonometry originated over 2,000 years ago, largely motivated by maritime navigation and understanding the relationship of the earth to the "heavenly bodies". Early contributors were from Greece, Persia and Arabia. The subject was completed by Europeans in the 18th and 19th centuries. Until the 1950s, spherical trigonometry was a standard part of the mathematics curriculum in U.S. high schools (Refs. 20 and 21).

4.1.2 Application to Navigation and Surveillance

In this memorandum, a distinction is made between "mathematical" and "navigation" spherical triangles. The three vertices of a "mathematical" spherical triangle can be arbitrarily located on the surface of a sphere — i.e., all three points can be problem-specific. The sides and interior angles are all positive numbers in the range (0, π). A "mathematical" spherical triangle does not have an defined relationship with the sphere's latitude/longitude grid.

In contrast, "navigation" spherical triangles involve only two problem-specific locations, typically labeled **U** and **S** in this chapter. The third vertex is chosen as the North Pole **P**[§§], enabling **U** and **S** to be related to the latitude/longitude grid. Six triangular elements (requiring seven variables) define a "navigation" spherical triangle (Figure 12):

(a) Angular lengths of sides **PU** and **PS** — complements of the latitudes of points **U** and **S**, respectively;

(b) Angle at **P** — the difference in the longitude of the points **U** and **S**;

(c) Angular length of side **US** — the geocentric angle between points **U** and **S**; and

[§§] While the North Pole is used in deriving navigation equations, the resulting expressions are valid for points in the southern hemisphere as well.

(d) Angles at **U** and **S** — the azimuth angles of the leg joining **U** and **S** with respect to north.

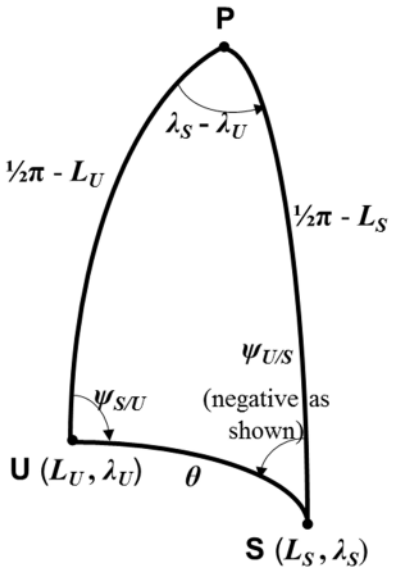

Figure 12 "Navigation" Spherical Triangle

This chapter is devoted to two-point problems that can be solved using navigation spherical triangles. Chapter 6 addresses situations involving three problem-specific points that require mathematical spherical triangles.

4.1.3 Applicability to Two-2D Problem Formulation

A drawback of spherical trigonometry is that it not suited to problems involving locations at finite distances above the earth's surface — i.e., it does not "handle" altitude. However, the vertical plane defined by two vertices of a spherical triangle and the center of the sphere conform to the assumptions employed in Chapter 3. Points directly above the two vertices lie in that plane as well. Thus, for situations involving two problem-specific points, plane and spherical trigonometry are complementary techniques that can be employed for their analysis. Moreover, situations involving three problem-specific points can be analyzed in the same way, so long as the altitude components can be handled in a pairwise manner. Generally, problems involving an aircraft and two navigation or surveillance sensors satisfy this condition.

4.1.4 General Characteristics of Spherical Triangles

The interior angles of a spherical triangle do not necessarily sum to π, and right triangles do not play as prominent a role as they do in plane trigonometry. Although Figure 11 and Figure 12 depicts all angles and sides as acute, angles and sides of mathematical spherical triangles lie in the range $(0, \pi)$. Angles in navigation spherical triangles have a wider range of values: latitude varies over $[-\pi/2, \pi/2]$, longitude varies over $[-\pi, \pi]$, geocentric angles vary over $(0, \pi)$ and azimuths vary over $[-\pi, \pi]$. Thus: latitudes are usually found with the arc sine function; longitudes with the two-argument arc tangent; geocentric angles with the arc cosine; and azimuths with the two-argument arc tangent. Difference between two longitudes or two azimuth angles may need to be adjusted by $\pm 2\pi$, so that the magnitude of the difference is less than or equal to π.

Two points on a sphere are diametrically opposite (antipodal) if the straight line connecting them passes through the center of the sphere. Mathematically, **U** and **S** are antipodal when $L_S = -L_U$ and $\lambda_S = \lambda_U \pm \pi$. If that is the case, the geocentric angle between **U** and **S** is π, and an infinite number of great circle paths connect **U** and **S**. Many spherical trigonometry equations, and particularly those for azimuth angles, are indeterminate for antipodal points.

4.1.5 Resources on the Web

The internet has many useful resources concerning spherical trigonometry. Examples, in approximate decreasing order of their complexity, are:

- I. Todhunter, *Spherical Trigonometry*, 5th Edition (Ref. 22) — Written by a British academic. Has been cited as the definitive work on the subject. Later editions were published but are not available without charge.
- W.M. Smart and R.M. Green, *Spherical Astronomy* (Ref. 23) — Also written by a British academics. Chapter 1 is devoted to spherical trigonometry. It has equations and their derivations (including more complex and useful ones).
- Wikipedia, *Spherical Trigonometry* (Ref. 24) — A fine collection of equations and background information.
- Wolfram MathWorld (Ref. 25) — Another good collection of equations
- Aviation Formulary (Ref. 26) — A website with equations similar to those in this chapter, without derivations. It also offers an Excel spreadsheet with formulas as macros.
- Spherical Trigonometry (Ref. 27) — An easily understood, unintimidating introduction to the topic.

4.1.6 Key Formulas

In general, the labeling of the angles and sides of a spherical triangle is arbitrary. Thus, cyclic substitutions — i.e., $\boldsymbol{A} \rightarrow \boldsymbol{B}$, $\boldsymbol{a} \rightarrow \boldsymbol{b}$, etc. — can be made to derive alternate versions of each identity. In addition to the formulas displayed below, there is a rich set of other identities that can be found in the literature.

Law of cosines for sides:

$$\cos(a) = \cos(b)\cos(c) + \sin(b)\sin(c)\cos(A) \qquad \text{Eq 56}$$

The right-hand side of this law contains two sides (here, ***b*** and ***c***) and their included angle (***A***). The left-hand side contains the third side (***a***), which is opposite to the included angle.

Primary applications: (1) finding the third side of a triangle, given two sides and their included angle; and (2) finding any angle of a triangle (using cyclic substitution), given three sides.

Law of cosines for angles:

$$\cos(A) = -\cos(B)\cos(C) + \sin(B)\sin(C)\cos(a) \qquad \text{Eq 57}$$

The right-hand side of this law contains two angles (here, ***B*** and ***C***) and their included side (***a***). The left-hand side contains the third angle (***A***), which is opposite to the included side.

Primary applications: (1) finding the third angle of a triangle, given the other two angles and their included side; and (2) finding any side of a triangle (by cyclic substitution) from all three angles.

Law of sines:

$$\frac{\sin(a)}{\sin(A)} = \frac{\sin(b)}{\sin(B)} = \frac{\sin(c)}{\sin(C)} \qquad \text{Eq 58}$$

Primary application: finding a side (or angle) of triangle, given the opposite angle (or side) and another opposite side-angle pair. The ambiguity of the arc sine function can be a concern.

Analogue of law of cosines for sides:

$$\begin{aligned} \sin(a)\cos(B) &= \cos(b)\sin(c) - \sin(b)\cos(c)\cos(A) \\ \sin(a)\cos(C) &= \cos(c)\sin(b) - \sin(c)\cos(b)\cos(A) \end{aligned} \qquad \text{Eq 59}$$

The right-hand sides of both lines of the above equation have the same sides and included angle (and almost identical functions) as the right-hand side of the law of cosines for sides. However, whereas the law of cosines for sides has cos(***a***) on the left-hand side, the analogue law has sin(***a***) cos(***B***) or sin(***a***) cos(***C***), with ***B*** and ***C*** being the angles adjacent to side ***a***.

Primary application: resolving ambiguities in situations where two sides and the included angle are known, and it is desired to find the other two angles directly from the known quantities.

Four-Part Cotangent Formula:

$$\begin{aligned} \cos(a)\cos(B) &= \sin(a)\cot(c) - \sin(B)\cot(C) \qquad (cBaC) \\ \cos(a)\cos(C) &= \sin(a)\cot(b) - \sin(C)\cot(B) \qquad (BaCb) \end{aligned} \qquad \text{Eq 60}$$

The six elements of a triangle may be written in cyclic order as (aCbAcB). The four-part cotangent formula relates two sides and two angles forming four consecutive elements around a triangle. The side and angle at the ends of such a sequence appear once on each line in Eq 60, as the argument of a cotangent function, whereas the middle elements appear twice on a line.

Primary applications: (1) given two angles (here, ***B*** and ***C***) and their included side (***a***), find the adjacent sides (***b*** and ***c***); and (2) Given two sides (***c*** and ***a,*** or ***a*** and ***b***) and their included angle (***B*** or ***C***), find the adjacent angles (***C*** and ***B***).

With same known quantities as the two cosine laws, the four-part cotangent formula provides solutions for the adjacent quantities that the cosine laws do not address. However, application (2) can also be accomplished by a combination of the law of sines and the analogue law (see solutions for longitude difference and azimuth angles below).

Napier's Analogies:

$$\tan\tfrac{1}{2}(A+B) = \frac{\cos\tfrac{1}{2}(a-b)}{\cos\tfrac{1}{2}(a+b)}\cot\tfrac{1}{2}C \qquad \tan\tfrac{1}{2}(a+b) = \frac{\cos\tfrac{1}{2}(A-B)}{\cos\tfrac{1}{2}(A+B)}\tan\tfrac{1}{2}c \qquad \text{Eq 61}$$

$$\tan\tfrac{1}{2}(A-B)=\frac{\sin\tfrac{1}{2}(a-b)}{\sin\tfrac{1}{2}(a+b)}\cot\tfrac{1}{2}C \qquad \tan\tfrac{1}{2}(a-b)=\frac{\sin\tfrac{1}{2}(A-B)}{\sin\tfrac{1}{2}(A+B)}\tan\tfrac{1}{2}c$$

Primary application: (1) given two sides (here, ***a*** and ***b***) and their opposite angles (***A*** and ***B***), find the remaining side (***c***) and remaining angle (***C***).

Same Affection for Sums/Difference of Opposite Sides/Angles:

Since all sides and angles of a "mathematical" spherical triangle are in (0, π), ½(***A***+***B***) and ½(***a***+***b***) are as well. Ref. 22 demonstrates that these sums are less than/equal to/greater than ½π synchronously. Also, ½(***A***-***B***) and ½(***a***-***b***) are both in (-½π, ½π). Ref. 22 demonstrates that these differences are less than/equal to/greater than 0 synchronously. Ref. 22 terms this characteristic "having the same affection".

Solving for Angles and Sides:

When solving for angles and sides after employing the above formulas, one must be aware of the possibility of ambiguous solutions to inverse trigonometric functions. In the realm of spherical trigonometry (versus navigation), where angles and sides are in the range (0, π), the arc sine function and the law of sines are the primary source of concern, as two angles in the range (0, π) can have the same sine value. However, some problems do have two solutions; in these cases, neither result from the arc sine function is extraneous. Additional comments are provided concerning specific problems and equations below.

4.1.7 Taxonomy of Mathematical Spherical Triangle Problems

A spherical triangle is defined by a total of six quantities. The case of five given (known) elements is trivial, requiring only a single application of either cosine law or the sine law. For four given elements there is one non-trivial case. For three given elements there are six cases. Each of the seven cases is illustrated in Figure 13 and enumerated below (Ref. 28), along with a solution approach. For some cases, others solutions may exist (Ref. 22).

(1) Three sides known — Eq 56, three times
(2) Two sides and the included angle known — Eq 56 for ***a***, Eq 58 and/or Eq 59 for ***B*** and ***C***
(3) Two sides and a non-included angle known — Eq 58 for ***C***, then follow case 7
(4) Two angles and the included side known — Eq 57 for ***A***, then Eq 58 or Eq 60 ***b*** and ***c***
(5) Two angles and a non-included side known — Eq 58 for ***b***, then follow case 7
(6) Three angles known — Eq 57, three times
(7) Two sides and their opposite angles known — Eq 61 for ***A*** and ***a***.

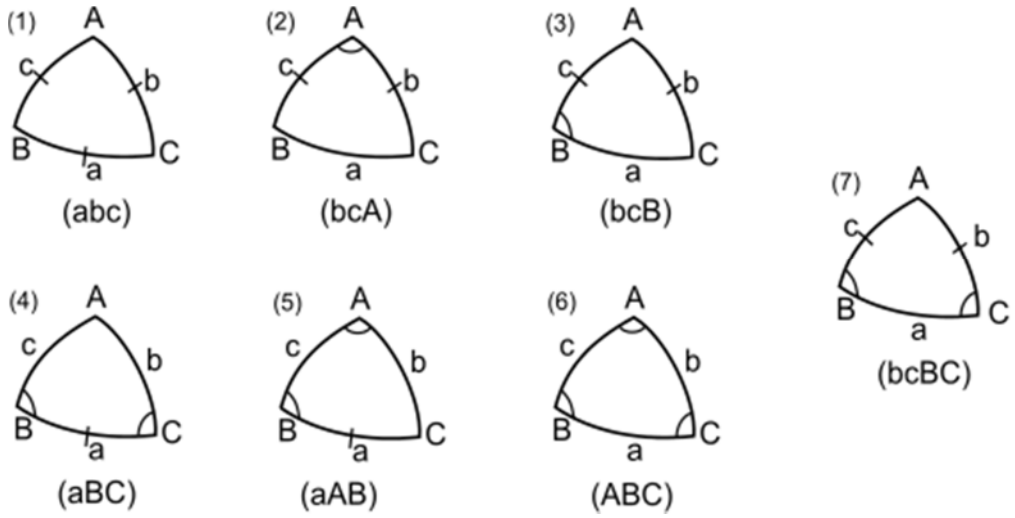

Figure 13 Illustrating the Taxonomy of Spherical Triangle Problems

4.1.8 Taxonomy of Navigation Spherical Surface Problems

The spherical surface formulation introduced in Section 1.3 involves seven variables. For a full solution to a given situation, four variables must be known, from which the remaining three can be found. Thus, 35 mathematical problems and 105 solution equations could be involved. However, the spherical surface formulation is symmetric in **U** and **S**; interchanging **U** and **S** only flips the left and right sides in Figure 12 but does not change the underlying problem. Of the 35 possible mathematical problems, three are self-symmetric (the mathematical problem does not change if **U** and **S** are interchanged) and 16 have symmetric versions — see Table 5. Table 5 notes the 3 of 19 problems summarized (and 5 of the full 35) do not involve either longitude being known; thus the solution can only yield a longitude difference rather than an actual longitude. Table 5 also references the corresponding spherical triangle case (Subsection 4.1.7) and the cases that are addressed in the remainder of this chapter. All seven spherical triangle cases presented in Subsection 4.1.7 occur in Table 5

Table 5 Taxonomy of Navigation Spherical Surface Problems

Case #	L_U	λ_U	$\psi_{S/U}$	L_S	λ_S	$\psi_{U/S}$	θ	SP[1]	SS[2]	No λ	ST Case[3]	Comment
1	X	X		X	X				X		2	Section 4.2
2	X	X	X	X				X			3	Section 4.6
3	X	X		X		X		X			3	Similar to #2
4	X	X		X			X	X			1	
5	X	X	X		X			X			4	Section 4.3.4
6	X	X			X	X		X			5	
7	X	X			X		X	X			3	
8	X	X	X			X		X			5	
9	X	X	X				X	X			2	Section 4.3
10	X	X				X	X	X			3	Section 4.4

Case #	L_U	λ_U	$\psi_{S/U}$	L_S	λ_S	$\psi_{U/S}$	θ	SP[1]	SS[2]	No λ	ST Case[3]	Comment
11	X		X	X		X			X	X	7	
12	X		X	X			X	X		X	1, 2, +	Over-specified
13	X		X		X	X		X			5	Similar to #8
14	X		X		X		X	X			2	Similar to #9
15	X				X	X	X	X			3	
16	X		X			X	X	X		X	2, 4, +	Over-specified
17		X	X		X	X			X		6	
18		X	X		X		X	X			5	
19		X	X			X	X	X			4	

[1] Symmetric Problem exists
[2] Self-Symmetric problem
[3] Spherical Triangle Case (Subsection 4.1.7)

4.2 The Indirect Problem of Geodesy

The indirect problem of geodesy is stated in Section 1.3 and is illustrated in Figure 14. The known elements (and their symbols/values) are sides **PU** ($\frac{1}{2}\pi - L_U$) and **PS** ($\frac{1}{2}\pi - L_S$) and the included angle **UPS** ($\lambda_S - \lambda_U$). In the taxonomy of spherical triangles of Subsection 4.1.7, this problem falls under Case (2).

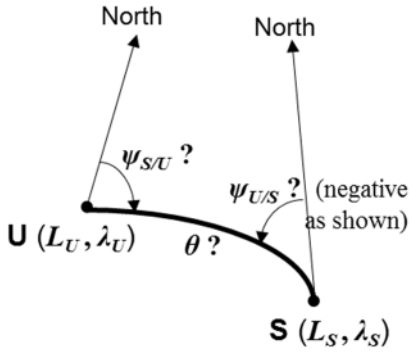

Figure 14 Indirect Problem of Geodesy

4.2.1 Computing the Geocentric Angle

Finding the geocentric angle between two locations on a spherical earth is fundamental question, and apparently was a motivating factor in the creation of spherical trigonometry during the first millennium AD.[***] Referring to Figure 12, the distance θ between **U** and **S** is readily derived from the law of cosines for sides (Eq 56), treating the leg connecting **U** and **S** as the unknown quantity

$$\cos(\theta) = \cos(L_U)\cos(L_S)\cos(\lambda_U - \lambda_S) + \sin(L_U)\sin(L_S) \qquad \text{Eq 62}$$

The right-hand side of Eq 62 should evaluate to a value in [-1, 1]; θ can then be found uniquely in [0, π]. Eq 62 was used by maritime navigators centuries ago, when precision was limited (their "tools" were paper-and-pencil and rudimentary trigonometry tables). It was found that Eq 62 is numerically ill-conditioned for small values of θ (Subsection 2.1.4) and alternatives were sought.

[***] When used at sea, presumably, a ship's navigator first estimated the vessel's latitude/longitude from celestial sightings, and then computed the distance to the destination and the course to follow.

To improve computational accuracy when the geocentric angle is small, over 1,000 years ago (Ref. 29) mathematicians defined the versine (in Latin, *sinus versus*) function as (Figure 15)

$$\text{vers}(\theta) \equiv 1 - \cos(\theta) = 2\sin^2\left(\frac{\theta}{2}\right) \qquad \text{Eq 63}$$

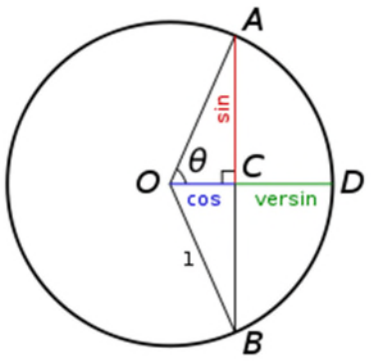

Figure 15 Sine, cosine and versine, and the unit circle

In early terminology, the familiar sine function was called *sinus rectus*, or vertical sine. Tables for the versine or the haversine (half of versine), and their inverses, date to the fourth century.

Using the haversine function, the geocentric angle can be found from what is sometimes called termed the "haversine formula"

$$\text{hav}(\theta) = \text{hav}(L_S - L_U) + \cos(L_S)\cos(L_U)\text{hav}(\lambda_S - \lambda_U) \qquad \text{Eq 64}$$

This historically significant formula eliminates the ill-conditioning of Eq 62 for small geocentric angles, and requires only a few calculations.

Without explicitly utilizing the versine or haversine (which are less needed today, due to the availability of modern computational capabilities), an analytically equivalent version of the haversine formula is

$$\sin\left(\frac{\theta}{2}\right) = \sqrt{\sin^2\left(\frac{L_S - L_U}{2}\right) + \cos(L_S)\cos(L_U)\sin^2\left(\frac{\lambda_S - \lambda_U}{2}\right)} \qquad \text{Eq 65}$$

The right-hand side of Eq 65 should evaluate to a value in [0, 1]; θ can then be found uniquely in [0, π]. The small latitude and longitude differences that occur when **U** and **S** are close only involve the sine function. This expression is reminiscent of Pythagoras's formula for the hypotenuse of a plane triangle. In fact, it reduces to Pythagoras's formula when the two points are close together and close to the equator.

A drawback of Eq 65 (although far less of an issue than the problem it solves) is that it's numerical ill-conditioned for angles near the antipodal point. One solution is to use the original equation (Eq 62) in these situations. Another is to use the following:

$$\cos\left(\frac{\theta}{2}\right) = \sqrt{\cos^2\left(\frac{L_S - L_U}{2}\right) - \cos(L_S)\cos(L_U)\sin^2\left(\frac{\lambda_S - \lambda_U}{2}\right)} = \sqrt{\cos\left(\frac{L_S - L_U}{2}\right) - \sqrt{\cos(L_S)\cos(L_U)}\sin\left(\frac{\lambda_S - \lambda_U}{2}\right)}\sqrt{\cos\left(\frac{L_S - L_U}{2}\right) + \sqrt{\cos(L_S)\cos(L_U)}\sin\left(\frac{\lambda_S - \lambda_U}{2}\right)} \qquad \text{Eq 66}$$

The previous two equations can be combined to create a form that is not ill-conditioned for any

value of θ when executing an inverse trigonometric function

$$\tan\left(\frac{\theta}{2}\right) = \frac{\sqrt{\sin^2\left(\frac{L_S - L_U}{2}\right) + \cos(L_S)\cos(L_U)\sin^2\left(\frac{\lambda_S - \lambda_U}{2}\right)}}{\sqrt{\cos\left(\frac{L_S - L_U}{2}\right) - \sqrt{\cos(L_S)\cos(L_U)}\sin\left(\frac{\lambda_S - \lambda_U}{2}\right)}\sqrt{\cos\left(\frac{L_S - L_U}{2}\right) + \sqrt{\cos(L_S)\cos(L_U)}\sin\left(\frac{\lambda_S - \lambda_U}{2}\right)}} \quad \text{Eq 67}$$

Remarks: (a) All of the equations in this subsection for θ are unchanged if **U** and **S** are interchanged; (b) When the three points **P**, **U** and **S** are aligned (so the triangle **PUS** is degenerate), the equations remain valid; and (c) An expression for $\sin(\theta)$ (vice that for $\sin(\frac{1}{2}\theta)$ in Eq 65) can be derived by vector analysis techniques, and is presented in Section 5.2 (Eq 121).

4.2.2 Computing the Azimuth Angles of the Connecting Arc

Having solved for the geocentric angle, the remaining "part" of the indirect problem of geodesy is finding the azimuth angles at **U** and **S** of the great circle arc connecting these two points. This determination is slightly complicated by the fact that azimuth angles can vary over the range $[-\pi, \pi]$, so that a two-argument arc tangent function must be used.

First, the spherical trigonometry law of sines (Eq 58), applied to the angles at **P** and at **U** yields

$$\sin(\psi_{S/U}) = \frac{\cos(L_S)\sin(\lambda_S - \lambda_U)}{\sin(\theta)} \quad \text{Eq 68}$$

Second, the analogue to the law of cosines for sides (Eq 59) yields

$$\cos(\psi_{S/U}) = \frac{\sin(L_S)\cos(L_U) - \cos(L_S)\sin(L_U)\cos(\lambda_S - \lambda_U)}{\sin(\theta)} \quad \text{Eq 69}$$

Thus

$$\tan(\psi_{S/U}) = \frac{\cos(L_S)\sin(\lambda_S - \lambda_U)}{\sin(L_S)\cos(L_U) - \cos(L_S)\sin(L_U)\cos(\lambda_S - \lambda_U)} \quad \text{Eq 70}$$

Observe that, while Eq 68 and Eq 69 depend upon the geocentric angle θ (which is not a "given" for the indirect problem), the solution (Eq 70) for $\psi_{S/U}$ only depends upon the latitudes and longitudes of the great circle arc end points, which are "givens". Thus, the solution for $\psi_{S/U}$ does not "daisy chain" from the solution for θ.

The spherical trigonometry method is symmetric with respect to the user and satellite, so

$$\tan(\psi_{U/S}) = \frac{\cos(L_U)\sin(\lambda_U - \lambda_S)}{\sin(L_U)\cos(L_S) - \cos(L_U)\sin(L_S)\cos(\lambda_U - \lambda_S)} \quad \text{Eq 71}$$

As mentioned previously, in navigation analyses it is useful to employ azimuths in the range [$-\pi$, π], where negative values denote angles west of north. In some expositions, the azimuth angle at the second point is taken to be the angle the path would take if it were to continue — i.e., implicitly or explicitly, the first point is taken as the origin and the second as the destination of a trajectory. However, herein, the two points are on an equal basis and the azimuth angle at the second point is that for the great circle path toward the first point. Eq 70 and Eq 71 reflect these points of view.

Remark: When the three points **P**, **U** and **S** are aligned (so the triangle **PUS** is degenerate), the equations in this subsection remain valid.

4.3 The Direct Problem of Geodesy

The direct problem of geodesy is stated in Section 1.3 and is illustrated in Figure 16. The known elements (and their symbols/values) are sides **PU** ($\frac{1}{2}\pi - L_U$) and **US** (θ), and their included angle **PUS** ($\psi_{S/U}$). In the taxonomy of Sub-section 4.1.7, this problem falls under case (2).

The coordinates L_U and λ_U and the azimuth angle $\psi_{S/U}$ define a great circle. The direct problem of geodesy can be thought of as determining the coordinates of location which is a given distance θ from **U**. Closely related problems are the subjects of Sections 4.4, 4.5 and 4.6.

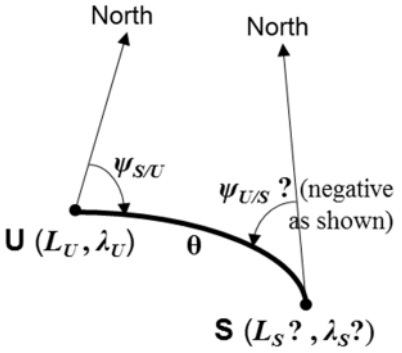

Figure 16 Direct Problem of Geodesy

4.3.1 Computing the Satellite Latitude

Applying the spherical law of cosines for sides, where the unknown is the side **PS**, yields

$$\sin\left(L_S\right) = \sin(L_U)\cos(\theta) + \cos(L_U)\sin(\theta)\cos\left(\psi_{S/U}\right) \qquad \text{Eq 72}$$

Note that latitude angles are restricted to the range [$-\pi/2$, $\pi/2$], so in this context, the principal value of the arc sine function always yields the correct solution.

4.3.2 Computing the Satellite Longitude

Finding the satellite longitude λ_S is more complex, as longitude angles are in the range [$-\pi$, π]. First, apply the spherical law of sines to the angels at **P** and **U**

$$\sin\left(\lambda_S - \lambda_U\right) = \sin\left(\theta\right)\frac{\sin\left(\psi_{S/U}\right)}{\cos\left(L_S\right)} \qquad \text{Eq 73}$$

Then apply the analogue to the law of cosines for sides

$$\cos\left(\lambda_S - \lambda_U\right) = \frac{\cos(L_U)\cos(\theta) - \sin(L_U)\sin(\theta)\cos\left(\psi_{S/U}\right)}{\cos\left(L_S\right)} \qquad \text{Eq 74}$$

Thus the satellite longitude can be found from

$$\tan\left(\lambda_S - \lambda_U\right) = \frac{\sin(\theta)\sin\left(\psi_{S/U}\right)}{\cos(L_U)\cos(\theta) - \sin(L_U)\sin(\theta)\cos\left(\psi_{S/U}\right)} \qquad \text{Eq 75}$$

The right-hand side of the above equation only depends upon "given" quantities for the direct problem, and not on the solution for $\boldsymbol{L_S}$. After employing a two-argument arc tangent function, the solution will yield a value of $\boldsymbol{\lambda_S - \lambda_U}$ in the range [$-\boldsymbol{\pi}$, $\boldsymbol{\pi}$]. If this is added to a value of $\boldsymbol{\lambda_U}$ (also in the range [$-\boldsymbol{\pi}$, $\boldsymbol{\pi}$]), the result will be in the range [$-2\boldsymbol{\pi}$, $2\boldsymbol{\pi}$]. Adjustments of $\pm 2\boldsymbol{\pi}$ must then be made to obtain a value of $\boldsymbol{\lambda_S}$ in the range ($-\boldsymbol{\pi}$, $\boldsymbol{\pi}$] — e.g., (1) If $\boldsymbol{\lambda_S} < 0$, then $\boldsymbol{\lambda_S} = \boldsymbol{\lambda_S} + 2\boldsymbol{\pi}$; (2) If $\boldsymbol{\lambda_S} > \boldsymbol{\pi}$, then $\boldsymbol{\lambda_S} = \boldsymbol{\lambda_S} - 2\boldsymbol{\pi}$.

4.3.3 Computing the Azimuth of the Connecting Path at the Satellite

After $\boldsymbol{L_S}$ and $\boldsymbol{\lambda_S}$ have been found, the direct problem solution can be completed by finding the azimuth of the great circle arc at the satellite's location, $\boldsymbol{\psi_{U/S}}$. using Eq 71. An alternative, preferred approach that does not daisy chain solutions is to first apply the law of sines,

$$\sin(\psi_{U/S}) = -\frac{\cos(L_U)\sin(\psi_{S/U})}{\cos(L_S)} \qquad \text{Eq 76}$$

A minus sign is introduced in the above equation to cause the two azimuth angles to have opposite signs.

Then apply the analogue to the law of cosines for sides

$$\cos(\psi_{U/S}) = \frac{\sin(L_U)\sin(\theta) - \cos(L_U)\cos(\theta)\cos(\psi_{S/U})}{\cos(L_S)} \qquad \text{Eq 77}$$

Thus

$$\tan(\psi_{U/S}) = \frac{-\cos(L_U)\sin(\psi_{S/U})}{\sin(L_U)\sin(\theta) - \cos(L_U)\cos(\theta)\cos(\psi_{S/U})} \qquad \text{Eq 78}$$

Eq 71 and Eq 78 have identical computational burdens.

4.3.4 Applications

Two applications of the equations in this Section to 'real world' problems are

- Finding intermediate points on the trajectory from **U** to **S** (using Eq 72 and Eq 75) by

replacing θ by $f \cdot \theta / N$, where $f \in [0, 1]$ (a similar functionality that applies to the vector approach is described in subsection 5.3.2)

- Determining the location of an aircraft **S** from the location of and range/bearing measurements for a VOR/DME ground station **U** (Subsection 4.8.6).

4.4 A Modified Direct Problem: Path Azimuth at Satellite Known

In this modification to the direct problem of geodesy, the azimuth angle $\psi_{U/S}$ of the path at **S** connecting **U** and **S** is known, and the azimuth angle $\psi_{S/U}$ of the path at **S** is unknown (the opposite of the assumptions for these quantities in unmodified problem). In taxonomy of spherical triangles in Subsection 4.1.7, this problem falls under case (3). In terms of the navigation triangle **UPS**, the known elements (and symbols) are sides **UP** ($\frac{1}{2}\pi - L_U$) and **US** (θ) and angle **USP** ($\psi_{U/S}$).

4.4.1 Computing the Satellite Longitude

The approach begins by applying the law of sines to triangle **UPS**

$$\sin(\lambda_S - \lambda_U) = \frac{\sin(\theta)\sin(\psi_{U/S})}{\cos(L_U)} \qquad \text{Eq 79}$$

In computing λ_S from Eq 79, two solutions are possible — one correct and one ambiguous. One satisfies $|\lambda_S - \lambda_U| \le \pi/2$ and the other satisfies $\pi/2 \le |\lambda_S - \lambda_U| \le \pi$. In aviation applications, the second will be "on the other side of the world" and not consistent with the range of available. It is discarded. It may be necessary to adjust λ_S to a value in the range $[-\pi, \pi]$.

4.4.2 Computing the Satellite Latitude

The satellite latitude L_S is found from Napier's Analogies (Eq 61), using the solutions for λ_S obtained from Eq 79

$$\begin{aligned}\tan\tfrac{1}{2}\left(\tfrac{\pi}{2} - L_S\right) &= \frac{\cos\frac{1}{2}(\psi_{U/S} + \lambda_S - \lambda_U)}{\cos\frac{1}{2}(\psi_{U/S} - \lambda_S + \lambda_U)} \tan\tfrac{1}{2}(\tfrac{\pi}{2} - L_U + \theta) \\ &= \frac{\sin\frac{1}{2}(\psi_{U/S} + \lambda_S - \lambda_U)}{\sin\frac{1}{2}(\psi_{U/S} - \lambda_S + \lambda_U)} \tan\tfrac{1}{2}(\tfrac{\pi}{2} - L_U - \theta)\end{aligned} \qquad \text{Eq 80}$$

The two expressions in Eq 80 are mathematically equivalent, but one may be preferred numerically in some situations.

4.4.3 Computing the Azimuth of the Connecting Arc at the User

There are multiple ways to find the azimuth angle $\psi_{S/U}$. Napier's Analogies (Eq 61) is used

because it raises the possibility of using the four-quadrant arc tangent function.

$$\begin{aligned}\tan\tfrac{1}{2}\psi_{S/U} &= \frac{\cos\frac{1}{2}(\theta-\frac{\pi}{2}+L_U)}{\cos\frac{1}{2}(\theta+\frac{\pi}{2}-L_U)}\tan\tfrac{1}{2}(\lambda_S-\lambda_S+\psi_{U/S}) \\ &= \frac{\sin\frac{1}{2}(\theta-\frac{\pi}{2}+L_U)}{\sin\frac{1}{2}(\theta+\frac{\pi}{2}-L_U)}\tan\tfrac{1}{2}(\lambda_S-\lambda_S-\psi_{U/S})\end{aligned} \qquad \text{Eq 81}$$

4.4.4 Application

An application of the equations in this Section is finding the aircraft's position using an on-board radar to measure the slant-range and azimuth angle to a location with known coordinates. Accurate determination of the geocentric angle $\boldsymbol{\theta}$ from the slant-range $\boldsymbol{d}$ requires taking into account the known altitude/elevation of the aircraft and target ground site relative to sea level. This is done using Eq 34, modified as described in Subsection 2.3.1.

$$\theta = 2\arcsin\left(\frac{1}{2}\sqrt{\frac{d-(h_S-h_U)}{R_e+h_U}\,\frac{d+(h_S-h_U)}{R_e+h_S}}\right) \qquad \text{Eq 82}$$

4.5 A Modified Direct Problem: Satellite Longitude Known

In this modification to the direct problem, the longitude of **S**, $\boldsymbol{\lambda_S}$, is known, and the geocentric angle, $\boldsymbol{\theta}$, between **U** and **S** is unknown (the opposite of the assumptions for these quantities in unmodified problem). In taxonomy of spherical triangles in Subsection 4.1.7, this problem falls under case (4). The known elements (and dimensions) are angles **UPS** ($\boldsymbol{\lambda_S - \lambda_U}$) and **SUP** ($\boldsymbol{\psi_{S/U}}$) and their included side **UP** ($\boldsymbol{\frac{1}{2}\pi - L_U}$).

In the development below, it is assumed that $\boldsymbol{\lambda_S \neq \lambda_U}$, as in that case there is either no solution ($\boldsymbol{\psi_{S/U}} \neq 0$ and $\boldsymbol{\psi_{S/U}} \neq \boldsymbol{\pi}$) or an infinite number of solutions. With this assumption, the problem is well-posed, because every non-meridian great circle crosses every line of longitude exactly once.

4.5.1 Computing the Satellite Latitude

The latitude $\boldsymbol{L_S}$ is found from the four-part cotangent formula (Eq 60)

$$\tan(L_S) = \frac{\sin(L_U)\cos(\lambda_S-\lambda_U)+\sin(\lambda_S-\lambda_U)\cot(\psi_{S/U})}{\cos(L_U)} \qquad \text{Eq 83}$$

In computing $\boldsymbol{L_S}$ from Eq 83, observe that, using the arc tangent function, it can be unambiguously found in $[-\boldsymbol{\pi}/\mathbf{2}, \boldsymbol{\pi}/\mathbf{2}]$.

4.5.2 Computing the Geocentric Angle

The geocentric angle θ is found from the four-part cotangent formula (Eq 60)

$$\cot(\theta) = \frac{\sin(L_U)\cos(\psi_{S/U}) + \sin(\psi_{S/U})\cot(\lambda_S - \lambda_U)}{\cos(L_U)} \quad \text{Eq 84}$$

In computing θ from Eq 84, observe that, using the arc cotangent function, it can be unambiguously found in [0, π].

4.5.3 Computing the Azimuth of the Connecting Arc at the Satellite

The azimuth angle $\psi_{U/S}$ is found from the law of cosines for angles (Eq 57)

$$\cos(\psi_{U/S}) = -\cos(\psi_{S/U})\cos(\lambda_S - \lambda_U) + \sin(\psi_{S/U})\sin(\lambda_S - \lambda_U)\sin(L_U) \quad \text{Eq 85}$$

In computing $\psi_{U/S}$ from Eq 85, observe that, using the arc cosine function, it can be unambiguously found in either [0, π] or [-π, 0]. The former is employed when **S** is west of **U**; the latter is employed when **S** is east of **U**.

4.6 A Modified Direct Problem: Satellite Latitude Known

In this modification to the direct problem, the latitude of **S**, L_S, is known, and the geocentric angle, θ, between **U** and **S** is unknown (the opposite of the assumptions for these quantities in unmodified problem). In the taxonomy of spherical triangle problems (Subsection 4.1.7), this situation falls into case (3). The known elements (and their dimensions) are sides **PU** ($\frac{1}{2}\pi - L_U$) and **PS** ($\frac{1}{2}\pi - L_S$) and adjacent angle **PUS** ($\psi_{S/U}$).

In the development below, it is assumed that $\psi_{S/U} \neq 0$ and $\psi_{S/U} \neq \pi$. If this assumption is not true, the problem either has no solution (either $L_U < L_S$ and $\psi_{S/U} = \pi$ or $L_S < L_U$ and $\psi_{S/U} = 0$) or the solution can be found trivially. Every great circle, except a meridian, has a maximum latitude L_{max} and minimum latitude $-L_{max}$. The $|L_{max}|$ associated with $\psi_{S/U}$ for a situation may be less than the value selected for $|L_S|$ for that situation (Subsection 4.6.1), in which case there is no solution (problem not well posed).

4.6.1 Computing the Azimuth of the Connecting Arc at the Satellite

The approach begins by applying the law of sines to finding $\psi_{U/S}$

$$\sin(\psi_{U/S}) = -\frac{\cos(L_U)\sin(\psi_{S/U})}{\cos(L_S)} \quad \text{Eq 86}$$

Consistent with the convention used herein, a minus sign is introduced on the right-hand side of the above equation, causing the two azimuth angles to have opposite signs. By assumption, the right-hand side of Eq 86 is not zero.

The absolute value of the right-hand side of Eq 86 can be: (a) greater than unity (in which case there is no solution, as $|\boldsymbol{L_S}| > \boldsymbol{L_{max}}$); (b) equal to unity (in which case there is one solution, as $|\boldsymbol{L_S}| = \boldsymbol{L_{max}}$); and (c) less than unity (in which case there are two solutions, as $|\boldsymbol{L_S}| < \boldsymbol{L_{max}}$). If (a) is true, the problem is ill posed and there's nothing more to be done. If (b) is true, refer to Section 4.7. If (c) is true, label the solutions $\boldsymbol{\psi_{U/S,1}}$ and $\boldsymbol{\psi_{U/S,2}}$ and proceed.

4.6.2 Computing the Satellite Longitude

The longitude $\boldsymbol{\lambda_S}$ is found using one of Napier's Analogies (Eq 61) and the solution for $\boldsymbol{\psi_{S/U}}$ found above with Eq 86

$$\tan\tfrac{1}{2}(\lambda_{S,i}-\lambda_U)=\frac{\cos\tfrac{1}{2}(L_U-L_S)}{\sin\tfrac{1}{2}(L_U+L_S)}\cot\tfrac{1}{2}(\psi_{S/U}-\psi_{U/S,i}) \qquad \text{Eq 87}$$

The discussion in Subsection 4.1.6 concerning sums and differences of sides and angles having the "same affection" is relevant here, but requires interpretation as a navigation (vice mathematical) spherical triangle is involved. Here, the cosine function is always positive and sine and cotangent functions change sign together. Thus, in computing $\boldsymbol{\lambda_{S,i}}$ (i = 1, 2) using the arc tangent function: (a) if **U** is west of **S**, the right-hand side is always positive and each solution can be unambiguously found in ($\boldsymbol{\lambda_U}$, $\boldsymbol{\lambda_U}+\boldsymbol{\pi}$); (b) if **S** is west of **U**, the right-hand side is always negative and each solution can be unambiguously found in ($\boldsymbol{\lambda_U}$ - $\boldsymbol{\pi}$, $\boldsymbol{\lambda_U}$).

Eq 87 is indeterminate when $\boldsymbol{L_U} = -\boldsymbol{L_S}$ (the sine term and the cotangent term are both zero). In this case, an alternate equation can be used:

$$\tan\tfrac{1}{2}(\lambda_{S,i}-\lambda_U)=\frac{\sin\tfrac{1}{2}(L_U-L_S)}{\cos\tfrac{1}{2}(L_U+L_S)}\cot\tfrac{1}{2}(\psi_{S/U}+\psi_{U/S,i}) \qquad \text{Eq 88}$$

Eq 88 is indeterminate when $\boldsymbol{L_U} = \boldsymbol{L_S}$ (the sine term is zero and the cotangent term is infinite).

4.6.3 Computing the Geocentric Angle

The geocentric angle $\boldsymbol{\theta}$ is also found from Napier's Analogies (Eq 61) using the solutions for $\boldsymbol{\psi_{S/U}}$ (Eq 86)

$$\tan\tfrac{1}{2}\theta_i = \frac{\cos\tfrac{1}{2}(\psi_{S/U} - \psi_{U/S,i})}{\cos\tfrac{1}{2}(\psi_{S/U} + \psi_{U/S,i})}\cot\tfrac{1}{2}(L_U + L_S) \qquad \text{Eq 89}$$

Here, the cosine function in the numerator and the cotangent function change signs together. Consequently, the right-hand side from Eq 89 is always positive. Thus, in computing $\boldsymbol{\theta_i}$ (i = 1, 2) using the arc tangent function, each solution can be unambiguously found in (0, $\boldsymbol{\pi}$).

Eq 89 is indeterminate when $\boldsymbol{L_U = -L_S}$ (the cosine term in the numerator is zero and the cotangent term is infinite). In this case, an alternate equation can be used:

$$\tan\tfrac{1}{2}\theta_i = \frac{\sin\tfrac{1}{2}(\psi_{S/U} - \psi_{U/S,i})}{\sin\tfrac{1}{2}(\psi_{S/U} + \psi_{U/S,i})}\tan\tfrac{1}{2}(L_U - L_S) \qquad \text{Eq 90}$$

Eq 90 is indeterminate when $\boldsymbol{L_U = L_S}$.

4.7 Latitude Extremes of a Great Circle

A special case of Clairaut's equation[†††] applies to full great circles (circling the earth), and can be simply derived using the law of sines applied to the angles at two end points of a navigation leg — **U** and **S**, in this case. If both azimuth angles are treated as positive

$$\cos(L_U)\sin(\psi_{S/U}) = \cos(L_S)\sin(\psi_{U/S}) \qquad \text{Eq 91}$$

Using the trigonometric identity $\sin(\boldsymbol{\psi}) = \sin(\boldsymbol{\pi}-\boldsymbol{\psi})$ yields

$$\cos(L)\sin(\psi) = C \qquad \text{Eq 92}$$

Thus all points on a given great circle have the same value, $\boldsymbol{C}$, for the product $\cos(\boldsymbol{L})\sin(\boldsymbol{\psi})$. Clearly, $|\boldsymbol{C}| \le 1$ and is positive for eastward routes and negative for westward routes. Satisfying Eq 92 is a necessary, but not sufficient, condition for the path to be a great circle — e.g., a counterexample is a constant-latitude route.

A common application of Eq 92 is finding the northern- and southern-most latitudes of a full great circle (termed vertices in Ref. 1). At a vertex, $\sin(\boldsymbol{\psi}) = \pm 1$, so

$$\cos(L_{\max}) = \left|\cos(L_U)\sin(\psi_{S/U})\right| = |C| \qquad \text{Eq 93}$$

At the two points displaced by $\pm\boldsymbol{\pi}/2$ from a vertex, the great circle crosses the equator. At those points, $\sin(\boldsymbol{\psi}) = \boldsymbol{C}$, so $|\boldsymbol{\psi}| = \boldsymbol{\pi}/2 - \boldsymbol{L_{max}}$.

[†††] Alexis Claude de Clairaut (or Clairault) (1713 –1765) was a prominent French mathematician, astronomer and geophysicist.

The great circle lies in a plane containing the locations **U** and **S** and center of the earth **O**. L_{max} is the angle between the great circle plane and the equatorial plane, and $|C|$ is the cosine of that angle. It follows from Eq 68 that

$$\cos(L_{\max}) = \left| \frac{\cos(L_U)\cos(L_S)\sin(\lambda_S - \lambda_U)}{\sin(\theta)} \right| \qquad \text{Eq 94}$$

Eq 94 enables L_{max} to be found from the coordinates of **U** and **S** and the distance between them.

Clearly, the latitude of the Southern Hemisphere vertex is $L_{min} = -L_{max}$

The longitude λ_{max} corresponding to L_{max} can be found using equations from Section 4.6. At L_{max}, the path azimuth ψ is $\pm\pi/2$. If that point is thought of as **S**, the sign of what would be $\psi_{U/S}$ is the opposite of the sign of $\psi_{S/U}$. Thus from Eq 88

$$\tan\tfrac{1}{2}(\lambda_{\max} - \lambda_U) = \frac{\sin\frac{1}{2}(L_U - L_{\max})}{\cos\frac{1}{2}(L_U + L_{\max})} \cot\tfrac{1}{2}\left(\psi_{S/U} - \operatorname{sgn}(\psi_{S/U})\frac{\pi}{2}\right) \qquad \text{Eq 95}$$

λ_{min} will occur at $\lambda_{max} \pm \pi$. Eq 95 is derived from the solution to the direct problem of geodesy. An alternate expression for λ_{max}, derived by vector analysis and based on the indirect problem of geodesy, is presented in Chapter 5 (Eq 133).

As stated in Section 4.6, not all great circle routes connecting **U** and **S** or pass through L_{max}, λ_{max} or its Southern Hemisphere equivalent. Stated informally, to pass through L_{max}, λ_{max} — or $-L_{max}$, $\lambda(-L_{max})$ — a route between **U** and **S** must have enough of a change in longitude to bend towards a pole. Mathematically, a route will pass through L_{max}, λ_{max} if the azimuth angles at **U** and **S** are both acute

$$|\psi_{S/U}| < \frac{\pi}{2} \quad \text{and} \quad |\psi_{U/S}| < \frac{\pi}{2} \qquad \text{Eq 96}$$

In this situation, the route will achieve larger latitude (pass closer to the North Pole) than either **U** or **S**. Alternatively both azimuth angles may be obtuse

$$|\psi_{S/U}| > \frac{\pi}{2} \quad \text{and} \quad |\psi_{U/S}| > \frac{\pi}{2} \qquad \text{Eq 97}$$

In this case, the route will pass closer to the South Pole than either **U** or **S**.

4.8 Example Applications

The example applications presented at the end of Chapter 3 are extended in the first three sub-sections below, to demonstrate the capabilities of spherical trigonometry to provide more

complete solutions to relevant technical problems. Three application examples are added — concerning planning a flight route, the display processing of radar measurements and determining an aircraft's latitude/longitude from a VOR/DME station.

4.8.1 Example 1, Continued: En Route Radar Coverage

Predictions of radar visibility of aircraft as a function of the aircraft's range and altitude, like those in Subsection 3.6.1, are useful. However, for a specific radar installation, a more valuable analysis product is a depiction of the radar's altitude coverage overlaid on a map. As an example, the ARSR-4/ATCBI-6 installation at North Truro, MA (FAA symbol: QEA) is selected. Its coordinates are L_U = 42.034531 deg and λ_U = -70.054272 deg, and its antenna elevation is h_U = 224 ft MSL. It is assumed that the terrain elevation in the coverage area is 0 ft MSL, which is correct for the nearby ocean and optimistic (in terms of coverage) for the nearby land.

The sequence of calculations is as follows:

- Using Eq 53 (third line), the radar's minimum usable elevation angle is found to be α_{min} = -0.230 deg
- Aircraft altitudes h_S of 3,000 ft, 10,000 ft and 25,000 ft MSL are selected for the contours to be depicted.
- Using Eq 53 (second line), the geocentric angles θ corresponding to the selected altitudes are found; the associated ground ranges are 85.7 NM, 141.2 NM and 212.6 NM, respectively.
- Using Eq 53 (first line), the minimum visible aircraft altitude at the maximum ground range (250 NM) is found to be h_S = 35,590 ft.
- For each contour, using special cases of Eq 65, four (L_S, λ_S) points on the contour — those at the same latitude or the same longitude as the radar — are found as follows:

$$L_S = L_U \qquad \lambda_S = \lambda_U - 2\arcsin\left(\frac{\sin\left(\frac{1}{2}\theta\right)}{\cos(L_U)}\right)$$

$$L_S = L_U \qquad \lambda_S = \lambda_U + 2\arcsin\left(\frac{\sin\left(\frac{1}{2}\theta\right)}{\cos(L_U)}\right) \qquad \text{Eq 98}$$

$$L_S = L_U - \theta \qquad \lambda_S = \lambda_U$$

$$L_S = L_U + \theta \qquad \lambda_S = \lambda_U$$

- With a graphics program, the remaining points for each contour are found by "interpolation" using a circle/ellipse.

An alternative to steps 5 and 6 is to compute four sets of points (one for each contour) using Eq 65, by assuming values for L_S, and solving for λ_S.

The result of carrying out steps 1-6 for the North Truro radar system is shown in Figure 17. The significance of the contour values is that: (a) Inside a contour, all aircraft having altitudes greater than the contour value are visible to the radar (and aircraft closer to the radar are visible at lower altitudes); and (b) Outside the contour, all aircraft having altitudes less than the contour value are not visible to the radar.

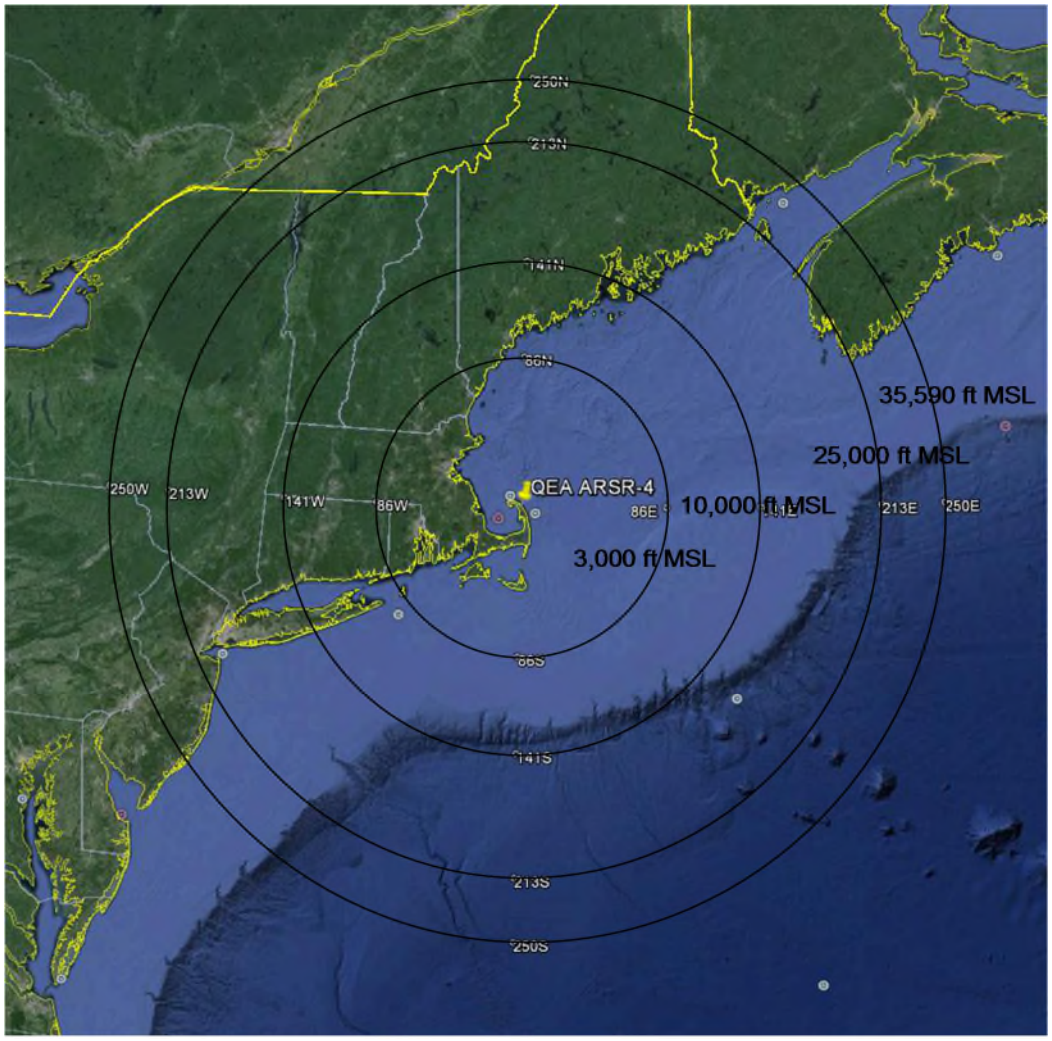

Figure 17 Aircraft Altitude Visibility Contours for the North Truro, MA, Radar System

Consistency Check — The primary purposes of QEA are (1) surveillance of higher altitude airspace, for use by ARTCC controllers; and (2) surveillance of much of the New England off shore airspace, for use by the Department of Defense (DoD). A third purpose is backup surveillance of the Boston TRACON airspace; horizontally, this airspace is a circle centered on Logan Airport with a radius of 60 NM. Boston TRACON controllers have stated that they consider QEA coverage to extend upward from an altitude of 3,000 ft MSL. Figure 17 is consistent with that statement.

Cone of Silence — As discussed in Subsection 3.6.1, ATC radars usually have a cone of silence directly above the antenna; targets within the relatively small cone of silence cannot be detected. Following the usual practice, contours for QEA's cone of silence are not shown in Figure 17.

The U.S. has an extensive ATC radar infrastructure. Generally, one radar station's cone of silence will be within the coverage area of one or more other radar stations. In the case of QEA, the Boston ARTCC also receives feeds from: the Nantucket, MA, terminal radar (46.5 NM from QEA, at essentially sea level), which covers QEA's cone of silence down to approximately 500 ft MSL; and the Cummington, MA, en route radar (132.1 NM from QEA, at an elevation of 2,000 ft MSL) which covers QEA's cone of silence down to approximately 5,000 ft MSL.

4.8.2 Example 2, Continued: Aircraft Precision Approach Procedure

Subsection 3.6.2 illustrates computation of the flight profile (altitude vs. distance from threshold) for an Aircraft Precision Approach procedure. However, for the procedure to be used operationally, the coordinates of the fixes are needed by ATC personnel. Computing them is a straightforward application of spherical geometry.

The sequence of calculations is as follows:

- Using the website AirNav (Ref. 30), the latitudes and longitudes of the ends of KMCI runway 19L / 1R are obtained.
- Associating **U** with the 1R end and **S** with the 19L end of the runway, the azimuth of the approach course in the direction away the 19R end is computed, using Eq 70, to be $\psi_{S/U}$ = 12.89 deg
- Associating **U** with the 19R end of the runway and **S** with the fix locations, the coordinates of the fixes are found using Eq 72 and Eq 75.

The results of carrying out steps 1-3 are shown in Table 6**.**

Table 6 Computed Fix Coordinates for MCI Runway 19L LPV Approach

Fix Name	UMREW	FELUR	REMNS	ZASBO	YOVNU	GAYLY
Range from Threshold, NM	1.9	4.9	6.2	9.3	12.4	15.5
Latitude, deg	39.337737	39.386470	39.407586	39.457940	39.508292	39.558642
Longitude, deg	-94.692345	-94.677907	-94.671645	-94.656696	-94.641725	-94.626732

4.8.3 Example 3, Continued: Satellite Visibility of/from Earth

Extending the analysis in Subsection 3.6.3 to calculating the latitude/longitude coordinates of the footprint of a geostationary satellite is a good example of the application of the equations in this chapter. Geostationary satellites have circular orbits. They are positioned directly above the earth's equator, and their altitude is selected so that their orbital speed matches the earth's rotation rate. Thus, from the earth, they appear to be stationary. Many communications satellites,

including those used for television, are geostationary.

The Wide Area Augmentation System (WAAS) satellites (which augment the Global Positioning System (GPS)) are chosen for this example. The FAA operates three geostationary WAAS satellites (Ref. 31) in order to satisfy the needs of the most demanding civil aviation operations or functions — e.g., guidance for low-visibility approaches or along narrow, obstacle-constrained routes. The parameters used in this calculation are:

- Altitude, $\boldsymbol{h}$ = 35,786,000 m = 19,323 NM
- Mask angle, $\boldsymbol{\alpha}$ = 5 deg
- Radius of the earth, $\boldsymbol{R_e}$ = 6,378,137 m = 3,444 NM (WGS-84 equatorial radius)

Substituting these values into Eq 27 yields $\boldsymbol{\theta}$ = 76.3 deg. Thus the user's position **U** can be up to 76.3 deg (in terms of the geocentric angle) away from the satellite nadir **N** and satellite will be visible. Since geostationary satellites are directly above the equator, the maximum user latitudes with visibility are ±76.3 deg if the user is at the same longitude as the satellite. Similarly, if the user is on the equator, the longitude extremes at which the satellite is visible are ±76.3 deg from the satellite longitude.

Obtaining the coordinates of perimeter of the visible region (satellite footprint) involves solving the following modified version of Eq 65:

$$\lambda_U = \lambda_S \pm 2\arcsin\left(\sqrt{\frac{\sin^2\left(\frac{\theta}{2}\right) - \sin^2\left(\frac{L_U}{2}\right)}{\cos(L_U)}}\right) \qquad \text{Eq 99}$$

A set values is assumed for $\boldsymbol{L_U}$ in the interval [$-\boldsymbol{\theta}$, $\boldsymbol{\theta}$], and the corresponding two sets of values for $\boldsymbol{\lambda_U}$ are computed (which are symmetrically located about $\boldsymbol{\lambda_S}$). The WAAS satellite labels and longitudes are: AMR, -98 deg; CRE, -107.3 deg; and CRW, -133 deg. When these calculations are carried out, the resulting footprints are depicted in Figure 18 below. To provide context, the locations of a few airports are also shown in Figure 18. As a check on the calculations herein, Ref. 31 has a page, "WAAS GEO Footprint", that is very similar to Figure 18.

4.8.4 Example 4: Great Circle Flight Route

For many reasons — e.g., siting of ground-based communications, navigation and surveillance equipment; estimation of fuel consumption; positioning of search and rescue assets; and analysis of over-flight routes — there is a need to calculate great circle paths between any two places on the earth. Such calculations are a straightforward application of the equations presented earlier in this chapter. The basic approach is: first solve the indirect problem of geodesy (Section 4.2), so

that geocentric angle (length) and the azimuth of the path starting point are known; then divide the path into equal-length segments and solve the direct problem of geodesy (Section 4.3) for each segment, starting at one end of the path and progressing to the other.

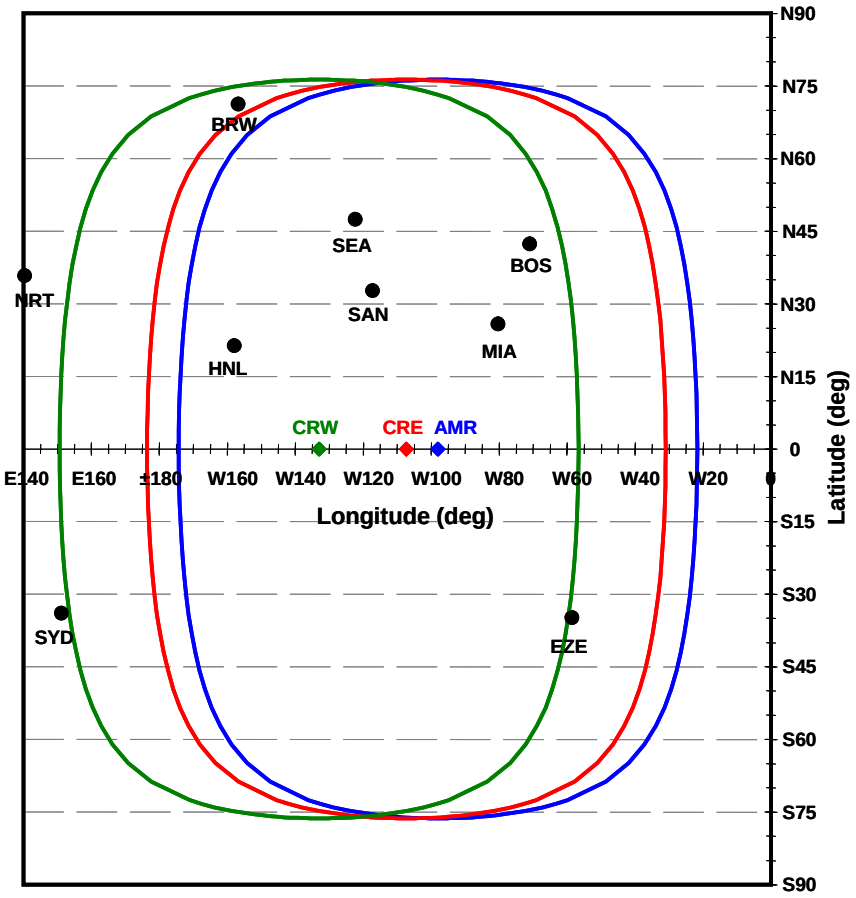

Figure 18 WAAS Satellite Visibility Contours for 5 deg Mask Angle

The result of carrying out these steps for the route between Boston Logan (BOS) and Tokyo Narita (NRT) airports is shown in Figure 19. In addition to showing the flight path for a spherical earth model (green curve), Figure 19 also shows the great circle path for an ellipsoidal earth model using Vincenty's algorithm (Subsection 2.2.3). For the scales and line thickness employed, the only perceptible separation between these curves is at the highest latitudes, where the ellipsoidal-model path is a maximum of 0.06 deg higher in latitude.

For the great circle/spherical earth route; the azimuth angle at BOS is 334.8 (-25.2) deg, the azimuth angle at NRT is 22.8 deg, and the geocentric angle is θ = 1.689 rad, or 53.8% of π rad (π rad being the longest possible great circle route). The computed distance (using the earth radius defined following Eq 23) is 5,810.4 NM, while the distance computed using Vincenty's algorithm is 5,823.5 NM. Thus, in this case, the ellipticity error in the path length is 0.2%.

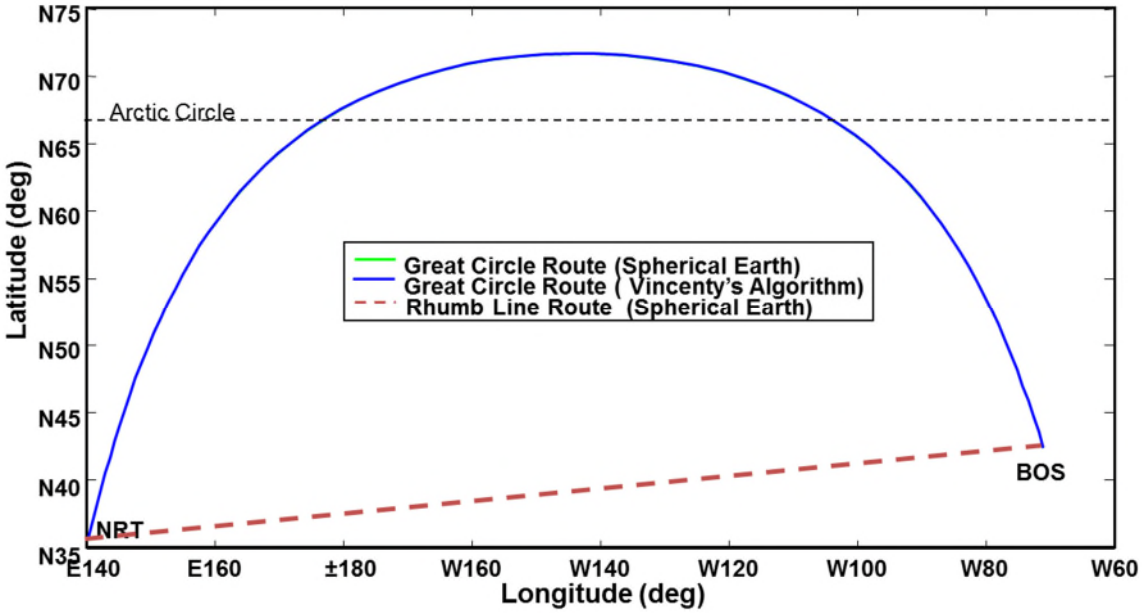

Figure 19 Mercator-like Depiction of Latitude/Longitude Coordinates for Great Circle and Rhumb Line Paths Connecting BOS and NRT

The trajectory's northern-most latitude is N71.7 deg (Eq 94), which occurs at a longitude of W143.42 deg. If the earth were sliced in half by a plane passing through BOS, NRT and the earth's center, the plane would make an angle of 71.7 deg with the plane of the equator and would intersect the equator at W53.42 deg and E126.58 deg. Equations from Section 4.6 predict that the trajectory crosses the Arctic Circle (N67 deg latitude) at longitudes of W104.7 deg and E177.9 deg. The trajectory is within the Arctic Circle for 29.2% of its length, although in Figure 19 it appears to be a larger fraction because the convergence of longitude lines at the Pole is not depicted.

Figure 19 also shows the course from BOS to NRT for the rhumb line (constant azimuth angle) method often used for marine navigation (Section 9.3). The azimuth angle for a rhumb line from BOS to NRT is 266.7 (-93.3) deg. The rhumb line path is 19% or 1,106.7 NM longer than the great circle route calculated using Vincenty's algorithm.

The BOS-NRT city pair has all three factors that favor great circle navigation over rhumb line navigation: widely separated origin and destination, essentially co-latitude origin and destination, and the end points are at mid-latitudes. A contrasting route is Boston (BOS) - Buenos Aires (EZE). It has a roughly similar length, but is oriented north-south. For BOS-EZE the rhumb line path is 0.007% (0.3 NM) longer than the great circle path.

Figure 20 depicts a polar view of the great circle and rhumb line routes. For this perspective, (a) the great circle route is almost a straight line while the rhumb line route is circular, and

(b) the difference in the lengths of the paths is obvious. Contrasting Figure 19 and Figure 20 illustrates value of matching the charting technique to the method for defining a route. Figure 19 is similar to a Mercator projection[‡‡‡], with both having the property that rhumb lines are straight; and Figure 20 similar to a gnomonic projection[§§§], which has the property that great circles are depicted as straight lines. It has been stated that Mercator projections were the preferred maps for maritime navigation, while gnomonic projections are the preferred maps for aircraft navigation.

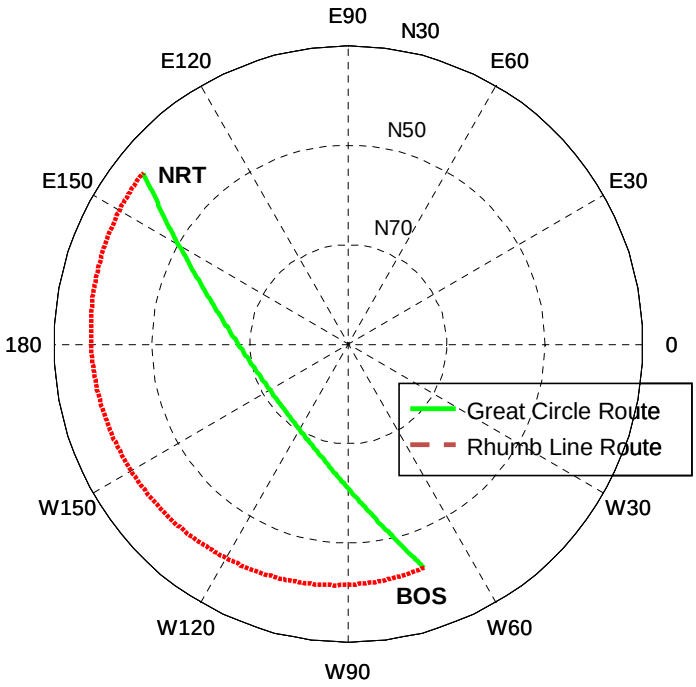

Figure 20 Polar View of BOS-NRT Great Circle and Rhumb Line Routes

4.8.5 Example 5: Radar Display Coordinate Transformations

In this subsection, an ATC radar is associated with the user **U** and an aircraft under surveillance with the satellite **S**. The radar's installation information will include:

$\boldsymbol{L_U}$ – Radar latitude

$\boldsymbol{\lambda_U}$ – Radar longitude

$\boldsymbol{h_U}$ – Radar antenna elevation above sea level

For each scan (antenna revolution), a secondary surveillance radar provides three quantities concerning an aircraft:

[‡‡‡] For a true Mercator projection, the distance between equal latitude increments increases towards the poles.

[§§§] For a true gnomonic projection, the distance between equal latitude increments increases toward the equator.

$\psi_{S/U}$ – Aircraft azimuth relative to North (from antenna direction)
d – Slant range between the aircraft and the radar (determined from interrogation-reply time)
h_S – Aircraft barometric elevation above sea level (reported by transponder)

Some long-range radars may correct for propagation phenomena (e.g., refraction), but those capabilities are not addressed here.

The first goal in ATC radar display is to accurately depict the horizontal separation between aircraft pairs. When two aircraft are only separated vertically (i.e., are at the same latitude and longitude) then their screen icons should overlay each other — or at least be close in comparison to the minimum allowable separation. Figure 21 shows the effect of directly displaying the slant range of two aircraft with only vertical separation (although it exaggerates the effect). Without altitude or elevation angle information, this may be the best that can be done — e.g., for two aircraft without Mode C altitude-reporting capability. Partly for this reason, operating in busy airspace typically requires Mode C capability.

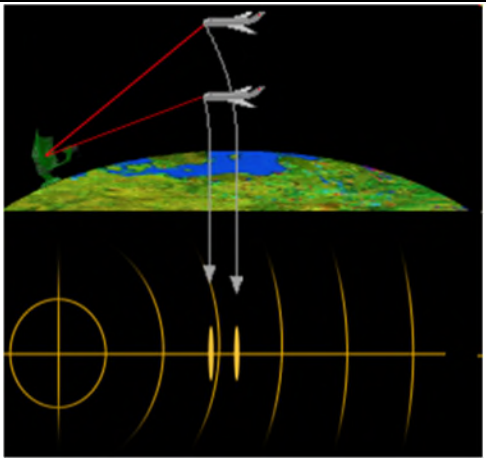

Figure 21 Effect of Displaying a Target's Slant Range

Generally, the display processing methodology depends upon the radar's maximum range. Two situations are addressed.

Tangent Plane Display — This method displays targets on a plane that is tangent to the earth at the radar's latitude/longitude and sea level. Locations on the plane can be computed in Cartesian (east/north) or polar (range/azimuth) coordinates. The steps in the calculation are:

- The aircraft elevation angle, α, is found using Eq 40, modified to account for the radar antenna elevation:

$$\alpha = \arcsin\left(\frac{(h_S - h_U)^2 + 2(h_S - h_U)(R_e + h_U) - d^2}{2d(R_e + h_U)}\right) \qquad \text{Eq 100}$$

- The aircraft range along the tangent plane, ***TPRng***, is found (sometimes called the slant-range correction)

$$TPRng = d\cos(\alpha) \qquad \text{Eq 101}$$

- If needed, ***TPRng*** can be resolved into east and north components

$$TPEast = TPRng\sin(\psi_{S/U})$$
$$TPNorth = TPRng\cos(\psi_{S/U}) \qquad \text{Eq 102}$$

If the earth were flat, this method would be error-free; however, it does not fully account for the curvature of the spherical earth. Figure 22 shows the slant range correction error (difference in

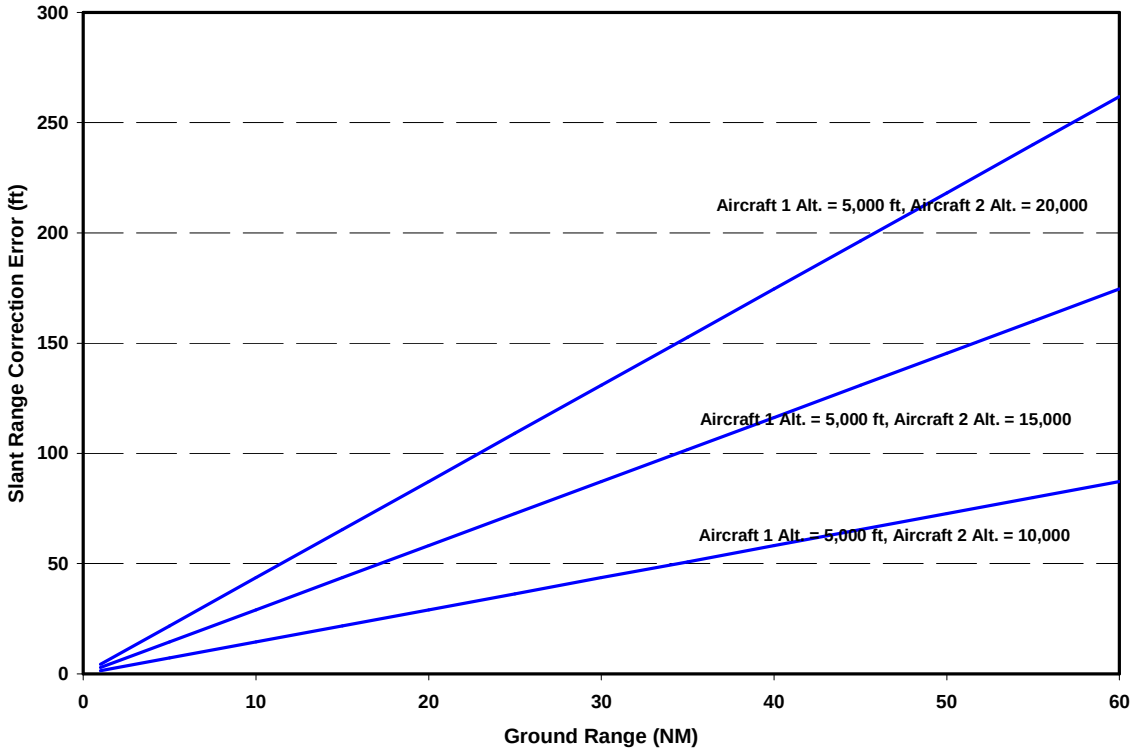

Figure 22 Slant-Range Correction Error for Tangent Plane Terminal Radar Display

computed ***TPRng*** values for two aircraft at the same latitude/longitude but different altitudes) for ranges/altitudes characteristic of a terminal area radar. The maximum error is approximately 250 ft. This value should be contrasted with the terminal area separation standard of 3 NM. Thus the maximum display processing error is less than 1.5% of the relevant standard, which is acceptable for engineering work.

Latitude/Longitude Display — Because errors for a tangent plane display increase with the ranges and altitude differences of targets, en route radars use a more accurate method that fully accounts for the earth's curvature.

- The target's geocentric angle relative to the radar is found using Eq 35
- The target's latitude/longitude are found from Eq 72 and Eq 75
- The target's latitude and longitude are converted to the coordinates of a map projection (e.g., Lambert conformal conic) for display to a controller.

En route radar coverage area will include multiple airports, and possibly several major ones. It's advantageous to display targets relative to the airport locations.

4.8.6 Example 6: Single-Station VOR / DME RNAV Fix

A single VOR/DME station **S** provides an aircraft **A** with its azimuth angle $\psi_{A/S}$ (VOR function) and slant range distance d_{SA} (DME function) relative to the station. For 'area navigation'

(RNAV), it may be necessary to use those measurements to determine the aircraft's latitude and longitude **A** (L_A, λ_A). The aircraft's altitude h_A is assumed known, as are the station coordinates (L_S, λ_S) and DME antenna altitude h_S.

The first step is to convert the slant range d_{SA} to the geocentric angle θ_{SA} utilizing Eq 35.

The aircraft's latitude and longitude are then found from Eq 72 and Eq 75, repeated here using the current notation:

$$L_A = \arcsin\left(\sin(L_S)\cos(\theta_{SA}) + \cos(L_S)\sin(\theta_{SA})\cos(\psi_{A/S})\right)$$
$$\lambda_A = \lambda_S + \arctan\left(\frac{\sin(\theta_{SA})\sin(\psi_{A/S})}{\cos(L_S)\cos(\theta_{SA}) - \sin(L_S)\sin(\theta_{SA})\cos(\psi_{A/S})}\right) \qquad \text{Eq 103}$$

Finally, the azimuth angle of the station relative to the aircraft is found from

$$\tan(\psi_{S/A}) = \frac{-\cos(L_S)\sin(\psi_{A/S})}{\sin(L_S)\sin(\theta_{SA}) - \cos(L_S)\cos(\theta_{SA})\cos(\psi_{A/S})} \qquad \text{Eq 104}$$

Remarks:

- Except for notation, the processing steps in this subsection are identical to those used for a radar latitude/longitude display in Subsection 4.8.5.
- While the slant-range correction of is usually considered a necessary step in en route radar processing, the slant-range correction is often not performed in navigation applications (as the distances and need for accuracy are both generally less, and many procedures are specified in terms of a DME reading). The approximation employed is $\theta_{SA} \approx d_{SA} / R_e$.
- Chapter 6 addresses computing fixes using measurements from the three possible combinations of two separate VOR and/or DME stations — i.e., VOR/VOR, DME/DME and VOR/DME. Chapter 7 address computing fixes using measurements from three DME stations.

4.8.7 Example 7: Path-Length Ellipticity Error for Selected Airport Pairs

As a partial check on the accuracy of the spherical earth approximation, a set of fourteen airports were selected. This set is intended to be representative of current aviation activity. However, in terms of frequency of operations, they over-emphasize longer routes (and some are too long for commercial transport aircraft at this time). The result is a total of 91 possible paths between airport pairs. For each pair, estimates of the length of the paths are computed for:

a) WGS-84 ellipsoidal earth model utilizing Vincenty's algorithm cited in Subsection 2.2.3 (which is treated as a "black box" herein), and

b) Spherical approximation of the earth utilizing the radius immediately following Eq 23 and Eq 67.

The airports are partitioned into two groups of seven each — CONUS (Table 7) and International (Table 8). The CONUS group essentially spans the CONUS land area and includes paths of various lengths and orientations. The International group, which includes one each in Alaska and Hawaii, provides additional pairs with greater separation but also with varying orientations. The longest path is HNL-JNB (10, 365 NM). As a point of interest, the current longest scheduled commercial flight route is 8,285 NM, between Newark and Singapore.

Table 7 CONUS Airports Used in Ellipticity Error Analysis

Airport Name (IATA Code)	Lat. (deg)	Lon. (deg)	Major City Served
Gen. Edward Lawrence Logan International (BOS)	42.3629722	-71.0064167	Boston, MA
Ronald Reagan Washington National (DCA)	38.8522	-77.0378	Washington, DC
O'Hare International (ORD)	41.9786	-87.9047	Chicago, IL
Miami International (MIA)	25.7933	-80.2906	Miami, FL
San Diego International (SAN)	32.7336	-117.1897	San Diego, CA
Dallas/Fort Worth International (DFW)	32.8969	-97.0381	Dallas/Fort Worth, TX
Seattle–Tacoma International (SEA)	47.4489	-122.3094	Seattle, WA

Table 8 International Airports Used in Ellipticity Error Analysis

Airport Name (IATA Code)	Lat. (deg)	Lon. (deg)	Major City Served
Wiley Post–Will Rogers Memorial (BRW)	71.2848889	-156.7685833	Barrow, Alaska
Honolulu International (HNL)	21.318681	-157.9224287	Honolulu, Hawaii
London Heathrow (LHR)	51.4775	-0.4614	London, England
Narita International (NRT)	35.7647	140.3864	Tokyo, Japan
Ministro Pistarini International (EZE)	-34.8222	-58.5358	Buenos Aires, Argentina
Oliver Reginald Tambo International (JNB)	-26.1392	28.246	Johannesburg, South Africa
Sydney (SYD)	-33.946111	151.177222	Sydney, Australia

Figure 23 is a histogram of the path length differences for the 91 paths analyzed using the methods labeled a) and b) above. Over 90% (all but eight) of the paths have ellipticity errors less than the “rule of thumb” of 0.3%, and none have errors greater that 0.5%. The average of the absolute values of the ellipticity errors is 0.17%. For the paths within CONUS, the maximum ellipticity error is 0.27%.

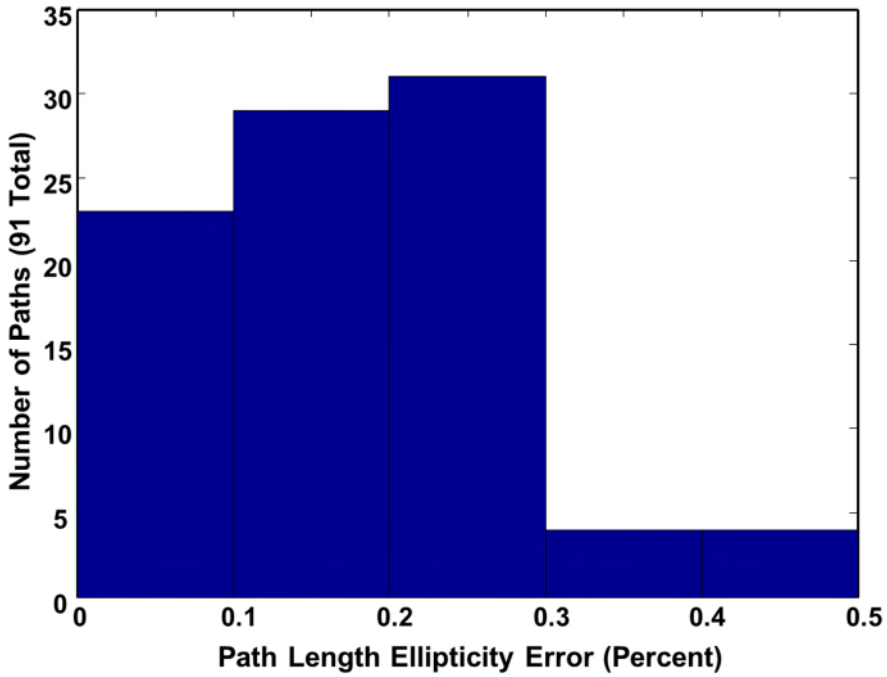

Figure 23 Histogram of Ellipticity Errors for Spherical-Earth Length of 91 Selected Paths

For some applications, a spherical model for the earth may not be sufficiently accurate. In some circumstances, sufficient improvement can be obtained by tailoring the radius of curvature to the path(s) involved — i.e., taking account of their latitude and azimuth angle, and possibly using multiple points to compute an average radius of curvature. However, there are limits to such an approach, as the radius of curvature generally cannot account for differences in the path itself. In high-accuracy applications, it is generally preferable to use an ellipsoidal earth model, possibly in conjunction with a least-squares solution technique such as that discussed in Chapter 8.

5. TWO-POINT / 3D-VECTOR PROBLEM FORMULATION

Section 5.1 provides definitions of the vectors and coordinate frames needed to analyze the geometry of user and aircraft or satellite relative to a spherical earth. Section 5.2 addresses the indirect problem of geodesy, and provides vector versions of the key equations in Section 4.2. Section 5.3 returns to the indirect problem, and demonstrate that for some combinations of known and unknown variables, vector analysis provides an alternative method of deriving solutions found in Chapter 4. Similarly, Section 5.4 demonstrates that vector analysis provides an alternative method of deriving certain solutions found in Chapter 3. Lastly, Section 5.5 addresses the direct problem of geodesy, and shows that, to a significant extent, the equations in Section 4.3 can be found by vector analysis as well.

A list of software packages which generally utilize the vector approach can be found at Ref. 32.

5.1 Vector and Coordinate Frame Definitions

5.1.1 Earth-Centered Earth-Fixed (ECEF) Coordinate Frame

The coordinates of the locations of interest on the earth's surface are:

- User position: latitude $\boldsymbol{L_U}$, longitude $\boldsymbol{\lambda_U}$ and altitude $\boldsymbol{h_U}$
- Satellite position: latitude $\boldsymbol{L_S}$, longitude $\boldsymbol{\lambda_S}$ and altitude $\boldsymbol{h_S}$

Define the earth-centered earth-fixed (ECEF) coordinate frame *e* by (see Figure 24, where the figure's **φ** is our $\boldsymbol{L}$):

- x-axis: lies in the plane of the equator and points toward Greenwich meridian
- y-axis: completes the right-hand orthogonal system
- z-axis: lies along the earth's spin axis.

The location of the user and satellite in the *e*-frame are

$$\underline{\mathbf{r}}^{\mathbf{e}}_{\mathbf{OU}} = \begin{bmatrix} r^e_{OU,x} \\ r^e_{OU,y} \\ r^e_{OU,z} \end{bmatrix} = \underline{\mathbf{1}}^{\mathbf{e}}_{\mathbf{OU}} (R_e + h_U) = \begin{bmatrix} 1^e_{OU,x} \\ 1^e_{OU,y} \\ 1^e_{OU,z} \end{bmatrix} (R_e + h_U) = \begin{bmatrix} \cos(L_U)\cos(\lambda_U) \\ \cos(L_U)\sin(\lambda_U) \\ \sin(L_U) \end{bmatrix} (R_e + h_U) \qquad \text{Eq 105}$$

and

$$\underline{\mathbf{r}}^{\mathbf{e}}_{\mathbf{OS}} = \begin{bmatrix} r^e_{OS,x} \\ r^e_{OS,y} \\ r^e_{OS,z} \end{bmatrix} = \underline{\mathbf{1}}^{\mathbf{e}}_{\mathbf{OS}} (R_e + h_S) = \begin{bmatrix} 1^e_{OS,x} \\ 1^e_{OS,y} \\ 1^e_{OS,z} \end{bmatrix} (R_e + h_S) = \begin{bmatrix} \cos(L_S)\cos(\lambda_S) \\ \cos(L_S)\sin(\lambda_S) \\ \sin(L_S) \end{bmatrix} (R_e + h_S) \qquad \text{Eq 106}$$

Here $\underline{\mathbf{1}}^{e}_{OU}$ and $\underline{\mathbf{1}}^{e}_{OS}$ are unit vectors associated with $\underline{\mathbf{r}}^{e}_{OU}$ and $\underline{\mathbf{r}}^{e}_{OS}$, respectively.

Given $\underline{\mathbf{r}}^{e}_{OU}$, the user's latitude, longitude and altitude can be found (respectively) from

$$L_U = \arctan\left(\frac{r^e_{OU,z}}{\sqrt{(r^e_{OU,x})^2 + (r^e_{OU,y})^2}}\right)$$
$$\lambda_U = \arctan\left(r^e_{OU,y}\ ,\ r^e_{OU,x}\right) \qquad \text{Eq 107}$$
$$h_U = \sqrt{(r^e_{OU,x})^2 + (r^e_{OU,y})^2 + (r^e_{OU,z})^2} - R_e$$

Similarly, given, $\underline{\mathbf{r}}^{e}_{OS}$, the satellite's latitude, longitude and altitude can be found (respectively) from

$$L_S = \arctan\left(\frac{r^e_{OS,z}}{\sqrt{(r^e_{OS,x})^2 + (r^e_{OS,y})^2}}\right) = \arcsin\left(\frac{r^e_{OS,z}}{R_e + h}\right)$$
$$\lambda_S = \arctan\left(r^e_{OS,y}\ ,\ r^e_{OS,x}\right) \qquad \text{Eq 108}$$
$$h_S = \sqrt{(r^e_{OS,x})^2 + (r^e_{OS,y})^2 + (r^e_{OS,z})^2} - R_e$$

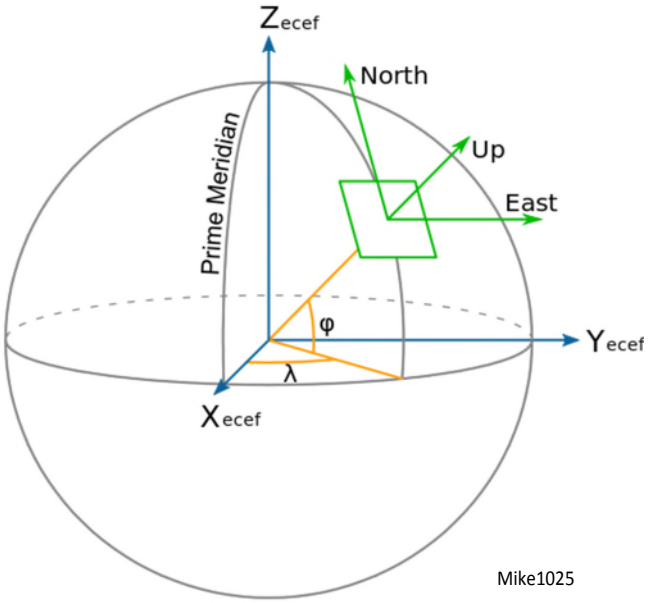

Figure 24 Vector Technique Coordinate Frames of Interest

5.1.2 Local-Level Coordinate Frame at User's Position

Define a local-level coordinate frame *u* corresponding to the user's position

- e-axis point east
- n-axis points north
- u-axis points up (away from earth's center).

The direction cosine matrix which rotates the *e*-frame into the *u*-frame is

$$\mathbf{C_e^u} = \mathbf{T}\,\mathbf{T_2}(-L_U)\,\mathbf{T_3}(\lambda_U) \qquad \text{Eq 109}$$

where $\mathbf{T_i}(\xi)$ denotes the rotation matrix about axis ***i*** by angle ξ.

$$\mathbf{T_1}(\xi) = \begin{bmatrix} 1 & 0 & 0 \\ 0 & \cos(\xi) & \sin(\xi) \\ 0 & -\sin(\xi) & \cos(\xi) \end{bmatrix}$$

$$\mathbf{T_2}(\xi) = \begin{bmatrix} \cos(\xi) & 0 & -\sin(\xi) \\ 0 & 1 & 0 \\ \sin(\xi) & 0 & \cos(\xi) \end{bmatrix} \qquad \text{Eq 110}$$

$$\mathbf{T_3}(\xi) = \begin{bmatrix} \cos(\xi) & \sin(\xi) & 0 \\ -\sin(\xi) & \cos(\xi) & 0 \\ 0 & 0 & 1 \end{bmatrix}$$

and **T** denotes the axis-permutation matrix

$$\mathbf{T} = \begin{bmatrix} 0 & 1 & 0 \\ 0 & 0 & 1 \\ 1 & 0 & 0 \end{bmatrix} \qquad \text{Eq 111}$$

Thus

$$\mathbf{C_e^u} = \begin{bmatrix} -\sin(\lambda_U) & \cos(\lambda_U) & 0 \\ \sin(-L_U)\cos(\lambda_U) & \sin(-L_U)\sin(\lambda_U) & \cos(-L_U) \\ \cos(-L_U)\cos(\lambda_U) & \cos(-L_U)\sin(\lambda_U) & -\sin(-L_U) \end{bmatrix} \qquad \text{Eq 112}$$

5.1.3 User and Satellite Positions in User's Local-Level Frame

The positions of the user and satellite in the *u*-frame are, respectively

$$\underline{\mathbf{r}}_{\mathbf{OU}}^{\mathbf{u}} = \mathbf{C_e^u}\begin{bmatrix} r_{OU,x}^e \\ r_{OU,y}^e \\ r_{OU,z}^e \end{bmatrix} = \begin{bmatrix} r_{OU,e}^u \\ r_{OU,n}^u \\ r_{OU,u}^u \end{bmatrix} = \begin{bmatrix} 0 \\ 0 \\ 1 \end{bmatrix} R_e \qquad \text{Eq 113}$$

and

$$\underline{\mathbf{r}}_{\mathbf{OS}}^{\mathbf{u}} = \mathbf{C_e^u}\begin{bmatrix} r_{OS,x}^e \\ r_{OS,y}^e \\ r_{OS,z}^e \end{bmatrix} = \begin{bmatrix} r_{OS,e}^u \\ r_{OS,n}^u \\ r_{OS,u}^u \end{bmatrix} = \begin{bmatrix} \cos(L_S)\sin(\lambda_S - \lambda_U) \\ -\cos(L_S)\sin(L_U)\cos(\lambda_S - \lambda_U) + \sin(L_S)\cos(L_U) \\ \cos(L_S)\cos(L_U)\cos(\lambda_S - \lambda_U) + \sin(L_S)\sin(L_U) \end{bmatrix} (R_e + h) \qquad \text{Eq 114}$$

Thus, using Eq 113 and Eq 114, the vector from **U** to **S** is

$$\underline{\mathbf{r}}^{\mathbf{u}}_{\mathbf{US}} = \underline{\mathbf{r}}^{\mathbf{u}}_{\mathbf{OS}} - \underline{\mathbf{r}}^{\mathbf{u}}_{\mathbf{OU}} = \begin{bmatrix} r^u_{US,e} \\ r^u_{US,n} \\ r^u_{US,u} \end{bmatrix} = \begin{bmatrix} (R_e + h)\cos(L_U)\sin(\lambda_S - \lambda_U) \\ -(R_e + h)\cos(L_S)\sin(L_S)\cos(\lambda_S - \lambda_U) + (R_e + h)\sin(L_S)\cos(L_U) \\ (R_e + h)\cos(L_S)\cos(L_U)\cos(\lambda_S - \lambda_U) + (R_e + h)\sin(L_S)\sin(L_U) - R_e \end{bmatrix} \quad \text{Eq 115}$$

The horizontal and vertical components of $\underline{\mathbf{r}}^{\mathbf{u}}_{\mathbf{US}}$ can be expressed as

$$\begin{aligned} r^u_{US,horiz} &= \sqrt{\left(r^u_{US,e}\right)^2 + \left(r^u_{US,n}\right)^2} = (R_e + h)\sin(\theta) \\ r^u_{US,vert} &= r^u_{US,u} = (R_e + h)\cos(\theta) - R_e \end{aligned} \quad \text{Eq 116}$$

Eq 116 can be found from Figure 1 by inspection. It can also be derived analytically from Eq 115 using Eq 62.

Two angles associated with $\underline{\mathbf{r}}^{\mathbf{u}}_{\mathbf{US}}$ are of interest

- $\psi_{S/U}$ – The azimuth angle of the horizontal component of $\underline{\mathbf{r}}^{\mathbf{u}}_{\mathbf{US}}$, measured clockwise from north
- α – The elevation angle of $\underline{\mathbf{r}}^{\mathbf{u}}_{\mathbf{US}}$, measured from the horizontal plane

$$\psi_{S/U} = \arctan\left(r^u_{US,e}, r^u_{US,n}\right) \quad \text{Eq 117}$$

$$\alpha = \arctan\left(\frac{r^u_{US,u}}{\sqrt{\left(r^u_{US,e}\right)^2 + \left(r^u_{US,n}\right)^2}}\right) \quad \text{Eq 118}$$

The two-argument arc tangent function is used in Eq 117 because azimuth angles lie in the range $(-\pi, \pi]$.

The Euclidean length d of $\underline{\mathbf{r}}^{\mathbf{u}}_{\mathbf{US}}$ is also of interest

$$d = \sqrt{\left(r^u_{US,e}\right)^2 + \left(r^u_{US,n}\right)^2 + \left(r^u_{US,u}\right)^2} \quad \text{Eq 119}$$

5.2 The Indirect Problem of Geodesy

5.2.1 Geocentric Angle from Latitudes and Longitudes, by Vector Dot Product

The vectors $\underline{\mathbf{r}}^{\mathbf{e}}_{\mathbf{OU}}$ and $\underline{\mathbf{r}}^{\mathbf{e}}_{\mathbf{OS}}$ meet at the earth's center, in geocentric angle θ. The dot product of these vectors, normalized by the product of their lengths, yields

$$\begin{aligned}\underline{\mathbf{1}}^{\mathbf{e}}_{\mathbf{OU}} \bullet \underline{\mathbf{1}}^{\mathbf{e}}_{\mathbf{OS}} &= \underline{1}^{e}_{OU,x}\underline{1}^{e}_{OS,x} + \underline{1}^{e}_{OU,y}\underline{1}^{e}_{OS,y} + \underline{1}^{e}_{OU,z}\underline{1}^{e}_{OS,z} \\ &= \cos(L_U)\cos(L_S)\cos(\lambda_U - \lambda_S) + \sin(L_U)\sin(L_S) \\ &= \cos(\theta)\end{aligned} \qquad \text{Eq 120}$$

Eq 120 demonstrates that if one forms the vector dot product indicated on the first line, the result will be the same as if one performed the scalar operations indicated on the second line, which in turn is equal to the equation for cos(θ) found by spherical trigonometry (Eq 62).

5.2.2 Geocentric Angle from Latitudes and Longitudes, by Vector Cross Product

The cross product of vectors $\underline{\mathbf{r}}^{\mathbf{e}}_{\mathbf{OU}}$ and $\underline{\mathbf{r}}^{\mathbf{e}}_{\mathbf{OS}}$, normalized by the product of their lengths, yields another expression for the geocentric angle:

$$\begin{aligned}\sin(\theta) &= \left|\underline{\mathbf{1}}^{\mathbf{e}}_{\mathbf{OU}} \times \underline{\mathbf{1}}^{\mathbf{e}}_{\mathbf{OS}}\right| \\ &= \sqrt{\begin{array}{l}\cos^2(L_U)\sin^2(L_S) + \cos^2(L_S)\sin^2(L_U) + \cos^2(L_U)\cos^2(L_S)\sin^2(\lambda_S - \lambda_U)\cdots \\ \cdots - 2\cos(L_U)\sin(L_U)\cos(L_S)\sin(L_S)\cos(\lambda_S - \lambda_U)\end{array}}\end{aligned} \qquad \text{Eq 121}$$

Since θ lies in [0, π], solving Eq 121 for θ using the arc sine function yields both the correct angle and an ambiguous solution. Another source of information, such as Eq 120, also must be used.

5.2.3 Path Azimuth Angles, from Latitudes and Longitudes

By substituting two elements of $\underline{\mathbf{r}}^{\mathbf{u}}_{\mathbf{US}}$ from Eq 115 into Eq 117, $\psi_{S/U}$ is found to be equal to

$$\psi_{S/U} = \arctan\left(r^{u}_{US,e}, r^{u}_{US,n}\right) = \arctan\left(\frac{\cos(L_S)\sin(\lambda_S - \lambda_U)}{\sin(L_S)\cos(L_U) - \cos(L_S)\sin(L_U)\cos(\lambda_S - \lambda_U)}\right) \qquad \text{Eq 122}$$

Eq 122 demonstrates that if one computes $\psi_{S/U}$ using the arc tangent function with two elements of the vector $\underline{\mathbf{r}}^{\mathbf{u}}_{\mathbf{US}}$ as arguments, the result will be the same as if one computed $\psi_{S/U}$ using the arc tangent indicated on the right-hand side. The latter is equal to the equation for $\psi_{S/U}$ found by spherical trigonometry (Eq 70).

The labeling of the points **U** and **S** in Eq 122 can be reversed, yielding

$$\psi_{U/S} = \arctan\left(\frac{\cos(L_U)\sin(\lambda_U - \lambda_S)}{\sin(L_U)\cos(L_S) - \cos(L_U)\sin(L_S)\cos(\lambda_U - \lambda_S)}\right) \qquad \text{Eq 123}$$

While the arguments on right-hand sides of Eq 122 and Eq 123 are shown (for convenience) as ratios, the azimuth angles should be computed using a two-argument arc tangent function.

Eq 123 is derived by vector analysis (rather than by spherical trigonometry). However, it not a vector equation *per se* — i.e., it does not make use of vectors or the components of vectors. The vector equation for $\psi_{U/S}$ is

$$\psi_{U/S} = \arctan\left(r^s_{SU,e}, r^s_{SU,n}\right) \qquad \text{Eq 124}$$

Vector $\underline{\mathbf{r}}^{\mathbf{s}}_{\mathbf{SU}}$ is found from

$$\underline{\mathbf{r}}^{\mathbf{s}}_{\mathbf{SU}} = \underline{\mathbf{r}}^{\mathbf{s}}_{\mathbf{OU}} - \underline{\mathbf{r}}^{\mathbf{s}}_{\mathbf{OS}} = \mathbf{C}^{\mathbf{s}}_{\mathbf{e}}\left(\underline{\mathbf{r}}^{\mathbf{e}}_{\mathbf{OU}} - \underline{\mathbf{r}}^{\mathbf{e}}_{\mathbf{OS}}\right) \qquad \text{Eq 125}$$

where $\underline{\mathbf{r}}^{\mathbf{e}}_{\mathbf{OU}}$ and $\underline{\mathbf{r}}^{\mathbf{e}}_{\mathbf{OS}}$ are given by Eq 105 and Eq 106, respectively, and (interpreting Eq 112)

$$\mathbf{C}^{\mathbf{s}}_{\mathbf{e}} = \begin{bmatrix} -\sin(\lambda_S) & \cos(\lambda_S) & 0 \\ \sin(-L_S)\cos(\lambda_S) & \sin(-L_S)\sin(\lambda_S) & \cos(-L_S) \\ \cos(-L_S)\cos(\lambda_S) & \cos(-L_S)\sin(\lambda_S) & -\sin(-L_S) \end{bmatrix} \qquad \text{Eq 126}$$

5.3 Corollaries of the Indirect Problem Solution

5.3.1 Intermediate Points between **U** and **S**: Dividing the Chord

Route planning generally requires that a set of intermediate path points between **U** and **S** be found. Any linear combination of $\underline{\mathbf{1}}^{\mathbf{e}}_{\mathbf{OU}}$ and $\underline{\mathbf{1}}^{\mathbf{e}}_{\mathbf{OS}}$ will be orthogonal to the vector $\underline{\mathbf{1}}^{\mathbf{e}}_{\mathbf{OU}} \times \underline{\mathbf{1}}^{\mathbf{e}}_{\mathbf{OS}}$, and thus will lie in the plane defined by **OUS**. Conversely, every point in the plane **OUS** can be expressed as a linear combination of $\underline{\mathbf{1}}^{\mathbf{e}}_{\mathbf{OU}}$ and $\underline{\mathbf{1}}^{\mathbf{e}}_{\mathbf{OS}}$.

A simple way to define a point along the arc between **U** and **S** is to choose a point along the chord $\underline{\mathbf{r}}^{\mathbf{e}}_{\mathbf{US}}$ between **U** and **S** then normalize it to unit length. Let $f \in [0, 1]$ be the fractional distance of point **X** from **U** to **S** along the chord $\underline{\mathbf{r}}^{\mathbf{e}}_{\mathbf{US}}$. Thus,

$$\underline{\mathbf{r}}^{\mathbf{e}}_{\mathbf{OX}} = \underline{1}^{\mathbf{e}}_{\mathbf{OU}} + f\left(\underline{1}^{\mathbf{e}}_{\mathbf{OS}} - \underline{1}^{\mathbf{s}}_{\mathbf{OU}}\right) = (1-f)\underline{1}^{\mathbf{e}}_{\mathbf{OU}} + f\,\underline{1}^{\mathbf{e}}_{\mathbf{OS}} = \begin{bmatrix} r^e_{OX,x} \\ r^e_{OX,y} \\ r^e_{OX,z} \end{bmatrix} = \begin{bmatrix} (1-f)1^e_{OU,x} + f\,1^e_{OS,x} \\ (1-f)1^e_{OU,y} + f\,1^e_{OS,y} \\ (1-f)1^e_{OU,z} + f\,1^e_{OS,z} \end{bmatrix} \qquad \text{Eq 127}$$

Then

$$L_X = \arctan\left(\frac{r^e_{OX,z}}{\sqrt{(r^e_{OX,x})^2 + (r^e_{OX,y})^2}}\right)$$
$$\lambda_X = \arctan\left(r^e_{OX,y}, r^e_{OX,x}\right) \qquad \text{Eq 128}$$

and

$$\underline{\mathbf{1}}^{\mathbf{e}}_{\mathbf{OX}} = \begin{bmatrix} \cos(L_X)\cos(\lambda_X) \\ \cos(L_X)\sin(\lambda_X) \\ \sin(L_X) \end{bmatrix} \qquad \text{Eq 129}$$

Equally-spaced points along the chord $\underline{\mathbf{r}}^{\mathbf{e}}_{\mathbf{US}}$ will not correspond to equally-spaced points along the arc connecting **U** and **S**. However, the midpoint of $\underline{\mathbf{r}}^{\mathbf{e}}_{\mathbf{US}}$ will correspond to the midpoint of arc **US**, and a grid of $N = 2^n$ equal-length arc segments can be generated by iteration.

5.3.2 Intermediate Points between **U** and **S**: Dividing the Arc

It's desirable to be able to find the coordinates of an arbitrary point along the arc between **U** and **S**. Toward that end, let $\boldsymbol{f} \in [0, 1]$ be the fractional distance of point **X** from **U** to **S** along the arc **US** of length θ. The unit vector $\underline{\mathbf{1}}^{\mathbf{e}}_{\mathbf{OX}}$ can be expressed as

$$\underline{1}^{\mathbf{e}}_{\mathbf{OX}} = \cos(f\theta)\underline{1}^{\mathbf{e}}_{\mathbf{OU}} + \frac{\sin(f\theta)}{\sin(\theta)}\left(\underline{\mathbf{1}}^{\mathbf{e}}_{\mathbf{OU}} \times \underline{\mathbf{1}}^{\mathbf{s}}_{\mathbf{OS}}\right) \times \underline{\mathbf{1}}^{\mathbf{e}}_{\mathbf{OU}} = \frac{\sin[(1-f)\theta]}{\sin(\theta)}\underline{1}^{\mathbf{e}}_{\mathbf{OU}} + \frac{\sin(f\theta)}{\sin(\theta)}\underline{\mathbf{1}}^{\mathbf{e}}_{\mathbf{OS}}$$

$$= \begin{bmatrix} 1^e_{OX,x} \\ 1^e_{OX,y} \\ 1^e_{OX,z} \end{bmatrix} = \begin{bmatrix} \frac{\sin[(1-f)\theta]}{\sin(\theta)}1^e_{OU,x} + \frac{\sin(f\theta)}{\sin(\theta)}1^e_{OS,x} \\ \frac{\sin[(1-f)\theta]}{\sin(\theta)}1^e_{OU,y} + \frac{\sin(f\theta)}{\sin(\theta)}1^e_{OS,y} \\ \frac{\sin[(1-f)\theta]}{\sin(\theta)}1^e_{OU,z} + \frac{\sin(f\theta)}{\sin(\theta)}1^e_{OS,z} \end{bmatrix} \qquad \text{Eq 130}$$

Eq 128 can be used to find the coordinates $\boldsymbol{L_X}$ and $\boldsymbol{\lambda_X}$. These equations (Eq 130 and Eq 128) provide essentially the same functionality for the vector technique that can be achieved with spherical trigonometry using Eq 72 and Eq 75.

5.3.3 Latitude Extremes of a Great Circle

I am not aware of a vector form of Clairaut's equation as used herein (Eq 92), or in general. However, the most useful application of Clairaut's equation, determining the vertices (northern- and southern-most latitudes of a great circle, is readily found by vector analysis. The cross product of unit vectors $\underline{\mathbf{1}}^{\mathbf{e}}_{\mathbf{OU}}$ (Eq 105) and $\underline{\mathbf{1}}^{\mathbf{e}}_{\mathbf{OS}}$ (Eq 106) is normal to the plane of the great circle containing **U** and **S**. In this subsection, it is assumed that **U** is west of **S**, so that **U × S** points toward the northern hemisphere.

$$\underline{\mathbf{1}}^{\mathbf{e}}_{\mathbf{OU}} \times \underline{\mathbf{1}}^{\mathbf{e}}_{\mathbf{OS}} = \begin{bmatrix} \left(\underline{\mathbf{1}}^{\mathbf{e}}_{\mathbf{OU}} \times \underline{\mathbf{1}}^{\mathbf{e}}_{\mathbf{OS}}\right)_x \\ \left(\underline{\mathbf{1}}^{\mathbf{e}}_{\mathbf{OU}} \times \underline{\mathbf{1}}^{\mathbf{e}}_{\mathbf{OS}}\right)_y \\ \left(\underline{\mathbf{1}}^{\mathbf{e}}_{\mathbf{OU}} \times \underline{\mathbf{1}}^{\mathbf{e}}_{\mathbf{OS}}\right)_z \end{bmatrix} = \begin{bmatrix} \underline{1}^e_{OU,y}\underline{1}^e_{OS,z} - \underline{1}^e_{OU,z}\underline{1}^e_{OS,y} \\ \underline{1}^e_{OU,z}\underline{1}^e_{OS,x} - \underline{1}^e_{OU,x}\underline{1}^e_{OS,z} \\ \underline{1}^e_{OU,x}\underline{1}^e_{OS,y} - \underline{1}^e_{OU,y}\underline{1}^e_{OS,x} \end{bmatrix} \quad \text{Eq 131}$$

$$= \begin{bmatrix} \cos(L_U)\sin(L_S)\sin(\lambda_U) - \sin(L_U)\cos(L_S)\sin(\lambda_S) \\ \sin(L_U)\cos(L_S)\cos(\lambda_S) - \cos(L_U)\sin(L_S)\cos(\lambda_U) \\ \cos(L_U)\cos(L_S)\sin(\lambda_S - \lambda_U) \end{bmatrix}$$

When $\underline{\mathbf{1}}^{\mathbf{e}}_{\mathbf{OU}} \times \underline{\mathbf{1}}^{\mathbf{e}}_{\mathbf{OS}}$ is adjusted to unit length of $\sin(\theta)$ (Eq 121), its z-component is equal to the cosine of the latitude of the highest (and lowest) point on the great circle that includes the route in question (projection of a unit vector onto the earth's spin axis). Thus,

$$\cos(L_{\max}) = \left| \frac{\cos(L_U)\cos(L_S)\sin(\lambda_S - \lambda_U)}{\sin(\theta)} \right| \quad \text{Eq 132}$$

Then $\boldsymbol{L_{min}} = \boldsymbol{-L_{max}}$. Eq 132 is identical to Eq 94, demonstrating that manipulating the components of $\underline{\mathbf{1}}^{\mathbf{e}}_{\mathbf{OU}}$ and $\underline{\mathbf{1}}^{\mathbf{e}}_{\mathbf{OS}}$ yields the same result that Clairaut's equation does.

The longitude where the highest/lowest latitudes are achieved can be found from the x- and y-components of vector $\underline{\mathbf{1}}^{\mathbf{e}}_{\mathbf{OU}} \times \underline{\mathbf{1}}^{\mathbf{e}}_{\mathbf{OS}}$ (from Eq 131).

$$\lambda_{\min} = \arctan\left(\frac{\left(\underline{\mathbf{1}}^{\mathbf{e}}_{\mathbf{OU}} \times \underline{\mathbf{1}}^{\mathbf{e}}_{\mathbf{OS}}\right)_y}{\left(\underline{\mathbf{1}}^{\mathbf{e}}_{\mathbf{OU}} \times \underline{\mathbf{1}}^{\mathbf{e}}_{\mathbf{OS}}\right)_x} \right) = \arctan\left(\frac{\sin(L_U)\cos(L_S)\cos(\lambda_S) - \cos(L_U)\sin(L_S)\cos(\lambda_U)}{\cos(L_U)\sin(L_S)\sin(\lambda_U) - \sin(L_U)\cos(L_S)\sin(\lambda_S)} \right) \quad \text{Eq 133}$$

Then $\boldsymbol{\lambda_{max}} = \boldsymbol{\lambda_{min}} \pm \boldsymbol{\pi}$. Not all great circle routes between two points on the earth's surface will contain a vertex. Criteria for when a route will include a vertex are given in Section 4.3.4.

5.3.4 Locus of Points on a Great Circle

From Eq 105, it follows that any point **X** on the earth has the *e*-frame coordinates $\underline{\mathbf{r}}^{\mathbf{e}}_{\mathbf{OX}}$

$$\underline{\mathbf{r}}^{\mathbf{e}}_{\mathbf{OX}} = \begin{bmatrix} r^e_{OX,x} \\ r^e_{OX,y} \\ r^e_{OX,z} \end{bmatrix} = \underline{\mathbf{1}}^{\mathbf{e}}_{\mathbf{OX}} R_e = \begin{bmatrix} 1^e_{OX,x} \\ 1^e_{OX,y} \\ 1^e_{OX,z} \end{bmatrix} R_e = \begin{bmatrix} \cos(L_X)\ \cos(\lambda_X) \\ \cos(L_X)\ \sin(\lambda_X) \\ \sin(L_X) \end{bmatrix} R_e \quad \text{Eq 134}$$

Here $\boldsymbol{L_X}$ and $\boldsymbol{\lambda_X}$ are the latitude and longitude of **X**, respectively. In order for **X** to be on the great circle containing **U** and **S**, the vector $\underline{\mathbf{r}}^{\mathbf{e}}_{\mathbf{OX}}$ must be orthogonal to the vector $\underline{\mathbf{1}}^{\mathbf{e}}_{\mathbf{OU}} \times \underline{\mathbf{1}}^{\mathbf{e}}_{\mathbf{OS}}$ — that is, the dot product of these two vectors must be zero. One can then solve for $\boldsymbol{L_X}$ in terms of $\boldsymbol{\lambda_X}$ and the coordinates of **U** and **S**.

$$\tan(L_X) = -\frac{\left(\underline{\mathbf{1}}^{\mathbf{e}}_{\mathbf{OU}} \times \underline{\mathbf{1}}^{\mathbf{e}}_{\mathbf{OS}}\right)_x \cos(\lambda_X) + \left(\underline{\mathbf{1}}^{\mathbf{e}}_{\mathbf{OU}} \times \underline{\mathbf{1}}^{\mathbf{e}}_{\mathbf{OS}}\right)_y \sin(\lambda_X)}{\left(\underline{\mathbf{1}}^{\mathbf{e}}_{\mathbf{OU}} \times \underline{\mathbf{1}}^{\mathbf{e}}_{\mathbf{OS}}\right)_z} \qquad \text{Eq 135}$$

Solving for $\boldsymbol{\lambda_X}$ in terms of $\boldsymbol{L_X}$ and the coordinates of **U** and **S** is more complicated. This is a consequence of the fact that while every great circle crosses every line of longitude exactly once, a great circle may cross a line of latitude zero, one or two times. Section 4.6 addresses this issue using spherical trigonometry.

5.4 Computing Satellite Elevation Angle and Slant Range

Section 5.2 shows that, if the latitude/longitude of locations **U** and **S** on the surface are known, the vector method can be used to find the three angles $\boldsymbol{\theta}$, $\boldsymbol{\psi_{S/U}}$ and $\boldsymbol{\psi_{U/S}}$. However, the equations in Section 5.2 do not include $\boldsymbol{h}$, $\boldsymbol{d}$ or $\boldsymbol{\alpha}$. (all of which are related to the height of the aircraft/ satellite above the earth's surface). The two subsections immediately below show that if $\boldsymbol{h}$ and $\boldsymbol{\theta}$ are known, then $\boldsymbol{d}$ and $\boldsymbol{\alpha}$ can be found by the vector method. Moreover, the expressions that are derived are identical to those found in Chapter 3 using the coordinate-free method.

The four other possible equations associated with an aircraft or satellite above the earth when the geocentric angle is known — finding $\boldsymbol{h}$ or $\boldsymbol{d}$ from $\boldsymbol{\alpha}$ and $\boldsymbol{\theta}$, and finding $\boldsymbol{h}$ or $\boldsymbol{\alpha}$ from $\boldsymbol{d}$ and $\boldsymbol{\theta}$ — are not pursued. For these variable combinations, the solutions for the unknown variables will involve manipulation of the scalar components of $\underline{\mathbf{r}}^{\mathbf{u}}_{\mathbf{US}}$. That being the case, one may as well utilize the scalar equations derived in Chapter 3.

5.4.1 Solution for Elevation Angle from Altitude and Geocentric Angle

As shown in Eq 118 the satellite elevation angle can be found from the components of $\underline{\mathbf{r}}^{\mathbf{u}}_{\mathbf{US}}$. Using Eq 116, Eq 118 can be expanded as

$$\tan(\alpha) = \frac{(R_e + h)\cos(\theta) - R_e}{(R_e + h)\sin(\theta)} = \frac{h\cos(\theta) - 2R_e \sin^2\left(\frac{1}{2}\theta\right)}{(R_e + h)\sin(\theta)} \qquad \text{Eq 136}$$

The right-hand side of Eq 136 is identical to the first line of Eq 38, demonstrating that manipulating the components of $\underline{\mathbf{r}}^{\mathbf{u}}_{\mathbf{US}}$ can yield the same value for $\boldsymbol{\alpha}$ as the scalar methodology used in Chapter 3.

5.4.2 Solution for Slant Range from Altitude and Geocentric Angle

The user-satellite slant range can be found by substituting both lines of Eq 116 into Eq 119, yielding:

$$d = \sqrt{h^2 + 4R_e\left(R_e + h\right)\sin^2\left(\frac{1}{2}\theta\right)} \qquad \text{Eq 137}$$

Eq 137 is identical to the second line of Eq 42. This demonstrates that applying Pythagoras's theorem to the components of $\underline{\mathbf{r}}^{\mathbf{u}}_{\mathbf{US}}$ (Eq 119) yields the same value for $\boldsymbol{d}$ as the scalar methodology used in Chapter 3.

5.5 The Direct Problem of Geodesy

The approach used to finding $\boldsymbol{L_S}$ and $\boldsymbol{\lambda_S}$ is to form $\mathbf{r}^{\mathbf{e}}_{\mathbf{OS}}$ and utilize its components. Then, $\boldsymbol{\psi_{U/S}}$ can be addressed utilizing $\boldsymbol{L_S}$ and/or $\boldsymbol{\lambda_S}$.

Given $\boldsymbol{L_U}$, $\boldsymbol{\lambda_U}$, $\boldsymbol{\theta}$ and $\boldsymbol{\psi_{S/U}}$, **N** is constrained but **S** is not. Consequently, form right triangle **OUS** with right angle at **U** and sides $\boldsymbol{R_e}$, $\boldsymbol{d}$ and hypotenuse ($\boldsymbol{R_e} + \boldsymbol{h}$), where

$$\begin{aligned} d &= R_e \tan(\theta) \\ R_e + h &= \frac{R_e}{\cos(\theta)} \end{aligned} \qquad \text{Eq 138}$$

Then $\underline{\mathbf{r}}^{\mathbf{u}}_{\mathbf{US}}$ is given by

$$\underline{\mathbf{r}}^{\mathbf{u}}_{\mathbf{US}} = \begin{bmatrix} r^u_{US,e} \\ r^u_{US,n} \\ r^u_{US,u} \end{bmatrix} = \begin{bmatrix} \tan(\theta)\sin(\psi_{S/U}) \\ \tan(\theta)\cos(\psi_{S/U}) \\ 0 \end{bmatrix} R_e \qquad \text{Eq 139}$$

Utilizing Eq 105 and Eq 112 yields

$$\begin{aligned} \underline{\mathbf{r}}^{\mathbf{e}}_{\mathbf{OS}} &= \underline{\mathbf{r}}^{\mathbf{e}}_{\mathbf{OU}} + \underline{\mathbf{r}}^{\mathbf{e}}_{\mathbf{US}} = \underline{\mathbf{r}}^{\mathbf{e}}_{\mathbf{OU}} + \left(\mathbf{C}^{\mathbf{u}}_{\mathbf{e}}\right)^T \underline{\mathbf{r}}^{\mathbf{u}}_{\mathbf{US}} = \begin{bmatrix} r^e_{OS,x} \\ r^e_{OS,y} \\ r^e_{OS,z} \end{bmatrix} \\ &= \begin{bmatrix} \cos(L_U)\cos(\lambda_U) - \sin(\lambda_U)\tan(\theta)\sin(\psi_{S/U}) + \sin(-L_U)\cos(\lambda_U)\tan(\theta)\cos(\psi_{S/U}) \\ \cos(L_U)\sin(\lambda_U) + \cos(\lambda_U)\tan(\theta)\sin(\psi_{S/U}) + \sin(-L_U)\sin(\lambda_U)\tan(\theta)\cos(\psi_{S/U}) \\ \sin(L_U) + \cos(-L_U)\tan(\theta)\cos(\psi_{S/U}) \end{bmatrix} R_e \end{aligned} \qquad \text{Eq 140}$$

From Eq 108 and Eq 140 it follows that

$$\begin{aligned} L_S &= \arcsin\left(\sin(L_U)\cos(\theta) + \cos(L_U)\sin(\theta)\cos(\psi_{S/U})\right) \\ \lambda_S &= \arctan\left(\frac{\cos(L_U)\sin(\lambda_U) + \cos(\lambda_U)\tan(\theta)\sin(\psi_{S/U}) - \sin(L_U)\sin(\lambda_U)\tan(\theta)\cos(\psi_{S/U})}{\cos(L_U)\cos(\lambda_U) - \sin(\lambda_U)\tan(\theta)\sin(\psi_{S/U}) - \sin(L_U)\cos(\lambda_U)\tan(\theta)\cos(\psi_{S/U})}\right) \end{aligned} \qquad \text{Eq 141}$$

While the right-hand side of the second line of Eq 141 involves a ratio, $\boldsymbol{\lambda_S}$ should be computed

using a two-argument arc tangent function. Eq 141 can be used to find a set of equally-spaced points on the trajectory from **U** to **S** by replacing $\boldsymbol{\theta}$ by $k{\cdot}\boldsymbol{\theta}$/N and letting k = 1,..,N**.**

Once $\boldsymbol{L_S}$ and $\boldsymbol{\lambda_S}$ have been found, $\boldsymbol{\psi_{U/S}}$ can be computed using Eq 123.

It's of interest to compare the equations in this section to those for the same/similar quantities developed using spherical trigonometry in Section 4.3. First, the expressions in Eq 141 for $\boldsymbol{L_S}$ and $\boldsymbol{\lambda_S}$ only involve known quantities — i.e., there is no "daisy chaining" of the solution for one unknown quantity to determine the other. The equations for $\boldsymbol{L_S}$ in Eq 141 and Eq 72 are identical. A difference is that Eq 141 is a solution for $\boldsymbol{\lambda_S}$ while Eq 75 is a solution for $\boldsymbol{\lambda_S} - \boldsymbol{\lambda_U}$; thus, the right-hand sides of these equations are necessarily different. In terms of the azimuth angle $\boldsymbol{\psi_{U/S}}$, Eq 123 in this chapter daisy chains from the solutions for $\boldsymbol{L_S}$ and $\boldsymbol{\lambda_S}$ in Eq 141, while Eq 78 in Chapter 5 does not involving daisy chaining of solutions.

6. AIRCRAFT POSITION FROM TWO RANGE AND/OR AZIMUTH MEASUREMENTS (TRIGONOMETRIC FORMULATIONS)

6.1 General Considerations

6.1.1 Problems Addressed

This chapter combines the formulations of Chapter 3 (involving plane trigonometry applied to a vertical-plane) and Chapter 4 (involving spherical trigonometry applied to the earth's surface). Whereas both of those formulations are limited to two problem-specific points, this chapter addresses situations involving three problem-specific points embedded in three dimensions. Relevant applications include aircraft navigation (specifically, Area Navigation, or RNAV) and aircraft surveillance (specifically, sensor fusion).

For this methodology, typically, one point corresponds to the aircraft (having an unknown latitude/longitude but known altitude), and the other two points correspond to sensor stations having fully-known locations. Each sensor station provides a scalar measurement that describes a geometric Surface-Of-Position (SOP) on which the aircraft lies. The solution for the aircraft position is the intersection of three SOPs. When attention is limited to the earth's surface, 3D SOPs reduce to 2D Lines-Of-Position (LOPs).[****]

Before circa 1950 (when synchronization of ground stations, and thus pseudorange measurements, became possible – see Chapter 7), the most common sensor systems measured

(a) Slant-range $\boldsymbol{d}$ – line-of-sight distance between a sensor station and the aircraft
(b) Spherical-range $\boldsymbol{R_e\,\theta}$ – distance along the earth's surface between a sensor's and the aircraft's ground points
(c) Azimuth $\boldsymbol{\psi_{A/S}}$ – angle of the great circle path from the sensor station to the aircraft
(d) Azimuth $\boldsymbol{\psi_{S/A}}$ – angle of the great circle path from the aircraft to the sensor station
(e) Altitude $\boldsymbol{h_A}$ – height of the aircraft above the mean sea level.

Slant-range measurements provide an SOP in the form of a sphere centered on the station. Spherical-range measurements provide an SOP in the form of a cone with apex at the earth's center and axis intersecting a known point on the surface. Azimuth measurements provide an SOP in the form of a vertical plane that passes through the sensor, the aircraft and the earth's center. A barometric altimeter provides an SOP in the form of a sphere that's concentric with the earth.

The most common civil aviation slant-range and azimuth sensors are

[****] The concept of LOPs was discovered by Thomas Hubbard Sumner, a U.S. Navy officer, in 1837. Sumner was born in Boston in1807, and graduated from Harvard University. In recognition of his achievements, two Navy survey ships were named the *USS Sumner*; also, the crater *Sumner* on the Moon is named after him.

- Slant-range between aircraft and station
  - Navigation: Distance Measuring Equipment (DME)
  - Surveillance: Secondary Surveillance Radar (SSR)
- Spherical-range between aircraft and station
  - Navigation: Star fix
- Azimuth angle from the station to the aircraft
  - Navigation: VHF Omnidirectional Range (VOR)
  - Navigation: Instrument Landing System (ILS) Localizer
  - Surveillance: Secondary Surveillance Radar (SSR)
- Azimuth angle from the aircraft to the station
  - Navigation: Non-Directional Beacon (NDB)
  - Navigation: Aircraft-based radar

This chapter addresses calculation of aircraft latitude and longitude from measurements of altitude in combination with those for slant-range and/or azimuth. However, in Sections 6.4 and 6.5, the slant-range measurements are converted to spherical-ranges at the start of each calculation; thus the material can be utilized for spherical-range measurements as well.

This chapter does not consider errors in the computed coordinates that result from measurement errors. That topic is addressed in Chapter 8. Also, there are several iterative methods for computing latitude and longitude from measurements of slant-range and/or azimuth on an ellipsoidal earth (e.g., Refs. 11 and 33). Those calculations can be initialized using solutions found using the approaches described in this chapter.

6.1.2 Geometric Concerns

The geometric relationship of two sensors and an aircraft is an important aspect of these analysis. Situations where the aircraft is directly above a ground station are excluded for several reasons: ground station antenna patterns are generally not designed to irradiate directly above the station; and the azimuth angle to an aircraft is undefined when an aircraft is above an azimuth determination station. Moreover, when an aircraft is directly above a ground station, that situation intrinsically constitutes a fix.

Restricting attention to the surface of the earth, when two measurements are available, several unfavorable geometries can occur. Figure 25 depicts examples involving aircraft **A** and stations **U** and **S**. Panel (a): Due to measurement errors, it is possible that the measurements are inconsistent and a solution does not exist. Panel (b): When the SOPs for two sensors overlap, only a partial position solution exists. Panel (c): When the two SOPs are tangent, measurement errors can cause the computed position error to increase significantly along the direction of the two LOPs. Panel (d): Multiple solutions occur when the LOPs intersect at more than one point.

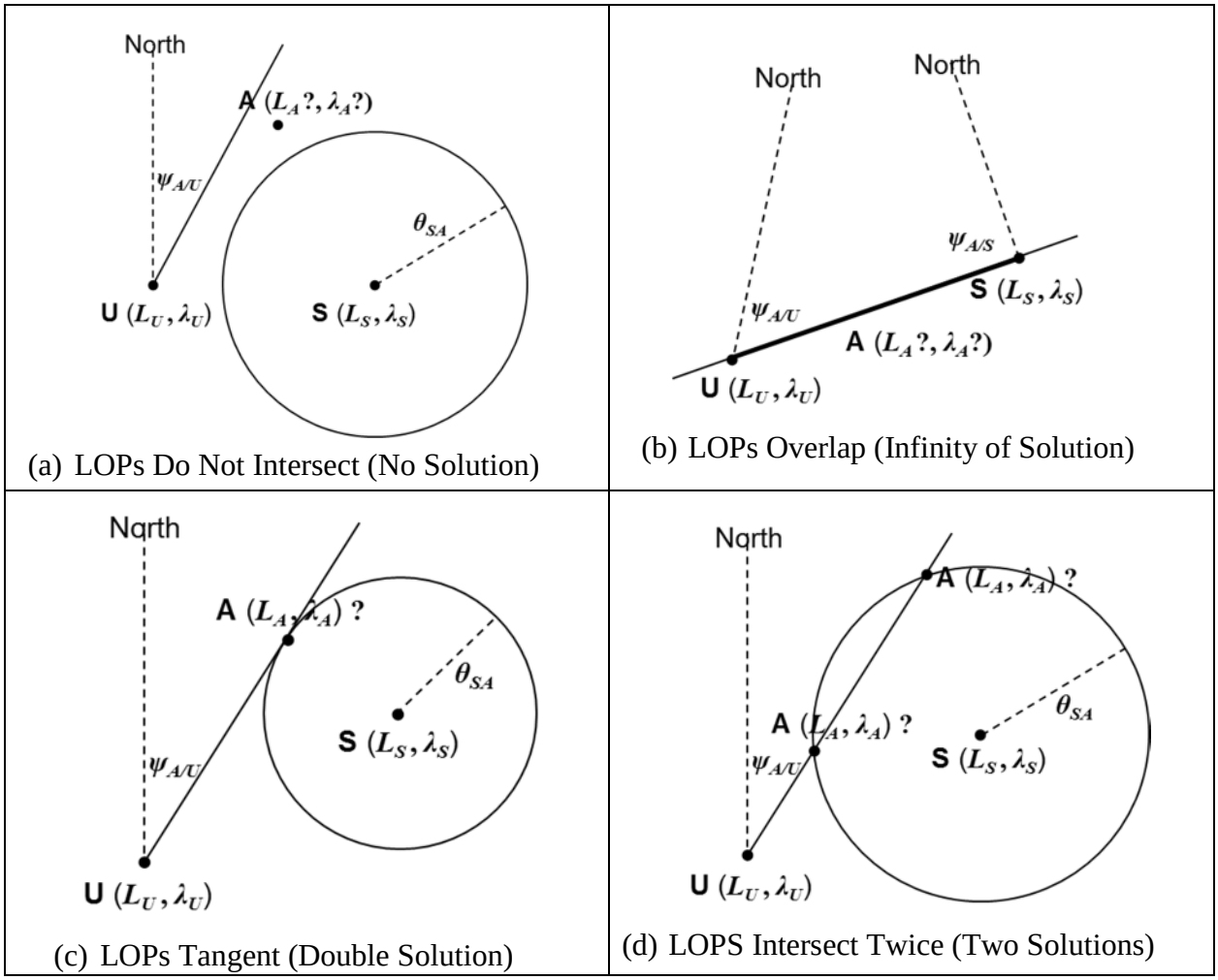

(a) LOPs Do Not Intersect (No Solution)

(b) LOPs Overlap (Infinity of Solution)

(c) LOPs Tangent (Double Solution)

(d) LOPS Intersect Twice (Two Solutions)

Figure 25 Possible Geometric Relationships involving an Aircraft and Two Ground Stations

6.1.3 Rationale for Two-Station Area Navigation (RNAV)

None of the geometric issues illustrated in Figure 25 arises when the slant-range and azimuth sensors are collocated. Since combined VOR/DME stations are prevalent in the NAS, the question naturally arises: Why not only use a single VOR/DME station to determine a vehicle's latitude and longitude (as is described in Subsection 4.8.6)? There are several reasons to utilize navigation fixes from two separate stations:

(1) Increased accuracy: When an aircraft is more than a few of miles from a VOR/DME station, the DME measurement is more accurate than the VOR measurement. Moreover, the difference increases with distance from the station. Thus utilizing two DME stations is generally preferable for RNAV

(2) Contingency/backup: When one of the functions of a VOR/DME station is out of service, utilizing a second station may allow a flight to continue when otherwise it could not. More broadly, RNAV using VOR/DME stations is likely to become the backup to GPS for en route and terminal area navigation.

(3) Advanced avionics: Aircraft with advanced navigation systems (navigation radios and

flight computers) are capable of utilizing measurements from multiple stations, whereas older and/or less sophisticated avionics cannot.

Standards for aircraft RNAV systems based on DME/DME measurements, but permitting VOR measurements, are presented in Ref. 34.

Items (1) and (2) pertain to SSR surveillance as well. The FAA is now incorporating 'sensor fusion' into its Automation (surveillance processing) systems to take advantage of these benefits.

6.1.4 Chapter Overview

Immediately following this introductory section, Section 6.2 analyzes the problem of a great circle and a point that is not necessarily on the great circle. The next three sections address situations involving two stations providing slant-range and/or azimuth measurements which are used (with aircraft altimeter information) to determine the aircraft location: Section 6.3, azimuth/ azimuth; Section 6.4, range/range; and Section 6.5, range/azimuth. Lastly, Section 6.6 addresses using a range measurement to crosscheck the altitude of an aircraft flying an approach procedure.

The solutions in Sections 6.3 - 6.5 follow a common pattern: (a) When a slant-range measurement $\boldsymbol{d}$ is involved, Eq 35 is used to obtain the corresponding geocentric angle $\boldsymbol{\theta}$. This reduces the problem to one of spherical trigonometry. (b) The parameters for the baseline joining the sensor stations are found as solutions to the indirect problem of geodesy (Section 4.2). (c) The possibility that the problem is ill-posed is investigated (e.g., Figure 25(a)). (d) The case (Subsection 4.1.7) of the mathematical spherical triangle comprised of the two stations and the aircraft is identified, and the corresponding solution is found. (d) Parameters for the mathematical triangle are used to determine the aircraft latitude/longitude coordinates.

6.2 Relationship between a Point and a Great Circle

6.2.1 Problem Statement

Often there is a need to find the relationship between a discrete point on the earth's surface and a great circle path. A possible scenario is shown in Figure 26: A vessel **V** intends to transit a great circle path from location **U** (coordinates ($\boldsymbol{L_U}$, $\boldsymbol{\lambda_U}$)) to location **S** (coordinates ($\boldsymbol{L_S}$, $\boldsymbol{\lambda_S}$)), with departure azimuth angle $\boldsymbol{\psi_{S/U}}$. However, while in en route, the crew determines that, due to currents and/or the lack of navigation equipment/ skills, the actual vessel location is ($\boldsymbol{L_V}$, $\boldsymbol{\lambda_V}$), which may not be on the intended path.

For such a scenario, the coordinates of **U**, **V** and **S** are all known. Thus, for triangle **UVS**, the side lengths and side azimuth angles can all be found from solutions to the Indirect Problem of Geodesy (Section 4.2).

In addition to the sides of **UVS**, the quantities of interest can include the coordinates of the nearest point **X** (L_X, λ_X) on the intended path, the distance θ_{VX} from the vessel to the nearest point on the intended path, the projection of the distance traveled onto the intended path θ_{UX} and the off-path angle β. Aviation applications of this methodology, involving the vertical dimension as well as the earth's surface, are discussed in Sections 6.5 and 6.6.

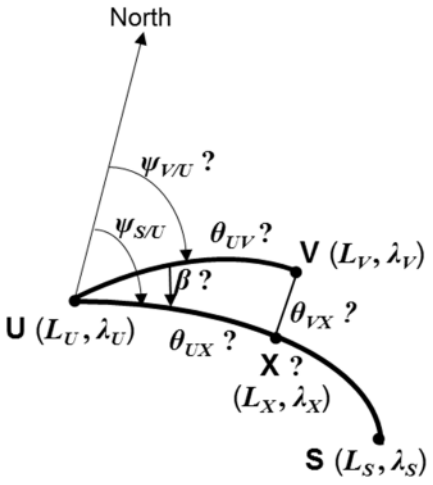

Figure 26 Vessel **V** and Intended Great Circle Path **US**

6.2.2 Problem Solution

Solution to this problem is a five-step process. The first step is to apply the Indirect Problem of Geodesy (Section 4.2) to the great circle path **UV**, thus finding the azimuth angle $\psi_{V/U}$ and the distance θ_{UV}. The fact that the vessel's actual track over the earth may not have been the great circle path **UV** is not relevant – only the end points are.

Because (a) the great circle through **U** and **S** encircles the earth and the vehicle may have traveled "in the wrong direction", and (b) azimuth (bearing) angles can vary over $(-\pi, \pi]$, the angle β between **US** and **UV** is computed in the range $[0, \pi]$ using

$$\beta = \min\left\{\left|\psi_{S/U} - \psi_{V/U}\right|, \left|\psi_{S/U} - \psi_{V/U} + 2\pi\right|, \left|\psi_{S/U} - \psi_{V/U} - 2\pi\right|\right\} \qquad \text{Eq 142}$$

When $\beta = 0$, the vessel is in fact on the intended path.

The third step addresses the mathematical spherical triangle **UVX**, where the angle at **X** is a right-angle. The law of sines (Eq 58) yields the off-course distance θ_{VX} in the range $[0, \pi/2]$

$$\theta_{VX} = \arcsin\left[\sin(\theta_{UV})\sin(\beta)\right] \qquad \text{Eq 143}$$

Again considering triangle **UVX**, the projection of the distance traveled onto the intended path θ_{UX} is found from the law of cosines for sides (Eq 56) and optionally Eq 12

$$\theta_{UX} = \arccos\left[\frac{\cos(\theta_{UV})}{\cos(\theta_{VX})}\right] = 2\arcsin\left(\sqrt{\frac{\sin\left(\frac{1}{2}(\theta_{UV} + \theta_{VX})\right)\sin\left(\frac{1}{2}(\theta_{UV} - \theta_{VX})\right)}{\cos(\theta_{VX})}}\right) \qquad \text{Eq 144}$$

Finally, the coordinates (L_X, λ_X) are found as a solution to the Direct Problem of Geodesy (Section 4.3) based on knowledge of (L_U, λ_U), θ_{UX} and $\psi_{S/U}$.

6.3 Position Solution for Two Azimuth Measurements

Here, the assumption is that the latitude/longitude coordinates of two stations, **U** (L_U, λ_U) and **S** (L_S, λ_S) are known, as are their azimuth (or bearing) angles, $\psi_{A/U}$ and $\psi_{A/S}$, to a third (aircraft) location **A**. The solution for the coordinates of **A** and related parameters follows the pattern described in Subsection 6.1.4.

6.3.1 Step 1: Solve the Navigation Spherical Triangle **PUS**

This step is a straightforward application of the Indirect Problem of Geodesy. Section 4.2 is used to find the geocentric angle θ_{US} between **U** and **S** (Eq 65) and the azimuth angles $\psi_{S/U}$ and $\psi_{U/S}$ (Eq 70 and Eq 71) of the great circle path between the stations.

6.3.2 Step 2: Determine if the Problem is Well-Posed

The problem must be physically and mathematically well posed. In terms of a spherical earth, two radials define two great circles which intersect at two antipodal points. The interior angles of triangle **USA** at **U** and **S**, both in (0, π), are given in the following equations.

$$\begin{aligned}\beta_U &= \min\left\{\left|\psi_{S/U}-\psi_{A/U}\right|, \left|\psi_{S/U}-\psi_{A/U}+2\pi\right|, \left|\psi_{S/U}-\psi_{A/U}-2\pi\right|\right\}\\ \beta_S &= \min\left\{\left|\psi_{U/S}-\psi_{A/S}\right|, \left|\psi_{U/S}-\psi_{A/S}+2\pi\right|, \left|\psi_{U/S}-\psi_{A/S}-2\pi\right|\right\}\end{aligned} \qquad \text{Eq 145}$$

For two intersections to occur, all of the following must be true:

- Solution Existence: The radials must point to the same side of the station baseline **US**. One and only one of the following conditions must be true:
  - $\psi_{A/U} = \psi_{S/U} + \beta_U$ and $\psi_{A/S} = \psi_{U/S} - \beta_S$
  - $\psi_{A/U} = \psi_{S/U} - \beta_U$ and $\psi_{A/S} = \psi_{U/S} + \beta_S$
- Solution Existence: It must be true that $0 < |\beta_U| + |\beta_S| < \pi$. Otherwise, the two intersections will either be equidistant (both at a geocentric angle of $\pi/2$ from the midpoint of the station baseline) or the closer intersection will be on the opposite side of the station baseline of that intended.
- Partial Solution: **A** cannot be found uniquely if it is on the station baseline **US** or its extensions, as the radials then do not have a single intersection. If both $\beta_U = 0$ and $\beta_U = 0$, then **A** is on the baseline between the stations; if $\beta_U = 0$ and $\beta_S = \pi$, then **A** is on the baseline extension from **S**; if $\beta_U = \pi$ and $\beta_S = 0$, then **A** is on the baseline extension from **U**.

If any of these conditions is not satisfied, then the problem is ill posed and does not have a valid solution.

6.3.3 Step 3: Solve the Mathematical Spherical Triangle **USA**

The third step is to solve the "mathematical" spherical triangle (Subsection 4.1.2) **USA**. This

situation falls under Case (4) in the spherical triangle taxonomy of Subsection 4.1.7 — two angles and the included side are known.

The unknown angle at which the two radials intersect at **A** is given by the law of cosines for angles (Eq 57)

$$\cos\left(\beta_A\right) = -\cos\left(\beta_U\right)\cos\left(\beta_S\right) + \sin\left(\beta_U\right)\sin\left(\beta_S\right)\cos(\theta_{US}) \qquad \text{Eq 146}$$

In computing $\boldsymbol{\beta_A}$ from Eq 146, observe that, using the arc cosine function, it can be unambiguously found in [0, $\boldsymbol{\pi}$].

The unknown sides (geocentric angles) $\boldsymbol{\theta_{UA}}$ and $\boldsymbol{\theta_{SA}}$ are found from the four-part cotangent formula (Eq 60)

$$\cot(\theta_{UA}) = \frac{\cos(\theta_{US})\cos\left(\beta_U\right) + \sin(\beta_U)\cot(\beta_S)}{\sin(\theta_{US})}$$
$$\cot(\theta_{SA}) = \frac{\cos(\theta_{US})\cos\left(\beta_S\right) + \sin(\beta_S)\cot(\beta_U)}{\sin(\theta_{US})} \qquad \text{Eq 147}$$

In computing $\boldsymbol{\theta_{UA}}$ and $\boldsymbol{\theta_{SA}}$ from Eq 147, observe that, using the arc cotangent function, they can be unambiguously found in [0, $\boldsymbol{\pi}$]. Also, observe that $\boldsymbol{\beta_A}$, $\boldsymbol{\theta_{UA}}$ and $\boldsymbol{\theta_{SA}}$ are found without daisy-chaining from one solution to another.

6.3.4 Step 4: Find the Coordinates/Path Azimuths for **A**

With $\boldsymbol{\theta_{UA}}$ or $\boldsymbol{\theta_{SA}}$ known, the latitude/longitude of **A** can be found from either the spherical triangle **PUA** or from triangle **PSA**. This is an application of the direct problem of geodesy (Section 4.3). The latitude can be found from either of these equations

$$\sin\left(L_A\right) = \sin(L_U)\cos(\theta_{UA}) + \cos(L_U)\sin(\theta_{UA})\cos\left(\psi_{A/U}\right)$$
$$\sin\left(L_A\right) = \sin(L_S)\cos(\theta_{SA}) + \cos(L_S)\sin(\theta_{SA})\cos\left(\psi_{A/S}\right) \qquad \text{Eq 148}$$

And the longitude can be found from either of these equations

$$\tan\left(\lambda_A - \lambda_U\right) = \frac{\sin(\theta_{UA})\sin\left(\psi_{A/U}\right)}{\cos(L_U)\cos(\theta_{UA}) - \sin(L_U)\sin(\theta_{UA})\cos\left(\psi_{A/U}\right)}$$
$$\tan\left(\lambda_A - \lambda_S\right) = \frac{\sin(\theta_{SA})\sin\left(\psi_{A/S}\right)}{\cos(L_S)\cos(\theta_{SA}) - \sin(L_S)\sin(\theta_{SA})\cos\left(\psi_{A/S}\right)} \qquad \text{Eq 149}$$

After employing a two-argument arc tangent function, the solutions will yield values of $\boldsymbol{\lambda_A - \lambda_U}$ and $\boldsymbol{\lambda_A - \lambda_S}$ in the range [$\boldsymbol{-\pi}$, $\boldsymbol{\pi}$].

Lastly, it may be of interest to know the azimuths of the paths to **U** and **S** from **A**.

$$\tan(\psi_{U/A}) = \frac{-\cos(L_U)\sin(\psi_{A/U})}{\sin(L_U)\sin(\theta_{UA}) - \cos(L_U)\cos(\theta_{UA})\cos(\psi_{A/U})}$$

$$\tan(\psi_{S/A}) = \frac{-\cos(L_S)\sin(\psi_{A/S})}{\sin(L_S)\sin(\theta_{SA}) - \cos(L_S)\cos(\theta_{SA})\cos(\psi_{A/S})} \qquad \text{Eq 150}$$

After employing a two-argument arc tangent function, the solutions will yield values of $\psi_{U/A}$ and $\psi_{S/A}$ in the range [$-\pi$, π].

6.3.5 Remarks

Solving the two-bearing (or VOR-VOR cross-fix) problem can be done using only spherical trigonometry, and does not require aircraft altitude. It is the only formulation in this chapter with that characteristic. If interest is limited to coordinates L_A and λ_A, then Eq 146 and Eq 150 are not needed, and only one line from each of Eq 147, Eq 148 and Eq 149 is needed. However, there is value to the added information.

- The crossing angle of the radials β_A (Eq 146) provides information about the accuracy of the solutions for L_A and λ_A. Some have suggested that the fix should only be used when $30° \leq \beta_A \leq 150°$. This would exclude locations near the baseline (including the extended baseline) and at large distances from both stations.
- The distances to the stations θ_{UA} and θ_{SA} (Eq 147) can provide information about the strength and visibility of the stations' signals at the aircraft.
- The azimuth angles $\psi_{U/A}$ and $\psi_{S/A}$ (Eq 150) may be useful for steering.

The solution process involves a potential total of 15 navigation variables (latitudes, longitudes, azimuth angles and geocentric angles). Of these, 6 are known at the start of the calculation.

A problem closely-related to the subject of this section is determining an aircraft's position from the coordinates of two stations **U** and **S** and measurements of the angles $\psi_{U/A}$ and $\psi_{S/A}$ from the aircraft to those stations. In aviation (or marine applications), the stations would typically be non-directional beacons or possibly commercial broadcast transmitters.

The information available for this related problem is mathematically insufficient for the direct use of spherical trigonometry — for triangle **USA**, only two quantities (the side θ_{US} and the opposite angle β_A are known. However, a viable approach is to set $\psi_{A/U} = \psi_{U/A} \pm \pi$ and $\psi_{A/S} = \psi_{S/A} \pm \pi$ — in each case, retaining the value in [-π. π]. Then carry out the calculations described in Subsections 6.3.1 to 6.3.4 above. If the computed value of $\psi_{U/A}$ and/or $\psi_{S/A}$ are significantly different than the measured values for these quantities — bearing in mind that azimuth measurements from moving vehicle are error-prone — adjust the estimates of $\psi_{A/U}$ and $\psi_{A/S}$ and repeat the calculations.

6.4 Position Solution for Two Slant Range Measurements

Here, the assumption is that the latitude/longitude/altitudes of stations **U** (L_U, λ_U, h_U) and **S** (L_S, λ_S, h_S) are known, as are the slant ranges, d_{UA} and d_{SA}, to the aircraft location **A**, about which only its altitude h_A is known. Following a preliminary step (Subsection 6.4.1), the solution for the latitude and longitude of **A** and related parameters is a four-step process, like that in Section 6.3.

6.4.1 Step 0: Convert Slant-Ranges to Spherical-Ranges/Geocentric Angles

Accurate calculation of the geocentric angles θ_{SA} and θ_{UA} takes account of the altitude/elevation of the aircraft and ground station above sea level. This is done using Eq 35, applied separately to each aircraft-station pair. Once the geocentric angles are found, the problem reduces to one of pure spherical trigonometry.

6.4.2 Step 1: Solve the Navigation Spherical Triangle **PUS**

This is an application of the Indirect Problem of Geodesy. The approach in Section 4.2 is employed to find the geocentric angle θ_{US} between the stations **U** and **S** (Eq 65) and the azimuth angles $\psi_{S/U}$ and $\psi_{U/S}$ (Eq 70 and Eq 71) of the path (baseline) joining the stations.

6.4.3 Step 2: Determine if the Problem is Well-Posed

The problem must be mathematically well posed for a solution to exist. Ranges (geocentric angles) from two stations define small circles on the surface which can intersect at zero, one or two points. If either of the following conditions is true, then the problem is ill posed and does not have a valid solution.

- If $\theta_{UA} + \theta_{SA} < \theta_{US}$, then the circle radii are too small (relative to the distance between their centers) to intersect.
- If $|\theta_{UA} - \theta_{SA}| > \theta_{US}$, then one circle encloses the other and they do not intersect.

If either $\theta_{UA} + \theta_{SA} = \theta_{US}$ or $|\theta_{UA} - \theta_{SA}| = \theta_{US}$ then the circles are tangent and there is only one solution, which lies on the baseline connecting **U** and **S**, or its extension as a great circle (see Subsection 6.4.6). Otherwise, there are two solutions, located symmetrically relative to the baseline **US**. Additional ("side") information must be used to choose between the two solutions (Subsection 6.4.6).

There is no partial solution case for this sensor combination. However, the one-solution case involves high sensitivity to measurement errors for the direction orthogonal to the baseline.

6.4.4 Step 3: Solve the Mathematical Spherical Triangle **USA**

The third step is to solve the mathematical spherical triangle (Subsection 4.1.2) **USA**. This situation falls under Case (1) in the taxonomy of Subsection 4.1.7 — all three sides are known. Denote the (positive) interior angles of **USA** by $\boldsymbol{\beta_U}$, $\boldsymbol{\beta_S}$ and $\boldsymbol{\beta_A}$. They can be found by applying the law of cosines (Eq 56) three times:

$$\begin{aligned}\cos(\beta_U) &= \frac{\cos(\theta_{SA}) - \cos(\theta_{US})\cos(\theta_{UA})}{\sin(\theta_{US})\sin(\theta_{UA})} \\ \cos(\beta_S) &= \frac{\cos(\theta_{UA}) - \cos(\theta_{US})\cos(\theta_{SA})}{\sin(\theta_{US})\sin(\theta_{SA})} \\ \cos(\beta_A) &= \frac{\cos(\theta_{US}) - \cos(\theta_{UA})\cos(\theta_{SA})}{\sin(\theta_{UA})\sin(\theta_{SA})}\end{aligned} \qquad \text{Eq 151}$$

In computing $\boldsymbol{\beta_U}$, $\boldsymbol{\beta_S}$ and $\boldsymbol{\beta_A}$ from Eq 151, observe that, using the arc cosine function, the angles can be unambiguously found in $(0, \boldsymbol{\pi})$. Also, $\boldsymbol{\beta_U}$, $\boldsymbol{\beta_S}$ and $\boldsymbol{\beta_A}$ are found without daisy-chaining from one solution to another.

6.4.5 Step 4: Find the Coordinates/Path Azimuths for **A**

With $\boldsymbol{\beta_U}$ and $\boldsymbol{\beta_S}$ known, azimuth angles $\boldsymbol{\psi_{A/U}}$ and $\boldsymbol{\psi_{A/S}}$ can be determined to within an ambiguity. The ambiguity arises because it is not known whether to add or subtract $\boldsymbol{\beta_U}$ from $\boldsymbol{\psi_{S/U}}$ ($\boldsymbol{\beta_S}$ from $\boldsymbol{\psi_{U/S}}$, respectively) to form $\boldsymbol{\psi_{A/U}}$ ($\boldsymbol{\psi_{A/S}}$). One and only one of the following is correct:

- $\boldsymbol{\psi_{A/U}} = \boldsymbol{\psi_{S/U}} + \boldsymbol{\beta_U}$ and $\boldsymbol{\psi_{A/S}} = \boldsymbol{\psi_{U/S}} - \boldsymbol{\beta_S}$
- $\boldsymbol{\psi_{A/U}} = \boldsymbol{\psi_{S/U}} - \boldsymbol{\beta_U}$ and $\boldsymbol{\psi_{A/S}} = \boldsymbol{\psi_{U/S}} + \boldsymbol{\beta_S}$.

The ambiguity may be resolvable from the azimuth angles $\boldsymbol{\psi_{A/U}}$ and $\boldsymbol{\psi_{A/S}}$ (because the vehicle operator often knows, approximately, $\boldsymbol{\psi_{U/A}}$ and/or $\boldsymbol{\psi_{S/A}}$). Alternatively, two solutions can be found for the coordinates of **A** and the azimuths of the paths from **A**, and the ambiguity resolved subsequently. In either case, the calculations set forth in Subsection 6.3.4 are performed last — specifically, Eq 148 for the aircraft' latitude $\boldsymbol{L_A}$, Eq 149 for the aircraft's longitude $\boldsymbol{\lambda_A}$, and Eq 150 for the azimuth angles $\boldsymbol{\psi_{U/A}}$ and $\boldsymbol{\psi_{S/A}}$ of the stations relative to the aircraft.

6.4.6 Remarks

This section could also be entitled "Position Solution for Two Geocentric Angle Measurements", since the first step in the solution is to convert the convert the slant ranges to geocentric angles.

Concerning resolution of the two-solution ambiguity:

- The ambiguity can often be resolved from knowledge of the station locations and the approximate route from the departure point. Using dead reckoning from either the departure point or a previous fix, the vehicle operator may know the side of the

station baseline on which the vehicle is currently located.

- If either station provides azimuth (in addition to range) information, that may be used to resolve the ambiguity.

To elaborate and provide context:

- The angle from the aircraft to the stations, β_A, provides information about the accuracy of the solutions for L_A and λ_A. Some have recommended that the fix only be accepted when $30° \leq \beta_A \leq 150°$. This would exclude locations near the baseline between stations (including its extensions) and at large distances from both stations.
- The solution presented above involves a total of 21 navigation variables (latitudes, longitudes, altitudes, azimuth angles, geocentric angles and slant ranges). Of these, 9 are known at the start of the calculation.
- The solution involves calculating parameters that may not be needed in all situations.
- The most commonly used method of celestial navigation, the "Altitude-Intercept Method," also involves the intersection of two small circles. A sextant is used to measure the angle between the horizon and each celestial body, which defines a small circle centered on celestial body's sub-point (nadir).

6.5 Position Solution for a Slant Range and an Azimuth Measurement

Here, the known quantities are: the coordinates of DME station **D** (L_D, λ_D, h_D) and VOR station **V** (L_V, λ_V); the aircraft **A** measured slant range to **D** d_{DA} and azimuth angle from **V** $\psi_{A/V}$; and the measured aircraft altitude h_A. The quantities sought are the coordinates of **A** (L_A, λ_A) and the parameters for paths **AD** and **AV** (similar those in Sections 6.2 - 6.4).

6.5.1 Step 0: Convert Slant-Range to Spherical-Range/Geocentric Angle

Convert the slant range d_{DA} to the geocentric angle θ_{DA} using Eq 35, in the same manner as discussed in Subsection 6.4.1.

6.5.2 Step 1: Solve the Navigation Spherical Triangle **PDV**

Apply the Indirect Problem of geodesy (Section 4.2) to find the geocentric angle θ_{DV} between stations **D** and **V** (Eq 65) and the azimuth angles $\psi_{D/V}$ and $\psi_{V/D}$ (Eq 70 and Eq 71) for the baseline joining the stations.

6.5.3 Step 2: Determine if the Problem is Well-Posed

In determining if the problem is well-posed, the first consideration is the magnitude of the measured geocentric angle between the aircraft **A** and station **D**, θ_{DA}, relative to the known geocentric angle between the stations **D** and **V**, θ_{DV}. There are three cases:

- Interior: If $\theta_{DV} < \theta_{DA}$, then **V** is within the perimeter of the circle of possible aircraft locations centered on **D**; there is one and only one intersection/solution

- Perimeter: If $\theta_{DV} = \theta_{DA}$, then **V** is on the perimeter of the circle centered on **D**; there can be zero or one solution
- Exterior: If $\theta_{DA} < \theta_{DV}$, then **V** is outside the perimeter of the circle centered on **D**; there can be zero, one or two solutions.

To further explore the scenario geometry, define the angle at **V**, β_V, between the great circle arcs to the aircraft **A** and the DME station **D**, in the range $0 \le \beta_V \le \pi$, by

$$\beta_V = \min\left\{\left|\psi_{A/V} - \psi_{D/V}\right|,\ \left|\psi_{A/V} - \psi_{D/V} + 2\pi\right|,\ \left|\psi_{A/V} - \psi_{D/V} - 2\pi\right|\right\} \qquad \text{Eq 152}$$

For the Perimeter case, there is a valid solution only if $0 \le \beta_V < \pi/2$. Otherwise, the problem is ill-posed and no solution exists.

For the Exterior case ($\theta_{DA} < \theta_{DV}$), define the critical value for β_V, $0 \le \beta_{V,crit} < \pi/2$, by

$$\sin(\beta_{V,crit}) = \frac{\sin(\theta_{DA})}{\sin(\theta_{DV})} \qquad \text{Eq 153}$$

Eq 153 is the law of sines applied to triangle **DVA** when β_A is a right angle. Three situations can occur: (a) when $\beta_{V,crit} < \beta_V$, the problem is ill-posed and there is no solution; (b) when $\beta_{V,crit} = \beta_V$, there is a single solution; and (c) when $\beta_V < \beta_{V,crit}$ there are two possible solutions.

There is no partial solution case for this sensor combination. However, the single-solution case involves high sensitivity to measurement errors for the direction along the radial from **V**.

6.5.4 Step 3: Solve the Mathematical Spherical Triangle **DVA**

When at least one solution exists, the third step is to solve the mathematical spherical triangle (Subsection 4.1.2) **DVA**. This problem falls under Case (3) in the taxonomy of Subsection 4.1.7 — two sides, θ_{DV} and θ_{DA}, and an adjacent (not included) angle β_V are known.

First, the interior angle at **A**, β_A, is found using the law of sines

$$\beta_A = \arcsin\left(\frac{\sin(\beta_V)\sin(\theta_{DV})}{\sin(\theta_{DA})}\right) \qquad \text{Eq 154}$$

Consistent with Subsection 6.5.3, for a well-posed problem the quantity within the large parentheses in Eq 154 will have a value in [0, 1]. Thus two angles will be found in [0, π] except when the right-hand side is unity, in which situation $\beta_A = \pi/2$ and $\beta_V = \beta_{V,crit}$. For the Interior case, the value for β_A in [0, $\pi/2$) is correct, and the value in ($\pi/2$, π] is extraneous (a mathematical artifact which is discarded). For the Exterior case, either value for β_A may be correct (the situation is ambiguous); these values are labeled $\beta_{A,1}$ and $\beta_{A,2}$, and both are retained. The value of β_A is indicative of the solution accuracy (Subsection 6.5.6).

The angles $\boldsymbol{\beta_{D,1}}$ and $\boldsymbol{\beta_{D,2}}$ corresponding to angles $\boldsymbol{\beta_{A,1}}$ and $\boldsymbol{\beta_{A,2}}$ are found using either of the following expressions from Napier's Analogies (Eq 61)

$$\begin{aligned}\tan\tfrac{1}{2}\beta_{D,i} &= \frac{\cos\frac{1}{2}(\theta_{DV}-\theta_{DA})}{\cos\frac{1}{2}(\theta_{DV}+\theta_{DA})}\cot\tfrac{1}{2}(\beta_{A,i}+\beta_V)\\ &= \frac{\sin\frac{1}{2}(\theta_{DV}-\theta_{DA})}{\sin\frac{1}{2}(\theta_{DV}+\theta_{DA})}\cot\tfrac{1}{2}(\beta_{A,i}-\beta_V)\end{aligned} \qquad \text{Eq 155}$$

The discussion in Subsection 4.1.6 concerning sums and differences of sides and angles having the "same affection" is relevant here. As a consequence, both expressions on the right-hand side of Eq 155 are positive. Thus, in computing $\boldsymbol{\beta_{D,i}}$ (i = 1, 2) from either line using the arc tangent function, each solution can be unambiguously found in (**0**, $\boldsymbol{\pi}$). The second line is preferred, as it cannot be indeterminate. There is a small possibility that first line can, by the two sums of angles equaling $\boldsymbol{\pi/2}$, resulting in the trigonometric functions of the sums both equaling zero.

The distance $\boldsymbol{\theta_{VA,i}}$ can be found from either of the following expressions. As is the case for Eq 155, both expressions on the right-hand side of Eq 156 are positive. Thus, in computing $\boldsymbol{\theta_{VA,i}}$ (i = 1, 2) from either line using the arc tangent function, each solution can be unambiguously found in (**0**, $\boldsymbol{\pi}$). The first line is usually preferred, as it cannot be indeterminate. There is a possibility that second line can, by the two differences equaling **0**, resulting in the trigonometric functions equaling zero.

$$\begin{aligned}\tan\tfrac{1}{2}\theta_{VA,i} &= \frac{\cos\frac{1}{2}(\beta_{A,i}+\beta_V)}{\cos\frac{1}{2}(\beta_{A,i}-\beta_V)}\tan\tfrac{1}{2}(\theta_{DV}+\theta_{DA})\\ &= \frac{\sin\frac{1}{2}(\beta_{A,i}+\beta_V)}{\sin\frac{1}{2}(\beta_{A,i}-\beta_V)}\tan\tfrac{1}{2}(\theta_{DV}-\theta_{DA})\end{aligned} \qquad \text{Eq 156}$$

6.5.5 Step 4: Find the Coordinates/Path Azimuths for **X**

One and only one of the following conditions is true:

- $\boldsymbol{\psi_{A/D}} = \boldsymbol{\psi_{V/D}} + \boldsymbol{\beta_D}$ and $\boldsymbol{\psi_{A/V}} = \boldsymbol{\psi_{D/V}} - \boldsymbol{\beta_V}$
- $\boldsymbol{\psi_{A/D}} = \boldsymbol{\psi_{V/D}} - \boldsymbol{\beta_D}$ and $\boldsymbol{\psi_{A/V}} = \boldsymbol{\psi_{D/V}} + \boldsymbol{\beta_V}$.

Since both $\boldsymbol{\psi_{A/V}}$ and $\boldsymbol{\psi_{D/V}}$ are now known, the correct line can be selected, yielding $\boldsymbol{\psi_{A/D}}$. Then the calculations set forth in Subsection 6.3.4 involving spherical triangles **PDA** and **PVA** can be performed — specifically, Eq 148 for the aircraft' latitude $\boldsymbol{L_A}$, Eq 149 for the aircraft's longitude $\boldsymbol{\lambda_A}$, and Eq 150 for the azimuth angles $\boldsymbol{\psi_{D/A}}$ and $\boldsymbol{\psi_{V/A}}$ of the stations relative to the aircraft.

6.5.6 Remarks

Concerning resolution of the two-solution ambiguity:

- The ambiguity can often be resolved from knowledge of the station locations and the approximate route from the departure point. Using dead reckoning, the vehicle operator may know the approximate distance to the VOR station.
- If the DME station provides azimuth (in addition to range) information, that may be used to resolve the ambiguity.

To elaborate and provide context:

- The angle from the aircraft to the stations, $\boldsymbol{\beta_A}$, provides information about the accuracy of the solutions for $\boldsymbol{L_A}$ and $\boldsymbol{\lambda_A}$. Some have recommended that the fix only be accepted when $0° \leq \boldsymbol{\beta_A} \leq 60°$ or $120° \leq \boldsymbol{\beta_A} \leq 180°$. This would exclude locations where the lines-of-sight to the stations are close to being orthogonal.
- The solution presented above involves a total of 18 navigation variables (latitudes, longitudes, altitudes, azimuth angles, geocentric angles and slant ranges). Of these, 8 are known at the start of the calculation.
- The solution involves calculating parameters that may not be needed in all situations.
- The aircraft-DME station geocentric angle can be approximated — e.g., by $\boldsymbol{d_{DA}} / \boldsymbol{R_e}$ — but Eq 35 provides a more accurate solution.
- The solution method described in this section uses Napier's Analogies. An alternative solution method can be based on the equations in Section 6.2. This method is employed in Section 6.6 to address a mathematically similar problem.

6.6 Crosscheck of Continuous Descent Approach Altitude

6.6.1 Application Context

FAA Advisory Circular AC 120-108 (Ref. 35) recommends and provides guidance for employing the Continuous Descent Final Approach (CDFA) technique, as an alternative to the Step Down technique, when conducting a Non-Precision Approach (NPA) procedure:[††††]

- "The goal of implementing CDFA is to incorporate the safety benefits derived from flying a continuous descent in a stabilized manner as a standard practice on an NPA.
- "CDFA starts from an altitude/height at or above the Final Approach Fix (FAF) and proceeds to an altitude/height approximately 50 feet (15 meters) above the landing runway threshold or to a point where the flare maneuver should begin for the type of aircraft being flown."

Simultaneous with publication of AC 120-108, the FAA began including CDFA Vertical Descent Angles (VDAs) on approach plates for NPAs. Figure 27, depicting part of the approach

[††††] CDFAs were not prohibited prior to publication of AC 120-108. However, the FAA did not recommend them nor provide information concerning their use. Some air carriers required utilization of CDFAs and supplied their flight crews with supplementary information on the company's approach plates.

plate for the LOC IAP to runway 35 at Norwood Memorial Airport (KOWD), is an example.[‡‡‡‡]

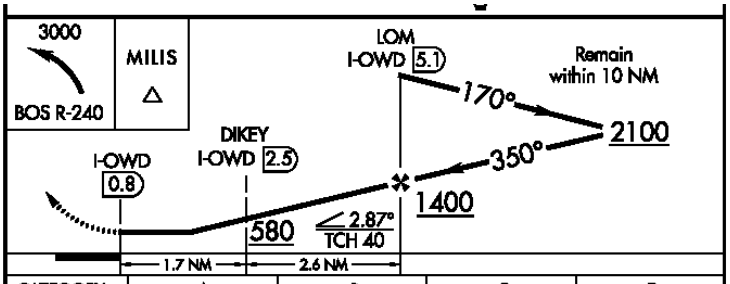

CATEGORY	A	B	C	D
S-35	580-¾ 531 (600-¾)		580-1½ 531 (600-1½)	580-1¾ 531 (600-1¾)
CIRCLING	600-1 551 (600-1)		700-1¾ 651 (700-1¾)	700-2 651 (700-2)
DIKEY FIX MINIMUMS				
S-35	500-¾ 451 (500-¾)		500-1¼ 451 (500-1¼)	500-1½ 451 (500-1½)
CIRCLING	600-1 551 (600-1)		700-1¾ 651 (700-1¾)	700-2 651 (700-2)

NORWOOD, MASSACHUSETTS

Figure 27 Portion of LOC IAP to KOWD Runway 35

When executing a CDFA in accordance with the LOC IAP to runway 35 at KOWD, upon passing the FAF (as determined either by a marker beacon receiver or a DME interrogator) at or above 1,400 ft MSL, the aircraft would descend to 580 ft MSL by following a CDFA with a VDA of 2.87 deg. Upon reaching 580 ft MSL, the aircraft should not descend further unless/until the fix DIKEY is identified utilizing a DME interrogator. If/when that occurs, the aircraft would be permitted to descend to 500 ft MSL — but no lower. If the airport environment is identified at that point, a visual landing could be performed; if not, a missed approach is recommended.

6.6.2 Altitude vs. DME Information for the Pilot

Employing the CDFA technique does not require additional equipment on the aircraft or on the ground — i.e., other than that required for the step down technique. Specifically, the avionics required for VNAV guidance specified in Advisory Circulars AC 90-105 (Ref. 36) and AC 20-138C (Ref. 37) are not required. However, if available, use of VNAV is recommended.

If VNAV avionics are not available, the pilot calculates a planned descent rate utilizing a table in AC 120-108, based on the charted VDA and planned ground speed. When executing a CDFA without VNAV, instrumentation errors in measuring airspeed and descent rate, variability in the headwind, the lack of a guidance display and other factors, will cause the aircraft's altitude flown to be less well controlled than it is for a VNAV operation. The contributions of some of error

[‡‡‡‡] Effective dates: May 1, 2014 – May 29, 2014

mechanisms accumulate, causing the difference between the altitude flown and the altitude desired to increase with time.

The safety aspect of an aircraft being at the incorrect altitude while performing a CDFA NPA is addressed by requiring the aircraft to remain above the Minimum Descent Altitude (MDA) along the entire approach track. However, a case has been made for the pilot having a readily available method for comparing the aircraft's measured altitude with the planned altitude on an almost continuous basis, particularly when VNAV is not used (Ref. 38). A technique adopted by some airlines has been to include a table of DME distance versus planned barometric altitude for each CDFA approach plate for an airport with a DME ground station. Generating such a table is the subject of this section. This analysis can also be used to determine the parameters of an approach fix defined by aircraft altitude or distance to a DME ground station.

Equations used to generate a DME distance – planned barometric altitude table must reflect the geometry of the DME ground station location relative to the approach ground track. Two types of DME stations are discussed:

- "ILS DME" — The DME ground station antenna is located close to the centerline of a runway equipped with an ILS localizer[§§§§] (regardless of whether an ILS glide slope system is present). These DME stations are generally low-powered and are only approved for use as an aid for approaches to the associated runway. On approach plates and other FAA documentation, ILS DMEs are designed with an "I-" prefix — e.g., I-OWD in Figure 27.
- "Airport DME" — The DME ground station is generally on the airport, but it is not associated with a runway.[*****] These DMEs generally have signal strengths sufficient to serve aircraft approaching all airport runway ends as well as in the surrounding airspace within a radius of at least 50 NM.

6.6.3 "ILS DME" Scenario

This scenario involves a straight-in CDFA at descent angle $\boldsymbol{\alpha'}$ to a runway with a DME ground station close to the runway centerline. Three locations, all on the same great circle, are involved. From the pilot's perspective, they are, in order: the aircraft, **A** (more precisely, its DME interrogator antenna); the runway threshold, **R** (more precisely, the threshold crossing location); and the DME ground station, **D** (more precisely, its antenna). In this analysis $\boldsymbol{h}$ denotes altitude above MSL, $\boldsymbol{\theta}$ denotes a geocentric angle and $\boldsymbol{d}$ denotes a slant range.

[§§§§] For some runways, the "ILS" DME ground station antenna is collocated with a Localizer antenna, and may be aligned with the centerline. It may serve both ends of the runway. For some other runways, the DME ground station antenna is between the ends of runway, as close to the centerline as possible, and serves both ends of the runway.

[*****] If it's off the airport, the "Airport" DME ground station antenna should be close to the runway centerline and either in front of or behind the aircraft throughout the approach.

The analysis is straightforward if the aircraft altitude $\boldsymbol{h_A}$ taken as the independent variable. From Section 9.2 (Eq 343) the geocentric angle $\boldsymbol{\theta_{RA}}$ between the aircraft and the threshold is

$$\theta_{RA} = \frac{\log\left(\frac{R_e + h_A}{R_e + h_R}\right)}{\tan(\alpha')} \qquad \text{Eq 157}$$

The geocentric angle between the runway threshold and the DME $\boldsymbol{\theta_{RD}}$ is known from the runway geometry and the approach plate. Reportedly, for some U.S. ILS DME installations, $\boldsymbol{\theta_{RD}}$ should be set to zero, because the fixed DME ground station delay (which is transparent to the pilot) is adjusted so that the aircraft DME reads zero at the runway threshold. This is not the case for the procedure shown in Figure 27, nor for others examined at random.

Thus the geocentric angle between the aircraft and the DME ground station $\boldsymbol{\theta_{DA}}$ is

$$\theta_{DA} = \theta_{RA} \pm \theta_{RD} \qquad \text{Eq 158}$$

The "+" sign applies if the DME is past the threshold and the "-" sign applies if the DME antanna is before the threshold.

Lastly, the slant range between the aircraft and the DME ground station $\boldsymbol{d_{DA}}$ is found from Subsection 3.4.1 (Eq 42).

$$d_{DA} = \sqrt{4(R_e + h_D)(R_e + h_A)\sin^2\left(\frac{1}{2}\theta_{DA}\right) + (h_A - h_D)^2} \qquad \text{Eq 159}$$

Remarks

- The solution for this scenario does not involve latitude or longitude coordinates — only altitudes and distances between the aircraft and destination runway.
- When generating a table for crosschecking aircraft altimeter readings against desired altitudes corresponding to DME readings, usually one would prefer to specify the slant range $\boldsymbol{d_{DA}}$ as a "nice number" (e.g., 3.0 NM) and determine the associated desired altitude $\boldsymbol{h_A}$. This is the inverse of the mathematically simpler solution approach described in this subsection. However, it can readily be achieved by "wrapping an iteration (e.g., Secant) method" around the equations of this subsection.

6.6.4 "Airport DME" Scenario

The "Airport DME" scenario is a generalization of the "ILS DME" scenario. The difference is that the aircraft location, runway threshold and DME location are not modeled as lying on the same great circle. Such situations can occur because (a) more often, the "Airport DME" is not located close to the destination runway centerline; and/or (b) less often, the approach course is

not aligned with the runway centerline (in which case a virtual threshold may be used in the analysis). In either situation, Eq 157 and Eq 159 remain valid; however, an alternative is needed for Eq 158.

The footprint on the earth's surface for this scenario is shown in Figure 28. In addition to the locations of the aircraft **A**, runway threshold **R** and DME ground station **D**, the figure shows the location **X** of the point on the approach course that is closest to the DME ground station. It is assumed that the coordinates of the threshold **R** (L_R, λ_R, h_R) and the DME station **D** (L_D, λ_D, h_D) are known, as are the azimuth angle $\psi_{A/R}$ of the approach course and the aircraft altitude h_A.

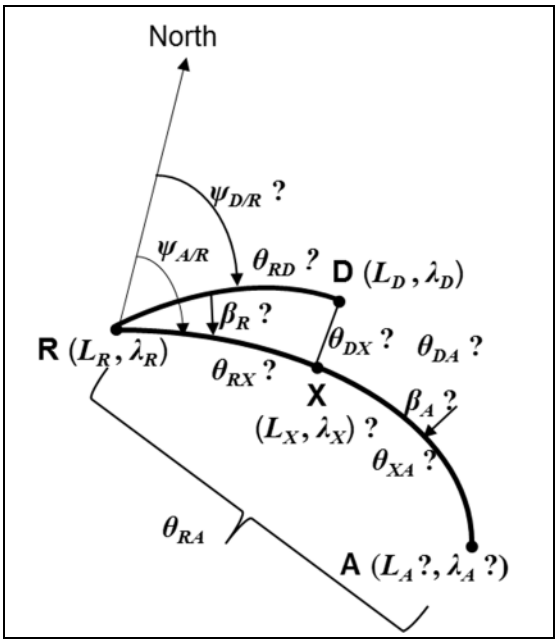

Figure 28 Relationship between Aircraft **A**, Runway **R** and DME **D**

In the case of an Airport DME, the simplest choice mathematically for the independent variable is the spherical range (angular distance along the ground) θ_{DA} between the aircraft and the DME antenna. When generating a table for operation use, one would generally prefer to perform altitude checks at defined DME readings. Or, conversely, one could perform DME checks at defined altitude readings. Tables for either of these options can be generated by iterating on Steps 1-9 in the following procedure.

Step 0 (executed once): Apply the Direct Problem of Geodesy to the path **RD** to find the distance θ_{RD} and azimuth angle $\psi_{D/R}$.

Step 1: Select θ_{DA}: A possible value for θ_{DA} is

$$\theta_{DA} = k\,\frac{\text{specified } d_{DA}}{R_e} \quad , \quad k \approx 1 \qquad \text{Eq 160}$$

Step 2: The angle β_R between **RD** and **RA** is computed in the range [0, π] using Eq 161. The cases of $\beta_R = 0$, $\beta_R = \pi/2$ and $\beta_R = \pi$ are handled separately below.

$$\beta_R = \min\left\{\left|\psi_{A/R} - \psi_{D/R}\right|,\ \left|\psi_{A/R} - \psi_{D/R} + 2\pi\right|,\ \left|\psi_{A/R} - \psi_{D/R} - 2\pi\right|\right\} \qquad \text{Eq 161}$$

Step 3: When β_R is not 0, π/2 or π, consider the spherical triangle **RXD**, where the angle at **X** is a right angle. The law of sines (Eq 58) yields the distance θ_{DX}.

$$\theta_{DX} = \arcsin\left[\sin(\theta_{RD})\sin(\beta_R)\right] \qquad \text{Eq 162}$$

While the arcsin function can have two solutions for θ_{DX} in [0, π], because $\theta_{DX} < \theta_{RD}$, only the smaller value will be consistent with signal coverage of a DME station.

Step 4: The angular distance θ_{RX} is found from the law of cosines for sides (Eq 56)

$$\theta_{RX} = \arccos\left[\frac{\cos(\theta_{RD})}{\cos(\theta_{DX})}\right] = 2\arcsin\left(\sqrt{\frac{\sin\left(\frac{1}{2}(\theta_{RD}+\theta_{DX})\right)\sin\left(\frac{1}{2}(\theta_{RD}-\theta_{DX})\right)}{\cos(\theta_{DX})}}\right) \quad \text{Eq 163}$$

Step 5: Consider the mathematical spherical triangle **AXD** The distance θ_{XA} is found from

$$\theta_{XA} = \arccos\left[\frac{\cos(\theta_{DA})}{\cos(\theta_{DX})}\right] = 2\arcsin\left(\sqrt{\frac{\sin\left(\frac{1}{2}(\theta_{DA}+\theta_{DX})\right)\sin\left(\frac{1}{2}(\theta_{DA}-\theta_{DX})\right)}{\cos(\theta_{DX})}}\right) \quad \text{Eq 164}$$

Step 6: The distance θ_{RA} is found from

$$\theta_{RA} = \left|\theta_{XA} \pm \theta_{RX}\right| \quad \text{Eq 165}$$

The plus sign is used when the DME ground station **D** lies between the runway threshold **R** and the aircraft **A**. Otherwise, the minus sign is used. The absolute value function is needed when the DME station **D** is behind the aircraft.

Step 7: To monitor the accuracy of the solution, the angle β_A is found from Eq 166. This topic is addressed in Subsection 6.6.5.

$$\beta_A = \arcsin\left[\frac{\sin(\theta_{DX})}{\sin(\theta_{DA})}\right] \quad \text{Eq 166}$$

Step 8: For an aircraft flying a CDFA with descent angle α', its planned altitude h_A for the location involved is

$$h_A = (R_e + h_R)\exp\left[\theta_{RA}\tan(\alpha')\right] - R_e \quad \text{Eq 167}$$

Step 9: Eq 159 is employed to find the aircraft-DME ground station slant range d_{DA} for the location and planned altitude involved.

Given the computed values for d_{DA} and h_A, the value for θ_{DA} can be adjusted and Steps 1-9 repeated until a specified value of d_{DA} or h_A is achieved.

If the aircraft location is to be designated as a fix, then the latitude and longitude coordinates of the fix (L_A, λ_A) are found as solutions to the Direct Problem of Geodesy (Section 4.3).

Two special cases must be considered. If $\boldsymbol{\beta_R} = 0$ or π, the DME ground station **D** lies on the great circle path containing the aircraft **A** and runway threshold **R**. In this case, Eq 162 through Eq 165 are replaced by

$$\theta_{RA} = \left| \theta_{DA} \pm \theta_{RD} \right| \qquad \text{Eq 168}$$

The plus sign is used when the DME ground station **D** lies between the runway threshold **R** and the aircraft **A**. Otherwise, the minus sign is used.

If $\boldsymbol{\beta_R} = \pi/2$ the DME station is abeam the runway threshold and the spherical triangle **ARD** has a right angle at **R**. In this case, Eq 162 through Eq 165 are replaced by

$$\theta_{RA} = \arccos\left[\frac{\cos(\theta_{DA})}{\cos(\theta_{RD})} \right] \qquad \text{Eq 169}$$

6.6.5 Remarks

For the problem formulation addressed in Subsection 6.6.4, in the majority of situations: (a) the aircraft-DME station distance is many times the aircraft altitude; and (b) high computational accuracy is not needed, since measurement errors are always present. In these situations, the aircraft-DME station ground range $\boldsymbol{\theta_{DA}}$ computed using Eq 160 with $\boldsymbol{k} = 1$ results in sufficiently accurate values of the aircraft's altitude $\boldsymbol{h_A}$ and coordinates ($\boldsymbol{L_A}$, $\boldsymbol{\lambda_A}$). In such situations, the computed slant-range $\boldsymbol{d_{DA}}$ (Eq 159) is not needed.

Two caveats are pertinent to the computations described in Subsection 6.6.4. First, in order to choose the proper sign in Eq 165 or Eq 168, the location on the approach course closest to the DME station in relation to the runway threshold and aircraft's position must be approximately known. The value of $\boldsymbol{\beta_R}$ aids in this choice — if $\boldsymbol{\beta_R} > \pi/2$ the DME station is "past" the runway threshold and a minus sign is used; this is usually the case. However, if $\boldsymbol{\beta_R} < \pi/2$, two solutions are possible — corresponding to the DME being "before" the aircraft (and, in most situations, on the airport) or "behind" the aircraft (and, in most situations, off the airport). The correct sign should not change over the entire approach.[†††††]

Related to this caveat is the fact that the angle $\boldsymbol{\beta_A}$ at the aircraft between the lines-of-sight to the runway threshold and the DME station influences the accuracy of the crosscheck on aircraft altitude. In Subsection 6.5.6, it's noted some have recommended that a DME-VOR fix only be accepted when $0° \leq \boldsymbol{\beta_A} \leq 60°$ or $120° \leq \boldsymbol{\beta_A} \leq 180°$. A similar rationale applies to this application

[†††††] This mathematical ambiguity is a manifestation of the physical fact that the locus of points at a given range from a DME station can intersect a great circle path at two points. When the DME station is beyond the runway threshold, only one intersection is meaningful.

($0° \le \boldsymbol{\beta_A} \le 60°$ applies when the DME station is ahead of the aircraft and $120° \le \boldsymbol{\beta_A} \le 180°$ when it is behind). Such a limitation on $\boldsymbol{\beta_A}$ would restrict use of this technique to portion of an NPA procedures where the DME is never abeam, or nearly abeam, the aircraft. Thus the sign in Eq 165 or Eq 168 would not change over an NPA segment where this technique is used.

The second caveat is that it is possible for to specify an aircraft-DME station slant range $\boldsymbol{d_{DA}}$ that is less than the minimum possible slant range $\boldsymbol{d_{DX}}$. Virtually always, this can be prevented by ensuring that $\boldsymbol{\theta_{DA}}$ (from Eq 160) exceeds the value of $\boldsymbol{\theta_{DX}}$ (from Eq 162, which does not require knowledge of the aircraft location).

Although the case for doing so is not as strong as it is for a NPA, the technique in this section can also be used to crosscheck aircraft altitude during an ILS or LPV approach with glide path angle $\boldsymbol{\alpha}$. Detecting capture of a false glide slope signal is perhaps the most compelling such reason (Ref. 39). To do so requires substituting for the two equations in this section that describe the vertical path. In place of Eq 157, the following (from Eq 27) would be used

$$\theta_{RA} = -\alpha + 2\arcsin\left(\sqrt{\frac{(R_e + h_R)\sin^2\left(\frac{1}{2}\alpha\right) + \frac{1}{2}(h_A - h_R)}{R_e + h_A}}\right) \qquad \text{Eq 170}$$

And in place of Eq 167, the following (from Eq 51) would be used

$$h_A = h_R + \left(\frac{\cos(\alpha)}{\cos(\alpha + \theta_{RA})} - 1\right)(R_e + h_R) \qquad \text{Eq 171}$$

7. AIRCRAFT POSITION FROM PSEUDORANGE MEASUREMENTS

7.1 Overview of Pseudoranges

7.1.1 Concept

Pseudoranges are measurements of the range (distance) between an aircraft and a set of ground‡‡‡‡‡ stations whereby all ranges are offset by the same unknown amount. This generally occurs when (a) there is a one-way transmission of energy (either from the aircraft to the ground stations [surveillance] or from the ground stations to the aircraft [navigation]), and (b) the ground stations have clocks that are synchronized but the aircraft does not. Use of pseudoranges, whereby the useful information is the difference between measured signal arrival times, has several advantages over true ranges; however, it does require deployment of an additional ground station. Pseudoranges became viable during the twentieth century, with development of technologies to synchronize widely separated ground stations, and is often the concept chosen for new system developments — e.g., GPS, Galileo and aircraft multilateration (surface and airborne).

The range involved in a pseudorange system can be either the geometric line-of-sight slant-range or the spherical-range (equivalently, the geocentric angle) between the aircraft and ground station. Currently deployed systems that employ pseudo slant-range measurements include aircraft multilateration (surveillance) and GPS (navigation). Low-frequency radionavigation systems provide pseudo spherical-range measurements based on ground-wave propagation. Examples (and their approximate station separations) are/were: Decca (100 NM), Loran-C (500-1,000 NM) and Omega (thousands of miles). All U.S. spherical-range systems are now decommissioned; however, systems are in operation in other parts of the world (Ref. 40).

When true ranges are involved and when the altitudes of the station and aircraft are known, conversion between slant- and spherical-ranges is straightforward (in either direction). For example, Eq 34 and Eq 42 demonstrate this conversion when one of the altitudes is zero, and Subsection 2.3.1 shows how to utilize two known, non-zero altitudes. Consequently, except for minor details, only one algorithm is needed to compute an aircraft's position from multiple slant- or spherical-range measurements.

However, the converse situation pertains when pseudorange measurements are involved. One cannot readily convert between pseudo slant-ranges and pseudo spherical-ranges. As a result, separate algorithms are required for each measurement type.

‡‡‡‡‡ In this terminology, navigation and surveillance satellites are "ground" stations, as they are external to the aircraft of interest and their locations are assumed to be known.

7.1.2 Pseudorange Lines-of-Position (LOPs) and Fix Geometry

One pseudorange station has no functional value. A pair of pseudorange stations measure the range difference from the stations to the aircraft (equivalent to the hyperboloid of revolution on which the aircraft is located). In a two-dimensional context, the hyperbola LOPs are shown in Figure 29(a).

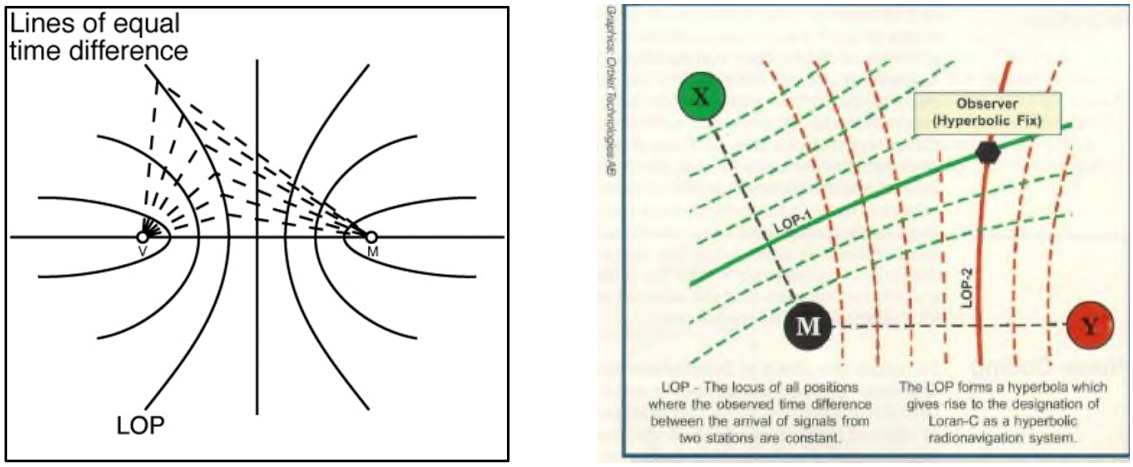

(a) Two-Station LOPs (b) Three Station Fix Geometry

Figure 29 Hyperbolic System Two-Dimensional Geometry

Hyperbolic LOPs are different from LOPs for either a true range-measuring sensor (concentric circles) or an angle-measuring sensor (radial straight lines). However, hyperbolic LOPs are closer in appearance/significance to those for an angle-measuring sensor. Specifically, LOPs for one angle station and a pair of pseudorange stations both: (a) emanate from the area when the station(s) are located and "radiate" outward; and (b) separate increasing with distance from the station(s). Conversely, a pseudorange station pair differs from a single-angle station in that its LOPs are curved and its effective coverage area is limited to approximately ±60 deg from the perpendicular bisector of the station baseline — i.e., provides coverage of only approximately ⅔ of a full circle, while one angle station provides useful information for a full circle.

Two pseudorange sensor pairs can be combined to obtain a position fix — e.g., Figure 29(b). Only one additional station is needed, as a station can be shared between pairs. To obtain an accurate measurement (e.g., LOP crossing angles between 30 deg and 150 deg), the angle between the two baselines joining station baselines should have a similar magnitude.

7.1.3 Algorithm Taxonomy

Generally, different algorithms are required for (a) different range measurement types (slant versus spherical and pseudo versus true) and (b) different analysis frameworks (two-dimensions versus three, Cartesian coordinates versus spherical) — see Table 9. Slant-range measurements

Table 9 Sources for Range-Type Algorithms and Example Applications

Measurements / Dimensions	True Slant-Ranges	Pseudo Slant-Ranges	Pseudo Spherical-Ranges
Two (Flatland or Sphere)	Unknown (Subsection 7.9.1)	Fang (Ref. 42) (Section 7.6)	Razin (Ref. 43) (Section 7.7-7.8)
	DME/DME approximation	Airport multilateration	Loran-C, Omega
Three (Physical Reality)	Unknown (Section 6.4*)	Bancroft (Ref. 41) (Sections 7.2-7.4)	N/A
	DME/DME/Altimeter	GPS, WAM	

*The algorithm for true spherical-ranges is embedded in this description.

(pseudo and true) are naturally addressed using Cartesian coordinates, while spherical-range measurements are naturally addressed using spherical coordinates.

The general three-dimensional / pseudo slant-range solution was derived by Bancroft in the 1980s, for application to GPS (Ref. 41 and Section 7.2). Bancroft's published algorithm applies to four stations that (a) measure pseudo slant-ranges, and (b) are synchronized to a single time standard. Bancroft's algorithm is derived using linear algebra, and solves for the time offset as well as the aircraft location. Bancroft's algorithm can be extended in several ways — e.g., to combinations of pseudo and true slant-range measurements, and to multiple synchronized clock groups. Sections 7.3 - 7.5 address three extensions relevant to aviation.

Prior to the publication of Bancroft's paper, individual algorithms were developed for specialized situations. These algorithms were derived based on geometry, and do not solve for the unknown time offset between the aircraft and ground station clocks. Fang's algorithm (Ref, 42 and Section 7.6) for aircraft and stations restricted to a plane, and Razin's algorithm (Ref, 43 and Section 7.7) for aircraft and stations restricted to the earth's surface, are representative examples. Section 7.8 extends Razin's algorithm to two separately-synchronized pairs of stations.

The algorithms presented in this chapter share several features with those presented in Chapter 6: (a) the earth is assumed to be a perfect sphere (except when the simpler Flatland assumption is used); (b) the number of measurements is the same as the number of unknown variables; and (c) the effects of measurement errors on the resulting position solutions are not considered. Chapter 8 addresses relaxation of all of these restrictions.

7.2 Solution for Pseudo Slant-Ranges/Cartesian Coordinates (Bancroft)

7.2.1 Background / Problem Formulation

Background — While this document emphasizes navigation/surveillance with respect to a spherical earth, situations involving a Cartesian or rectangular coordinate framework are of

interest (e.g., Chapter 5) for several reasons: (1) slant-range and pseudo slant-range measurements are more compatible with the rectangular framework than the spherical; (2) many persons find the Cartesian framework more intuitive, so it can be used to gain insights into situations where a spherical framework is more convenient for obtaining numerical results; and (3) a Cartesian framework is often required when the earth's ellipticity must be taken into account.

For emphasis, it's noted that this section addresses a situation involving four pseudo slant-range (i.e., homogeneous) measurements. Bancroft's algorithm can be extended situations involving only true slant-range measurements (including aircraft altitude), or a combination of pseudo and true slant-range measurements — Sections 7.3 and 7.4, respectively. Bancroft's algorithm can also be employed in situations involving multiple clock synchronization groups — Section 7.5.

Coordinate Frame — The first step is the selection of an analysis origin. The analysis origin must be is different from the location of any station, and must satisfy other conditions discussed below. As will become evident, the Bancroft method is an elegant application of the cosine law of plane trigonometry, and involves triangles with vertices at the analysis origin (known), the station location (known) and the aircraft location (unknown). The side connecting the analysis origin and the aircraft is common to all triangles, and is found first. The other two sides of each triangle then follow readily.

For most problems, the Earth-Centered, Earth-Fixed (ECEF, Subsection 5.1.1) is a good choice. In ECEF coordinates, the physical stations are located at

$$\underline{\mathbf{r}}_i^{\mathbf{e}} = \begin{bmatrix} x_i^e \\ y_i^e \\ z_i^e \end{bmatrix} = \begin{bmatrix} \cos(L_i)\cos(\lambda_i) \\ \cos(L_i)\sin(\lambda_i) \\ \sin(L_i) \end{bmatrix} (R_e + h_i) \qquad i = 1,2,3,4 \qquad \text{Eq 172}$$

Here, $\boldsymbol{L_i}$, $\boldsymbol{\lambda_i}$ and $\boldsymbol{h_i}$ denote the latitude, longitude and altitude (respectively) of station *i*.

Using similar notation, the (unknown) coordinates of the aircraft are

$$\underline{\mathbf{r}}_A^e = \begin{bmatrix} x_A^e & y_A^e & z_A^e \end{bmatrix}^T \qquad \text{Eq 173}$$

For convenience, since quadratic quantities will be involved, use of the superscript **e** on $\underline{\mathbf{r}}_A^e$ and $\underline{\mathbf{r}}_i^e$ and their components is discontinued until the end of this section.

The aircraft-station pseudo slant-range measurements satisfy an equation of the form

$$\begin{aligned} &(x_A - x_i)^2 + (y_A - y_i)^2 + (z_A - z_i)^2 = (ct_i - ct_A)^2 \\ &\left((x_A)^2 + (y_A)^2 + (z_A)^2 - (ct_A)^2\right) + \left((x_i)^2 + (y_i)^2 + (z_i)^2 - (ct_i)^2\right) = \cdots \\ &\qquad \cdots 2\left(x_i x_A + y_i y_A + z_i z_A - c^2 t_i t_A\right) \qquad i = 1,2,3,4 \end{aligned} \qquad \text{Eq 174}$$

Here t_A denotes the unknown time of transmission by the aircraft and t_i the measured time of reception by ground station *i*.

In vector-matrix notation, the second lines of Eq 174 thru Eq 197 can be combined as

$$2\mathbf{B}\underline{\mathbf{s}}_A = \lambda\mathbf{1} + \mathbf{b} \qquad \text{Eq 175}$$

$$\underline{\mathbf{s}}_A \equiv \begin{bmatrix} \underline{\mathbf{r}}_A \\ ct_A \end{bmatrix} = \begin{bmatrix} x_A & y_A & z_A & ct_A \end{bmatrix}^T$$

$$\mathbf{B} = \begin{bmatrix} x_1 & y_1 & z_1 & -ct_1 \\ x_2 & y_2 & z_2 & -ct_2 \\ x_3 & y_3 & z_3 & -ct_3 \\ x_4 & y_4 & z_4 & -ct_4 \end{bmatrix}$$

$$\lambda = \langle \underline{\mathbf{s}}_A, \underline{\mathbf{s}}_A \rangle = (x_A)^2 + (y_A)^2 + (z_A)^2 - (ct_A)^2$$

$$\mathbf{1} = \begin{bmatrix} 1 & 1 & 1 & 1 \end{bmatrix}^T$$

$$\mathbf{b} = \begin{bmatrix} (x_1)^2 + (y_1)^2 + (z_1)^2 - (ct_1)^2 \\ (x_2)^2 + (y_2)^2 + (z_2)^2 - (ct_2)^2 \\ (x_3)^2 + (y_3)^2 + (z_3)^2 - (ct_3)^2 \\ (x_4)^2 + (y_4)^2 + (z_4)^2 - (ct_4)^2 \end{bmatrix}$$

Eq 175 relates $\underline{\mathbf{s}}_A$ to its Lorentzian norm λ.

7.2.2 Problem Solution

Matrix **B** is nonsingular when (and only when) its rows are linearly independent. Assuming that to be true, the formal solution for $\underline{\mathbf{s}}_A$ is

$$\underline{\mathbf{s}}_A = \tfrac{1}{2}\lambda\mathbf{B}^{-1}\mathbf{1} + \tfrac{1}{2}\mathbf{B}^{-1}\mathbf{b} \qquad \text{Eq 176}$$

Eq 176 can be written as

$$\underline{\mathbf{s}}_A = \lambda\underline{\mathbf{u}} + \underline{\mathbf{v}} \qquad \text{Eq 177}$$

$$\underline{\mathbf{u}} = \tfrac{1}{2}\mathbf{B}^{-1}\mathbf{1} = \begin{bmatrix} u_x & u_y & u_z & u_t \end{bmatrix}^T$$
$$\underline{\mathbf{v}} = \tfrac{1}{2}\mathbf{B}^{-1}\mathbf{b} = \begin{bmatrix} v_x & v_y & v_z & v_t \end{bmatrix}^T$$

The Lorentzian norm λ of $\underline{\mathbf{s}}_A$ in Eq 177 can be found by (a) left-multiplying both sides of the equation by the diagonal matrix with diagonal elements (1,1,1,-1), then (b) left-multiplying both sides by the transpose of Eq 177. Upon collecting like terms, the result is

$$\alpha\lambda^2 + \beta\lambda + \gamma = 0 \qquad \text{Eq 178}$$

$$\alpha = \langle \underline{\mathbf{u}}, \underline{\mathbf{u}} \rangle = u_x^2 + u_y^2 + u_z^2 - u_t^2$$
$$\beta = 2\langle \underline{\mathbf{u}}, \underline{\mathbf{v}} \rangle - 1 = 2u_x v_x + 2u_y v_y + 2u_z v_z - 2u_t v_t - 1$$
$$\gamma = \langle \underline{\mathbf{v}}, \underline{\mathbf{v}} \rangle = v_x^2 + v_y^2 + v_z^2 - v_t^2$$

Usually, Eq 178 has two real roots

$$\lambda_+ = \frac{1}{2\alpha}\left(-\beta + \sqrt{\beta^2 - 4\alpha\gamma}\right)$$
$$\lambda_- = \frac{1}{2\alpha}\left(-\beta - \sqrt{\beta^2 - 4\alpha\gamma}\right) \qquad \text{Eq 179}$$

Thus there are two possible solutions for the aircraft state $\underline{\mathbf{s}}_A$

$$\underline{\mathbf{s}}_A(\pm) = \lambda_\pm \underline{\mathbf{u}} + \underline{\mathbf{v}} = \begin{bmatrix} x_A(\pm) \\ y_A(\pm) \\ z_A(\pm) \\ ct_A(\pm) \end{bmatrix} = \begin{bmatrix} \underline{\mathbf{r}}_A(\pm) \\ ct_A(\pm) \end{bmatrix} \qquad \text{Eq 180}$$

One of the two solutions is correct; the other may be either

- Ambiguous — mathematically and physically possible, but not correct.
- Extraneous — mathematically but not physically possible, introduced by analytic manipulations.

The penultimate step is determining the two possible sets of aircraft latitude/longitude/altitude coordinates. Reintroducing the superscript **e** to denote coordinate frames

$$L_A(\pm) = \arctan\left(\frac{z_A^e(\pm)}{\sqrt{\left(x_A^e(\pm)\right)^2 + \left(y_A^e(\pm)\right)^2}}\right)$$
$$\lambda_A(\pm) = \arctan\left(y_A^e(\pm)\,,\, x_A^e(\pm)\right) \qquad \text{Eq 181}$$
$$h_A(\pm) = \sqrt{\left(x_A^e(\pm)\right)^2 + \left(y_A^e(\pm)\right)^2 + \left(z_A^e(\pm)\right)^2} - R_e$$

In Eq 180 and Eq 181, a single sign, + or -, must be used consistently. The final step is selecting between the two possible solutions.

7.2.3 Remarks

Coordinate Frames — Cartesian coordinate frame employed for Bancroft's algorithm can be related to either a spherical or ellipsoidal earth model. Compatibility with an ellipsoidal earth is

an advantage when the sensor-aircraft ranges are several hundred miles or more.

If a spherical-earth model underlies the Cartesian frame, then aircraft altitude can be used as a measurement without additional considerations. If an ellipsoidal earth model underlies the Cartesian frame, then obtaining the maximum benefit from aircraft altitude may require iteration.

Invertibility of Matrix B — General, physically meaningful conditions for the invertibility of the 4x4 matrix **B** (Eq 175) are not obvious. However, when only slant-range and altitude measurements are involved, **B** reduces to a 3x3 matrix containing the components of the three origin-to-station vectors. This is a well-known situation, and yields the requirements that the analysis origin cannot (a) lie in the plane containing the three stations, or (b) lie along any baseline connecting two stations (or the extensions past the stations). With three physical slant-range stations, selecting the origin to be below the plane of the stations, and with its latitude/ longitude near the middle of the triangle formed by the stations, appears to be a good choice. For the situation involving two physical stations and an altitude measurement, the analysis origin should be well removed from the baseline connecting the stations (and its extensions).

When only slant-range and altitude measurements are involved, matrix **B** is independent of the measurements. It is possible to compute the inverse once and utilize it for several sets of measurements. However, for pseudo slant-range measurements, matrix **B** does depend on measured times-of-arrival of signals at the pseudo slant-range stations. If a sequence of measurements are collected over time, matrix **B** and its inverse must be recomputed for each set of measurements.

Number / Types of Solutions — Solution possibilities for Eq 178 are (bearing in mind that not all problems have all solution types):

(a) No real roots: Mathematically, $\beta^2 < 4\alpha\gamma$; geometrically, the LOPs/SOPs do not intersect; practically, this situation is generally the result of measurement error

(b) One real single root: Mathematically, $\alpha = 0$; geometrically, the LOPs cannot all be closed curves/surfaces (e.g., circles); physically, the problem must involve pseudoranges, so that the LOPs/SOPs have two branches, one pair crosses and the other pair does not; practically, this is a rare situation

(c) A real double root: Mathematically, $\beta^2 = 4\alpha\gamma$; geometrically, two or more of the SOPs are tangent, and in a three dimensional problem, the other SOP passes through the point of tangency; practically, this is a rare situation

(d) Two real roots: Mathematically, $4\alpha\gamma < \beta^2$; physically, the LOPs/SOPs intersect at two distinct points; practically, this is the most common situation, and is discussed below.

Elaborating on case (d): When two real solutions occur, one solution is correct and the other is

either ambiguous or extraneous. An ambiguous solution satisfies the measurement equations; additional information is required to determine which solution is correct. When only real slant-range measurements are involved, only an ambiguous solution will occur. An extraneous solution does not satisfy measurement equations. When only pseudo slant-range measurements are involved, an either an ambiguous or an extraneous solution may occur. One method of detection is to substitute the solutions into the measurement equations.

When pseudo slant-range measurements are involved, an ambiguous or extraneous solution can arise from the squaring of the time differences in Eq 174, as squaring destroys the sign of the time differences t_i - t_A. When there is an extraneous solution, the solution for the aircraft time of transmission t_A can be used to detect it — the correct value for t_A being less than min(t_1, t_2) and the extraneous value being greater than max(t_1, t_2). Generally, for pseudo slant-range systems, ambiguous solutions only occur when the aircraft is near an extended baseline connecting two stations; when the measurement geometry is more favorable (i.e., at locations where the system intended to be used), only detectable extraneous solutions occur (Ref. 44).

Relationship to Traditional Solutions — Bancroft's algorithm is readily programmed, but is not conducive to developing analytic expressions for the aircraft's position as a function of the measurements. Thus, when available, traditional solutions to problems involving real and pseudo slant-ranges (e.g., three of the four problem cases shown in Table 9) — which are analytically equivalent to Bancroft's — remain valuable, particularly during the planning and design stages of a project.

Other Comments

- Bancroft noted that his algorithm "performs better than an iterative solution in regions of poor GDOP". The most common Gauss-Newton iterative, linearized least-squares solution method is addressed in Chapter 8.
- Bancroft's solution has been extended to situations involving more measurements than unknown variables (Ref. 45). Those equations are not employed herein, as the linearized least squares method addressed in Chapter 8 is preferred (Ref. 46).
- Alternative solutions to the four-pseudo slant-range problem were published after Bancroft's paper (e.g., Ref. 47).
- There are scenarios where Bancroft's algorithm can used in lieu of other solution methods. An example is two real slant-range and one altimeter measurement; the alternative solution method is described in Section 6.4.

7.3 Solution for Slant-Ranges/Cartesian Coordinates (Bancroft Extensions)

7.3.1 Background / Motivation

Bancroft's algorithm (Section 7.2) was derived for four pseudo slant-range measurements. Its

extension to three true slant-range measurements, or to two true slant-range measurements and an altitude measurement, is the topic of this Section. Bancroft's algorithm can also be extended to situations involving a combination of pseudo slant-range and true slant-range measurements; however, the analysis is more complex; Sections 7.4 and 0 address two relevant situations.

7.3.2 Three Slant-Range Measurements

The situation involving three true slant-range measurements is similar to the topic of Section 7.2 (involving four pseudo slant-range measurements); thus, only the differences will be pointed out. In this case, the slant-range measurement between the aircraft **A** and ground station *i* is

$$\begin{gathered}(x_A-x_i)^2+(y_A-y_i)^2+(z_A-z_i)^2=d_{iA}^2 \qquad i=1,2,3 \\ \left((x_A)^2+(y_A)^2+(z_A)^2\right)+\left((x_i)^2+(y_i)^2+(z_i)^2-d_{iA}^2\right)=2\left(x_i x_A+y_i y_A+z_i z_A\right)\end{gathered} \qquad \text{Eq 182}$$

As a consequence of omitting the time component, the Lorentzian norm is replaced by the Euclidean norm

$$\lambda=\langle \underline{\mathbf{r}}_A,\underline{\mathbf{r}}_A\rangle=(x_A)^2+(y_A)^2+(z_A)^2 \qquad \text{Eq 183}$$

Also, matrix **B** and vectors **b** and **1** become

$$\mathbf{B}=\begin{bmatrix}x_1 & y_1 & z_1\\ x_2 & y_2 & z_2\\ x_3 & y_3 & z_3\end{bmatrix} \qquad \text{Eq 184}$$

$$\mathbf{b}=\begin{bmatrix}(x_1)^2+(y_1)^2+(z_1)^2-(d_{1A})^2\\ (x_2)^2+(y_2)^2+(z_2)^2-(d_{2A})^2\\ (x_3)^2+(y_3)^2+(z_3)^2-(d_{3A})^2\end{bmatrix} \qquad \mathbf{1}=\begin{bmatrix}1\\1\\1\end{bmatrix} \qquad \text{Eq 185}$$

With these substitutions, Eq 175 becomes (with $\underline{\mathbf{s}}_A$ is replaced by $\underline{\mathbf{r}}_A$)

$$2\mathbf{B}\underline{\mathbf{r}}_A=\lambda\mathbf{1}+\mathbf{b} \qquad \text{Eq 186}$$

The solution then proceeds as in Section 7.2 using three-element vectors in place of four-element vectors (i.e., without involving transmission time).

Remarks:

- Two-dimensional application of this subsection is presented in Subsection 7.9.1.
- Subsection 7.2.3 addresses the invertibility of matrix **B**.

7.3.3 Two Slant-Ranges and an Altitude Measurement

Bancroft's algorithm can also be applied to situations involving two slant-range measurements and a measurement of aircraft altitude, as (for a spherical-earth formulation) an altitude measurement can be converted to a slant-range from the center of the earth. However, when altitude is used as the third measurement, an extra step is involved in the solution. For the Bancroft **B** matrix (e.g., Eq 184) to be inverted, the analysis origin must be is different from the location of any station. Thus, an analysis origin offset from the center of the earth must be used.

One possible analysis origin, in ECEF coordinates, is of the form

$$\underline{\mathbf{r}}_o^{\mathbf{e}} = \begin{bmatrix} x_o^e \\ y_o^e \\ z_o^e \end{bmatrix} = \begin{bmatrix} \cos(L_o)\cos(\lambda_o) \\ \cos(L_o)\sin(\lambda_o) \\ \sin(L_o) \end{bmatrix} kR_e \qquad \text{Eq 187}$$

Here $\boldsymbol{L_o}$ and $\boldsymbol{\lambda_o}$ are the latitude and longitude of an arbitrary point not on the baseline connecting the stations and k is a number slightly less than 1 — e.g., 0.97.

In ECEF coordinates, the physical stations locations are given by Eq 172, with i=1,2. The associated measurements equations are given by Eq 182, with i=1,2.

The aircraft altitude h_A measurement equation is

$$(x_A)^2 + (y_A)^2 + (z_A)^2 = (R_e + h_A)^2 \qquad \text{Eq 188}$$

The altitude measurement "station" is the earth's center, with ECEF coordinates given by:

$$\underline{\mathbf{r}}_3^{\mathbf{e}} = \begin{bmatrix} 0 & 0 & 0 \end{bmatrix}^T \qquad \text{Eq 189}$$

Bancroft's algorithm is then applied using offset station coordinates

$$\Delta\underline{\mathbf{r}}_i^{\mathbf{e}} = \underline{\mathbf{r}}_i^{\mathbf{e}} - \underline{\mathbf{r}}_o^{\mathbf{e}} = \begin{bmatrix} x_i^e \\ y_i^e \\ z_i^e \end{bmatrix} - \begin{bmatrix} x_o^e \\ y_o^e \\ z_o^e \end{bmatrix} = \begin{bmatrix} x_i^e - x_o^e \\ y_i^e - y_o^e \\ z_i^e - z_o^e \end{bmatrix} = \begin{bmatrix} \Delta x_i^e \\ \Delta y_i^e \\ \Delta z_i^e \end{bmatrix} \qquad i = 1,2,3 \qquad \text{Eq 190}$$

Matrix **B** and vector **b** are

$$\mathbf{B} = \begin{bmatrix} \Delta x_1 & \Delta y_1 & \Delta z_1 \\ \Delta x_2 & \Delta y_2 & \Delta z_2 \\ \Delta x_3 & \Delta y_3 & \Delta z_3 \end{bmatrix} \qquad \text{Eq 191}$$

$$\mathbf{b} = \begin{bmatrix} (\Delta x_1)^2 + (\Delta y_1)^2 + (\Delta z_1)^2 - (d_{1A})^2 \\ (\Delta x_2)^2 + (\Delta y_2)^2 + (\Delta z_2)^2 - (d_{2A})^2 \\ (\Delta x_3)^2 + (\Delta y_3)^2 + (\Delta z_3)^2 - (R_e + h_A)^2 \end{bmatrix} \qquad \text{Eq 192}$$

The aircraft's location is found relative to the analysis origin

$$\Delta \underline{\mathbf{r}}_A^e \equiv \begin{bmatrix} \Delta x_A^e & \Delta y_A^e & \Delta z_A^e \end{bmatrix}^T \qquad \text{Eq 193}$$

The solution for $\Delta \underline{\mathbf{r}}_A^e$ is then converted to ECEF coordinates using Eq 190, which in turn is used to find the aircraft latitude and longitude using Eq 181.

The solution method described in this subsection is an alternative to that in Section 6.4.

7.4 Solution for Three Pseudo Slant-Ranges and an Altitude Measurement

7.4.1 Introduction

In terms of system functionality, this section is closely related to Sections 7.6 and 7.7. Each section addresses the determination of an aircraft's location based on the time difference of arrival of signals at/from a triad of stations. The difference is the analysis framework: whereas the following two sections assume that the aircraft is restricted to a flat earth (Section 7.6) or that its altitude does not affect the pseudo spherical-range measurements (Section 7.7), this section considers a spherical earth and all three dimensions.

A modified version of Bancroft's algorithm is employed for this task. Three scalar equations describe the pseudorange measurements by the multilateration ground stations, and one equation describes the altitude measurement. As often occurs when more than one measurement type are utilized, the resulting expressions are more complex than are the expressions for a homogeneous set of measurements.

7.4.2 Problem Formulation

The three physical ground stations have the known locations latitude $\boldsymbol{L_i}$, longitude $\boldsymbol{\lambda_i}$, and altitude $\boldsymbol{h_i}$, where i = 1, 2 or 3. In ECEF coordinates, their locations are

$$\underline{\mathbf{r}}_i^{\mathbf{e}} = \begin{bmatrix} x_i^e \\ y_i^e \\ z_i^e \end{bmatrix} = \begin{bmatrix} \cos(L_i)\cos(\lambda_i) \\ \cos(L_i)\sin(\lambda_i) \\ \sin(L_i) \end{bmatrix} (R_e + h_i) \qquad i = 1,2,3 \qquad \text{Eq 194}$$

The unknown ECEF coordinates of the aircraft are

$$\underline{\mathbf{r}}_A^e = \begin{bmatrix} x_A^e & y_A^e & z_A^e \end{bmatrix}^T \qquad \text{Eq 195}$$

For convenience, since quadratic quantities will be involved, use of the superscript **e** on $\underline{\mathbf{r}}_A^e$ and $\underline{\mathbf{r}}_i^e$ and their components is discontinued until the end of this section.

The aircraft-station pseudo slant-range measurements satisfy equations of the form

$$\begin{aligned} &\left((x_A)^2+(y_A)^2+(z_A)^2-(ct_A)^2\right)+\left((x_i)^2+(y_i)^2+(z_i)^2-(ct_i)^2\right)=\cdots \\ &\cdots 2\left(x_i x_A + y_i y_A + z_i z_A - c^2 t_i t_A\right) \qquad i=1,2,3 \end{aligned} \qquad \text{Eq 196}$$

Here t_A denotes the unknown time of transmission by the aircraft and t_i the measured time of reception by ground station *i*.

The aircraft altitude h_A measurement equation is

$$(x_A)^2+(y_A)^2+(z_A)^2=(R_e+h_A)^2 \qquad \text{Eq 197}$$

In vector-matrix notation, Eq 196 and Eq 197 can be written as

$$2\,\mathbf{B}\,\underline{\mathbf{r}}_A = \mathbf{b} + (R_e+h_A)^2\mathbf{1} + 2c^2\mathbf{t}\,t_A - c^2\mathbf{1}(t_A)^2 \qquad \text{Eq 198}$$

$$\mathbf{B}=\begin{bmatrix} x_1 & y_1 & z_1 \\ x_2 & y_2 & z_2 \\ x_3 & y_3 & z_3 \end{bmatrix}$$

$$\mathbf{b}=\begin{bmatrix} (x_1)^2+(y_1)^2+(z_1)^2-(ct_1)^2 \\ (x_2)^2+(y_2)^2+(z_2)^2-(ct_2)^2 \\ (x_3)^2+(y_3)^2+(z_3)^2-(ct_3)^2 \end{bmatrix} \qquad \mathbf{1}=\begin{bmatrix} 1 \\ 1 \\ 1 \end{bmatrix} \qquad \mathbf{t}=\begin{bmatrix} t_1 \\ t_2 \\ t_3 \end{bmatrix}$$

7.4.3 Problem Solution

Inverting matrix **B** and solving Eq 198 for $\underline{\mathbf{r}}_A$ yields

$$\underline{\mathbf{r}}_A = \mathbf{u} + \mathbf{v}\,t_A + \mathbf{w}(t_A)^2 \qquad \text{Eq 199}$$

$$\mathbf{u} = \tfrac{1}{2}\mathbf{B}^{-1}\left(\mathbf{b} + (R_e+h_A)^2\mathbf{1}\right) \qquad \mathbf{v} = c^2\mathbf{B}^{-1}\mathbf{t} \qquad \mathbf{w} = -\tfrac{1}{2}c^2\mathbf{B}^{-1}\mathbf{1}$$

Taking the Euclidian norm of $\underline{\mathbf{r}}_A$ in Eq 199 and using Eq 197 yields a quartic equation in t_A

$$a_4(t_A)^4 + a_3(t_A)^3 + a_2(t_A)^2 + a_1 t_A + a_0 = 0 \qquad \text{Eq 200}$$

$$a_4 = \mathbf{w}^T\mathbf{w} \qquad a_3 = 2\mathbf{v}^T\mathbf{w} \qquad a_2 = 2\mathbf{u}^T\mathbf{w} + \mathbf{v}^T\mathbf{v}$$

$$a_1 = 2\mathbf{u}^T\mathbf{v} \qquad a_0 = \mathbf{u}^T\mathbf{u} - (R_e+h_A)^2$$

When t_A is found as a root of Eq 200 (see Remarks below), $\underline{\mathbf{r}}_A^e$ follows from Eq 199. Then the aircraft latitude $\boldsymbol{L_A}$ and longitude $\boldsymbol{\lambda_A}$ are given by Eq 181.

7.4.4 Remarks

Fang's algorithm (Section 7.6) considers the situation of three pseudo slant-range stations in a Cartesian plane. The simplicity of that situation enables development of insights into the three-station pseudorange problem which are less apparent in a spherical context. However, the behavior of the solutions are qualitatively similar — particularly, the occurrence of a readily-identified extraneous solution when the aircraft in the service area and the the occurrence of a unresolvable ambiguous solution when the aircraft is near a baseline extension.

There is an algebraic formula for the roots of a quartic polynomial equation such as Eq 200. Thus the algorithm presented herein can be classified as non-iterative. The Matlab routine 'roots' implements a version of the quartic formula; in limited testing, it performed reliably (Example 12, Subsection 7.9.5). During those tests, for aircraft locations in the service area, the correct root of Eq 200 was obvious based on physical considerations.

7.5 Solution for Two Pairs of Pseudo Slant-Ranges and Altitude

7.5.1 Introduction

In terms of the functionality of the system involved, this section is most closely related to Section 7.4. Each addresses the determination of an aircraft's location based on of time-difference-of-arrival measurements of slant-range signals for a set of ground stations, plus knowledge of the aircraft's altitude. However, whereas the preceding section assumes three ground stations with synchronized clocks, this section assumes two pairs of ground stations with the clocks for each pair being separately synchronized. This section is also related to Section 7.8, which addresses the determination of an aircraft's location based on time-difference-of-arrival measurements of spherical-range signals for two pairs of separately synchronized ground stations.

Unsynchronized slant-range differences can arise if one were to combine measurements from two separate navigation systems — e.g., GPS and Galileo. In the context of multilateration, it could arise as the result of a failure in the ground station synchronization network or intentionally, as an aspect of the system design. Loran-C 'cross-chaining' involves similar assumptions concerning station time synchronization.

7.5.2 Problem Formulation

One ground station pair is labeled **R** and **S**; the other is labeled **U** and **V**. The ground stations

have the known locations latitude $\boldsymbol{L_i}$, longitude $\boldsymbol{\lambda_i}$, and altitude $\boldsymbol{h_i}$, where i = R, S, U or V. In ECEF coordinates, their locations are

$$\underline{\mathbf{r}}_i^{\mathbf{e}} = \begin{bmatrix} x_i^e \\ y_i^e \\ z_i^e \end{bmatrix} = \begin{bmatrix} \cos(L_i)\cos(\lambda_i) \\ \cos(L_i)\sin(\lambda_i) \\ \sin(L_i) \end{bmatrix} (R_e + h_i) \qquad i = R,S,U,V \qquad \text{Eq 201}$$

The altitude measurement "station", labeled **H**, is the earth's center, with ECEF coordinates given by:

$$\underline{\mathbf{r}}_H^{\mathbf{e}} = \begin{bmatrix} 0 & 0 & 0 \end{bmatrix}^T \qquad \text{Eq 202}$$

The unknown ECEF coordinates of the aircraft labeled **A**, are

$$\underline{\mathbf{r}}_A^{\,e} = \begin{bmatrix} x_A^{\,e} & y_A^{\,e} & z_A^{\,e} \end{bmatrix}^T \qquad \text{Eq 203}$$

Since altitude will be utilized as a measurement — rather than as a constraint, as in Section 7.4 — an analysis origin offset from the earth's center must be used. One possible origin, in ECEF coordinates, is of the form

$$\underline{\mathbf{r}}_o^{\mathbf{e}} = \begin{bmatrix} x_o^e \\ y_o^e \\ z_o^e \end{bmatrix} = \begin{bmatrix} \cos(L_o)\cos(\lambda_o) \\ \cos(L_o)\sin(\lambda_o) \\ \sin(L_o) \end{bmatrix} kR_e \qquad \text{Eq 204}$$

Here $\boldsymbol{L_o}$ and $\boldsymbol{\lambda_o}$ are the latitude and longitude of an arbitrary point not on the baseline connecting the stations and k is a number slightly less than 1 — e.g., 0.97. Bancroft's algorithm is then applied using offset station coordinates

$$\Delta\underline{\mathbf{r}}_i^{\mathbf{e}} = \underline{\mathbf{r}}_i^{\mathbf{e}} - \underline{\mathbf{r}}_o^{\mathbf{e}} = \begin{bmatrix} x_i^e \\ y_i^e \\ z_i^e \end{bmatrix} - \begin{bmatrix} x_o^e \\ y_o^e \\ z_o^e \end{bmatrix} = \begin{bmatrix} x_i^e - x_o^e \\ y_i^e - y_o^e \\ z_i^e - z_o^e \end{bmatrix} = \begin{bmatrix} \Delta x_i^e \\ \Delta y_i^e \\ \Delta z_i^e \end{bmatrix} \qquad i = R,S,U,V,H \qquad \text{Eq 205}$$

Thus the aircraft's location is first found relative to the analysis origin

$$\Delta\underline{\mathbf{r}}_A^{\mathbf{e}} = \underline{\mathbf{r}}_A^{\mathbf{e}} - \underline{\mathbf{r}}_o^{\mathbf{e}} = \begin{bmatrix} \Delta x_A^e & \Delta y_A^e & \Delta z_A^e \end{bmatrix}^T \qquad \text{Eq 206}$$

For convenience, since quadratic quantities will be involved, use of the superscript **e** on $\underline{\mathbf{r}}_A^{\mathbf{e}}$ and $\underline{\mathbf{r}}_i^{\mathbf{e}}$ and their components is discontinued until the end of this section. Also, without loss of generality, the description will use the terminology of a multilateration system.

For stations **R** and **S**, the aircraft-station pseudo slant-range measurements satisfy

$$\begin{aligned}\left((\Delta x_A)^2+(\Delta y_A)^2+(\Delta z_A)^2-(ct_{RS})^2\right)+\left((\Delta x_i)^2+(\Delta y_i)^2+(\Delta z_i)^2-(ct_i)^2\right)=\cdots\\ \cdots 2\left(\Delta x_i\Delta x_A+\Delta y_i\Delta y_A+\Delta z_i\Delta z_A-c^2t_it_{RS}\right)\qquad i=R,S\end{aligned}\qquad \text{Eq 207}$$

Similarly, for stations **U** and **V**, the aircraft-station pseudo slant-range measurements satisfy

$$\begin{aligned}\left((\Delta x_A)^2+(\Delta y_A)^2+(\Delta z_A)^2-(ct_{UV})^2\right)+\left((\Delta x_i)^2+(\Delta y_i)^2+(\Delta z_i)^2-(ct_i)^2\right)=\cdots\\ \cdots 2\left(\Delta x_i\Delta x_A+\Delta y_i\Delta y_A+\Delta z_i\Delta z_A-c^2t_it_{UV}\right)\qquad i=U,V\end{aligned}\qquad \text{Eq 208}$$

Here t_{RS} denotes the unknown time of transmission by the aircraft based on the clock for stations **R** and **S**. Similarly t_{UV} denotes the unknown time of transmission by the aircraft based on the clock for stations **U** and **V**. Also, t_i the measured time of reception by ground station *i* based on its clock group.

The aircraft altitude h_A measurement equation is

$$\begin{aligned}\left((\Delta x_A)^2+(\Delta y_A)^2+(\Delta z_A)^2\right)+\left((\Delta x_H)^2+(\Delta y_H)^2+(\Delta z_H)^2-(R_e+h_A)^2\right)=\cdots\\ \cdots 2\left(\Delta x_H\Delta x_A+\Delta y_H\Delta y_A+\Delta z_H\Delta z_A\right)\end{aligned}\qquad \text{Eq 209}$$

7.5.3 Problem Solution

The solution approach is to: (1) consider station pair **R** and **S**, in conjunction with "station" **H**, and find a relationship between the aircraft time of transmission t_{RS} and the square of the distance between the analysis origin and the aircraft λ; (2) consider station pair **U** and **V** in conjunction with **H**, and find a relationship between t_{UV} and λ; and (3) consider both pairs of stations and find an additional relationship between t_{RS} and λ (and/or between t_{UV} and λ). Combining the relationships found in (1) and (3) (or (2) and (3)) results in a quartic polynomial in t_{RS} (and/or t_{UV}) for which a closed-form solution exists. All other results then follow readily.

Analysis of Stations R and S — First selecting stations **R** and **S** and the altitude measurement for analysis, Eq 207 and Eq 209 can be written as

$$2\,\mathbf{B}_{RS}\,\Delta\underline{\mathbf{r}}_A=\mathbf{b}_{RS}+\lambda\mathbf{1}_3+2c^2\mathbf{t}_{RS}\,t_{RS}-c^2\mathbf{1}_2t_{RS}^2 \qquad \text{Eq 210}$$

$$\mathbf{B}_{RS}=\begin{bmatrix}\Delta\underline{\mathbf{r}}_R^T\\ \Delta\underline{\mathbf{r}}_S^T\\ \Delta\underline{\mathbf{r}}_H^T\end{bmatrix}=\begin{bmatrix}\Delta x_R & \Delta y_R & \Delta z_R\\ \Delta x_S & \Delta y_S & \Delta z_S\\ \Delta x_H & \Delta y_H & \Delta z_H\end{bmatrix}$$

$$\mathbf{b}_{RS}=\begin{bmatrix}(\Delta x_R)^2+(\Delta y_R)^2+(\Delta z_R)^2-(ct_R)^2\\ (\Delta x_S)^2+(\Delta y_S)^2+(\Delta z_S)^2-(ct_S)^2\\ (\Delta x_H)^2+(\Delta y_H)^2+(\Delta z_H)^2-(R_e+h_A)^2\end{bmatrix}$$

$$\lambda = (\Delta x_A)^2 + (\Delta y_A)^2 + (\Delta z_A)^2$$

$$\mathbf{1}_3 = \begin{bmatrix} 1 & 1 & 1 \end{bmatrix}^T \qquad \mathbf{1}_2 = \begin{bmatrix} 1 & 1 & 0 \end{bmatrix}^T \qquad \mathbf{t}_{RS} = \begin{bmatrix} t_R & t_S & 0 \end{bmatrix}^T$$

Inverting matrix $\mathbf{B}_{RS}$ yields

$$\Delta \underline{\mathbf{r}}_A = \mathbf{c}_{RS} + \mathbf{d}_{RS}\lambda + \mathbf{e}_{RS} t_{RS} + \mathbf{f}_{RS} t_{RS}^2 \qquad \text{Eq 211}$$

$$\mathbf{c}_{RS} = \tfrac{1}{2}\mathbf{B}_{RS}^{-1}\,\mathbf{b}_{RS} \qquad \mathbf{d}_{RS} = \tfrac{1}{2}\mathbf{B}_{RS}^{-1}\,\mathbf{1}_3$$

$$\mathbf{e}_{RS} = c^2\mathbf{B}_{RS}^{-1}\,\mathbf{t}_{RS} \qquad \mathbf{f}_{RS} = -\tfrac{1}{2}c^2\mathbf{B}_{RS}^{-1}\,\mathbf{1}_2$$

Taking the Euclidian norm of $\Delta\underline{\mathbf{r}}_A$ in Eq 211 and collecting terms yields

$$\begin{aligned} &a_{RS,40}\,t_{RS}^4 + a_{RS,30}\,t_{RS}^3 + a_{RS,20}\,t_{RS}^2 + a_{RS,10}\,t_{RS} + a_{RS,00} \cdots \\ &\cdots + a_{RS,02}\lambda^2 + a_{RS,01}\lambda + a_{RS,21}t_{RS}^2\lambda + a_{RS,11}t_{RS}\lambda = 0 \end{aligned} \qquad \text{Eq 212}$$

$$a_{RS,40} = \mathbf{f}_{RS}^T\mathbf{f}_{RS} \qquad a_{RS,30} = 2\mathbf{e}_{RS}^T\mathbf{f}_{RS} \qquad a_{RS,20} = 2\mathbf{c}_{RS}^T\mathbf{f}_{RS} + \mathbf{e}_{RS}^T\mathbf{e}_{RS}$$

$$a_{RS,10} = 2\mathbf{c}_{RS}^T\mathbf{e}_{RS} \qquad a_{RS,00} = \mathbf{c}_{RS}^T\mathbf{c}_{RS} \qquad a_{RS,02} = \mathbf{d}_{RS}^T\mathbf{d}_{RS}$$

$$a_{RS,01} = 2\mathbf{c}_{RS}^T\mathbf{d}_{RS} - 1 \qquad a_{RS,21} = 2\mathbf{d}_{RS}^T\mathbf{f}_{RS} \qquad a_{RS,11} = 2\mathbf{d}_{RS}^T\mathbf{e}_{RS}$$

The above steps transform a situation (Eq 210) involving four unknown variable and three scalar equations into involving: (a) one scalar polynomial equation (Eq 212) relating two unknown variables (t_{RS} and λ), and (b) a vector equation (Eq 211) for finding the unknown aircraft coordinates from t_{RS} and λ.

Analysis of Stations U and V — Analysis for stations **U** and **V** is identical (except for subscripts designating stations) to that for stations **R** and **S**. Thus Eq 208 and Eq 209 can be written as

$$2\,\mathbf{B}_{UV}\,\Delta\underline{\mathbf{r}}_A = \mathbf{b}_{UV} + \lambda\mathbf{1}_3 + 2c^2\mathbf{t}_{UV}\,t_{UV} - c^2\mathbf{1}_2\,t_{UV}^2 \qquad \text{Eq 213}$$

$$\mathbf{B}_{UV} = \begin{bmatrix} \Delta\underline{\mathbf{r}}_U^T \\ \Delta\underline{\mathbf{r}}_V^T \\ \Delta\underline{\mathbf{r}}_H^T \end{bmatrix} = \begin{bmatrix} \Delta x_U & \Delta y_U & \Delta z_U \\ \Delta x_V & \Delta y_V & \Delta z_V \\ \Delta x_H & \Delta y_H & \Delta z_H \end{bmatrix}$$

$$\mathbf{b}_{UV} = \begin{bmatrix} (\Delta x_U)^2 + (\Delta y_U)^2 + (\Delta z_U)^2 - (ct_U)^2 \\ (\Delta x_V)^2 + (\Delta y_V)^2 + (\Delta z_V)^2 - (ct_V)^2 \\ (\Delta x_H)^2 + (\Delta y_H)^2 + (\Delta z_H)^2 - (R_e + h_A)^2 \end{bmatrix}$$

$$\lambda = (\Delta x_A)^2 + (\Delta y_A)^2 + (\Delta z_A)^2$$

$$\mathbf{1}_3 = \begin{bmatrix} 1 & 1 & 1 \end{bmatrix}^T \qquad \mathbf{1}_2 = \begin{bmatrix} 1 & 1 & 0 \end{bmatrix}^T \qquad \mathbf{t}_{UV} = \begin{bmatrix} t_U & t_V & 0 \end{bmatrix}^T$$

Inverting matrix $\mathbf{B}_{UV}$ yields

$$\Delta\underline{\mathbf{r}}_A = \mathbf{c}_{UV} + \mathbf{d}_{UV}\lambda + \mathbf{e}_{UV}t_{UV} + \mathbf{f}_{UV}t_{UV}^2 \qquad \text{Eq 214}$$

$$\mathbf{c}_{UV} = \tfrac{1}{2}\mathbf{B}_{UV}^{-1}\mathbf{b}_{UV} \qquad \mathbf{d}_{UV} = \tfrac{1}{2}\mathbf{B}_{UV}^{-1}\mathbf{1}_3$$

$$\mathbf{e}_{UV} = c^2\mathbf{B}_{UV}^{-1}\mathbf{t}_{UV} \qquad \mathbf{f}_{UV} = -\tfrac{1}{2}c^2\mathbf{B}_{UV}^{-1}\mathbf{1}_2$$

Taking the Euclidian norm of $\Delta\underline{\mathbf{r}}_A$ in Eq 214 and collecting terms yields

$$a_{UV,40}t_{UV}^4 + a_{UV,30}t_{UV}^3 + a_{UV,20}t_{UV}^2 + a_{UV,10}t_{UV} + a_{UV,00}\cdots$$
$$\cdots + a_{UV,02}\lambda^2 + a_{UV,01}\lambda + a_{UV,21}t_{UV}^2\lambda + a_{UV,11}t_{UV}\lambda = 0 \qquad \text{Eq 215}$$

$$a_{UV,40} = \mathbf{f}_{UV}^T\mathbf{f}_{UV} \qquad a_{UV,30} = 2\mathbf{e}_{UV}^T\mathbf{f}_{UV} \qquad a_{UV,20} = 2\mathbf{c}_{UV}^T\mathbf{f}_{UV} + \mathbf{e}_{UV}^T\mathbf{e}_{UV}$$

$$a_{UV,10} = 2\mathbf{c}_{UV}^T\mathbf{e}_{UV} \qquad a_{UV,00} = \mathbf{c}_{UV}^T\mathbf{c}_{UV} \qquad a_{UV,02} = \mathbf{d}_{UV}^T\mathbf{d}_{UV}$$

$$a_{UV,01} = 2\mathbf{c}_{UV}^T\mathbf{d}_{UV} - 1 \qquad a_{UV,21} = 2\mathbf{d}_{UV}^T\mathbf{f}_{UV} \qquad a_{UV,11} = 2\mathbf{d}_{UV}^T\mathbf{e}_{UV}$$

The above steps result in one scalar polynomial equation (Eq 215) relating two unknown variables (t_{UV} and λ).

Analysis for Both Station Pairs — Both Eq 212 and Eq 215 are relationships between an aircraft time-of-transmission, t_{RS} or t_{UV}, and the square of the distance between the analysis origin and the aircraft λ. Thus a second relationship between the same two quantities is needed. To that end, observe that the right-hand sides of Eq 211 and Eq 214 are equal. Thus, multiplying both by $\mathbf{B}_{UV}$ and equating them yields

$$\tfrac{1}{2}\mathbf{b}_{UV} + \tfrac{1}{2}\lambda\mathbf{1}_3 + c^2\mathbf{t}_{UV}\,t_{UV} - \tfrac{1}{2}c^2\mathbf{1}_2\,t_{UV}^2 = \mathbf{B}_{UV}\left(\mathbf{c}_{RS} + \mathbf{d}_{RS}\lambda + \mathbf{e}_{RS}t_{RS} + \mathbf{f}_{RS}t_{RS}^2\right) \qquad \text{Eq 216}$$

The third line of Eq 216 relates t_{RS} and λ as follows:

$$\lambda = \beta_{RS,2}t_{RS}^2 + \beta_{RS,1}t_{RS} + \beta_{RS,0} \qquad \text{Eq 217}$$

$$\beta_{RS,2} = \frac{\Delta\underline{\mathbf{r}}_H^T\mathbf{f}_{RS}}{\tfrac{1}{2} - \Delta\underline{\mathbf{r}}_H^T\mathbf{d}_{RS}} \qquad \beta_{RS,1} = \frac{\Delta\underline{\mathbf{r}}_H^T\mathbf{e}_{RS}}{\tfrac{1}{2} - \Delta\underline{\mathbf{r}}_H^T\mathbf{d}_{RS}}$$

$$\beta_{RS,0} = \frac{\Delta\underline{\mathbf{r}}_H^T\mathbf{c}_{RS} - \tfrac{1}{2}\left(\Delta\underline{\mathbf{r}}_H^T\Delta\underline{\mathbf{r}}_H - (R_e + h_A)^2\right)}{\tfrac{1}{2} - \Delta\underline{\mathbf{r}}_H^T\mathbf{d}_{RS}}$$

Using Eq 217 to replace λ in Eq 212 yields

$$\alpha_{RS,4}t_{RS}^4 + \alpha_{RS,3}t_{RS}^3 + \alpha_{RS,2}t_{RS}^2 + \alpha_{RS,1}t_{RS} + \alpha_{RS,0} = 0 \qquad \text{Eq 218}$$

$$\alpha_{RS,4} = a_{RS,40} + a_{RS,02}\beta_{RS,2}^2$$

$$\alpha_{RS,3} = a_{RS,30} + 2a_{RS,02}\beta_{RS,2}\beta_{RS,1} + a_{RS,21}\beta_{RS,1} + a_{RS,11}\beta_{RS,2}$$

$$\alpha_{RS,2} = a_{RS,20} + 2a_{RS,02}\beta_{RS,2}\beta_{RS,0} + a_{RS,02}\beta_{RS,1}^2 + a_{RS,01}\beta_{RS,2} + a_{RS,21}\beta_{RS,0} + a_{RS,11}\beta_{RS,1}$$

$$\alpha_{RS,1} = a_{RS,10} + a_{RS,11}\beta_{RS,0} + a_{RS,01}\beta_{RS,1} + 2a_{RS,02}\beta_{RS,0}\beta_{RS,1}$$

$$\alpha_{RS,0} = a_{RS,00} + a_{RS,01}\beta_{RS,0} + a_{RS,02}\beta_{RS,0}^2$$

As noted in Subsection 7.4.4, a closed-form solution is available for quartic polynomials such as Eq 218. After finding the solution for t_{RS}, it is substituted into Eq 217 to obtain λ. Then t_{RS} and λ are substituted into Eq 211 to find $\Delta\underline{\mathbf{r}}_{\boldsymbol{A}}$. Next, $\underline{\mathbf{r}}_A^{\mathbf{e}}$ is found from $\underline{\mathbf{r}}_A^{\mathbf{e}} = \Delta\underline{\mathbf{r}}_{\boldsymbol{A}} + \underline{\mathbf{r}}_o^{\mathbf{e}}$. Finally, the aircraft latitude and longitude are found from Eq 181.

7.5.4 Remarks

The computation of the solution for $\Delta\underline{\mathbf{r}}_{\boldsymbol{A}}$ described above does not utilize either Eq 214 or Eq 215. However, if t_{UV} is needed, then Eq 214 and Eq 215 are both used. (When λ is known, Eq 215 reduces to a quartic polynomial in t_{UV}.) One reason for computing t_{UV} is to determine the offset between the clocks for the two station pairs.

7.6 Solution for Three Pseudo Slant-Range Stations in Flatland (Fang)

7.6.1 Problem Statement

Flatland is a useful construct for developing a conceptual understanding of a situation. Moreover, Flatland can be a useful approximation for physical problems involving limited geographical areas — e.g., the surface of an airport.

Assume that an aircraft in Flatland is within the coverage region of a multilateration surveillance system that has three stations — **M**, **U** and **V** — with known coordinates (see figure). The stations have synchronized clocks, and each station measures the time-of-arrival at its location — t_M, t_U and t_V, respectively — of the same aircraft transmission. (An equivalent situation can be posed as a navigation problem, whereby the times-of-transmission of three ground stations are synchronized.) The unknown variables to be found are the aircraft coordinates ξ_A and ζ_A. The time of the aircraft's transmission t_A can also be found.

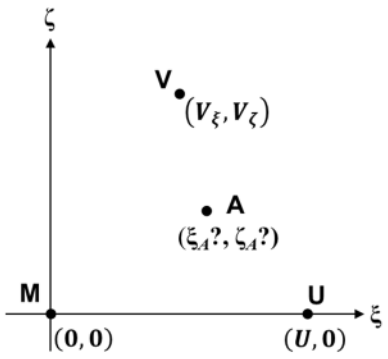

This formulation can be considered to be a simplified version of multilateration surveillance of an airport surface. Qualitatively, the results are similar to those for the two-dimensional, spherical earth pseudorange problem addressed in Section 7.7.

7.6.2 General Solution

The solution that follows utilizes the traditional (non-Bancroft) approach as described in Ref. 42. The expressions found in this way are the same as those that would be found using Bancroft's algorithm, but fewer algebraic manipulations are needed. Implicit in this development is that:

$$\begin{aligned} &\left|\Delta d_{MU}\right| \le U && \left|\Delta d_{MV}\right| \le V \\ &\Delta d_{MU} = c\left(t_M - t_U\right) = d_{MA} - d_{UA} && \Delta d_{MV} = c\left(t_M - t_V\right) = d_{MA} - d_{VA} \end{aligned} \qquad \text{Eq 219}$$

The approach begins with formulation of the pseudo slant-range differences. Taking **M** as the common station, these are

$$\begin{aligned} \Delta d_{MU} &= \sqrt{\xi_A^2 + \zeta_A^2} - \sqrt{\left(\xi_A - U\right)^2 + \zeta_A^2} \\ \Delta d_{MV} &= \sqrt{\xi_A^2 + \zeta_A^2} - \sqrt{\left(\xi_A - V_\xi\right)^2 + \left(\zeta_A - V_\zeta\right)^2} \end{aligned} \qquad \text{Eq 220}$$

In Eq 220: (a) each equation describes a hyperbola, and (b) the left-hand side of each of equation can be either positive or negative. The solution is the intersection of a specific branch of each hyperbola. After re-arranging, then squaring, each equation in Eq 220, the result is

$$\begin{aligned} U^2 - 2U\xi_A - \Delta d_{MU}^2 &= -2\Delta d_{MU}\sqrt{\xi_A^2 + \zeta_A^2} \\ V^2 - 2V_\xi\xi_A - 2V_\zeta\zeta_A - \Delta d_{MV}^2 &= -2\Delta d_{MV}\sqrt{\xi_A^2 + \zeta_A^2} \end{aligned} \qquad \text{Eq 221}$$

In Eq 221, $V^2 = V_\xi^2 + V_\zeta^2$. Dividing one equation by the other, and re-arranging, yields

$$\zeta_A = C\xi_A + D \qquad \text{Eq 222}$$

$$C = \frac{\Delta d_{MV}}{V_\zeta}\left(\frac{U}{\Delta d_{MU}}\right) - \frac{V_\xi}{V_\zeta} \qquad V_\zeta \neq 0 \qquad \Delta d_{MU} \neq 0$$

$$D = \frac{V^2}{2V_\zeta} - \frac{\Delta d_{MV}^2}{2V_\zeta} - \frac{\Delta d_{MU}\Delta d_{MV}}{2V_\zeta}\left(\left(\frac{U}{\Delta d_{MU}}\right)^2 - 1\right) \qquad V_\zeta \neq 0 \quad \Delta d_{MU} \neq 0$$

The condition $V_\zeta \neq 0$ is equivalent to requiring that the stations not form a straight line, and the condition $\Delta d_{MU} \neq 0$ is equivalent to requiring that the aircraft not be on the perpendicular bisector of the baseline **MU**. These special cases are addressed in Subsection 7.6.3.

Eq 222 defines a line in the $\xi - \zeta$ plane which contains the aircraft location. Using this equation to substitute for ζ_A in the first equation in Eq 221, then squaring and collecting like terms, yields:

$$E\xi_A^2 + F\xi_A + G = 0 \qquad V_\zeta \neq 0 \qquad \Delta d_{MU} \neq 0 \qquad \text{Eq 223}$$

$$E = 1 - \left(\frac{U}{\Delta d_{MU}} \right)^2 + C^2 \qquad \Delta d_{MU} \neq 0$$

$$F = 2CD + U\left(\left(\frac{U}{\Delta d_{MU}} \right)^2 - 1 \right) \qquad \Delta d_{MU} \neq 0$$

$$G = D^2 - \frac{\Delta d_{MU}^2}{4}\left(\left(\frac{U}{\Delta d_{MU}} \right)^2 - 1 \right)^2 \qquad \Delta d_{MU} \neq 0$$

Thus the general solution of the "three pseudo slant-range system in Flatland" problem can be reduced to:

- Solve the quadratic equation that is first line of Eq 223 to obtain (usually) two candidate values for ξ_A
- Substitute the two candidate values for ξ_A into the first line of Eq 222 to find the corresponding values for ζ_A
- Attempt to determine which candidate solution-pair (ξ_A, ζ_A) is correct by substituting each into Eq 220.

The squaring steps in the solution process can generate a second candidate solution that corresponds to pseudo slant-range differences of $-d_{MU}$ and $-d_{MV}$. (i.e., the negation of the measured slant-range differences, with both having the same sign). When a sign reversal is involved, the incorrect candidate solution can be detected by substituting the two candidates into the original equations to be solved (Eq 220).

If needed, the time of the aircraft's transmission can be found from the correct solution using

$$t_A = t_M - \frac{1}{c}\sqrt{\xi_A^2 + \zeta_A^2} \qquad \text{Eq 224}$$

7.6.3 Solution Cases

As noted in conjunction with Bancroft's algorithm (Subsection 7.2.3), solutions to a quadratic equation such as Eq 223 can be grouped into categories. Six possibilities relevant to this situation are explored in this subsection. The first four are "special cases" resulting from arrangements of the aircraft and stations and corresponding to lines in the $\xi - \zeta$ plane. The other two possibilities are "general cases" and correspond to areas of the $\xi - \zeta$ plane.

Stations Form a Straight Line — If the station locations form a straight line, the solution to Eq 221 is (in order):

$$\xi_A = \frac{\left(V^2 \Delta d_{MU} - U^2 \Delta d_{MV}\right) + \Delta d_{MU} \Delta d_{MV} \left(\Delta d_{MU} - \Delta d_{MV}\right)}{2\left(U \Delta d_{MV} - V \Delta d_{MU}\right)}$$

$$\zeta_A = \pm \sqrt{\frac{\left(U^2 - 2U\xi_A - \Delta d_{MU}^2\right)^2}{4\Delta d_{MU}^2} - \xi_A^2} \qquad \text{Eq 225}$$

This is a geometrical special case of the problem formulation, rather than a mathematical special case of Eq 223.

Aircraft Equidistant from Stations M and U — Eq 222 and Eq 223 fail when an aircraft is equi-distant to stations **M** and **U**. When this occurs, Eq 221 reduces to

$$\xi_A = \frac{U}{2} \qquad H\zeta_A^2 + J\zeta_A + K = 0 \qquad \text{Eq 226}$$

$$H = 4\Delta d_{MV}^2 - 4V_\zeta^2$$

$$J = 4V_\zeta \left(V^2 - V_\xi U - \Delta d_{MV}^2\right)$$

$$K = \Delta d_{MV}^2 U^2 - \left(V^2 - V_\xi U - \Delta d_{MV}^2\right)^2$$

Two double-special cases of Eq 226 are of interest. When an aircraft is equidistant between both station pairs **MU** and **MV**, the quadratic equation has a double root and the aircraft location is:

$$\xi_A = \frac{U}{2} \qquad \zeta_A = \frac{V^2 - UV_\xi}{2V_\zeta} \qquad \text{Eq 227}$$

When ***H*** is zero, the quadratic equation is degenerate and Eq 226 has a single root at:

$$\xi_A = \frac{U}{2} \qquad \zeta_A = \frac{U^2 V_\zeta}{4V_\xi\left(U - V_\xi\right)} - \frac{V_\xi\left(U - V_\xi\right)}{4V_\zeta} \qquad \text{Eq 228}$$

Double Root – Aircraft on a Baseline Extension — When an aircraft is at a station or on a baseline extension, the associated slant-range difference is the same for any position on that extension and is equal in magnitude to the baseline length. In the double special case where the three stations form a straight line and the aircraft is on an extension of that baseline, then $\Delta d_{MU} = \pm U$ and $\Delta d_{MV} = \pm V$, with the same sign applying to both measurements. Thus the expression for ξ_A in Eq 225 is singular.

For the more usual two-dimensional station geometry, assume that the aircraft is on the ξ-axis to the left of **M**. Then $\Delta d_{MU} = -U$, so the discriminant for Eq 223 is zero, indicating the occurrence of a double-root. The aircraft position is given by

$$\xi_A = -\frac{D}{C} = \frac{V^2 - \Delta d_{MV}^2}{2\left(V_\xi + \Delta d_{MV}\right)} \qquad \zeta_A = 0 \qquad \text{Eq 229}$$

The expression for the location of the aircraft relative to the nearest station (i.e., ξ_A in Eq 229) does not depend upon the length of that baseline.

The solution in Eq 229 depends on both conditions $|\Delta d_{MU}| = U$ and $|\Delta d_{MV}| \leq V$ being valid. If either is violated due to measurement errors, the solution will change in character — either it may not exist (the discriminant is negative) or the double root may divide into two single roots (the discriminant is positive). For this reason, it is sometimes said that locations on the baseline extensions are unstable. Also, while Eq 229 is derived for only one of six baseline extensions, by transforming the coordinate axes and the slant-range differences, it can be applied to any baseline extension.

Single Root – Degenerate Quadratic — While Eq 223 is nominally a quadratic function of ξ_A, it reduces to a linear function of ξ_A when $\boldsymbol{E}$ = 0, or when

$$V^2 \Delta d_{MU}^2 + U^2 d_{MV}^2 - 2UV_\xi \Delta d_{MU} \Delta d_{MV} - U^2 V_\zeta^2 = 0 \qquad \text{Eq 230}$$

Eq 230 is analytically intractable, as it involves all three possible products of the three radicals in Eq 220; thus, repeated isolating and squaring will result in a 8th order polynomial. However, Eq 230 can be readily solved numerically — e.g., using the secant method (Subsection 2.1.6). The result of such a calculation, for stations that form an equilateral triangle with unit baselines, is shown as the green curves in Figure 30. Geometrically, the single-solution case occurs when the two hyperbola have asymptotes that are parallel to each other.

The loci of single-root solutions (three green curves in Figure 30) partition the $\xi - \zeta$ plane into four regions. From numerical trials, it has been found that in the two-root case, both solutions are always located in the same region (Ref. 44). When the aircraft is near this boundary, the incorrect solution is very distant from the correct solution

For the square area shown in Figure 30 (3 x 3 Base Line Units [BLUs]), the ‘extraneous’ region is 62.5% of the total area, and each of the three ‘ambiguous’ regions is 12.5%. If attention is limited to an area of 1.5 x 1.5 BLUs (which better resembles one of operational interest), the ‘extraneous’ region is 79.8% of the total and each of the three ‘ambiguous’ regions is 6.7%.

Two Roots – Different Branches — This situation occurs when the aircraft is in the larger, ‘extraneous solution’ area of the $\xi - \zeta$ plane in Figure 30. An algebraic indicator of this situation is that $\boldsymbol{E}$ in Eq 223 is negative. Geometrically, each solution is formed by the intersection of hyperbola branches which are distinct from those which form the other solution (Figure 31(a)).

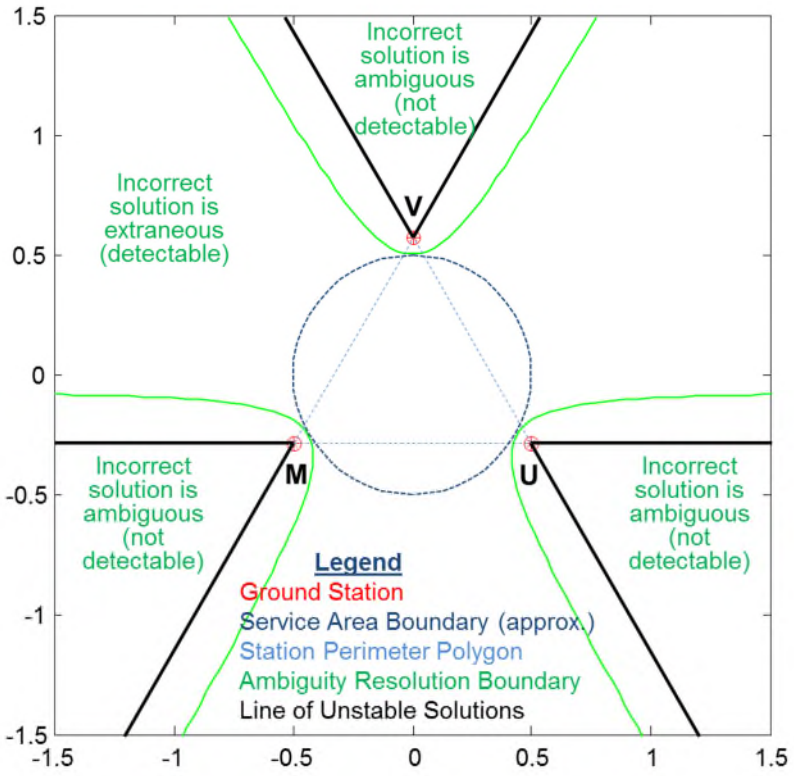

Figure 30 Solution Regions for Three Pseudo Slant-Range Stations in Flatland

The filled circle corresponds to the correct slant-range differences, and the unfilled circle to their sign-reversed versions. Thus the correct solution can be identified.

Two Roots – Same Branches — This situation occurs when the aircraft is in one of the three rounded-V-shaped 'ambiguous solution' areas in Figure 30. An algebraic indicator of this situation is that ***E*** in Eq 223 is positive. Both solutions are formed by intersections of the branches of the hyperbolas which correspond to the correct slant-range differences (Figure 31(b)). Thus, the correct solution cannot be identified without additional information.

7.6.4 Remarks

Service Area — Every navigation or surveillance system is intended to provide service in a defined area or volume. Generally, in the service area/volume, the measurement geometry (e.g., crossing angles of LOPs) is satisfactory, and the signal-to-noise ratio is adequate. For a three-station pseudorange system with equal baselines, the service area is approximately a circle with its center at the mid-point of the station locations and radius equal to one-half the baseline length (Figure 30). This includes almost all on the triangle connecting the stations, plus three circle segments adjacent to the baselines. The maximum "bulge" outward from each baseline is 21% of a baseline length. Subsection 8.4.2 provides additional information about pseudo slant-range systems' service areas.

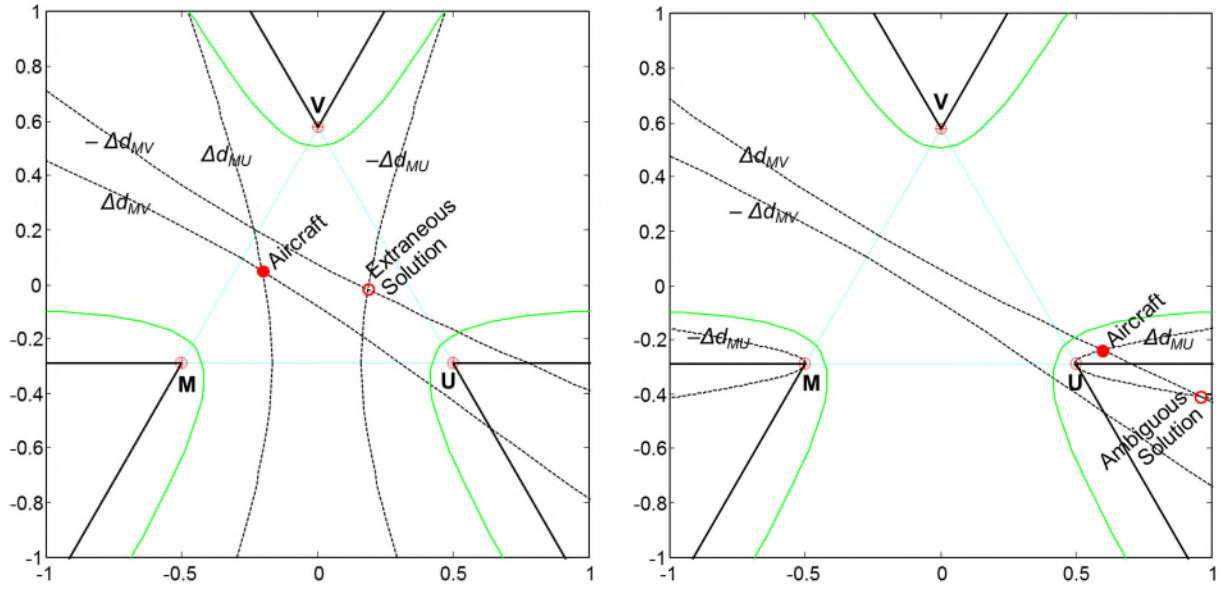

(a) Different Branches (Extraneous Soln.) (b) Same Branches (Ambiguous Soln.)

Figure 31 Types of Solutions for Three Pseudo Slant-Range Stations

Contribution of Derivation — The development in Subsection 7.6.2 is the least-complicated derivation of a solution to the 'three pseudo slant-ranges in Flatland' problem. This solution only requires finding the roots of a quadratic equation in one position coordinate. Also, it provides insight into the effects of the geometry on the solution. In contrast, Bancroft's algorithm requires solution of a quadratic equation in a quadratic quantity — the Lorentzian norm of the aircraft location. A third derivation takes a coordinate-free approach and only utilizes distances and angles (Ref. 48). It does not provide as much insight.

Keys to Derivation — A key step in Fang's derivation is dividing the two equations in Eq 221. If, instead, one were to square the two equations separately to eliminate the radicals, the result would be two fourth-order polynomial equations. Geometrically, two families of hyperbolas, one associated with each baseline, intersect at up to four points and thus may require a fourth-order polynomial for computing all the intersections. Fang's derivation takes advantage of the fact that the two slant-range differences have one station in common. A similar step occurs in the derivation of Razin's algorithm for a spherical earth.

Numerical Results — When numerical results are needed, Bancroft's algorithm may be preferable to implementing Eq 222 and Eq 223. One reason is that, if vector-matrix software is available, the coding task is simpler. A second is that Bancroft's algorithm places all the stations on an equal footing, while Fang's algorithm makes **MU** the primary baseline. A consequence is that the solution code must handle $\Delta d_{MU} = 0$ as a special case. Another may be that the solution is more sensitive to measurement errors in Δd_{MU}.

Two Station Pairs — One could define a hyperbolic system involving four stations comprised of two separately synchronized pairs of stations (similar to Loran-C cross-chaining). A derivation similar to the above would require two squaring operations to remove all radicals, which would result in a fourth-order polynomial.

Application to Ellipsoid LOPs — Reference 42 makes the point that — with some sign reversals — the equations of this section would apply equally well to measurements of the two sums of the slant-ranges for three ground stations to an aircraft. While not commonly implemented (e.g., by a multi-static radar), it is a point worth noting.

Relationship to Classic Hyperbola Parameters — Figure 32 shows the classic form of a hyperbola which satisfies the equation

$$\frac{x^2}{a^2} - \frac{y^2}{b^2} = 1 \qquad \text{Eq 231}$$

This classic hyperbola can be easily related to the hyperbola described by the first line of Eq 220. Equating the distances between the vertices and the foci of the two hyperbolas, respectively, yields:

$$2a = \left|\Delta d_{MU}\right|$$
$$2\sqrt{a^2 + b^2} = U \qquad \text{Eq 232}$$

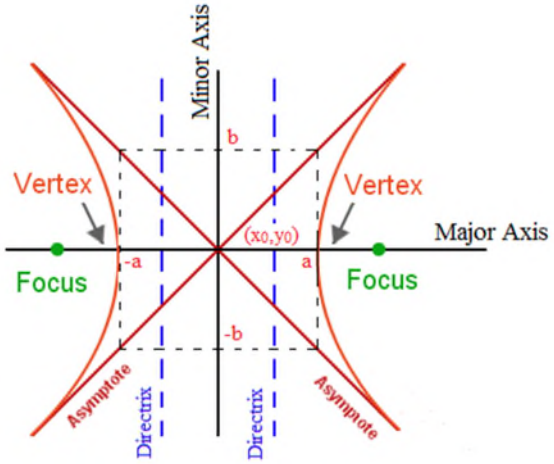

Figure 32 Classic Hyperbola

Thus the tangent of the acute angle that an asymptote makes with the baseline is:

$$\frac{b}{a} = \sqrt{\left(\frac{U}{\Delta d_{MU}}\right)^2 - 1} \qquad \text{Eq 233}$$

The quantity under the radical in Eq 233 is fundamental to this formulation, and also appears in the expressions for ***D*** (Eq 222) and ***E***, ***F*** and ***G*** (Eq 223).

Insight into More Complex Situations — The problems addressed in this section, three-pseudorange-stations-in-Flatland, is a simplified version of the problems addressed in Sections 7.4 and 7.7. Qualitatively, the solutions behave similarly.

7.7 Solution for Three Pseudo Spherical-Range Stations (Razin)

7.7.1 Problem Formulation

Pseudo (or differences in) spherical-ranges are the basis upon which several radionavigation systems have been developed, most prominently Loran-C. Spherical ranging systems are intended for use on or near the earth's surface; altitude has no role in their concepts or solutions. The Loran community developed an advanced concept involving user-carriage of an atomic standard, enabling measurement of spherical-ranges (vice differences). Such measurements can be handled by the method described in Section 6.4 and are not addressed here.

Figure 33 illustrates a basic scenario using Loran-C station labels: **M** at latitude/longitude (L_M, λ_M) is the master station, and **X** (L_X, λ_X) and **Y** (L_Y, λ_Y) are secondary stations whose transmissions are synchronized with those from **M**. The coordinates of all stations are known. The assumption is that aircraft **A** is employing the system for navigation, and wishes to determine its latitude and longitude (L_A, λ_A).

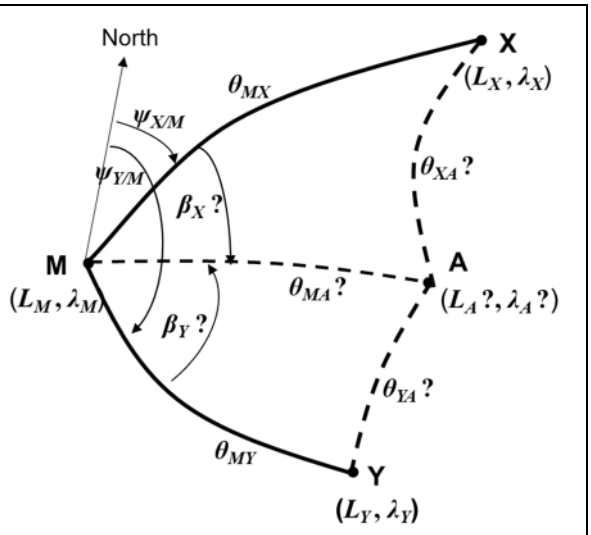

Figure 33 Pseudo Spherical-Range Scenario Involving Stations **M**, **X** and **Y** and Aircraft **A**

Two time-difference-of-arrival (TDOA) measurements available from the station's transmissions; these are grouped as "**M** minus **X**" and "**M** and **Y**". The TDOAs are equivalent to two spherical-range differences with constrained magnitudes:

$$\Delta\theta_{MXA} = \theta_{MA} - \theta_{XA} \qquad |\Delta\theta_{MXA}| \le \theta_{MX}$$
$$\Delta\theta_{MYA} = \theta_{MA} - \theta_{YA} \qquad |\Delta\theta_{MYA}| \le \theta_{MY} \qquad \text{Eq 234}$$

7.7.2 Problem Solution

Figure 33 depicts two mathematical spherical triangles **MXA** and **MYA** with common side **MA**. The goal in analyzing these triangles is to find θ_{MA} and either β_X or β_Y, as having these quantities reduces the task to solution of the Direct Problem of Geodesy. As occurs for position determination based of two real slant-range measurements (Section 6.4) — which devolves into position determination based of two real circular-range measurements — multiple solutions can occur.

Step 0: Solve the Indirect Problem of Geodesy (Section 4.2) for the paths **MX** and **MY**, yielding the geocentric angles θ_{MX} and θ_{MY} and the azimuth angles $\psi_{X/M}$ and $\psi_{Y/M}$.

Step 1: Form the difference of the azimuth angles $\psi_{X/M}$ and $\psi_{Y/M}$, yielding the angle β between great circle arcs **MX** and **MY** satisfying $0 < \beta < \pi$

$$\beta = \min\left(\left|\psi_{Y/M} - \psi_{X/M}\right|,\ \left|\psi_{Y/M} - \psi_{X/M} + 2\pi\right|,\ \left|\psi_{Y/M} - \psi_{X/M} - 2\pi\right| \right) \qquad \text{Eq 235}$$

To establish the sign conventions, assume that the vehicle is within the V-shaped region with sides **MX** and **MY**. Then both β_X and β_Y are positive as shown. The following is always true:

$$\beta = \beta_X + \beta_Y \qquad \text{Eq 236}$$

Step 2: Solve Eq 234 for θ_{XA} and θ_{YA}, then take the cosine of both sides, yielding:

$$\begin{aligned} \cos(\theta_{XA}) &= \cos(\theta_{MA})\cos(\Delta\theta_{MXA}) + \sin(\theta_{MA})\sin(\Delta\theta_{MXA}) \\ \cos(\theta_{YA}) &= \cos(\theta_{MA})\cos(\Delta\theta_{MYA}) + \sin(\theta_{MA})\sin(\Delta\theta_{MYA}) \end{aligned} \qquad \text{Eq 237}$$

Step 3: Apply the spherical triangle law of cosines for sides (Eq 56) to **MXA** and **MYA**, yielding:

$$\begin{aligned} \cos(\theta_{XA}) &= \cos(\theta_{MA})\cos(\theta_{MX}) + \sin(\theta_{MA})\sin(\theta_{MX})\cos(\beta_X) \\ \cos(\theta_{YA}) &= \cos(\theta_{MA})\cos(\theta_{MY}) + \sin(\theta_{MA})\sin(\theta_{MY})\cos(\beta_Y) \end{aligned} \qquad \text{Eq 238}$$

Step 4: The first and second lines, respectively, of Eq 237 and Eq 238 are equated, eliminating θ_{XA} and θ_{YA}. Then solving for θ_{MA} yields:

$$\begin{aligned} \tan(\theta_{MA}) &= \frac{\cos(\theta_{MX}) - \cos(\Delta\theta_{MXA})}{\sin(\Delta\theta_{MXA}) - \sin(\theta_{MX})\cos(\beta_X)} \\ \tan(\theta_{MA}) &= \frac{\cos(\theta_{MY}) - \cos(\Delta\theta_{MYA})}{\sin(\Delta\theta_{MYA}) - \sin(\theta_{MY})\cos(\beta_Y)} \end{aligned} \qquad \text{Eq 239}$$

Step 5: Equate the two expressions for θ_{MA} in Eq 239 and eliminate β_Y using Eq 236, yielding:

$$\frac{\cos(\theta_{MX}) - \cos(\Delta\theta_{MXA})}{\sin(\Delta\theta_{MXA}) - \sin(\theta_{MX})\cos(\beta_X)} = \frac{\cos(\theta_{MY}) - \cos(\Delta\theta_{MYA})}{\sin(\Delta\theta_{MYA}) - \sin(\theta_{MY})\cos(\beta - \beta_X)} \qquad \text{Eq 240}$$

Step 6: Re-write Eq 240 as:

$$\begin{aligned} B_c\cos(\beta_X) + B_s\sin(\beta_X) &= C \\ B_c &= \sin(\theta_{MX})[\cos(\theta_{MY}) - \cos(\Delta\theta_{MYA})] - \sin(\theta_{MY})[\cos(\theta_{MX}) - \cos(\Delta\theta_{MXA})]\cos(\beta) \\ B_s &= -\sin(\theta_{MY})[\cos(\theta_{MX}) - \cos(\Delta\theta_{MXA})]\sin(\beta) \\ C &= \sin(\Delta\theta_{MXA})[\cos(\theta_{MY}) - \cos(\Delta\theta_{MYA})] - \sin(\Delta\theta_{MYA})[\cos(\theta_{MX}) - \cos(\Delta\theta_{MXA})] \end{aligned} \qquad \text{Eq 241}$$

Step 7: Re-write Eq 241 as:

$$\begin{aligned} B_m\cos(\beta_X - \gamma) &= C \\ B_m &= \sqrt{(B_c)^2 + (B_s)^2} \qquad \gamma = \arctan(B_s, B_c) \end{aligned} \qquad \text{Eq 242}$$

The four-quadrant arc tangent function is used in Eq 242.

Step 8: Find $\boldsymbol{\beta}_X$ using Eq 243.

$$\beta_X = \arctan(B_s, B_c) + \arccos\left(\frac{C}{B_m}\right) = \arctan(B_s, B_c) \pm \mathrm{ArcCos}\left(\frac{C}{B_m}\right) \qquad \text{Eq 243}$$

In Eq 243, ArcCos denotes the principal value of the arccos function — i.e., the value in the range [0, π]. Thus, in general, two solutions are possible.

Step 9: For both possible solutions, find $\boldsymbol{\theta}_{MA}$ using the first line of Eq 239.

Step 10: For both possible solutions, find the aircraft's latitude and longitude ($\boldsymbol{L}_A$, $\boldsymbol{\lambda}_A$) as a solution to the Direct Problem of Geodesy, given the latitude/longitude ($\boldsymbol{L}_M$, $\boldsymbol{\lambda}_M$), the geocentric angle $\boldsymbol{\theta}_{MA}$ and the azimuth angle $\boldsymbol{\psi}_{A/M} = \boldsymbol{\psi}_{X/M} + \boldsymbol{\beta}_X$.

Step 11: For both possible solutions, the geocentric angles $\boldsymbol{\theta}_{XA}$ and $\boldsymbol{\theta}_{YA}$ are found from the aircraft and station latitudes and longitudes as solutions to the indirect problem of geodesy.

Step 12: For both possible solutions, substitute the angles $\boldsymbol{\theta}_{MA}$, $\boldsymbol{\theta}_{XA}$ and $\boldsymbol{\theta}_{YA}$ in the right-hand side of Eq 234. Compare the resulting spherical range difference to the measured values for these quantities. Discard a possible solution when agreement does not occur.

7.7.3 Types of Solutions

No Solution — Measurement errors can cause one of the inequalities in Eq 234 to be violated. That, in turn, can cause the argument of the arc cosine function in Eq 243 to be greater than one in magnitude, in which case a solution does not exist.

Double-Root Solution — If the aircraft is on a baseline extension, including at a station, then Eq 240 becomes indeterminate and the equations immediately before it must be used. For example, assume the aircraft is on the extension of **MX**, closer to **X**. Then $\theta_{MA} = \Delta\theta_{MXA}$, and equating the first two lines of Eq 237 and Eq 238 yields $\boldsymbol{\beta}_X = 0$, hence $\boldsymbol{\beta}_Y = \boldsymbol{\beta}$. Thus, since $0 < \boldsymbol{\beta} < \pi$, there is a single solution for $\boldsymbol{\theta}_{MA}$ given by the second line of Eq 239.

Single Solution — In Eq 243, if $B_m = C$ then the ArcCos term is zero and there is only one solution for $\boldsymbol{\beta}_X$. The locus of latitudes/longitudes for which $B_m = C$ can be found numerically.

Two Solutions: Ambiguous vs. Extraneous — In most instances, two candidate solutions are found by the method described in Subsection 7.7.2. One is always correct. The other is either: (a) extraneous, corresponding to the negation of the measured spherical-range differences (thus will be detected in Step 12); or (b) ambiguous, also corresponding to the measured spherical-

range differences, and thus not resolvable without additional information.

The intended service area for a pseudorange system is, approximately, the region within the perimeter of the polygon enclosing the stations (but not close to a station) or the border area outside the perimeter but near the bisector of the baseline joining the closest two stations. In the service area, one candidate solution is extraneous and corresponds to the "+" sign in Eq 243, while the correct solution corresponds to the "–" sign. Example 10 in Subsection 7.9.3 illustrates where both ambiguous and extraneous solutions occur.

7.7.4 Remarks

System Applications — The primary examples of long-range pseudo spherical-range systems are Loran-C and Omega. For their combinations of system characteristics (long-ranges between stations and aircraft, low-frequency radio waves and ground propagation paths), processing steps in addition to those described in Subsection 7.7.2 were generally needed to achieve the systems' potential accuracies.

Accuracy Enhancements — Two areas have been addressed to improve the accuracy of low-frequency spherical-range difference systems:

- Earth Geometry — For distances of more than a few hundred miles, the ellipticity error incurred by using a spherical-earth model is usually unacceptably large. One approach is to employ approximations to an ellipsoid (Refs. 10-12 and 14-16) which are not amenable to closed-form solution. These can be utilized in an iterative solution technique that is initialized with the solution obtained from Razin's algorithm (see Chapter 8). A second approach is to tailor the spherical-earth model to the service area involved (Refs. 43 and 49).
- Radiowave Propagation — Low-frequency electromagnetic ground waves cannot be assumed to travel with constant speed, since their propagation depends upon the conductivity of the ground over which they travel. Modeling and measurements have both been used to address this issue. The resulting adjustments are easily incorporated in the pseudo spherical-range difference measurements.

Validation — Reference 49 contains the findings of a comparison, using Loran-C measurements, of Razin's algorithm and the semi-official, iterative algorithm published by the Radio Technical Commission for Maritime Services (RTCM) (Ref. 50). Differences between the computed latitude/longitude coordinates for the two algorithms are between 3 ft and 5 ft.

Similarity to Flatland Solution — Although the analysis formulations are different (rectangular versus spherical), the qualitative characteristics of the solutions for the Flatland/Fang and spherical-earth/Razin algorithms are qualitatively virtually the same. Both have two solutions with the incorrect one being detectable (i.e., extraneous) in the useful service area for a system, but not detectable (i.e., ambiguous) between and near the baseline extensions for the stations.

7.8 Solution for Two Pairs of Stations Measuring Pseudo Spherical-Ranges

7.8.1 Problem Formulation

This section addresses a problem that is close to the topic of the previous section: determining an aircraft's position from two spherical-range difference measurements. However, in this section, the measurements are obtained from four stations comprising two distinct pairs, rather than from three stations comprising two pairs having a common station. It is also close to the topic of Section 7.5, which addresses two pairs of stations that measure pseudo slant-ranges.

Figure 34 illustrates the scenario using Loran-C-like station labels. Station **M** at latitude/longitude (L_M, λ_M) is a master station, and station **X** (L_X, λ_X) is an associated secondary station. Similarly, station **N** (L_N, λ_N) is the master for a separate set of stations (chain), and station **Y** (L_Y, λ_Y) is an associated secondary. The transmissions of each master-secondary pair are synchronized, but not with those of the other pair.

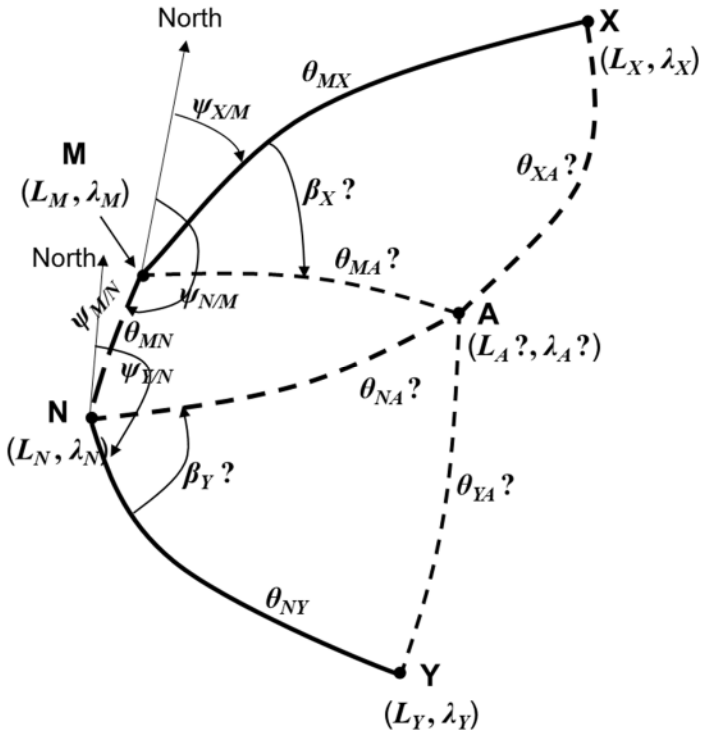

Figure 34 Pseudo Spherical-Range Measurement Scenario Involving Two Station Pairs and Aircraft

The assumption is that aircraft **A** is employing this set of stations for navigation. The aircraft's first priority is to determine its latitude/longitude (L_A, λ_A) coordinates. A second priority is to determine the spherical-range to and azimuth angle toward each of the four stations.

Two time-difference-of-arrival (TDOA) measurements are available from the station's transmis-

sions; these follow the convention "**M** minus **X**" and "**N** minus **Y**". These TDOAs are equivalent to two spherical-range differences. These are, together with the limitations on their magnitudes:

$$\begin{aligned} \Delta\theta_{MXA} &= \theta_{MA} - \theta_{XA} \qquad \left|\Delta\theta_{MXA}\right| \le \theta_{MX} \\ \Delta\theta_{NYA} &= \theta_{NA} - \theta_{YA} \qquad \left|\Delta\theta_{NYA}\right| \le \theta_{NY} \end{aligned} \qquad \text{Eq 244}$$

7.8.2 Problem Solution

Figure 34 depicts three mathematical spherical triangles: **MXA**, **NYA** and **MNA**. The goal in analyzing these triangles is to find values for the two spherical-range/bearing pairs $\boldsymbol{\theta_{MA}}$ and $\boldsymbol{\beta_X}$ and $\boldsymbol{\theta_{NA}}$ and $\boldsymbol{\beta_Y}$. Knowing these quantities reduces the task of finding ($\boldsymbol{L_A}$, $\boldsymbol{\lambda_A}$) to a solution of the Direct Problem of Geodesy. As in other multi-dimensional problems, multiple solutions for ($\boldsymbol{L_A}$, $\boldsymbol{\lambda_A}$) may occur; when they do, the validity of each must be checked.

The immediate goal is to find $\boldsymbol{\beta_X}$, as the quantities $\boldsymbol{\theta_{MA}}$, $\boldsymbol{\theta_{NA}}$ and $\boldsymbol{\beta_Y}$ follow readily.

Step 0: Solve the Indirect Problem of Geodesy for three paths between stations:

- **MX** (master and associated secondary): Provides $\boldsymbol{\theta_{MX}}$ and $\boldsymbol{\psi_{X/M}}$
- **NY** (master and associated secondary): Provides $\boldsymbol{\theta_{NY}}$ and $\boldsymbol{\psi_{Y/N}}$
- **MN** (two master stations): Provides $\boldsymbol{\theta_{MN}}$, $\boldsymbol{\psi_{M/N}}$ and $\boldsymbol{\psi_{N/M}}$

Define the positive angles between the path **MN** and, respectively, the paths **MX** and **NY**

$$\begin{aligned} \psi_M &= \min\left\{ \left|\psi_{N/M} - \psi_{X/M}\right|, \left|\psi_{N/M} - \psi_{X/M} + 2\pi\right|, \left|\psi_{N/M} - \psi_{X/M} - 2\pi\right| \right\} \\ \psi_N &= \min\left\{ \left|\psi_{Y/N} - \psi_{M/N}\right|, \left|\psi_{Y/N} - \psi_{M/N} + 2\pi\right|, \left|\psi_{Y/N} - \psi_{M/N} - 2\pi\right| \right\} \end{aligned} \qquad \text{Eq 245}$$

Formally define $\boldsymbol{\beta_X}$ as the angle **XMA**, measured clockwise from **XM**. Similarly, define $\boldsymbol{\beta_Y}$ as the angle **YNA**, measured counter-clockwise from **YN**.

Step 1: Solve Eq 244 for $\boldsymbol{\theta_{XA}}$ and $\boldsymbol{\theta_{YA}}$, then take the cosine of both sides, yielding:

$$\begin{aligned} \cos(\theta_{XA}) &= \cos(\theta_{MA})\cos(\Delta\theta_{MXA}) + \sin(\theta_{MA})\sin(\Delta\theta_{MXA}) \\ \cos(\theta_{YA}) &= \cos(\theta_{NA})\cos(\Delta\theta_{NYA}) + \sin(\theta_{NA})\sin(\Delta\theta_{NYA}) \end{aligned} \qquad \text{Eq 246}$$

Step 2: Apply the spherical law of cosines for sides to triangles **MXA** and **NYA**, yielding:

$$\begin{aligned} \cos(\theta_{XA}) &= \cos(\theta_{MA})\cos(\theta_{MX}) + \sin(\theta_{MA})\sin(\theta_{MX})\cos(\beta_X) \\ \cos(\theta_{YA}) &= \cos(\theta_{NA})\cos(\theta_{NY}) + \sin(\theta_{NA})\sin(\theta_{NY})\cos(\beta_Y) \end{aligned} \qquad \text{Eq 247}$$

Step 3: The first lines of Eq 246 and Eq 247 are equated, eliminating $\boldsymbol{\theta_{XA}}$. Then solving for the master station-aircraft distance yields $\boldsymbol{\theta_{MA}}$ as a function of $\boldsymbol{\beta_X}$ and known quantities

$$\theta_{MA} = \arctan\left(\frac{\cos(\theta_{MX}) - \cos(\Delta\theta_{MXA})}{\sin(\Delta\theta_{MXA}) - \sin(\theta_{MX})\cos(\beta_X)}\right) \quad \text{Eq 248}$$

In Eq 248, the single-argument arc tangent function should be used.

Step 4: Consider spherical triangle **MNA**. The four-part cotangent formula yields an expression for $\boldsymbol{\beta_Y}$ as an explicit function of $\boldsymbol{\beta_X}$ and quantities that are either known or are functions of $\boldsymbol{\beta_X}$:

$$\beta_Y = \psi_N - \arctan\left(\frac{\sin(\psi_M - \beta_X)}{\sin(\theta_{MN})\cot(\theta_{MA}) - \cos(\theta_{MN})\cos(\psi_M - \beta_X)}\right) \quad \text{Eq 249}$$

In Eq 249, the two-argument arc tangent function should be used.

Step 5: The second lines of Eq 246 and Eq 247 are equated, eliminating $\boldsymbol{\theta_{YA}}$. Then solving for the master station-aircraft distance yields $\boldsymbol{\theta_{NA}}$ as a function of $\boldsymbol{\beta_Y}$ and known quantities

$$\theta_{NA} = \arctan\left(\frac{\cos(\theta_{NY}) - \cos(\Delta\theta_{NYA})}{\sin(\Delta\theta_{NYA}) - \sin(\theta_{NY})\cos(\beta_Y)}\right) \quad \text{Eq 250}$$

In Eq 250, the single-argument arc tangent function should be used.

Step 6: The value of $\boldsymbol{\beta_X}$ sought is a root of the following equation (application of the Law of Sines to spherical triangle **MNA**)

$$\frac{\sin(\psi_M - \beta_X)}{\sin(\theta_{NA})} = \frac{\sin(\psi_N - \beta_Y)}{\sin(\theta_{MA})} \quad \text{Eq 251}$$

By substituting and re-substituting Eq 248, Eq 249 and Eq 250 into Eq 251, the result would be an explicit function of $\boldsymbol{\beta_X}$ and known quantities. There is no point in doing so, however, since the expression would be too complex to be solved analytically for $\boldsymbol{\beta_X}$. Instead, a root finding technique (such as the secant method) can used to find one or more values for $\boldsymbol{\beta_X}$.

Step 7: For each candidate solution for $\boldsymbol{\beta_X}$, find the corresponding value for $\boldsymbol{\theta_{MA}}$ using Eq 248.

Step 8: For each candidate solution pair for bearing $\boldsymbol{\beta_X}$ and range $\boldsymbol{\theta_{MA}}$, find the aircraft's latitude and longitude ($\boldsymbol{L_A}$, $\boldsymbol{\lambda_A}$) as a solution to the Direct Problem of Geodesy.

Step 9: If multiple solutions to Eq 251 occur, for each solution set, find the geocentric angles $\boldsymbol{\theta_{XA}}$ and $\boldsymbol{\theta_{YA}}$ from the aircraft and station coordinates as solutions to the Indirect Problem of Geodesy.

Step 10: For each solution set, substitute the angles $\boldsymbol{\theta_{MA}}$, $\boldsymbol{\theta_{XA}}$ and $\boldsymbol{\theta_{NA}}$, $\boldsymbol{\theta_{YA}}$ in the right-hand side of Eq 244. Compare the resulting spherical range difference to the measured values for these quantities. Discard a candidate solution when agreement does not occur.

7.8.3 Remarks

- An obvious application of this algorithm is to Loran-C "cross-chaining" — finding position solutions using TDOA measurements from two separate chains. Loran-C cross-chaining can involve three stations, with one station being dual-rated. However, in terms of the position-solution algorithm, three-station cross-chaining is no different than three stations from a single chain. This section addresses the more-complex situation involving two pairs of stations, one pair from each chain.
- Sequences of equations other than those in Subsection 7.8.2 can be used arrive at a function of $\boldsymbol{\beta_X}$ (only) whose root is to be found. The solution sequence presented herein follows Razin (Ref. 43) and appears to yield satisfactory results (Subsection 7.9.4).
- When a closed-form solution to a problem does not exist, reducing the solution to finding the root of a scalar equation over a pre-defined range of values is the next best option.

7.9 Example Applications

Example applications are presented in this section, with the intent of providing a sense of how the equations presented earlier in this chapter might be utilized.

7.9.1 Example 8: Slant-Range Measurement System in Flatland

Problem Statement — Consider the simplest application of Bancroft's algorithm — finding the intersections of two circles in a plane. Stated as a navigation problem, an aviator in Flatland measures his/her slant-range to two stations — say, d_{1A} to station **S₁** having known coordinates, and d_{2A} to station **S₂** also having known coordinates. This formulation can be considered to be a simplified version of the problem of computing a DME/DME/altitude fix (Section 6.4).

The first step toward a solution is selecting the coordinate frame. Because Bancroft's algorithm involves calculating a matrix inverse, the origin cannot be in-line with the two stations (Subsection 7.2.3). A good choice is to place each station on one axis, equidistant from the origin (illustrated at the right). A normalized distance scale is chosen such that the separation between the stations is one unit — i.e., distances are quantified in Base Line Units (BLUs).

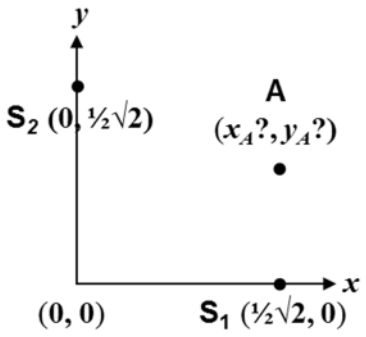

Solution — Carrying out the steps indicated in Subsections 7.2.1 and 7.2.2 yields

$$\mathbf{B} = \begin{bmatrix} \frac{1}{2}\sqrt{2} & 0 \\ 0 & \frac{1}{2}\sqrt{2} \end{bmatrix} \qquad \mathbf{B}^{-1} = \begin{bmatrix} \sqrt{2} & 0 \\ 0 & \sqrt{2} \end{bmatrix} \qquad \text{Eq 252}$$

$$\mathbf{b} = \begin{bmatrix} (x_1)^2 + (y_1)^2 - d_{1A}^2 \\ (x_2)^2 + (y_2)^2 - d_{2A}^2 \end{bmatrix} = \begin{bmatrix} \frac{1}{2} - d_{1A}^2 \\ \frac{1}{2} - d_{2A}^2 \end{bmatrix} \qquad \text{Eq 253}$$

$$\underline{\mathbf{u}} = \begin{bmatrix} u_x \\ u_y \end{bmatrix} = \tfrac{1}{2}\mathbf{B}^{-1}\mathbf{1} = \begin{bmatrix} \frac{1}{2}\sqrt{2} \\ \frac{1}{2}\sqrt{2} \end{bmatrix} = \tfrac{1}{2}\sqrt{2}\begin{bmatrix} 1 \\ 1 \end{bmatrix}$$

$$\underline{\mathbf{v}} = \begin{bmatrix} v_x \\ v_y \end{bmatrix} = \tfrac{1}{2}\mathbf{B}^{-1}\mathbf{b} = \begin{bmatrix} \frac{1}{4}\sqrt{2} - \frac{1}{2}\sqrt{2}d_{1A}^2 \\ \frac{1}{4}\sqrt{2} - \frac{1}{2}\sqrt{2}d_{2A}^2 \end{bmatrix} = \tfrac{1}{2}\sqrt{2}\begin{bmatrix} \frac{1}{2} - d_{1A}^2 \\ \frac{1}{2} - d_{2A}^2 \end{bmatrix} \qquad \text{Eq 254}$$

$$\alpha\lambda^2 + \beta\lambda + \gamma = 0$$

$$\begin{aligned} \alpha &= \langle \underline{\mathbf{u}}, \underline{\mathbf{u}} \rangle = u_x^2 + u_y^2 = 1 \\ \beta &= 2\langle \underline{\mathbf{u}}, \underline{\mathbf{v}} \rangle - 1 = 2u_x v_x + 2u_y v_y - 1 = 1 - d_{1A}^2 - d_{2A}^2 - 1 = -\left(d_{1A}^2 + d_{2A}^2\right) \\ \gamma &= \langle \underline{\mathbf{v}}, \underline{\mathbf{v}} \rangle = v_x^2 + v_y^2 = \tfrac{1}{2}\left(\tfrac{1}{2} - d_{1A}^2\right)^2 + \tfrac{1}{2}\left(\tfrac{1}{2} - d_{2A}^2\right)^2 \end{aligned} \qquad \text{Eq 255}$$

$$\begin{aligned} \text{Disc} &= \beta^2 - 4\alpha\gamma = \left(d_{1A}^2 + d_{1A}^2\right)^2 - 2\left(\tfrac{1}{2} - d_{1A}^2\right)^2 - 2\left(\tfrac{1}{2} - d_{2A}^2\right)^2 \\ &= 2\left(d_{1A}^2 + d_{2A}^2\right) - \left(d_{1A}^2 - d_{2A}^2\right)^2 - 1 \end{aligned} \qquad \text{Eq 256}$$

Thus

$$\lambda_{\pm} = \frac{1}{2}\left(d_{1A}^2 + d_{2A}^2 \pm \sqrt{2\left(d_{1A}^2 + d_{2A}^2\right) - \left(d_{1A}^2 - d_{2A}^2\right)^2 - 1} \right) \qquad \text{Eq 257}$$

The two possible solutions for the aircraft location are

$$\begin{bmatrix} x_A(\pm) \\ y_A(\pm) \end{bmatrix} = \lambda_{\pm}\underline{\mathbf{u}} + \underline{\mathbf{v}} = \lambda_{\pm}\tfrac{1}{2}\sqrt{2}\begin{bmatrix} 1 \\ 1 \end{bmatrix} + \tfrac{1}{2}\sqrt{2}\begin{bmatrix} \frac{1}{2} - d_{1A}^2 \\ \frac{1}{2} - d_{2A}^2 \end{bmatrix} \qquad \text{Eq 258}$$

Types of and Conditions on Solutions — Insight into the solution can be obtained by examining the sum and difference of the slant-ranges. Thus let

$$\begin{aligned} \Sigma d &= d_{1A} + d_{2A} & \Delta d &= d_{1A} - d_{2A} \\ d_{1A} &= \tfrac{1}{2}\left(\Sigma d + \Delta d\right) & d_{2A} &= \tfrac{1}{2}\left(\Sigma d - \Delta d\right) \end{aligned} \qquad \text{Eq 259}$$

Upon substituting into Eq 256, the discriminant Disc can be written as

$$\text{Disc} = \beta^2 - 4\alpha\gamma = \left(\left(\Sigma d\right)^2 - 1\right)\left(1 - \left(\Delta d\right)^2\right) \qquad \text{Eq 260}$$

The four types of possible solutions for the norm λ are enumerated in Subsection 7.2.3. It follows from Eq 255 that, since $\alpha = 1$, a single real root cannot occur. Geometrically, this is because two circles in a plane must cross at two points, be tangent at a point, or not cross.

The other three solution types can occur, depending upon the value of the discriminant. For real roots to occur, both of the following conditions must be true:

$$\Sigma d \;\geq\; 1 \qquad\qquad |\Delta d| \;\leq\; 1 \qquad\qquad \text{Eq 261}$$

Since the two stations are separated by one BLU, Eq 261 "says" that (a) the sum of the ranges to the stations must be at least equal to the separation between the stations, and (b) the absolute value of the difference between the ranges to the stations must be no more than the separation between the stations. Based on geometric reasoning, when Σd is unity, the aircraft must be on the baseline separating the stations, and when $|\Delta d|$ is unity the aircraft must be on an extension of the baseline. Similar conditions are derived in Subsection 6.4.3 for the analogous problem involving a spherical earth.

Aircraft locations along the baseline connecting the stations and its extensions are unstable because small measurement errors can change the character of the solution — to a situation where a solution does not exist or to one where there are two separate candidate solutions.

It follows from Eq 257 and Eq 260 that

$$\lambda_{\pm} = \frac{1}{4}\left((\Sigma d)^2 + (\Delta d)^2\right) \pm \frac{1}{2}\sqrt{\left((\Sigma d)^2 - 1\right)\left(1 - (\Delta d)^2\right)} \qquad \text{Eq 262}$$

Either solution to Eq 262 (and to Eq 257 as well) may be correct. Of course, only one solution is actually equal to the vehicle's true position — the other solution is ambiguous. Two slant ranges do not provide enough information to make a decision.

"Natural" Coordinate System — While the (x, y) frame is compatible with Bancroft's algorithm, it is not the natural frame for this problem. Thus, consider the (ξ, ζ) frame (Figure 35) which is generated by rotating the (x, y) frame counter clockwise by 45 deg, then offsetting it by one-half a BLU to the right. The result is that (a) both stations lie on the ζ-axis, and (b) the ξ-axis is the perpendicular bisector of the baseline connecting the stations. The solutions for the aircraft location can be expressed in the (ξ, ζ) frame as:

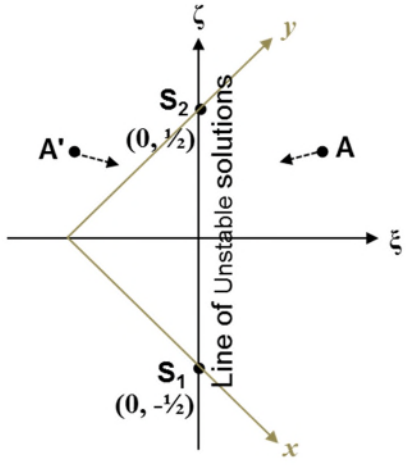

Figure 35 Two Slant-Range Stations and Aircraft in Flatland

$$\begin{bmatrix} \xi_A \\ \zeta_A \end{bmatrix} = \frac{1}{2}\begin{bmatrix} \pm\sqrt{2\left(d_{1A}^2 + d_{2A}^2\right) - \left(d_{1A}^2 - d_{2A}^2\right)^2 - 1} \\ d_{1A}^2 - d_{2A}^2 \end{bmatrix} \qquad \text{Eq 263}$$

This solution can also be written as

$$\begin{bmatrix} \xi_A \\ \zeta_A \end{bmatrix} = \frac{1}{2}\begin{bmatrix} \pm\sqrt{\left((\Sigma d)^2 - 1\right)\left(1-(\Delta d)^2\right)} \\ \Sigma d\ \Delta d \end{bmatrix} \qquad \text{Eq 264}$$

Let a breve diacritic mark above a normalized quantity denote its un-normalized version; thus, e.g., $\breve{\xi} = B\xi$ and $\breve{\zeta} = B\zeta$, where B is the baseline length. The un-normalized version Eq 264 then is

$$\begin{bmatrix} \breve{\xi}_A \\ \breve{\zeta}_A \end{bmatrix} = \frac{1}{2B}\begin{bmatrix} \pm\sqrt{\left((\Sigma \breve{d})^2 - B^2\right)\left(B^2-(\Delta \breve{d})^2\right)} \\ \Sigma \breve{d}\ \Delta \breve{d} \end{bmatrix} \qquad \text{Eq 265}$$

Geometry-Based Derivation — There is an older, more direct, geometry-based derivation of Eq 263. Referring to Figure 35, the two slant-ranges satisfy Pythagoras' theorem:

$$\begin{aligned} d_{1A}^2 &= \xi_A^2 + \left(\zeta_A + \tfrac{1}{2}\right)^2 \\ d_{2A}^2 &= \xi_A^2 + \left(\zeta_A - \tfrac{1}{2}\right)^2 \end{aligned} \qquad \text{Eq 266}$$

Completing the squares and subtracting the second equation from the first in Eq 266 yields

$$\zeta_A = \tfrac{1}{2}\left(d_{1A}^2 - d_{2A}^2\right) \qquad \text{Eq 267}$$

Lastly, substituting for ζ_A in the first equation in Eq 266 yields

$$\begin{aligned} \xi_A &= \pm\sqrt{d_{1A}^2 - \left(\tfrac{1}{2}\left(d_{1A}^2 - d_{2A}^2\right) + \tfrac{1}{2}\right)^2} \\ &= \pm\tfrac{1}{2}\sqrt{2\left(d_{1A}^2 + d_{2A}^2\right) - \left(d_{1A}^2 - d_{2A}^2\right)^2 - 1} \end{aligned} \qquad \text{Eq 268}$$

Remarks

- In the absence of slant-range measurement errors that cause one or both of the inequalities of Eq 261 to be violated, there are no aircraft positions where either line in Eq 263 fails — i.e., the equations do not have any singularities.
- If the aircraft position is on the ζ-axis — either on the baseline connecting the stations or on an extension — the discriminant (Eq 256 and Eq 260) is zero and Eq 255 has an unstable double root. This different than the situation for three pseudorange stations in a plane (Section 7.7); there, only positions on the baseline extensions are unstable.
- If the aircraft is not on the ζ-axis, then Eq 255 has two separate real roots that correspond to the actual and ambiguous aircraft locations.
- The correct and ambiguous solutions are symmetrically located with respect to the ζ-axis but cannot be distinguished based on two slant-range measurements.

- Movement of the aircraft with a component toward or away from the ζ-axis is a method for determining the correct solution.
- The effect of measurement errors on the solution depends strongly on the location of the aircraft. This is the topic of Subsection 8.4.1.
- The two-ranging-stations-in-Flatland problem is a simplified version of the DME/DME/Altitude problem addressed in Section 6.4. Qualitatively, the solutions behave similarly.

7.9.2 Example 9: Three Pseudo Slant-Range Stations in Flatland

This subsection presents examples of results obtained using Fang's algorithm described in Section 7.3 for finding the two-dimensional position of an aircraft from three pseudo slant-range measurements. Figure 36 depicts three such stations, labeled **M**, **U** and **V**. The three green curves partition the space into four regions that contain the incorrect (ambiguous or extraneous) solution when the correct solution is in the same region (Figure 30).

The thicker, solid blue and red lines with filled symbols at their ends represent hypothetical aircraft flight tracks. The thinner dashed blue and red lines with unfilled symbols at their ends depict the incorrect solutions yielded by the algorithm for the hypothetical tracks of the same color. An asterisk marks the center of each hypothetical or incorrect track.

The blue track corresponding to the correct solution is well within the service area, as is its corresponding incorrect track (which is in approximately the opposite direction, and is slightly curved). In the 'extraneous' region, the correct solution can be identified by inspection. For

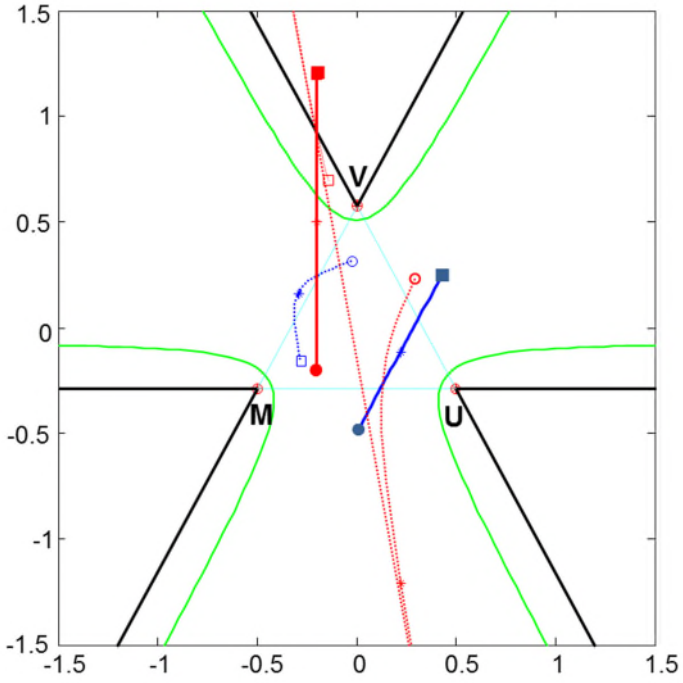

Figure 36 Three Pseudo Slant-Range Stations in Flatland and Two Aircraft Tracks

example, the filled blue circle is equidistant from **M** and **U** and furthest from **V**. In contrast, its counterpart, the unfilled blue circle, is equidistant from **M** and **U** and closest to **V** (i.e., the order is reversed). Similar statements can be made about every point in this region. Calculations reveal that the magnitudes of the slant-range differences are the same for the correct and incorrect solutions; however, their signs are reversed.

In contrast to the blue track, the red track corresponding to the incorrect solution transitions from the 'extraneous' region to the 'ambiguous' region. Starting from the circle symbols the correct solution moves directly "north" in a straight line, while the incorrect solution moves largely "south" in a slightly curved path. As the aircraft approaches and crosses the transition between the regions, the incorrect solution moves at a high rate to the "south" then reappears at the far "north" and again moves at a high rate to the "south". As the aircraft moves away from the transition curve, the incorrect solution moves close to the correct solution.

7.9.3 Example 10: Three Pseudo Spherical-Range Stations

This subsection presents an example application of Razin's algorithm (Section 7.7) utilizing three pseudo spherical-range navigation stations in the U.S. Northeast Loran-C chain (Ref. 51). In Figure 37: **M** represents the master station at Seneca, NY; **W** represents the secondary station at Caribou, ME; and **X** represents the secondary station at Nantucket, MA. For a spherical-earth formulation, the baselines and their extensions for these stations are great circles.

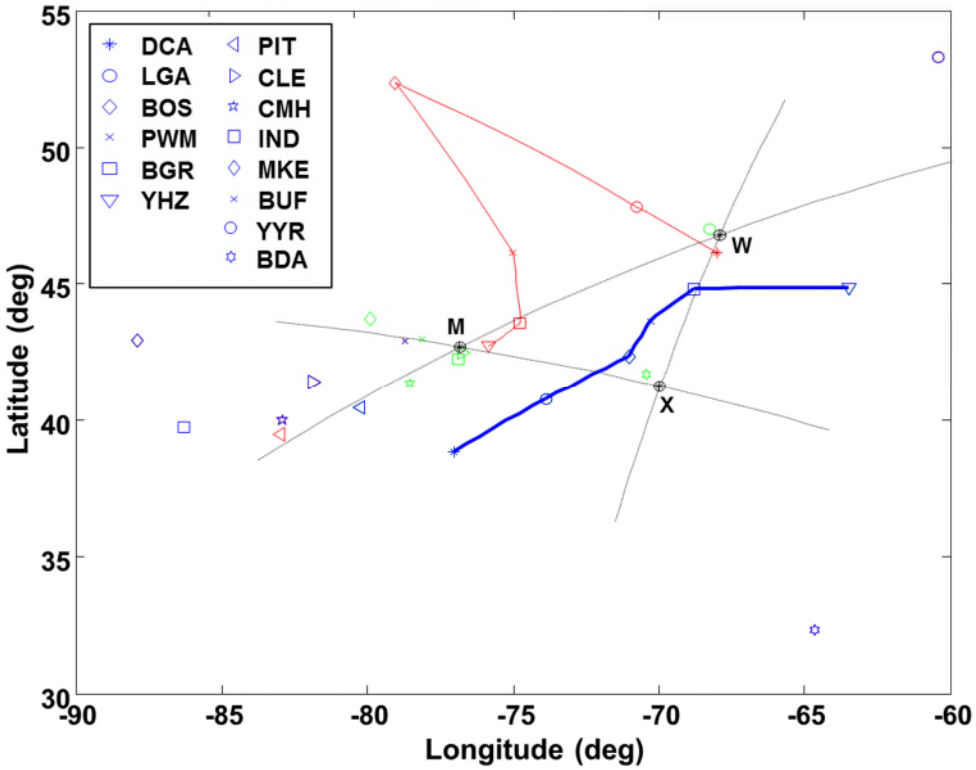

Figure 37 Position Solutions for Triad of Stations from the Northeast U.S. Loran-C Chain

Fourteen airport locations were selected, and spherical-range differences for the station pairs **M**-**W** and **M**-**X** were calculated using a spherical-earth model. The methodology of Section 7.7 was used to find solutions for the airport locations from the range differences. Green ("–" solution) and red ("+" solution) icons of the same shapes represent the algorithm's solutions for the same airport. Blue-colored symbols depict the actual airport locations, and overprint the correct solution (in all cases, they agree to machine precision).

Six airports are in the service area for these stations: Reagan National, VA (DCA); LaGuardia, NY (LGA); Boston, MA (BOS); Portland, ME (PWM); Bangor, ME (BGR); and Halifax, Nova Scotia (YHZ). A blue line represents a hypothetical flight path connecting these airports. A thinner red line connects the incorrect "+"solutions.

For airports in the service area, the incorrect solutions can be detected by inspection. For example, DCA is closest to station **M** and furthest from **W**. However, its extraneous version is closest to **W** and furthest from **M**. More generally, for locations in the service area, the range differences for an extraneous solution will be negative versions of the range differences for the correct solution. Another method for detecting the correct solution is to examine the flight path. In this case, the incorrect "flight path" is, overall, in the opposite direction of the correct track.

Eight other airports are also depicted by blue symbols: Pittsburgh, PA (PIT); Cleveland, OH (CLE); Columbus, OH (CMH); Indianapolis, IN (IND); Milwaukee, WI (MKE); Buffalo, NY (BUF); Goose Bay, Labrador (YYR); and Bermuda (BDA). These airports are all outside the nominal service area for the stations, and are in or near the three regions bounded by baseline extensions. The incorrect solutions, which may be either the "–" or "+" solution of Eq 243, are all ambiguous — i.e., the range differences calculated from the correct and incorrect airport locations are identical.

This example is revisited in Subsection 8.4.4, which addresses the effect of mis-modeling the earth as a sphere (i.e., the ellipticity error), and presents a solution.

7.9.4 Example 11: Two Pairs of Pseudo Spherical-Range Stations

This subsection presents an example of the solution algorithm for two pairs of pseudo spherical-range navigation stations described in Section 7.8. Figure 38 depicts the master station at Seneca, NY for the U.S. Northeast Loran-C chain and a secondary station at Nantucket, MA. It also depicts the master station for the U.S. Great Lakes Loran-C chain at Dana, IN, and a secondary station at Malone, FL.

Figure 38 also shows seven airports which represent possible locations of aircraft employing these stations for navigation: LaGuardia, NY (LGA); Elizabeth City, NC (ECG); Charleston, SC

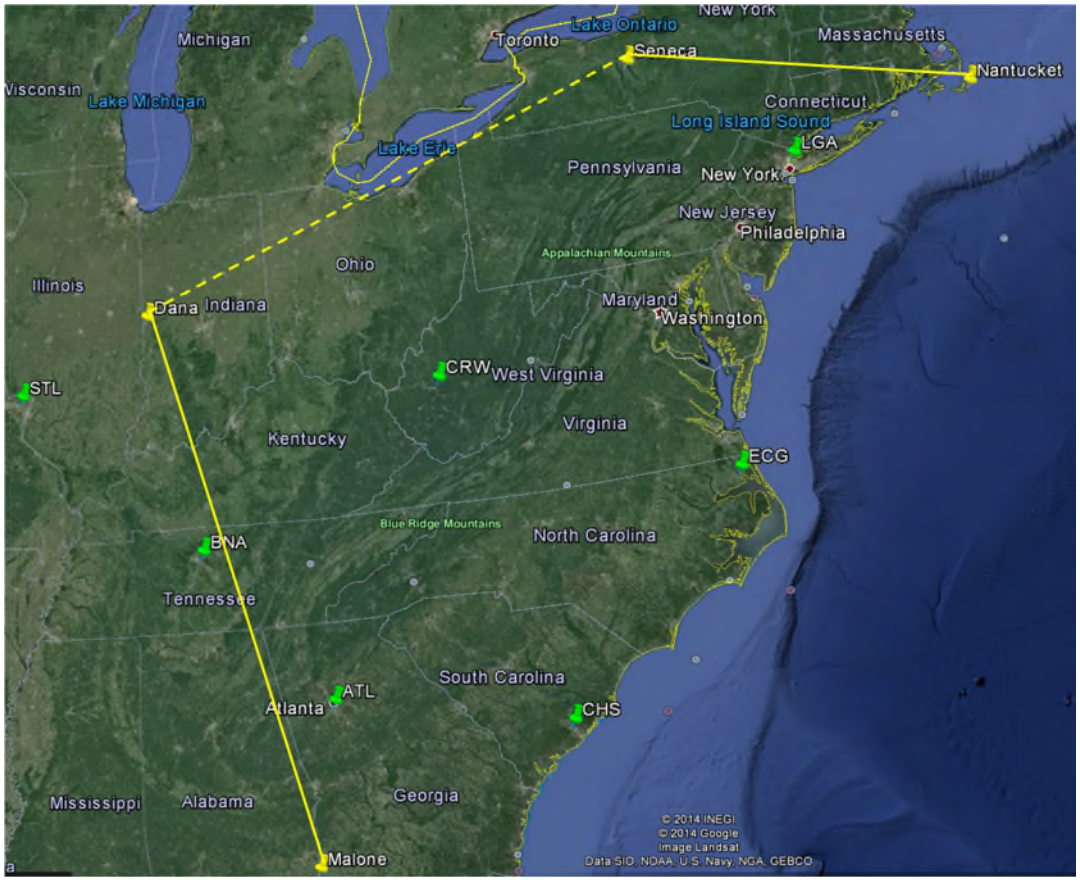

Figure 38 Two Pairs of Loran-C Stations and Seven Airport Locations

(CHS); Charleston, WV (CRW); Atlanta, GA (ATL); Nashville, TN (BNA); and St. Louis, MO (STL). All of the airports locations are within the expected service area for such a navigation system.

The solution algorithm presented in Section 7.8 is straightforward except for the process of finding values for $\boldsymbol{\beta}_X$ that are roots of Eq 251. Thus the primary issue explored is the behavior of Eq 251 as a function of $\boldsymbol{\beta}_X$ — i.e., with $\boldsymbol{\theta}_{MA}$, $\boldsymbol{\theta}_{NA}$ and $\boldsymbol{\beta}_Y$ determined from $\boldsymbol{\beta}_X$. (Here, $\boldsymbol{\beta}_X$ is the angle, measured clockwise, from (a) the baseline from Seneca to Nantucket to (b) a great circle path from Seneca to the aircraft.)

Figure 39 shows the difference between the left- and right-hand sides of Eq 251 as a function of assumed values for $\boldsymbol{\beta}_X$ in the range $(\psi_M - \pi) \leq \beta_X \leq \psi_M$. Each of the seven possible aircraft locations are considered for the half-sphere on the southeast side of the great circle path through Dana and Seneca. The curves for six of the seven airports (all except STL) have the same basic shape — a “sideways S”. Most important is that each curve in Figure 39, including that for STL, has only one root, so ambiguous and extraneous solutions do not occur for locations in the area of interest. If the roots for $\boldsymbol{\beta}_X$ shown in Figure 39 are substituted into Steps 7-10 of the algorithm in Section 7.8, the original aircraft locations result.

A plot similar to Figure 39 was generated for the area on the northwest side of the great circle path through Dana and Seneca. Four of the airports of interest (LGA, ECG, CRW and BNA) had a single extraneous solution in this area. CHS and ATL did not have a second solution, and STL has two additional solutions.

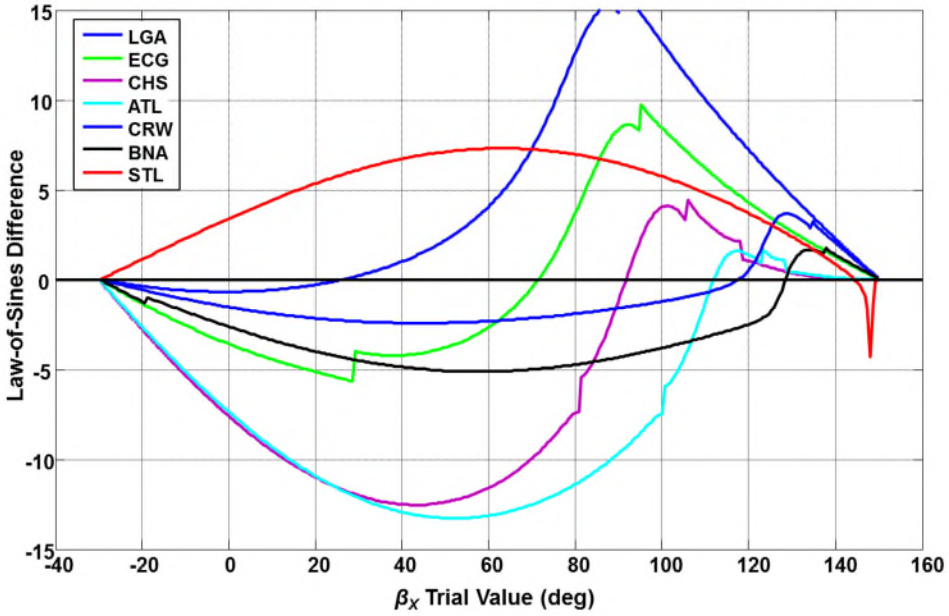

Figure 39 Example 11: Sensitivity of Law-of-Sines Difference to Trial Values of $\boldsymbol{\beta_X}$

This example is re-visited in Subsection 8.4.5.

7.9.5 Example 12: Wide Area Multilateration (WAM)

As an example of the solution technique presented in Section 7.4, a WAM system is postulated which has ground stations at three airports: Boston, MA (BOS); Manchester, NH (MHT); and Hartford, CT (BDL) — see Figure 40. An aircraft at an altitude of 25,000 ft over-flies five airports in the system's service area: Westfield-Barnes Regional, MA (BAF); Dillant-Hopkins, Keene NH (EEN); Fitchburg Municipal, MA (FIT); Lawrence Municipal, MA (LWM); and Hanscom Field, Bedford MA (BED). To provide insight into the algorithm's behavior outside the service area, solutions are found for three possible aircraft locations outside the service area and near extended baselines: Barnstable Municipal, MA (HYA); Stewart International, NY (SWF); and Portland International, ME (PWM).

Interest in the algorithm of Section 7.4 centers on the solution to Eq 200 for the aircraft time of transmission t_A. In this example, the times of reception at the ground stations t_i were shifted by the same amount, so that the earliest occurred at $t_i = 0$. As a result, the correct value for t_A must be negative. The four roots of Eq 200 were found using the Matlab routine 'roots'. These were multiplied by the speed of light, *c*, converting their units to nautical miles. Thus, the correct

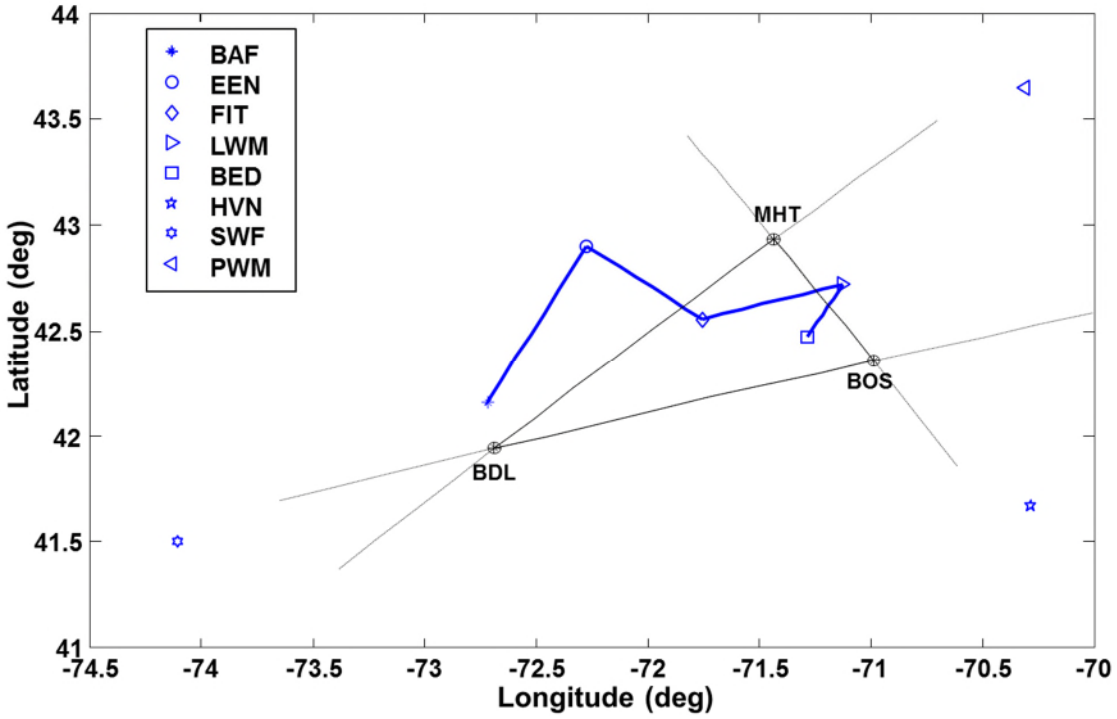

Figure 40 Three-Station WAM System and Example Flight Track

solution is the negative of the slant-range between the aircraft and the nearest ground station. Since the reception range of a WAM ground station is similar to that of an en route SSR (Figure 7), ranges beyond a few hundred nautical miles are not feasible.

The calculated roots (potential values for t_A) are displayed in Table 10. Positive roots cannot be correct, nor can complex roots. Thus, for each airport, only the two negative roots are possible solutions. For the five airports in the WAM system's service area, the negative root nearer to zero is clearly the correct choice. (The magnitude of other negative root is approximately an earth-radius.) In fact, the negated values of the calculated correct roots were equal to the slant-ranges used to generate the simulated measurements, to machine precision. For the three airport locations outside the service area, either negative root could be correct. Similar situations, involving extraneous and ambiguous solutions, occur in Examples 9 and 10.

Table 10 Roots for Aircraft Transmission Time, in NM, for Example 12

Aircraft	Root 1		Root 2		Root 3		Root 4	
Location	Real	Imag	Real	Imag	Real	Imag	Real	Imag
BAF	-4,002.6	0.0	-13.3	0.0	82.8	0.0	4,066.4	0.0
EEN	-4,748.8	0.0	-36.9	0.0	78.9	0.0	4,795.0	0.0
FIT	-6,361.5	0.0	-27.0	0.0	58.9	0.0	6,397.5	0.0
LWM	-4,022.4	0.0	-19.0	0.0	74.1	0.0	4,094.9	0.0
BED	-4,771.9	0.0	-15.1	0.0	86.0	0.0	4,812.5	0.0
HYA	-52.1	0.0	-29.5	0.0	106.1	-3,508.9	106.1	3,508.9
SWF	-68.7	0.0	-35.6	0.0	135.6	-1,072.8	135.6	1,072.8
PWM	-177.1	0.0	-65.3	0.0	211.6	-1,053.7	211.6	1,053.7

This example is re-visited in Subsection 8.4.6, where an ellipsoidal earth model is considered.

8. LINEARIZED LEAST-SQUARES (LLS) METHOD (GAUSS-NEWTON)

8.1 General LLS Method

8.1.1 Background / Context

This final chapter is a fundamental departure from the foregoing chapters in several aspects. Situations addressed in Chapters 3-7 explicitly or implicitly assume that

- There are exactly as many measurements (equations) as there are unknown variables — i.e., there is no role for redundant measurements
- The available measurements can be described by simple equations that can be inverted to find the aircraft's coordinates or other unknown quantities of interest — i.e., there is no role for complex expressions, recursive algorithms or tabular data.

One implication of the second item is that the problem setting must be a spherical earth or (less commonly) a two- or three-dimensional rectangular Cartesian frame.

This chapter removes the above restrictions, enabling more general situations to be addressed. Simply put, Chapters 3-7 provide exact solutions to approximate problems, while this chapter provides approximate solutions to exact problems.

A cost of this generality is that the solution techniques are iterative/numerical rather than analytic and closed-form. This results in a loss insight into problems. For example, an iterative method does not reveal how many solutions may exist, or their nature (extraneous, ambiguous, etc.). Moreover, iterative techniques require that an initial value be provided. Thus there are useful roles for both analytic and iterative techniques.

The form of the iterative equations depends upon the sensors involved and the coordinate system employed. There are two basic alternatives. When a spherical or ellipsoidal earth model is employed, the unknown aircraft position variables will generally be its latitude $\boldsymbol{L_A}$ and longitude $\boldsymbol{\lambda_A}$, and possibly altitude $\boldsymbol{h_A}$. When an earth-fixed rectangular coordinate system is used, the unknown aircraft position variables will be its Cartesian $\boldsymbol{x_A}$, $\boldsymbol{y_A}$ and $\boldsymbol{z_A}$ components. (Appendix Section 9.3 shows how to convert between these formulations.) When pseudorange measurements are involved, the time of transmission by the aircraft $\boldsymbol{t_A}$ (surveillance) or ground stations $\boldsymbol{t_S}$ (navigation) may also be an unknown variable.

In terms of mathematical techniques, the Linear Least Squares (LLS) technical utilizes vectors and matrices. In contrast, Chapters 3-4 and 6-7 rely on multiple scalar equations.

8.1.2 Linearized Least Squares Problem and Solution

In this section, a spherical/ellipsoidal coordinate system is used, but the basic technique also

applies to a rectangular coordinate system. It is assumed that there are measurements $\tilde{z}_i$ available (combinations of slant-ranges, angles, etc.) of the unknown variables of the form

$$\begin{aligned} \tilde{z}_i &= z_i + v_i \qquad\qquad i = 1, \cdots, m \\ z_i &= f_i(L_A, \lambda_A, h_A, t_X) = f_i(\mathbf{x}) \end{aligned} \qquad \text{Eq 269}$$

$$\mathbf{x} \equiv \begin{bmatrix} L_A & \lambda_A & h_A & t_X \end{bmatrix}^T \qquad \text{Eq 270}$$

Here: (a) **x** denotes the vector of unknown variables; (b) *m* is the number of measurements (which must be at least equal to the number of unknown variables); (c) $\boldsymbol{v}_i$ is the measurement error that is inevitably present; and (d) $\boldsymbol{t}_X$ is either $\boldsymbol{t}_A$ or $\boldsymbol{t}_S$. The vector of measurement errors is characterized by a zero mean and known covariance matrix (Subsection 8.1.3).

Often Eq 269 is termed the scalar measurement model. In Eq 269, the measurement function $f_i(L_A, \lambda_A, h_A, t_X)$ is known but need not be invertible; it can be any combination of analytic expressions, recursive algorithms and tables that, when the variables $(L_A, \lambda_A, h_A, t_X)$ are known, yields a value for z_i (Subsection 8.1.4).

Each unknown variable is expressed as the sum of an "initial" estimate for the iteration step involved, denoted by an overbar, and a perturbation term. For the first iteration step, the initial estimate must be provided by an external source; for subsequent steps, the initial estimate is the updated value for the previous step.

$$\begin{aligned} \mathbf{x} &= \bar{\mathbf{x}} + \boldsymbol{\delta}\mathbf{x} \\ \bar{\mathbf{x}} = \begin{bmatrix} \bar{L}_A & \bar{\lambda}_A & \bar{h}_A & \bar{t}_X \end{bmatrix}^T & \qquad \boldsymbol{\delta}\mathbf{x} = [\delta L_A \;\; \delta\lambda_A \;\; \delta h_A \;\; \delta t_X]^T \end{aligned} \qquad \text{Eq 271}$$

The scalar measurement $\tilde{z}_i$ can thus be replaced by the <u>first-order (or linearized) scalar measurement</u>

$$\begin{aligned} \delta z_i &\equiv \tilde{z}_i - f_i(\bar{L}_A, \bar{\lambda}_A, \bar{h}_A, \bar{t}_X) \qquad i = 1, \ldots, m \\ &= \frac{\partial f_i}{\partial L_A}\delta L_A + \frac{\partial f_i}{\partial \lambda_A}\delta\lambda_A + \frac{\partial f_i}{\partial h_A}\delta h_A + \frac{\partial f_i}{\partial \Delta t}\delta t_X + v_i \end{aligned} \qquad \text{Eq 272}$$

In Eq 272, all partial derivatives are evaluated at the initial estimates for the unknown variables.

In Eq 272, the quantity $\delta z_i = \tilde{z}_i - f_i(\bar{L}_A, \bar{\lambda}_A, \bar{h}_A, \bar{t}_X)$ is often called the measurement residual. An abnormally large measurement residual can be the basis for rejecting a measurement as anomalous. A scalar cost function *C* that quantifies the measurement residuals is:

$$C \equiv \boldsymbol{\delta}\mathbf{z}^T \mathbf{W}\, \boldsymbol{\delta}\mathbf{z} \qquad \text{Eq 273}$$

$$\begin{aligned} \boldsymbol{\delta}\mathbf{z} &= \tilde{\mathbf{z}} - \mathbf{f}(\bar{L}_A, \bar{\lambda}_A, \bar{h}_A, \bar{t}_X) \\ \boldsymbol{\delta}\mathbf{z} \equiv \begin{bmatrix} \delta z_1 \cdots \delta z_m \end{bmatrix}^T & \qquad \tilde{\mathbf{z}} \equiv \begin{bmatrix} \tilde{z}_1 \cdots \tilde{z}_m \end{bmatrix}^T \qquad \mathbf{f} \equiv \begin{bmatrix} f_1 \cdots f_m \end{bmatrix}^T \end{aligned} \qquad \text{Eq 274}$$

Here, **W** is an analyst-defined positive-definite, symmetric (and often diagonal) matrix that weights the measurement equations. A method for selecting **W** is given in Subsection 8.1.3.

The full set of equations for the linearize measurement model (Eq 272) can be written as

$$\begin{bmatrix} \delta z_1 \\ \vdots \\ \vdots \\ \vdots \\ \delta z_m \end{bmatrix} = \begin{bmatrix} \frac{\partial f_1}{\partial L_A} & \frac{\partial f_1}{\partial \lambda_A} & \frac{\partial f_1}{\partial h_A} & \frac{\partial f_1}{\partial t_X} \\ \vdots & \vdots & \vdots & \vdots \\ \vdots & \vdots & \vdots & \vdots \\ \frac{\partial f_m}{\partial L_A} & \frac{\partial f_m}{\partial \lambda_A} & \frac{\partial f_m}{\partial h_A} & \frac{\partial f_m}{\partial t_X} \end{bmatrix} \begin{bmatrix} \delta L_A \\ \delta \lambda_A \\ \delta h_A \\ \delta t_X \end{bmatrix} + \begin{bmatrix} v_1 \\ \vdots \\ \vdots \\ \vdots \\ v_m \end{bmatrix} \qquad \text{Eq 275}$$

Denoting the matrix of partial derivatives as **J** (for Jacobian), Eq 275 can be written as the linearized matrix measurement model

$$\boldsymbol{\delta z} = \mathbf{J}\,\boldsymbol{\delta x} + \mathbf{v} \qquad \text{Eq 276}$$

$$\mathbf{J} \equiv \begin{bmatrix} \frac{\partial f_1}{\partial L_A} & \frac{\partial f_1}{\partial \lambda_A} & \frac{\partial f_1}{\partial h_A} & \frac{\partial f_1}{\partial t_X} \\ \vdots & \vdots & \vdots & \vdots \\ \frac{\partial f_m}{\partial L_A} & \frac{\partial f_m}{\partial \lambda_A} & \frac{\partial f_m}{\partial h_A} & \frac{\partial f_m}{\partial t_X} \end{bmatrix} \qquad \mathbf{v} \equiv \begin{bmatrix} v_1 \\ \vdots \\ \vdots \\ v_m \end{bmatrix}$$

In general, matrix **J** is non-square and cannot be inverted. The standard approach is to compute **δx** as the value that minimizes the weighted sum of the squared residuals after being adjusted by an estimate for **δx**. Thus, denoting $\hat{C}$ as the cost function to be minimized:

$$\hat{C} \equiv (\boldsymbol{\delta z} - \mathbf{J}\,\boldsymbol{\delta x})^T\,\mathbf{W}(\boldsymbol{\delta z} - \mathbf{J}\,\boldsymbol{\delta x}) = \boldsymbol{\delta z}^T\mathbf{W}\boldsymbol{\delta z} - 2\boldsymbol{\delta x}^T\mathbf{J}^T\mathbf{W}\,\boldsymbol{\delta z} + \boldsymbol{\delta x}^T\mathbf{J}^T\mathbf{W}\,\mathbf{J}\,\boldsymbol{\delta x} \qquad \text{Eq 277}$$

The value **δx** that minimizes $\hat{C}$ in Eq 277 is

$$\boldsymbol{\delta \hat{x}} = \left(\mathbf{J}^T\,\mathbf{W}\,\mathbf{J}\right)^{-1}\mathbf{J}^T\,\mathbf{W}\,\boldsymbol{\delta z} \qquad \text{Eq 278}$$

Existence of the matrix inverse indicated in Eq 278 requires that **J** be of full rank, i.e., to have linearly independent columns. For the situation where the number of measurements is the same as the number of unknown variables, Eq 278 reduces to Eq 279 below. In this situation, there is no role for a weighting matrix **W**.

$$\boldsymbol{\delta \hat{x}} = \mathbf{J}^{-1}\boldsymbol{\delta z} \qquad \text{Eq 279}$$

Given the solution for **δx̂**, the unknown variables are updated in accordance with

$$\hat{\mathbf{x}} = \bar{\mathbf{x}} + \boldsymbol{\delta \hat{x}} \qquad \text{Eq 280}$$

$$\hat{L}_A = \bar{L}_A + \delta\hat{L}_A \qquad \hat{\lambda}_A = \bar{\lambda}_A + \delta\hat{\lambda}_A \qquad \hat{h}_A = \bar{h}_A + \delta\hat{h}_A \qquad \hat{t}_X = \bar{t}_X + \delta\hat{t}_X$$

Combining Eq 280, Eq 279 and Eq 274 yields

$$\hat{\mathbf{x}} = \overline{\mathbf{x}} + \mathbf{J}^{-1}[\tilde{\mathbf{z}} - \mathbf{f}(\overline{\mathbf{x}})] \qquad \text{Eq 281}$$

This (Eq 281) is the multi-dimensional Newton-Raphson formula for solving $\tilde{\mathbf{z}} = \mathbf{f}(\mathbf{x})$ by iteration. It applies when the number of equations is equal to the number of unknown variables — a common situation in navigation.

Combining Eq 280, Eq 278 and Eq 274 yields

$$\hat{\mathbf{x}} = \overline{\mathbf{x}} + (\mathbf{J}^T \mathbf{W} \mathbf{J})^{-1} \mathbf{J}^T \mathbf{W} [\tilde{\mathbf{z}} - \mathbf{f}(\overline{\mathbf{x}})] \qquad \text{Eq 282}$$

This (Eq 281) is the Gauss formula for solving $\tilde{\mathbf{z}} \approx \mathbf{f}(\mathbf{x})$ by iteration, and applies when the number of equations exceeds the number of unknown variables.

In contrast to Eq 281 and Eq 282, in the vector/matrix notation employed in this chapter, the solution methods of Chapters 3-7 can be written as $\mathbf{x} = \mathbf{f}^{-1}(\tilde{\mathbf{z}})$. By taking advantage of the structure of specific problems, the measurement equations involved can be inverted.

For $\boldsymbol{\delta}\hat{\mathbf{x}}$ given by Eq 278, $\hat{C}$ (Eq 277) evaluates to

$$\hat{C} = \boldsymbol{\delta}\mathbf{z}^T \left(\mathbf{W} - \mathbf{W}\,\mathbf{J} \left(\mathbf{J}^T\,\mathbf{W}\,\mathbf{J} \right)^{-1} \mathbf{J}^T\,\mathbf{W} \right) \boldsymbol{\delta}\mathbf{z} = C - \Delta C \qquad \text{Eq 283}$$

$\hat{C}$ can be interpreted as the difference between C (the weighted sum of the squared measurement residuals for $\tilde{\mathbf{z}} - \mathbf{f}(\overline{\mathbf{x}})$ and ΔC (the estimated amount that the residual would be reduced after using $\boldsymbol{\delta}\hat{\mathbf{x}}$ to adjust the unknown variables). By employing a matrix inequality, it can be shown (Ref. 52) that $\hat{C}$ must be non-negative. When the number of equations is equal to the number of unknowns (and noting that $\mathbf{J}$ must be invertible in that situation), $\hat{C}$ is equal to zero.

A convergence check is performed at the end of each iteration step. This involves comparing the updated value of each unknown variable with its initial estimate. If the measurement equations (Eq 269) are linear functions of the unknown variables, then only one iteration is needed. However, when the measurements are nonlinear functions of the unknown variables, at least two iterations should be performed — the last step confirming that the changes in the values of the variables sought are negligible.

The value of the cost function (Eq 273) is usually monitored for each iteration. Temporarily using an additional subscript to denote the iteration number, the cost function for the next iteration (say C_{n+1}) will be different than the value of Eq 283 for the current iteration (say $\hat{C}_n$). The latter can be regarded as a prediction of the former based on first-order perturbations.

If convergence is not achieved in an iteration step, the updated value for each unknown variable

becomes the initial estimate for that variable in the next step:

$$\bar{L}_{A,n+1} = \hat{L}_{A,n} \qquad \bar{\lambda}_{A,n+1} = \hat{\lambda}_{A,n} \qquad \bar{h}_{A,n+1} = \hat{h}_{A,n} \qquad \bar{t}_{X,n+1} = \hat{t}_{X,n} \qquad \text{Eq 284}$$

The solution process (Eq 271 - Eq 283) is then repeated.

8.1.3 Solution Properties

Here Eq 278 defines $\boldsymbol{\delta\hat{x}}$, and is the formal solution to the Normal Equation (Eq 285).

$$\left(\mathbf{J}^T\,\mathbf{W}\,\mathbf{J}\right)\boldsymbol{\delta x} = \mathbf{J}^T\,\mathbf{W}\,\boldsymbol{\delta z} \qquad \text{Eq 285}$$

Numerical methods for solving the Normal Equation are available that are more stable than directly computing the inverse of the matrix on the left-hand side of Eq 285. Perhaps the best approach is to not compute that matrix, and to perform orthogonal decomposition on $\mathbf{W}^{½}\,\mathbf{J}$, where $\mathbf{W}^{½}\,\mathbf{W}^{½} = \mathbf{W}$ (i.e., utilize the antecedent of the normal equations, similar to Eq 276). This can be accomplished in some mathematical software packages using the '\' operator. In the syntax of such packages, $\boldsymbol{\delta\hat{x}}$ is computed using

$$\boldsymbol{\delta\hat{x}} = \left(\mathbf{W}^{1/2}\,\mathbf{J}\right) \backslash \left(\mathbf{W}^{1/2}\,\boldsymbol{\delta z}\right) \qquad \text{Eq 286}$$

Returning to conventional notation, if Eq 276 is substituted into Eq 278, the result is

$$\boldsymbol{\delta\hat{x}} = \boldsymbol{\delta x} + \left(\mathbf{J}^T\,\mathbf{W}\,\mathbf{J}\right)^{-1}\mathbf{J}^T\,\mathbf{W}\,\mathbf{v} \qquad \text{Eq 287}$$

Thus, in the context of the linearized measurement model, $\boldsymbol{\delta\hat{x}}$ from Eq 278 is an unbiased estimate of $\boldsymbol{\delta x}$ and is corrupted only by measurement errors. The covariance matrix of the estimation error for the unknown variables is

$$E\left(\boldsymbol{\delta\hat{x}} - \boldsymbol{\delta x}\right)\left(\boldsymbol{\delta\hat{x}} - \boldsymbol{\delta x}\right)^T = \left(\mathbf{J}^T\,\mathbf{W}\,\mathbf{J}\right)^{-1}\mathbf{J}^T\,\mathbf{W}\,\mathbf{R}\,\mathbf{W}\,\mathbf{J}\left(\mathbf{J}^T\,\mathbf{W}\,\mathbf{J}\right)^{-1} \qquad \text{Eq 288}$$

Here, $\mathbf{R}$ is the measurement error covariance matrix:

$$E\left(\mathbf{v}\right) = \mathbf{0} \qquad E\left(\mathbf{v}\mathbf{v}^T\right) = \mathbf{R} \qquad \text{Eq 289}$$

It can be shown that (Ref. 52) that the estimation error covariance (Eq 288) has the following lower bound

$$E\left(\boldsymbol{\delta\hat{x}} - \boldsymbol{\delta x}\right)\left(\boldsymbol{\delta\hat{x}} - \boldsymbol{\delta x}\right)^T = \left(\mathbf{J}^T\,\mathbf{W}\,\mathbf{J}\right)^{-1}\mathbf{J}^T\,\mathbf{W}\,\mathbf{R}\,\mathbf{W}\,\mathbf{J}\left(\mathbf{J}^T\,\mathbf{W}\,\mathbf{J}\right)^{-1} \geq \left(\mathbf{J}^T\,\mathbf{R}^{-1}\,\mathbf{J}\right)^{-1} \qquad \text{Eq 290}$$

It can further shown that the lower bound is only achieved when $\mathbf{W} = \mathbf{R}^{-1}$. For this reason, the weight matrix is often chosen to be the inverse of the measurement error covariance matrix.

When the number of measurements and unknown variables are equal, $\mathbf{W}$ is the identify matrix and Eq 290 becomes

$$E\left(\delta\hat{\mathbf{x}} - \delta\mathbf{x}\right)\left(\delta\hat{\mathbf{x}} - \delta\mathbf{x}\right)^T = \left(\mathbf{J}^T\,\mathbf{J}\right)^{-1}\mathbf{J}^T\mathbf{R}\,\mathbf{J}\left(\mathbf{J}^T\,\mathbf{J}\right)^{-1} \geq \left(\mathbf{J}^T\mathbf{R}^{-1}\,\mathbf{J}\right)^{-1} \quad \text{Eq 291}$$

For the situation (often-assumed for convenience) when the measurement errors are independent and have a common variance σ^2_{meas}, both Eq 290 (provided that $\mathbf{W} = \mathbf{R}^{-1}$.) and Eq 291 reduce to

$$E\left(\delta\hat{\mathbf{x}} - \delta\mathbf{x}\right)\left(\delta\hat{\mathbf{x}} - \delta\mathbf{x}\right)^T = \sigma^2_{meas}\left(\mathbf{J}^T\,\mathbf{J}\right)^{-1} \quad \text{Eq 292}$$

An alternate to Eq 283 for computing $\hat{C}$ is

$$\hat{C} = \left(\delta\mathbf{z} - \mathbf{J}\,\delta\hat{\mathbf{x}}\right)^T\mathbf{W}\,\delta\mathbf{z} = \delta\mathbf{z}^T\mathbf{W}\,\delta\mathbf{z} - \delta\hat{\mathbf{x}}^T\,\mathbf{J}^T\mathbf{W}\,\delta\mathbf{z} \quad \text{Eq 293}$$

This is true because

$$\left(\delta\mathbf{z} - \mathbf{J}\,\delta\hat{\mathbf{x}}\right)^T\mathbf{W}\,\mathbf{J}\,\delta\hat{\mathbf{x}} = 0 \quad \text{Eq 294}$$

8.1.4 Advantages of the LLS Technique

Uses All Measurements — One reason for employing the LLS technique is to be able to utilize more measurements than there are unknown variables. Using redundant equations enables some averaging of measurement errors and often eliminates the ambiguous/extraneous solutions that can occur with the minimum required number of equations.

Utilizes Uninvertible Measurement Equations — While all of the measurement equations in Chapters 3-7 are analytically invertible (i.e., expressions exist for the unknown variables as functions of the measurements), invertibility is not always possible. Thus, another motivation for utilizing the LLS approach is its capability to utilize measurement equations that cannot be inverted. Such situations generally arise because an expression that accurately characterizes a measurement is too complex to be inverted.

Utilizes Non-Equation "Measurement Equations" — In most applications, the measurement equations (symbolized by $f_i(L_A, \lambda_A, h_A, t_X)$ in Eq 269) is the most accurate available representation of the quantities which are measured. Since invertibility is not required, the "measurement equations" need not be equations in the analytic sense. Rather, what is needed is a process to compute the measured quantities (e.g., ranges and/or angles) as a function of the independent variables (e.g., L_A, λ_A, h_A and t_X). A combination of analytic expressions, recursive algorithms (such as Vincenty's) and table lookup have been used as "measurement equations".

Approximate Jacobians Useful — Because the LLS solution technique is recursive, the elements of the Jacobian matrix (**J** in Eq 276) need not be precisely equal to the partial derivatives of the measurement equations (which may not even have derivatives). This situation is analogous to the secant method for finding the root of a scalar equation using approximations to the derivative of the equation (Subsection 2.1.6). In navigation and surveillance applications,

an obvious source of such approximations is the spherical earth model (Subsection 8.3.2).

Provides Accuracy Estimates — An important feature of the LLS technique is that it provides estimates of the accuracy of a solution to the measurement equations. Characterizations for both the measurement residuals (Eq 273) and the navigation variables (Eq 288 – Eq 292) are available, including for the situation where the number of measurements and unknown variables are equal. With an equal number of measurements and variables, a closed-form solution can be obtained (Chapters 3-7) and the solution error can be estimated separately (Eq 288 - Eq 292).

Role of Accuracy Estimates — Estimating position error statistics from station locations and measurement error statistics is often used in planning studies — e.g., to determine the stations should be placed for a proposed system. Since measurement error statistics are approximate and virtually never regarded as having the same level of precision as a position solution, characterizing the earth as an ellipsoid is usually not necessary.

Useful Optimization Criterion — The LLS technique employs an optimization criterion that has proven to be useful in a wide variety of application areas for over 200 years. Focusing on navigation, Ref. 46 contains a case study of several solution techniques; its conclusion is that the linearized least-squares technique always yields a "good", and often the "best", solution.

Proven in Navigation Applications — Several important navigation systems have been deployed with the assumption that user's would use the LLS technique or an evolved form of it (e.g., Kalman Filter) to convert a set of measurements to latitude/longitude coordinates. Prominent examples are Loran-C, Omega and GPS. [*]

8.1.5 Remarks

Historical Credit — Ascribing the LLS technique to Gauss and Newton is established usage, if not completely accurate historically. While the least-squares technique is usually credited to Carl Friedrich Gauss, a case has been made for Adrien-Marie Legendre. Isaac Newton is often credited with the technique for iterative solution of an equation whereby the value of the independent variable is changed by the ratio of value of the dependent variable to its derivative. Joseph Raphson frequently shares credit.

Dilution of Precision (DoP) — When the measurement errors for individual stations are independent and have a common variance, then the estimate of the accuracy for navigation variables in Eq 292 is the product of: (a) a factor, $\mathbf{(J^T J)^{-1}}$, that depends only on the geometry of

[*] These systems now (or did) involve station-vehicle separations of up to twelve thousand nautical miles. To achieve achieve useful accuracies over such distances, the ellipticity of the earth is/was characterized in the measurement equations.

the aircraft and the stations; and (b) a factor, σ^2_{meas}, that depends only on the electronic systems involved (including their installations). Often only the geometric factor is analyzed, and various Dilution of Precision (DoP) metrics are defined for the elements of $\mathbf{(J^T J)^{-1}}$ — see Subsections 8.2.5, 8.4.1, 8.4.2, 8.4.4 and 8.4.5.

Jacobian Rank — The necessity that the Jacobian matrix **J** be of full rank is an observability requirement. Essentially, in order for an unknown variable to be determined, a change from the assumed initial value must cause a unique signature in the available measurements.

Initial Estimate — The first iteration step requires that initial estimates be provided for the quantities sought. Potential sources for the initial estimates are: (1) a solution based on an assumed spherical-earth; (2) a previous estimate, possibly updated by changes from the previous solution (obtained from, e.g., a "tracker" or dead-reckoning system); and (3) user-provided.

Qualitative Characteristics — While the LLS technique has been applied to many fields, qualitative conclusions drawn in one field may not be valid in another. Much of the modern LLS literature involves its application to model parameter identification. Often parameter identification can be characterized as fitting an equation with a few unknown parameters and heuristically chosen functions to many (hundreds or even thousands) measurements (e.g., Ref. 53). While this literature is mathematically relevant, judgment must be exercised before adopting qualitative conclusions to navigation and surveillance applications.

In contrast to parameter identification, navigation/surveillance applications usually involve: (a) at most, only a few more measurements than unknown variables;[*] (b) a scientific basis for the functions being fitted; and (c) reasonably good initial values for the unknown variables. These factors reduce the likelihood that a solution will yield a local (rather than a global) minimum and largely eliminate concerns about computational resources.

Geometric Interpretation — A geometric interpretation of Eq 294 is that the measurement residual after correction by $\boldsymbol{\delta\hat{x}}$ is orthogonal to the estimate of the perturbation of the unknown variables. Informally, the interpretation is that — within the limitations of linear perturbation models — the estimate $\boldsymbol{\delta\hat{x}}$ embodies all the information available from the measurements.

Probabilistic Interpretation — Although not done herein, probability distributions can be assigned to the measurement errors. This enables determination of additional statistical quantities — e.g., confidence bounds on the unknown variables. Such analyses are most meaningful when there are many more measurements than there are unknown variables.

[*] Generally, the cost of providing an additional real-time navigation or surveillance measurement is the cost of a ground station (real estate, equipment, installation and maintenance). This is usually significantly more than the cost of an additional parameter identification measurement (e.g., that of extending a data collection period).

Numerical Examples — Examples 10 (Subsection 8.4.4) and 12 (Subsection 8.4.6) illustrate the convergence of the LLS iterative method for ellipsoidal earth measurements and spheroidal Jacobian elements. In these examples, the iteration process is initialized by the solution for a spherical earth, and four or fewer iterations are needed to reduce the residual aircraft location error to less than the error in the location of the ground stations involved.

8.2 Solution Employing Cartesian Coordinates

8.2.1 Introduction

Application of the linearized least-squares technique described in Section 8.1 only requires specification of the measurement equations (Eq 269) and the weight matrix (Eq 273). Moreover, the latter is not needed if the number of measurements and unknown variables are equal. Among the most common least-squares applications are those involving 'range-type' measurements of the distance between an aircraft and a known location. These include:

- Actual slant-range measurements of the distance between an aircraft and a station — such as a radar or a DME transponder. Usually, these involve transmission and reception of signals by both the station and the aircraft (two-way ranging).
- Pseudo slant-range measurements of the distance, plus an offset common to all stations, between an aircraft and one of set of stations with synchronized clocks — such as a multilateration remote unit or GPS satellite. Usually, these involve transmission of signals by one entity and reception by the other (one-way ranging).
- Altitude measurements of the distance between an aircraft and the center of the earth — usually performed by a barometric altimeter (see Appendix Section 9.1).

Range-type measurements can be processed/analyzed using any rectangular coordinate frame, since the form of Pythagoras's equation is the same in all frames. Thus the choice generally depends upon the application. One option, suitable for small areas, is a local tangent plane frame (Subsection 5.1.2). For larger areas, the earth-centered earth-fixed (ECEF) frame **e** introduced in Section 5.1.1 is more suitable, and is used in this section. If station **S** is has latitude $\boldsymbol{L_S}$, longitude $\boldsymbol{\lambda_S}$ and altitude $\boldsymbol{h_S}$, its ECEF coordinates are

$$\underline{\mathbf{r}}^{\mathbf{e}}_{Si} = \begin{bmatrix} \cos(L_S)\cos(\lambda_S) \\ \cos(L_S)\sin(\lambda_S) \\ \sin(L_S) \end{bmatrix} (R_e + h_S) = \begin{bmatrix} x_S \\ y_S \\ z_S \end{bmatrix} \qquad \text{Eq 295}$$

Assuming that the aircraft **A** is has unknown latitude $\boldsymbol{L_A}$, unknown longitude $\boldsymbol{\lambda_A}$ and unknown altitude $\boldsymbol{h_A}$, then its unknown ECEF coordinates are

$$\underline{\mathbf{r}}_A^{\mathbf{e}} = \begin{bmatrix} \cos(L_A)\cos(\lambda_A) \\ \cos(L_A)\sin(\lambda_A) \\ \sin(L_A) \end{bmatrix} (R_e + h_A) = \begin{bmatrix} x_A \\ y_A \\ z_A \end{bmatrix} \qquad \text{Eq 296}$$

A caveat concerning notation: In this section, ***z*** denotes one axis in the ECEF system, while in Section 8.1, ***z*** denotes a generic measurement. Hopefully, this will not cause confusion.

8.2.2 Measurement Equations

Range Measurement — The non-linear scalar measurement model, corresponding to Eq 269, for the slant range $\boldsymbol{d_{ri}}$ between ranging station $\mathbf{S}_{ri}$ and aircraft **A** is

$$\begin{aligned} \tilde{d}_{ri} &= d_{ri} + v_{ri} \\ d_{ri} &= \sqrt{(x_A - x_{ri})^2 + (y_A - y_{ri})^2 + (z_A - z_{ri})^2} \end{aligned} \qquad \text{Eq 297}$$

Here, x_{ri}, y_{ri}, z_{ri} are the ECEF coordinates of $\mathbf{S}_{ri}$. The partial derivatives of $\boldsymbol{d}_{ri}$ with respect to the unknown aircraft position variables (corresponding to the partial derivatives in Eq 272) are

$$\frac{\partial d_{ri}}{\partial x_A} = \frac{x_A - x_{ri}}{d_{ri}} \qquad \frac{\partial d_{ri}}{\partial y_A} = \frac{y_A - y_{ri}}{d_{ri}} \qquad \frac{\partial d_{ri}}{\partial z_A} = \frac{z_A - z_{ri}}{d_{ri}} \qquad \text{Eq 298}$$

The measurement residual, corresponding to the left-hand side of Eq 272, is

$$\delta d_{ri} = \tilde{d}_{ri} - \bar{d}_{ri} = \tilde{d}_{ri} - \sqrt{(\bar{x}_A - x_{ri})^2 + (\bar{y}_A - y_{ri})^2 + (\bar{z}_A - z_{ri})^2} \qquad \text{Eq 299}$$

Here $\tilde{d}_{ri}$ denotes the output of ranging instrument/system (e.g., DME) i and $\bar{x}_A, \bar{y}_A, \bar{z}_A$ are initial estimates for the unknown variables, which be computed from initial estimate of latitude, longitude and altitude using Eq 296.

Pseudo Slant-Range Measurement — The non-linear scalar measurement model, corresponding to Eq 269, for the pseudo slant-range $\boldsymbol{p_{pi}}$ between station $\mathbf{S}_{pi}$ and aircraft **A** is

$$\begin{aligned} \tilde{p}_{pi} &= p_{pi} + v_{pi} \\ p_{pi} &= \sqrt{(x_A - x_{pi})^2 + (y_A - y_{pi})^2 + (z_A - z_{pi})^2} + c\,t_X \end{aligned} \qquad \text{Eq 300}$$

Here, x_{pi}, y_{pi}, z_{pi} are the ECEF coordinates of $\mathbf{S}_{pi}$ and $\boldsymbol{c}$ is the known speed of propagation.

The partial derivatives of $\boldsymbol{p}_{pi}$ with respect to the unknown variables (corresponding to the partial derivatives in Eq 272) are

$$\frac{\partial p_{pi}}{\partial x_A} = \frac{x_A - x_{pi}}{d_{pi}} \qquad \frac{\partial p_{pi}}{\partial y_A} = \frac{y_A - y_{pi}}{d_{pi}} \qquad \frac{\partial p_{pi}}{\partial z_A} = \frac{z_A - z_{pi}}{d_{pi}} \qquad \frac{\partial p_{pi}}{\partial t_X} = c \qquad \text{Eq 301}$$

In Eq 301, $\boldsymbol{d}_{pi}$ is given by

$$d_{pi} = \sqrt{\left(x_A - x_{pi}\right)^2 + \left(y_A - y_{pi}\right)^2 + \left(z_A - z_{pi}\right)^2} \qquad \text{Eq 302}$$

The measurement residual, corresponding to the left-hand side of Eq 272, is

$$\delta p_i = \tilde{p}_i - \bar{p}_i = \tilde{p}_i - \sqrt{\left(\bar{x}_A - x_{pi}\right)^2 + \left(\bar{y}_A - y_{pi}\right)^2 + \left(\bar{z}_A - z_{pi}\right)^2} - c\bar{t}_X \qquad \text{Eq 303}$$

Here $\tilde{p}_i$ denotes the output of pseudo slant-range station *i* (e.g., multilateration system Remote Unit) and $\overline{\Delta t}$ is the initial estimates for the unknown clock synchronization difference.

Altitude Measurement — Let $\boldsymbol{r_A}$ be the distance from the aircraft **A** to the earth's center. Then the non-linear scalar measurement model, corresponding to Eq 269, for an altimeter measurement is

$$\begin{aligned} \tilde{r}_A &= R_e + \tilde{h}_A = R_e + h_A + v_{alt} \\ r_A &= R_e + h_A = \sqrt{\left(x_A\right)^2 + \left(y_A\right)^2 + \left(z_A\right)^2} \end{aligned} \qquad \text{Eq 304}$$

The partial derivatives of $\boldsymbol{r_A}$ with respect to the unknown variables (corresponding to the partial derivatives in Eq 272) are

$$\frac{\partial r_A}{\partial x_A} = \frac{x_A}{r_A} \qquad \frac{\partial r_A}{\partial y_A} = \frac{y_A}{r_A} \qquad \frac{\partial r_A}{\partial z_A} = \frac{z_A}{r_A} \qquad \text{Eq 305}$$

The measurement residual, corresponding to the left-hand side of Eq 272, is

$$\delta r_A = \tilde{h}_A - \bar{h}_A = \tilde{h}_A + R_e - \sqrt{\left(\bar{x}_A\right)^2 + \left(\bar{y}_A\right)^2 + \left(\bar{z}_A\right)^2} \qquad \text{Eq 306}$$

Here $\tilde{h}_A$ denotes the altimetry system output.

Rather than treat the altimeter output as a measurement (as is done in this subsection), it is also possible to treat it as a constraint, as is done in Subsection 8.2.4.

Weight Matrix / Measurement Error Covariance — The weight matrix **W** (which is not needed when the number of measurements and unknown variables are equal) is selected — usually as the inverse of measurement error covariance **R**. The latter is usually chosen as a diagonal matrix whose elements are the measurement error variances (i.e., the measurement errors are assumed to be uncorrelated).

$$\mathbf{R} = \text{diag}[\ \sigma_{r1}^2 \ldots \sigma_{p1}^2 \ldots \sigma_{alt}^2\ ] \qquad \text{Eq 307}$$

8.2.3 Solution Process

The vector of measurement residuals (e.g., left-hand side of Eq 275) is assembled, one element

per measurement, from Eq 299, Eq 303 and Eq 306. The Jacobian matrix **J** (as in Eq 275) is assembled, one row per measurement, from Eq 298, Eq 301 and Eq 305. Except for notation, the iteration process is identical to that described in Subsection 8.1.2. For each iteration, the initial estimates of the unknown variable $\bar{x}_A, \bar{y}_A, \bar{z}_A$ and $\bar{t}_X$ (if applicable) are employed to generate updated estimates $\hat{x}_A, \hat{y}_A, \hat{z}_A$ and $\hat{t}_X$ (if applicable) using Eq 278. The process is terminated when the change between the initial and updated estimates are insignificant.

When the iteration process has converged, the values for $\hat{x}_A, \hat{y}_A, \hat{z}_A$ and $\hat{t}_X$ (if applicable) during the last iteration are employed to determine the aircraft latitude, longitude and altitude using Eq 181.

8.2.4 Altitude Constraint

Rationale — In aviation applications, it's often the case that altimeter reading, which may or may not be considered to be error-free, cannot be improved upon by slant-range and pseudo slant-range measurements whose signal paths are essentially parallel to the earth's surface. Mathematically, altimeter information constitutes a constraint rather than a measurement. The linearized measurement model corresponding to Eq 272 then is

$$\delta r_A = \frac{x_A}{r_A}\delta x_A + \frac{y_A}{r_A}\delta y_A + \frac{z_A}{r_A}\delta z_A + v_{alt} = 0 \qquad \text{Eq 308}$$

This equation can be solved for any one of the three unknown position variables in terms of the other two. Upon selecting, δz_A as the variable to be found in terms of the other two position coordinates, Eq 308 can be re-written as

$$\delta z_A = -\frac{\frac{x_A}{r_A}\delta x_A + \frac{y_A}{r_A}\delta y_A + v_{alt}}{\frac{z_A}{r_A}} = -\frac{x_A}{z_A}\delta x_A - \frac{y_A}{z_A}\delta y_A - \frac{r_A}{z_A}v_{alt} \qquad \text{Eq 309}$$

Slant-Range and Pseudo Slant-Range Measurements — By substituting for δz_A using Eq 309, the number of unknown variable is reduced by one, and the analysis can be re-cast in terms of the remaining unknown variables. The linearized measurement models then become

$$\begin{aligned} \delta d_{ri} &= \frac{\partial d_{ri}}{\partial x_A}\delta x_A + \frac{\partial d_{ri}}{\partial y_A}\delta y_A + v_{di} - \frac{z_A - z_{di}}{d_{ri}}\frac{r_A}{z_A}v_{alt} \\ \delta p_{pi} &= \frac{\partial p_{pi}}{\partial x_A}\delta x_A + \frac{\partial p_{pi}}{\partial y_A}\delta y_A + c\delta\Delta t + v_{pi} - \frac{z_A - z_{pi}}{d_{pi}}\frac{r_A}{z_A}v_{alt} \end{aligned} \qquad \text{Eq 310}$$

In Eq 310, the partial derivatives of $\boldsymbol{d}_{ri}$ and $\boldsymbol{p}_{pi}$ with respect to the two remaining unknown position variables are

$$\frac{\partial d_{ri}}{\partial x_A} = \frac{x_A - x_{ri}}{d_{ri}} - \frac{z_A - z_{ri}}{d_{ri}}\frac{x_A}{z_A} \qquad \frac{\partial d_{ri}}{\partial y_A} = \frac{y_A - y_{ri}}{d_{ri}} - \frac{z_A - z_{ri}}{d_{ri}}\frac{y_A}{z_A}$$
$$\frac{\partial p_{pi}}{\partial x_A} = \frac{x_A - x_{pi}}{d_{pi}} - \frac{z_A - z_{pi}}{d_{pi}}\frac{x_A}{z_A} \qquad \frac{\partial p_{pi}}{\partial y_A} = \frac{y_A - y_{pi}}{d_{pi}} - \frac{z_A - z_{pi}}{d_{pi}}\frac{y_A}{z_A} \qquad \text{Eq 311}$$

The re-cast problem thus involves a Jacobian matrix having dimensions $m\times2$ or $m\times3$, where the first dimension, m, is the total number of slant-range and pseudo slant-range measurements, and the second dimension is the number of remaining unknown variables. The measurement residuals are computed as in Eq 299 and Eq 303.

Measurement Error Covariance — Assuming that the altimeter error is not neglected, the re-cast problem also involves a different measurement error covariance matrix. It has larger diagonal terms and off-diagonal terms, and is a function of both the aircraft's and station's position. If the slant-range, pseudo slant-range and altimeter errors are assumed to be uncorrelated, then the re-cast measurement error covariance matrix is:

$$\mathbf{R} = \begin{bmatrix} \sigma_{r1}^2 & 0 & \cdots & 0 & \cdots \\ 0 & \sigma_{r2}^2 & \cdots & 0 & \cdots \\ \vdots & \vdots & \ddots & \vdots & \\ 0 & 0 & \cdots & \sigma_{p1}^2 & \cdots \\ \vdots & \vdots & & \vdots & \ddots \end{bmatrix} +$$

$$\begin{bmatrix} \left(\frac{z_A - z_{r1}}{d_{r1}}\right)^2 & \frac{z_A - z_{r1}}{d_{r1}}\frac{z_A - z_{r2}}{d_{r2}} & \cdots & \frac{z_A - z_{r1}}{d_{r1}}\frac{z_A - z_{p1}}{d_{p1}} & \cdots \\ \frac{z_A - z_{r1}}{d_{r1}}\frac{z_A - z_{r2}}{d_{r2}} & \left(\frac{z_A - z_{r2}}{d_{r2}}\right)^2 & \cdots & \frac{z_A - z_{r2}}{d_{r2}}\frac{z_A - z_{p1}}{d_{p1}} & \cdots \\ \vdots & \vdots & \ddots & \vdots & \\ \frac{z_A - z_{r1}}{d_{r1}}\frac{z_A - z_{p1}}{d_{p1}} & \frac{z_A - z_{r2}}{d_{r2}}\frac{z_A - z_{p1}}{d_{p1}} & \cdots & \left(\frac{z_A - z_{p1}}{d_{p1}}\right)^2 & \cdots \\ \vdots & \vdots & & \vdots & \ddots \end{bmatrix} \left(\frac{r_A}{z_A}\right)^2 \sigma_{alt}^2 \qquad \text{Eq 312}$$

Solution Process — The iterative process for finding the unknown variables is similar to that described in the first paragraph of Subsection 8.2.3. A difference is that, at each iteration, the value of $\delta\hat{z}_A$ is updated using

$$\delta\hat{z}_A = -\frac{\bar{x}_A}{\bar{z}_A}\delta\hat{x}_A - \frac{\bar{y}_A}{\bar{z}_A}\delta\hat{y}_A \qquad \text{Eq 313}$$

When the iteration process has converged, the values for $\hat{x}_A, \hat{y}_A, \hat{z}_A$ and $\hat{t}_X$ (if applicable) from the last iteration are employed to determine the aircraft latitude and longitude using Eq 181.

8.2.5 Dilution of Precision (DoP)

When the measurement are all the same type — e.g., slant-ranges or pseudo slant-ranges — frequently it's assumed that the measurement errors are independent and have the same variance, σ^2_{meas}. Then the estimation error covariance for the unknown variables (Eq 292) is the product of σ^2_{meas} and a term $\mathbf{(J^T J)^{-1}}$ that depends only on the measurement geometry.

Since, the formulation in this section utilizes the ECEF frame, in some instances it's convenient to rotate the Dilution of Precision (DoP) matrix $\mathbf{(J^T J)^{-1}}$ into the local-level frame at the estimated aircraft location using an expanded version of the direction cosine matrix of Eq 112:

$$\mathbf{C} = \begin{bmatrix} -\sin(\hat{\lambda}_A) & \cos(\hat{\lambda}_A) & 0 & 0 \\ \sin(-\hat{L}_A)\cos(\hat{\lambda}_A) & \sin(-\hat{L}_A)\sin(\hat{\lambda}_A) & \cos(-\hat{L}_A) & 0 \\ \cos(-\hat{L}_A)\cos(\hat{\lambda}_A) & \cos(-\hat{L}_A)\sin(\hat{\lambda}_A) & -\sin(-\hat{L}_A) & 0 \\ 0 & 0 & 0 & 1 \end{bmatrix} \qquad \text{Eq 314}$$

Thus the DoP matrix in the east-north-up frame at the estimated aircraft location is

$$\mathbf{M} = \mathbf{C}\left(\mathbf{J}^T\mathbf{J}\right)^{-1}\mathbf{C}^T = \begin{bmatrix} m_{ee} & m_{en} & m_{eu} & m_{e\Delta t} \\ m_{ne} & m_{nn} & m_{nu} & m_{n\Delta t} \\ m_{ue} & m_{un} & m_{uu} & m_{u\Delta t} \\ m_{\Delta te} & m_{\Delta tn} & m_{\Delta tu} & m_{\Delta t\Delta t} \end{bmatrix} \qquad \text{Eq 315}$$

The fourth row and column of **C** and **M** are not present when pseudo slant-range measurements are not involved. Various DoP quantities are computed from **M**, including Horizontal Dilution of Precision (HDoP), Vertical Dilution of Precision (VDoP), Time Dilution of Precision (TDoP) and Geometric Dilution of Precision (GDoP):

$$\begin{aligned} \text{HDoP} &= \sqrt{m_{ee} + m_{nn}} & \text{VDoP} &= \sqrt{m_{uu}} \\ \text{TDoP} &= \sqrt{m_{\Delta t\Delta t}} & \text{GDoP} &= \sqrt{m_{ee} + m_{nn} + m_{uu} + m_{\Delta t\Delta t}} \end{aligned} \qquad \text{Eq 316}$$

8.2.6 Remarks

Multilateration Application — An airport surface is a small enough region that the earth can be treated as flat within its perimeter, and a tangent plane coordinate system can be used. Also, aircraft on the surface can be assumed to be at the same altitude. Thus the multilateration pseudo

slant-range equations can be processed with two position variables. If low-altitude aircraft are involved, altitude information provided by aircraft can be employed for the vertical dimension, and combined with the multilateration horizontal solution.

GPS Application — GPS is 'at the other end' of the size scale from airport multilateration. The "ground stations" are satellites in orbit approximately 10,900 NM above the surface — about three times the radius of the earth. At this scale, and using only pseudo slant-range measurements, the ECEF frame is the natural setting.

Solution Option — When a set of pseudo slant-range measurements (Eq 300) is being processed, a solution method is to subtract one pseudo slant-range from the others. Analytically, this reduces the number of measurement equations by one, eliminates $\boldsymbol{\Delta t}$ as an unknown variable and increases the measurement error per equation. The hyperbolic geometry associated with range differences can provide insights into regions where a set of stations provides (and does not provide) effective measurements (e.g., Section 7.3). However, this solution method is not preferred for numerical results; knowing the clock offset and associated TDoP may be useful in some situations, and the additional computational cost is insignificant.

8.3 Solution Employing Spherical Coordinates (Latitude/Longitude/Altitude)

8.3.1 Introduction / Rationale

As shown in Chapter 7, Cartesian coordinates and range-type measurements result in simple measurement equations. However, in the context of much of aircraft navigation — involving station-aircraft distances of hundreds of miles — ECEF coordinates have important limitations:

- In contrast with range-type measurements, ECEF coordinates do not handle angular measurements well — e.g., the aircraft azimuth or geocentric angle from a station
- Each of the unknown ECEF variables x_A, y_A, z_A is a function of the aircraft latitude, longitude and altitude, complicating the placing of restrictions on the latter, more natural set of unknown variables.

A second reason to utilize spherical coordinates in an LLS solution is noted in Subsection 8.1.4, under the title "Approximate Jacobians Useful". Accurate solutions can be readily found when the Jacobian matrix elements are approximations (rather than exactly equal) to derivatives of the measurement equation. This is particularly important when the measurements pertain to an ellipsoidal earth; then Jacobian elements for a spherical earth are usually satisfactory.

In this section, it is assumed that station **S** is has known latitude $\boldsymbol{L_S}$, longitude $\boldsymbol{\lambda_S}$ and altitude $\boldsymbol{h_S}$. It is similarly assumed that the aircraft **A** is has unknown latitude $\boldsymbol{L_A}$ and longitude $\boldsymbol{\lambda_A}$ and possibly unknown altitude $\boldsymbol{h_A}$. It is further assumed that initial estimates for the unknown aircraft

coordinates $\bar{L}_A, \bar{\lambda}_A, \bar{h}_A$ and the time of transmission $\bar{t}_X$ by **A** or **S** (if applicable) are available.

8.3.2 Measurement Equations

Slant Range Measurement — The slant range between station **S** and aircraft **A** can be expressed in terms of $\boldsymbol{L}_A$, $\boldsymbol{\lambda}_A$ and $\boldsymbol{h}_A$ by substituting Eq 65 into Eq 159. Thus the nonlinear slant range measurement model is:

$$\begin{aligned}\tilde{d}_{AS} &= d_{AS} + v_{rS} \\ d_{AS} &= \sqrt{4(R_e + h_A)(R_e + h_S)\sin^2\left(\tfrac{1}{2}\theta_{AS}\right) + (h_A - h_S)^2} \\ &= \sqrt{4(R_e + h_A)(R_e + h_S)\left[\sin^2\left(\tfrac{1}{2}(L_A - L_S)\right) + \cos(L_A)\cos(L_S)\sin^2\left(\tfrac{1}{2}(\lambda_A - \lambda_S)\right)\right] + (h_A - h_S)^2}\end{aligned} \qquad \text{Eq 317}$$

Here $\tilde{d}_{AS}$ denotes the error-corrupted measurement, d_{AS} denotes the error-free slant range and $\boldsymbol{v}_{rS}$ denotes the additive measurement error.

The partial derivatives of $\boldsymbol{d}_{AS}$ with respect to the unknown aircraft position variables (corresponding to the partial derivatives in Eq 272) are

$$\begin{aligned}\frac{\partial d_{AS}}{\partial L_A} &= \frac{(R_e + h_A)(R_e + h_S)}{d_{AS}}\left[\sin(L_A - L_S) - 2\sin(L_A)\cos(L_S)\sin^2\left(\tfrac{1}{2}(\lambda_A - \lambda_S)\right)\right] \\ \frac{\partial d_{AS}}{\partial \lambda_A} &= \frac{(R_e + h_A)(R_e + h_S)}{d_{AS}}\cos(L_A)\cos(L_S)\sin(\lambda_A - \lambda_S) \\ \frac{\partial d_{AS}}{\partial h_A} &= \frac{2(R_e + h_S)}{d_{AS}}\left[\sin^2\left(\tfrac{1}{2}(L_A - L_S)\right) + \cos(L_A)\cos(L_S)\sin^2\left(\tfrac{1}{2}(\lambda_A - \lambda_S)\right)\right] + \frac{1}{d_{AS}}(h_A - h_S)\end{aligned} \qquad \text{Eq 318}$$

The measurement residual, corresponding to the left-hand side of Eq 272, is

$$\delta d_{AS} = \tilde{d}_{AS} - \bar{d}_{AS} \qquad \text{Eq 319}$$

Here $\tilde{d}_{AS}$ denotes the output of a ranging system (e.g., DME) and $\bar{d}_{AS}$ denotes the initial estimate for d_{AS}, computed from Eq 317 using the initial values of the unknown variables $\bar{L}_A, \bar{\lambda}_A, \bar{h}_A$.

Pseudo Slant-Range Measurement — The pseudo slant-range between station **S** and aircraft **A** can be expressed in terms of $\boldsymbol{L}_A$, $\boldsymbol{\lambda}_A$ and $\boldsymbol{h}_A$ by modifying Eq 317 to include the clock synchronization offset Δt. Thus the nonlinear slant range measurement model is:

$$\begin{aligned}\tilde{p}_{AS} &= p_{AS} + v_{pS} \\ p_{AS} &= d_{AS} + ct_X\end{aligned} \qquad \text{Eq 320}$$

Here $\tilde{p}_{AS}$ denotes the error-corrupted measurement, p_{AS} denotes the error-free pseudo slant-range and $\boldsymbol{v}_{pS}$ denotes the measurement error.

The partial derivatives of p_{AS} with respect to the unknown variables (corresponding to the partial

derivatives in Eq 272) are

$$\frac{\partial p_{AS}}{\partial L_A} = \frac{\partial d_{AS}}{\partial L_A} \qquad \frac{\partial p_{AS}}{\partial \lambda_A} = \frac{\partial d_{AS}}{\partial \lambda_A} \qquad \frac{\partial p_{AS}}{\partial h_A} = \frac{\partial d_{AS}}{\partial h_A} \qquad \frac{\partial p_{AS}}{\partial t_X} = c \qquad \text{Eq 321}$$

The measurement residual, corresponding to the left-hand side of Eq 272, is

$$\delta p_{AS} = \tilde{p}_{AS} - \bar{p}_{AS} \qquad \text{Eq 322}$$

Here $\tilde{p}_{AS}$ denotes the output of a pseudorange station and $\bar{p}_{AS}$ denotes the initial estimate for p_{AS}, computed from Eq 320 using the initial values of the unknown variables $\bar{L}_A, \bar{\lambda}_A, \bar{h}_A$ and $\overline{\Delta t}$.

Altitude Measurement — The measurement model for the altitude of the aircraft **A** is simply:

$$\tilde{h}_A = h_A + v_{alt} \qquad \text{Eq 323}$$

Here $\tilde{h}_A$ denotes the error-corrupted measurement, h_A denotes the error-free altitude and $\boldsymbol{v}_{alt}$ denotes the measurement error.

The partial derivatives of h_A with respect to the unknown variables (corresponding to the partial derivatives in Eq 272) are

$$\frac{\partial h_A}{\partial L_A} = 0 \qquad \frac{\partial h_A}{\partial \lambda_A} = 0 \qquad \frac{\partial h_A}{\partial h_A} = 1 \qquad \text{Eq 324}$$

The measurement residual, corresponding to the left-hand side of Eq 272, is

$$\delta h_A = \tilde{h}_{AS} - \bar{h}_A \qquad \text{Eq 325}$$

Here $\tilde{h}_A$ denotes the output of a pseuodrange station and $\bar{h}_A$ denotes the initial estimate for h_A.

Azimuth Measurement — The azimuth angle $\boldsymbol{\psi}_{A/S}$ of the aircraft **A** with respect to station **S** is expressed in terms of $\boldsymbol{L}_A$ and $\boldsymbol{\lambda}_A$ by Eq 71. Thus the nonlinear measurement model is:

$$\tilde{\psi}_{A/S} = \psi_{A/S} + v_{\psi S}$$
$$\psi_{A/S} = \arctan\left(\frac{\cos(L_A)\sin(\lambda_A - \lambda_S)}{\sin(L_A)\cos(L_S) - \cos(L_A)\sin(L_S)\cos(\lambda_A - \lambda_S)}\right) \qquad \text{Eq 326}$$

Here $\boldsymbol{v}_{\psi S}$ denotes the angle measurement error.

The partial derivatives of $\boldsymbol{\psi}_{A/S}$ o with respect to the unknown aircraft position variables (corresponding to the partial derivatives in Eq 272) are

$$\frac{\partial \psi_{A/S}}{\partial L_A} = -\frac{\sin(L_A)\sin(\lambda_A-\lambda_S)\mathrm{Den}\left[\tan(\psi_{A/S})\right]}{\left(\mathrm{Num}\left[\tan(\psi_{A/S})\right]\right)^2+\left(\mathrm{Den}\left[\tan(\psi_{A/S})\right]\right)^2}\cdots$$
$$\cdots\cdots-\frac{\left(\cos(L_A)\cos(L_S)+\sin(L_A)\sin(L_S)\cos(\lambda_A-\lambda_S)\right)\mathrm{Num}\left[\tan(\psi_{A/S})\right]}{\left(\mathrm{Num}\left[\tan(\psi_{A/S})\right]\right)^2+\left(\mathrm{Den}\left[\tan(\psi_{A/S})\right]\right)^2}$$
$$\frac{\partial \psi_{A/S}}{\partial \lambda_A} = \frac{\cos(L_A)\cos(\lambda_A-\lambda_S)\mathrm{Den}\left[\tan(\psi_{A/S})\right]}{\left(\mathrm{Num}\left[\tan(\psi_{A/S})\right]\right)^2+\left(\mathrm{Den}\left[\tan(\psi_{A/S})\right]\right)^2}\cdots \qquad \text{Eq 327}$$
$$\cdots\cdots-\frac{\cos(L_A)\sin(L_S)\sin(\lambda_A-\lambda_S)\mathrm{Num}\left[\tan(\psi_{A/S})\right]}{\left(\mathrm{Num}\left[\tan(\psi_{A/S})\right]\right)^2+\left(\mathrm{Den}\left[\tan(\psi_{A/S})\right]\right)^2}$$
$$\frac{\partial \psi_{A/S}}{\partial h_A} = 0$$

In Eq 327:

$$\mathrm{Num}[\tan(\psi_{A/S})] \equiv \cos(L_A)\sin(\lambda_A-\lambda_S)$$
$$\mathrm{Den}[\tan(\psi_{A/S})] \equiv \sin(L_A)\cos(L_S)-\cos(L_A)\sin(L_S)\cos(\lambda_A-\lambda_S) \qquad \text{Eq 328}$$

The measurement residual, corresponding to the left-hand side of Eq 272, is

$$\delta\psi_{A/S} = \tilde{\psi}_{A/S} - \bar{\psi}_{A/S} \qquad \text{Eq 329}$$

Here $\tilde{\psi}_{A/S}$ denotes the output of an azimuth measurement system (e.g., VOR) and $\bar{\psi}_{A/S}$ denotes the initial estimate for $\psi_{A/S}$, computed from Eq 326 using the initial values of the unknown variables $\bar{L}_A$ and $\bar{\lambda}_A$.

Geocentric Angle Measurement — The geocentric angle (or spherical range) between station **S** and aircraft **A** can be expressed in terms of $\boldsymbol{L}_A$ and $\boldsymbol{\lambda}_A$ using Eq 65. Thus the nonlinear slant range measurement model is:

$$\tilde{\theta}_{AS} = \theta_{AS} + \nu_{\theta S}$$
$$\theta_{AS} = 2\arcsin\left(\sqrt{\sin^2\left(\tfrac{1}{2}(L_A-L_S)\right)+\cos(L_A)\cos(L_S)\sin^2\left(\tfrac{1}{2}(\lambda_A-\lambda_S)\right)}\right) \qquad \text{Eq 330}$$

Here $\tilde{\theta}_{AS}$ denotes the error-corrupted measurement, θ_{AS} denotes the error-free geocentric angle and $\boldsymbol{\nu}_{\theta S}$ denotes the measurement error.

The partial derivatives of θ_{AS} with respect to the unknown aircraft position variables (corresponding to the partial derivatives in Eq 272) are

$$\frac{\partial \theta_{AS}}{\partial L_A} = \frac{1}{\sin(\theta_{AS})}\left[\sin(L_A-L_S)-2\sin(L_A)\cos(L_S)\sin^2\left(\tfrac{1}{2}(\lambda_A-\lambda_S)\right)\right]$$
$$\frac{\partial \theta_{AS}}{\partial \lambda_A} = \frac{1}{\sin(\theta_{AS})}\cos(L_A)\cos(L_S)\sin(\lambda_A-\lambda_S) \qquad \text{Eq 331}$$

$$\frac{\partial \theta_{AS}}{\partial h_A} = 0$$

The measurement residual, corresponding to the left-hand side of Eq 272, is

$$\delta\theta_{AS} = \tilde{\theta}_{AS} - \bar{\theta}_{AS} \qquad \text{Eq 332}$$

Here $\tilde{\theta}_{AS}$ denotes the output of a measurement system and $\bar{\theta}_{AS}$ denotes the initial estimate for θ_{AS}, computed from Eq 330 using the initial values of the unknown variables $\bar{L}_A$ and $\bar{\lambda}_A$.

8.3.3 Dilution of Precision (DoP)

The concept of Dilution of Precision (DoP) applies to the spherical-earth framework as well as to the Cartesian/rectangular framework. Thus, the discussion in Subsection 8.2.5 is relevant here as well.

A minor difference in the spherical-earth framework is that the horizontal variables are taken to be δL_A and $\cos(L_A)\delta\lambda_A$, to maintain consistency in horizontal distance changes for different azimuth angles. To accommodate this adjustment, in the Jacobian matrix employed for DoP calculations, partial derivations with respect to λ_A are divided by $\cos(L_A)$ — e.g.,

$$\frac{\partial \theta_{SA}}{\partial \lambda_A} \quad \text{becomes} \quad \frac{1}{\cos(L_A)} \frac{\partial \theta_{SA}}{\partial \lambda_A} \qquad \text{Eq 333}$$

Here θ_{SA} denotes the geocentric angle between station **S** and aircraft **A**. Examples in Subsection 8.4.4 and 8.4.5 reflect this change.

8.3.4 Remarks

The measurement residuals vector (e.g., left-hand side of Eq 275) is assembled, one element per measurement, from Eq 319, Eq 322, Eq 325, Eq 329 and Eq 332. The Jacobian matrix **J** (also in Eq 275) is assembled, one row per measurement, from Eq 318, Eq 321, Eq 324, Eq 327 and Eq 331. The iteration process for determining a solution is identical to that described in Subsection 8.1.2. For each iteration, the initial estimates of the unknown variables $\bar{L}_A, \bar{\lambda}_A, \bar{h}_A$ and $\overline{\Delta t}$ (if applicable) are employed to generate updated estimates $\hat{L}_A, \hat{\lambda}_A, \hat{h}_A$ and $\widehat{\Delta t}$ (if applicable) using Eq 278, which become the initial estimates for the next iteration. The process is terminated when the change between the initial and updated estimates are insignificant.

Advantages of using L_A, λ_A, h_A and t_X (if applicable) as the unknown variables include:

- Almost any form of measurement equation can be accommodated, including some that are not compatible with Cartesian coordinates:
  (1) Those extending the spherical earth model in order to better represent the ellipsoidal

shape of the earth;

(2) Measurements of the aircraft azimuth relative to a station; and

(3) Measurements of the geocentric angle between the aircraft and a station

- Any one or more of the variables L_A, λ_A, h_A and t_X (if applicable), but typically h_A, can be constrained to its initial value by omitting its perturbed value from the variables to be estimated

Historically, sextants provided geocentric angle measurements to the nadir of a star. During the twentieth century, Loran-C, Omega, Decca and other radionavigation systems provided measurements of the geocentric angle between a user and their low-frequency transmitters.

8.4 Example Applications

8.4.1 Example 8 Continued: Slant-Range Measurement Systems in Flatland

This subsection continues the analysis, begun in Subsection 7.9.1, of a surveillance or navigation system operating in Flatland. The systems employs ground stations which can be used to measure the slant-range to an aircraft. The stations are separated by one Base Line Unit (BLU). The analysis in this subsection is focused on Horizontal Dilution of Precision (HDoP), a measure of system accuracy. The methodology employed is described in Subsection 8.2.5, and utilizes the partial derivatives in Eq 298 (without the z-component). Upon carrying out the straightforward calculations involved, the HDoP contours are shown in Figure 41.

In Figure 41, the left-hand side pertains to a two-station configuration, and the right-hand side to three stations. The calculations employed assumed each station's signal could be received up to 3.5 BLUs in range. The HDoPs for both configurations are symmetrical about a vertical axis, and thus can be truncated to the "west".

Considering the two-station configuration, there is strong directionality to the HDoP pattern. Coverage is best perpendicular to the baseline, and non-existent along the baseline extensions (where the solution is unstable). Using HDoP equal to five as a criterion, the service area can be approximated by a 7 BLU x 1 BLU "north-south" rectangle bordered by four right triangles with sides of 3 BLU and 1 BLU. Thus the service area can be approximated by:
$(7 \times 1) + 4 \times (\frac{1}{2} \times 3 \times 1) = 13$ BLU^2.

The three-station configuration eliminates the unstable solutions present in the two-station case. As a result, the service area (maximum HDoP equal to five) is roughly circular. There is some directionality (partly due to the assumed range limitation) but it is not pronounced. Thus the service area is approximately π 3.5 BLU x 3.5 BLU $\approx$ 36 BLU^2.

Subsection 8.4.3 contains a more detailed analysis of service areas.

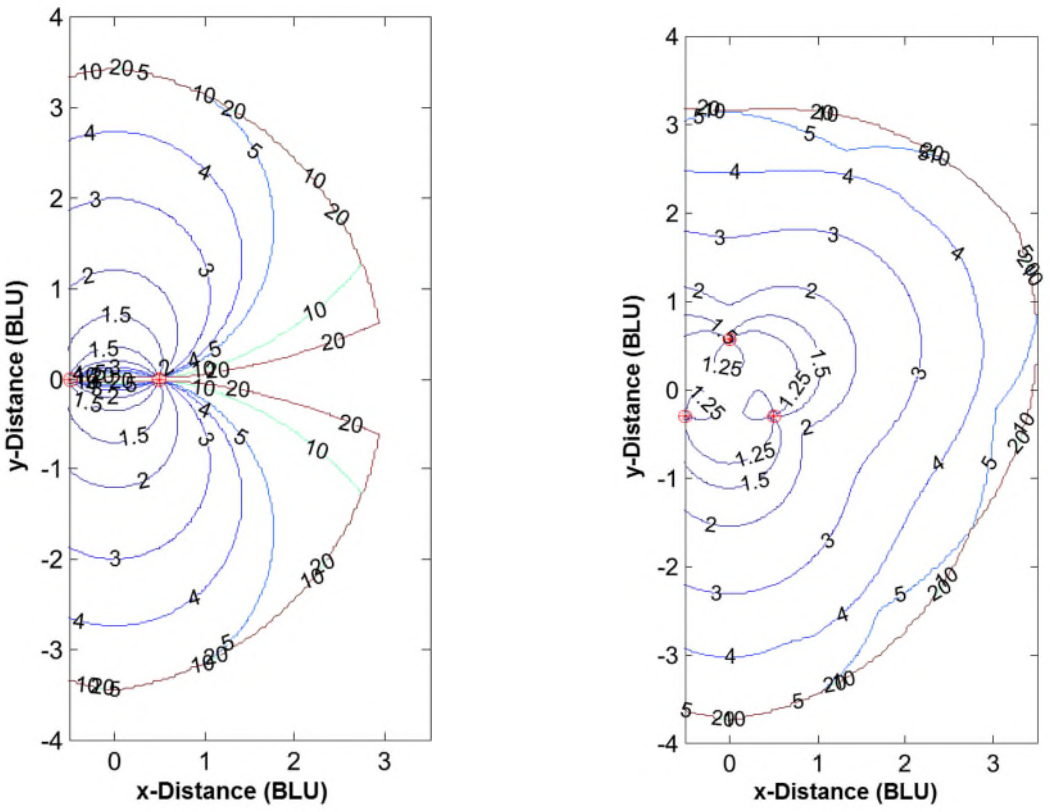

(a) Two Stations (b) Three Stations

Figure 41 HDoP Contours for Slant-Range Measurement Systems in Flatland

8.4.2 Example 9 Continued: Pseudo Slant-Range Measurement Systems in Flatland

This subsection continues the analysis, begun in Subsection 7.3, of a surveillance or navigation system operating in Flatland. The system employs ground stations which are used to measure the pseudo slant-range to an aircraft, and are separated by one Base Line Unit (BLU). This sub-section is focused on Horizontal Dilution of Precision (HDoP), a measure of accuracy. The methodology employed is described in Subsection 8.2.5, and utilizes the partial derivatives in Eq 301 without the z-component. Upon carrying out the straightforward calculations involved, the HDoP contours are shown in Figure 43.

In Figure 43, the left-hand side pertains to a three-station equilateral triangle configuration, and the right-hand side to four stations arranged in a square. The calculations assume that each station's signal can be received up to 3.5 BLUs in range. HDoPs for both configurations are symmetrical about a vertical axis, and thus can be truncated "to the west". Two facts concerning Figure 43 are immediately evident

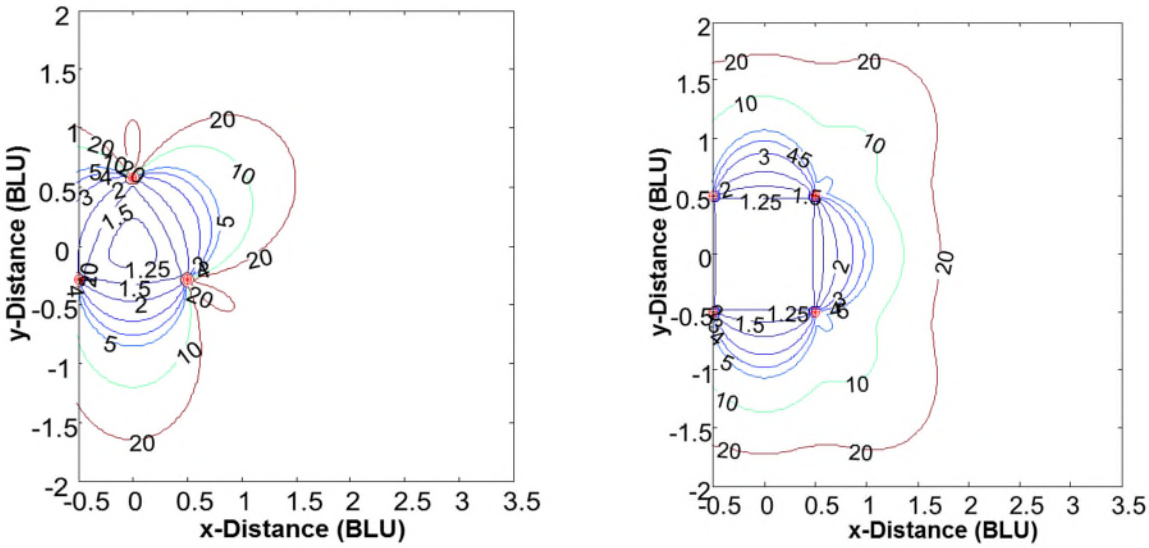

(a) Three-Station Equilateral Triangle (b) Four-Station Square

Figure 43 HDoP Contours for Pseudo Slant-Range Measurement Systems in Flatland

- Coverage of a network of pseudo slant-range ground stations does not extend much past the perimeter polygon formed by connecting the stations
- Within the perimeter polygon, pseudo slant-range systems HDoPs are comparable to those of a system that measures slant ranges.

As is the case for slant-range systems, using a redundant ground station eliminates unstable solutions — in this case, along the baseline extensions for a station triad. A redundant station also provides a small increase in the service area — approximately from a circle of radius of ½ BLU to a circle of radius ¾ BLU.

An alternative four-station configuration, more suited to situations when as much coverage as possible is sought, is the four-station Wye configuration (Figure 42). In this case, a BLU is the distance from the center station (which served as the Master in certain radionavigation systems) to each of the three outlying, secondary stations.

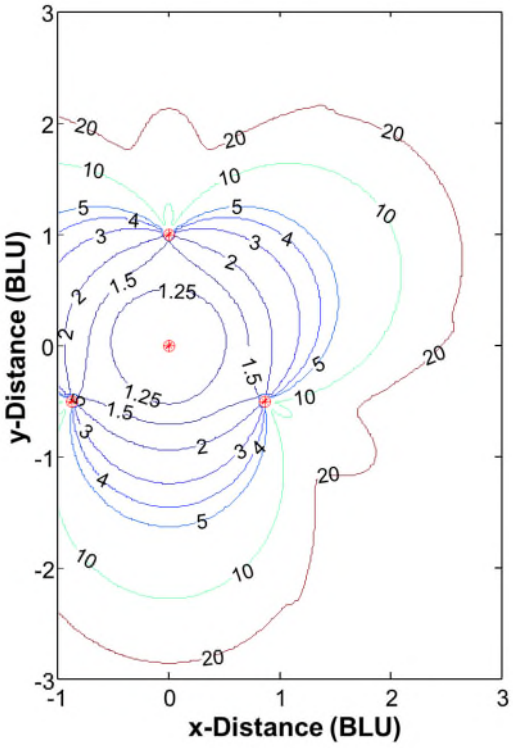

Figure 42 HDoP Contours for Wye Configuration Using All Stations

8.4.3 Interpretation: Pseudo vs. Real Slant-Range Systems

Service Area Comparison — Figure 44 is a quantitative comparison of the service areas for the five system configurations addressed in Subsections 8.4.1 and 0, assuming a common baseline length. Figure 44 indicates that a navigation or surveillance system utilizing real slant-range measurements will have a substantially larger (e.g., ten times) service area than one

utilizing pseudo slant-range measurements, assuming that common station baseline lengths are used. However, having equal or comparable baselines for different systems is only a convenience for analysis purposes, and is not a constraint.

Siting Flexibility — A more meaningful conclusion that can be drawn from this analysis is that real slant-range systems have greater station siting flexibility. Pseudo slant-range systems must have station locations that almost surround the service area, while real slant-range systems do not. To address this limitation, pseudo slant-range systems have been built with extremely long baselines. The ultimate system in this regard is GPS, which has its stations on satellites, resulting in stations separated by on the order of 20,000 NM.

GPS Service Area — Interestingly, GPS users on or near the earth's surface are outside the perimeter of the polygonal surfaces formed by the stations in use. Instead, GPS users are in the "border area" adjacent to and near the center of the baselines connecting the satellites with the lowest elevation angles (Figure 30 shows the Flatland equivalent).

Geometry Advantage of Range Measurements — Figure 45 helps explain why HDoPs for pseudo slant-range systems degrade much more rapidly with distance from the stations than do HDoPs for real slant-range systems. The figure shows two stations and the circular LOPs they

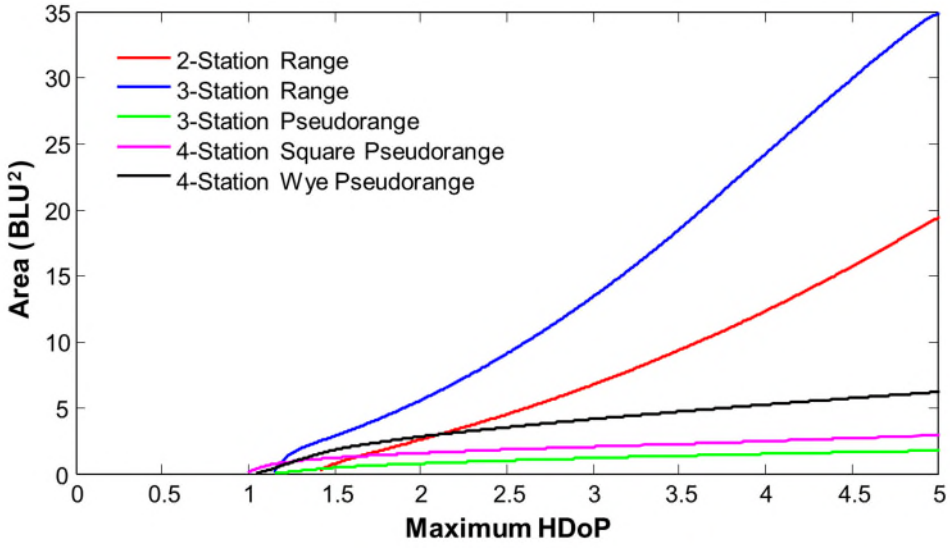

Figure 44 Service Area with HDOP ≤ Max. HDOP for Five System Concepts

would generate if the stations were used for real slant-range measurements. The LOP crossing angles starts at zero on the baseline, where the solution is unstable. Moving perpendicular to the baseline, the crossing angle becomes useful within perhaps one-eighth of the baseline length, and remains useful to about 3.5 baseline lengths (outside of the limits of the figure) where the crossing angle becomes too shallow. An important aspect of this figure is that the separation between LOPs for each station remains constant with distance from the station.

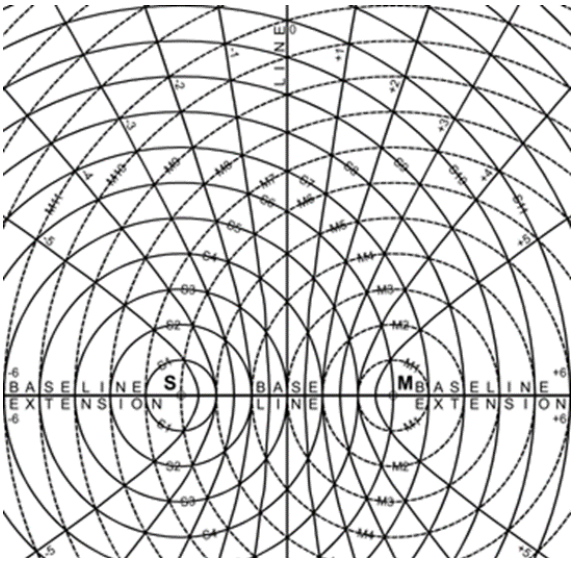

Figure 45 LOPs for Slant-Rang and Pseudo Slant-Range Systems

Figure 45 also shows a family of LOPs for a pair pseudo slant-range stations. If there were two pairs of stations, degradation in their crossing angles with distance from the stations would be evident (e.g., Figure 29). However, a second source of accuracy degradation is involved for pseudo slant-range systems: the LOPs become further apart with distance from the stations, much as the LOPs for an angle measurement system. This divergence of the LOPs limits the service area of a pseudo slant-range system to, roughly, the region surrounded by the stations.

8.4.4 Example 10 Continued: Three Pseudo Spherical-Range Stations

Introduction — This subsection continues the example, begun in Subsection 7.9.3, of an aircraft that utilizes three stations in the U.S. Northeast Loran-C chain (**M** at Seneca, NY; **W** at Caribou, ME; and **X** at Nantucket, MA) for navigation. Two topics are addressed which are relevant to the material in this chapter: Horizontal Dilution of Precision (HDoP) and accounting for the earth's ellipticity using the Gauss-Newton LLS technique.

HDoP Contours — While more commonly used for rectangular geometries (e.g., Subsections 8.4.1-8.4.3), Horizontal Dilution of Precision (HDoP) is also applicable to spherical geometries — see Subsections 8.2.5 and 8.3.3. Here, the modified Jacobian matrix is

$$J_{DOP} = \begin{bmatrix} \dfrac{\partial\theta_{MA}}{\partial L_A} - \dfrac{\partial\theta_{WA}}{\partial L_A} & \dfrac{1}{\cos(L_A)}\left(\dfrac{\partial\theta_{MA}}{\partial\lambda_A} - \dfrac{\partial\theta_{WA}}{\partial\lambda_A}\right) \\ \dfrac{\partial\theta_{MA}}{\partial L_A} - \dfrac{\partial\theta_{XA}}{\partial L_A} & \dfrac{1}{\cos(L_A)}\left(\dfrac{\partial\theta_{MA}}{\partial\lambda_A} - \dfrac{\partial\theta_{XA}}{\partial\lambda_A}\right) \end{bmatrix} \qquad \text{Eq 334}$$

HDoP is then given by

$$\text{HDoP} = \sqrt{\left(J_{DOP}^{T}\, J_{DOP}\right)^{-1}\Big|_{11} + \left(J_{DOP}^{T}\, J_{DOP}\right)^{-1}\Big|_{22}} \qquad \text{Eq 335}$$

Results of this calculation are shown in Figure 46. This figure is qualitatively similar to Figure 43(a), which applies to a two-dimensional Cartesian setting. The information in Subsection 7.6.3 concerning extraneous and ambiguous solutions is relevant here as well.

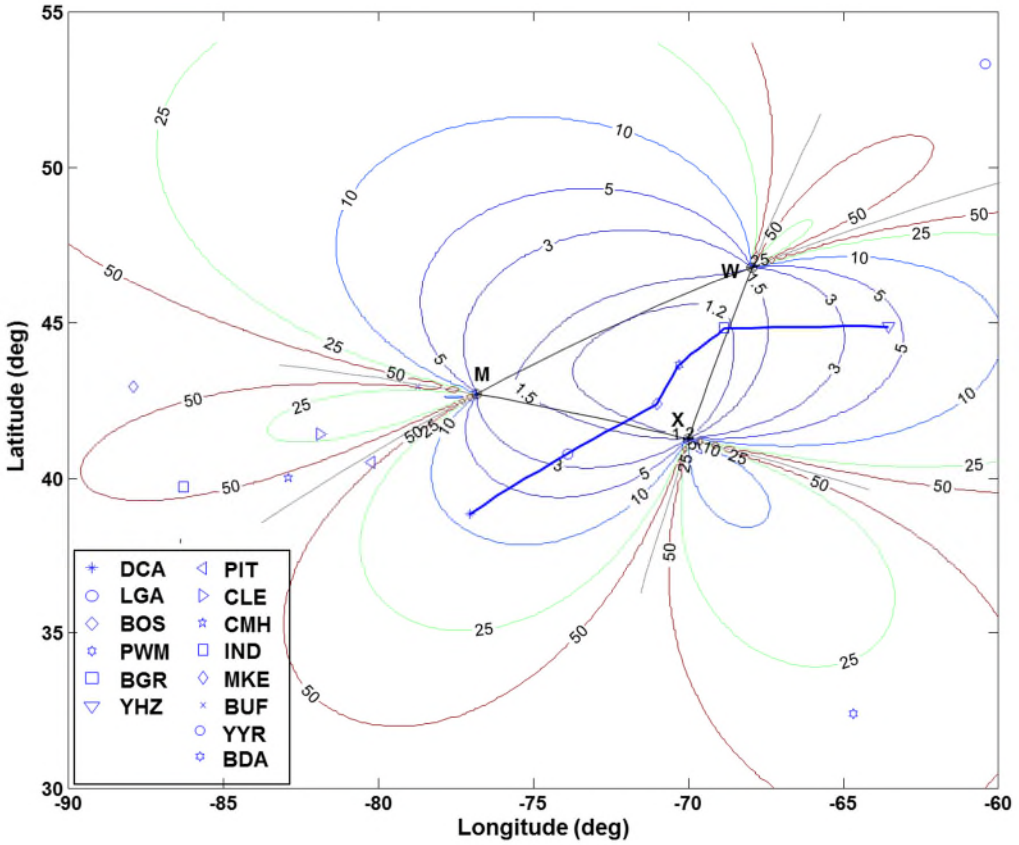

Figure 46 HDOP Contours for a Triad of Pseudo Spherical-Range Stations

Need to Consider Ellipsoidal Earth —If the earth were a sphere, Razin's algorithm (Section 7.7) could be used without modification. However, the earth is better modeled as an ellipsoid of revolution (Section 2.2). Since errors resulting from modeling the earth as a sphere (ellipticity error) tend to increase with distance, they can become important for accurate, long-range systems. For example, consider four airport locations: LaGuardia, NY (LGA); Boston, MA (BOS); Portland, ME (PWM); and Bangor, ME (BGR). The path lengths between the three ground stations and these airports vary from 81.0 NM (**X** and BOS) to 444.3 NM (**W** and LGA); the average is 233.5 NM. Based on (a) the distances involved, (b) the "rule of thumb" for the spherical earth approximation that the distance error is roughly 0.3% of the distance, and (c) the Coast Guard's Loran-C accuracy goal of 0.25 NM, the effect of mis-modeling the earth's

geometry should be addressed.

Table 11 shows the position error resulting from applying Razin's algorithm to range-differences generated using Vincenty's algorithm (Subsection 2.2.3), rather than those for a spherical earth (as assumed by the algorithm). The ellipticity error values, between 0.38 NM and 1.13 NM, are consistent with the 0.3% of distance "rule of thumb".

Table 11 Example of Ellipticity Errors for Razin's Algorithm

Airport	True Latitude (deg)	Lat Error* (deg)	True Longitude (deg)	Lon Error* (deg)	Distance Error (NM)
LGA	40.7772500	-0.0062000	-73.8726111	0.0011000	0.38
BOS	42.3629418	-0.0006300	-71.0063931	-0.0102000	0.45
PWM	43.6456435	0.0036400	-70.3086164	-0.0148100	0.68
BGR	44.8074444	0.0061100	-68.8281389	-0.0250500	1.13

* True minus estimated coordinate value

Application of LLS — The LLS technique is used to improve the solution accuracy of Razin's algorithm. Following Subsection 8.1.2, each spherical-range difference measurement is computed using Vincenty's algorithm* for the distance $s(\mathbf{S},\mathbf{A})$ along the surface of the ellipsoid between a station **S** at (L_S, λ_S) and aircraft **A** at (L_A, λ_A). The first line of Eq 269 becomes

$$\begin{aligned} \tilde{z}_1 &= s(M,A) - s(W,A) \\ \tilde{z}_2 &= s(M,A) - s(X,A) \end{aligned} \qquad \text{Eq 336}$$

The measurement equation for each spherical-range difference also employs Vincenty's algorithm. However, the aircraft location replaced by the current estimate $\hat{\mathbf{A}}$ of its location. Thus the second line of Eq 269 becomes

$$\begin{aligned} f_1(M,W,X,\hat{A}) &= s(M,\hat{A}) - s(W,\hat{A}) \\ f_2(M,W,X,\hat{A}) &= s(M,\hat{A}) - s(X,\hat{A}) \end{aligned} \qquad \text{Eq 337}$$

The Jacobian (Eq 276) is composed of the partial derivatives of the measurements with respect to the unknown variables — L_A and λ_A in this case. However, it is not necessary that the elements of the Jacobian used in computations be exact derivatives of the measurement equation. Because the LLS technique is recursive, approximations of the derivatives are sufficient (Subsection 8.1.4). This is fortuitous, because Vincenty's technique is not an equation in the analytic sense, but a recursive procedure; expressions for its derivatives cannot be computed easily.

In place of the derivatives with respect to L_A and λ_A of the distance along the surface of an ellipse for Vincenty's algorithm, scaled derivatives of the geocentric angle θ_{SA} are used. Thus, the

* Selection of Vincenty's algorithm was based on the availability of validated computer code. Other methods could have been used.

Jacobian is computed using Eq 331

$$\frac{\partial s(S,A)}{\partial L_A} \approx R_e \frac{\partial \theta_{SA}}{\partial L_A} \qquad \frac{\partial s(S,A)}{\partial \lambda_A} \approx R_e \frac{\partial \theta_{SA}}{\partial \lambda_A} \qquad \text{Eq 338}$$

Any reasonable value for $\boldsymbol{R_e}$ can be used; here the value following Eq 23 is employed.

The LLS process is initialized using values for $\bar{L}_A$ and $\bar{\lambda}_A$ found using Razin's algorithm for a spherical earth. The perturbation corrections $\delta\hat{L}_A$ and $\delta\hat{\lambda}_A$ are found using Eq 279, since a weight matrix **W** is not used in the absence of redundant measurements.

Calculation of Results — Carrying out the LLS process for five iterations yields a sequence of increasingly accurate position estimates for four airport locations. The associated residual errors are shown in Table 12. Convergence of the LLS technique is rapid in this situation. Each of the first four iterations reduces the error by a minimum factor of 76; the average latitude or longitude error reduction by one iteration is a factor of 539. The fifth iteration appears to approach the limits of machine precision (calculations were done in double precision).

Table 12 Gauss-Newton Residual Error for Spherical-Range Difference Measurements

Iter-ation	LaGuardia (LGA)		Boston (BOS)	
	Lat Error* (deg)	Lon Error* (deg)	Lat Error* (deg)	Lon Error* (deg)
0	-0.006,204,297,044,61	0.001,098,559,038,59	-0.000,627,450,377,91	-0.010,195,811,988,10
1	-0.000,020,505,170,77	-0.000,001,816,926,14	-0.000,008,177,955,56	0.000,045,180,746,10
2	-0.000,000,027,423,43	0.000,000,018,116,62	-0.000,000,014,339,68	-0.000,000,157,274,01
3	-0.000,000,000,083,93	-0.000,000,000,062,20	-0.000,000,000,032,53	0.000,000,000,565,15
4	0.000,000,000,000,01	0.000,000,000,000,29	-0.000,000,000,000,04	-0.000,000,000,002,02
5	0.000,000,000,000,01	-0.000,000,000,000,01	0.000,000,000,000,01	0.000,000,000,000,03
Iter-ation	**Portland (PWM)**		**Bangor (BGR)**	
	Lat Error* (deg)	**Lon Error* (deg)**	**Lat Error* (deg)**	**Lon Error* (deg)**
0	0.003,642,517,508,14	-0.014,811,819,575,26	0.006,109,544,331,55	-0.025,054,253,476,51
1	0.000,001,297,312,66	0.000,072,399,332,72	0.000,018,565,242,40	0.000,160,340,474,51
2	-0.000,000,016,162,69	-0.000,000,244,802,54	-0.000,000,084,834,17	-0.000,000,437,980,97
3	0.000,000,000,041,82	0.000,000,000,817,39	0.000,000,000,213,29	0.000,000,001,148,99
4	-0.000,000,000,000,15	-0.000,000,000,002,72	-0.000,000,000,000,57	-0.000,000,000,003,05
5	0.000,000,000,000,01	0.000,000,000,000,04	-0.000,000,000,000,01	0.000,000,000,000,00

* True minus estimated coordinate value

Useful Solution Precision — Aside from demonstrations of the LLS technique (such as this), in practice, when applied to Loran-C measurements, one or two iterations would generally be sufficient. Even with error-free measurements (e.g., as can be assumed during system analyses), there usually is no point in computing an aircraft's position to greater precision than that to

which the ground stations are known. Loran-C station locations are known to 0.001 arc second, or approximately 0.1 ft, or 0.000,000,3 deg (Ref. 51), which is achieved with two iterations in the calculations employed here. For real-time operational use, if one optimistically takes the Loran-C measurement accuracy to be 10 ft (it is often quoted as "100 ft or better"), then computing the aircraft location to a precision of 0.000,03 deg would be sufficient.

Related Work — Razin's paper (Ref. 43) recognized the need to modify a solution to the 'two spherical-range difference' problem based on an assumed spherical earth, and contained a technique to do so. References 48 and 49 did as well. This solution is closest to that in Ref. 48.

8.4.5 Example 11 Continued: Two Pairs of Pseudo Spherical-Range Stations

This subsection is a continuation of the example, begun in Subsection 7.9.4, concerning two distinct pairs of pseudo spherical-range navigation stations. For such a configuration, the solution algorithm for a spherical earth is described in Section 7.8. The ellipticity error inherent in a solution that assumes a spherical earth can be corrected by the Gauss-Jordan LLS technique demonstrated in Subsection 8.4.4. However, that topic is not pursued here.

Since two distinct pairs of stations is not as common as a triad of stations, Horizontal Dilution of Precision (HDoP) is utilized to obtain insight into this configuration's performance. The Jacobian matrix and HDoP expressions follow directly from Eq 334 and Eq 335, respectively. Figure 47 depicts HDoP contours for the four stations and seven airport shown in Figure 38. For all airports depicted, HDoP is 10 or less. As expected, the solution becomes unstable along the extensions for the baselines connecting a station pair (Seneca-Nantucket and Dana-Malone). However, the solution is not unstable along the extensions for the paths connecting stations from different chains. For this example, there is a region where HDoP exceeds 50 close to the Dana-Seneca path, as the hyperbolic LOPs for the two chains are nearly parallel in this area.

As noted earlier, navigation and surveillance systems are developed/deployed to provide service in a defined area. In the case of the U.S. East Coast Loran-C Chain, the station at Carolina Beach, NC, was intended to support service in much of the U.S.Southeast. However, stations are occasionally be out-of-service. In such a circumstance, cross-chaining was an advanced capability that enabled operations to continue during a station outage (for appropriately equipped aircraft).

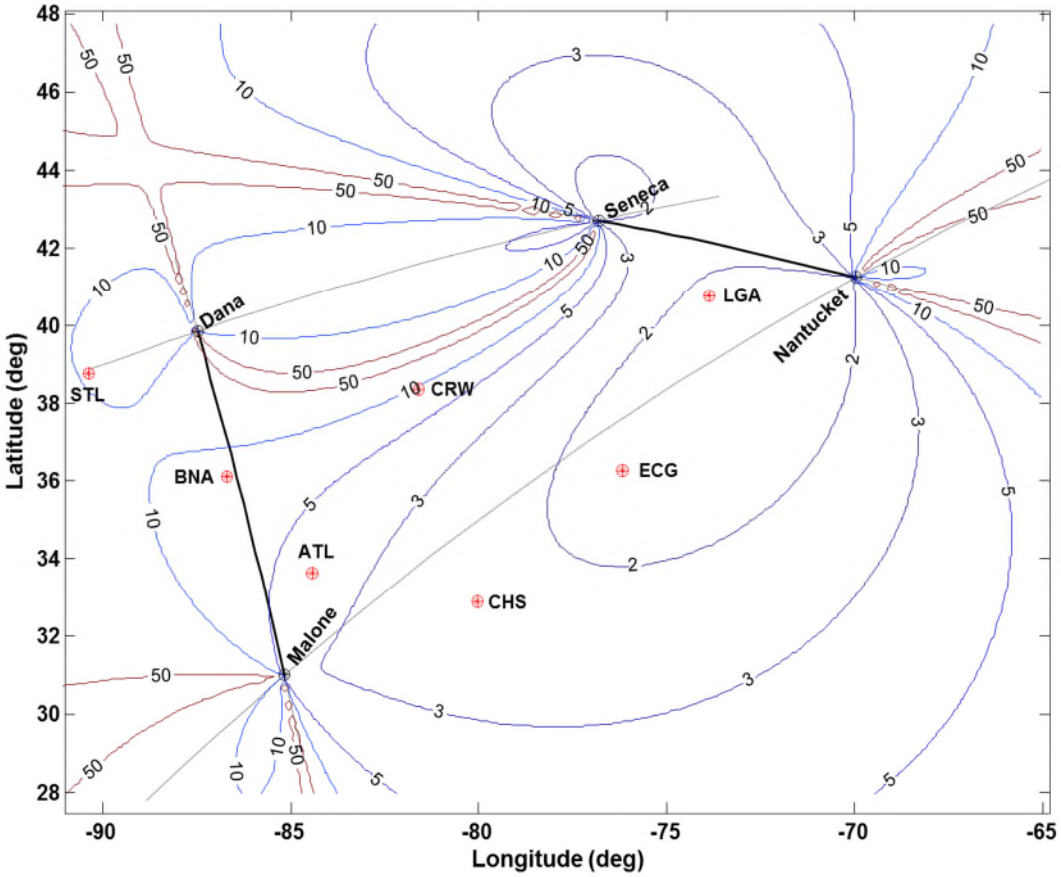

Figure 47 HDoP Contours for Two Pairs of Pseudo Spherical-Range Stations

A second advanced capability (relative to traditional Loran-C) was employing redundant stations to improve measurement geometry. The Dana station was in fact dual-rated: it was the master for the Great Lakes Chain and a secondary for the East Coast Chain. Figure 48 depicts the HDoP contours when measurements by the Seneca-Dana pair are used with those for the Seneca-Nantucket and Dana-Malone pairs. HDoPs adjacent to the Seneca-Dana baseline are improved markedly (e.g., six of the seven airports shown have HDoPs less than two), while HDoPs for the area further to the southeast are only marginally improved.

The geographic size of service areas involved in Figure 47 and Figure 48 are quite large. For the two figures, HDoP is 5 or less for approximately 798,493 (Figure 47) and 1,165,883 (Figure 48) square nautical miles, respectively. The major reason for large coverages is use of long baselines: for Dana-Malone, approximately 544 NM; and for Seneca-Dana, approximately 510 NM.

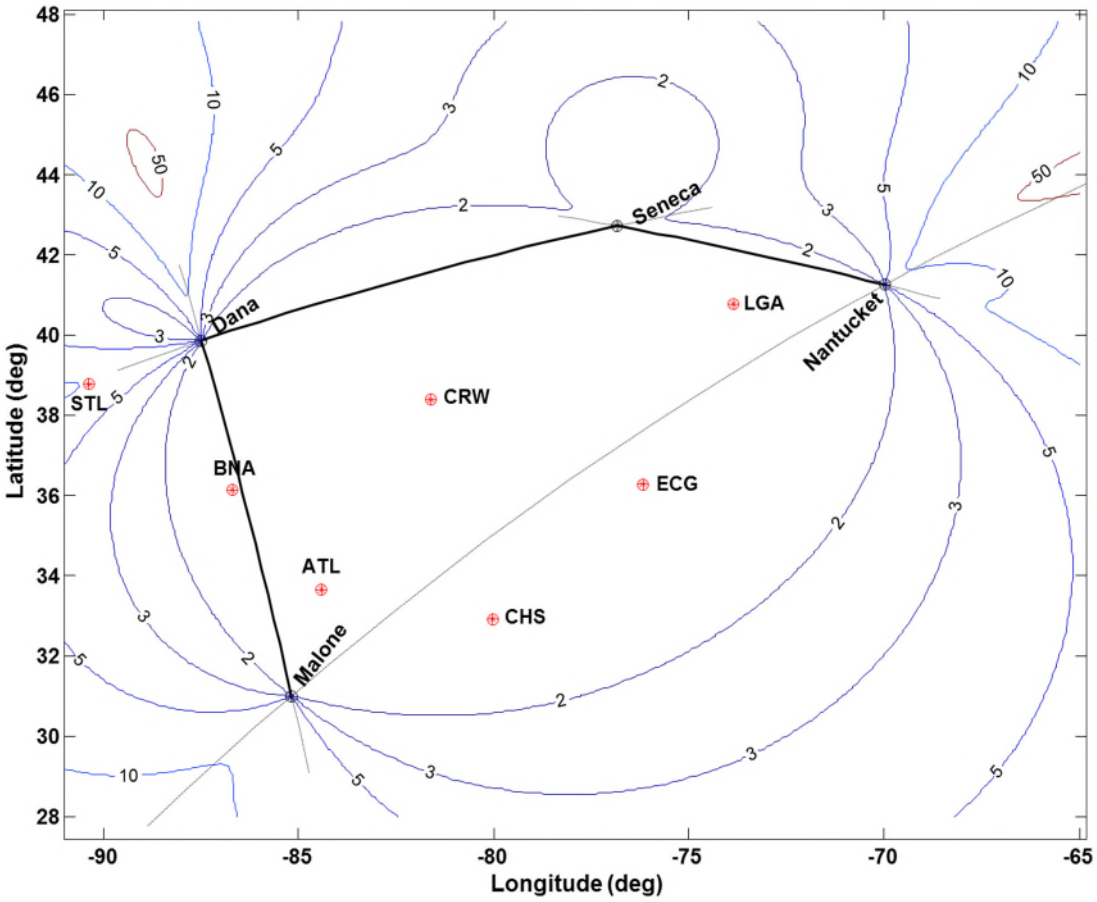

Figure 48 HDoP Contours for Three Pairs of Pseudo Spherical-Range Stations

8.4.6 Example 12 Continued: Wide Area Multilateration (WAM)

Introduction — This subsection continues the example, begun in Subsection 7.9.5, of a WAM system that utilizes aircraft altitude reports and pseudo slant-range measurements at ground sites on three airports: Boston, MA (BOS); Manchester, NH (MHT); and Hartford, CT (BDL). The analysis in Subsection 7.9.5 assumes a spherical earth; this subsection accounts for the earth's ellipticity using the Gauss-Newton LLS technique.

Equations Employed — Following Subsection 8.1.2, each slant-range difference measurement is computed using Appendix Section 9.3 (particularly Eq 350) for the slant-range $\boldsymbol{d(S,A)}$ between a station **S** at coordinates $(\boldsymbol{L_S, \lambda_S, h_S})$ and aircraft **A** at coordinates $(\boldsymbol{L_A, \lambda_A, h_A})$. The first line of Eq 269 thus becomes

$$\begin{aligned} \tilde{z}_1 &= d(BOS, A) - d(MHT, A) \\ \tilde{z}_2 &= d(MHT, A) - d(BDL, A) \end{aligned} \qquad \text{Eq 339}$$

The measurement equation for each slant-range difference also employs Eq 350. However, the aircraft location replaced by the current estimate $\hat{\mathbf{A}}$ of its location. Thus the second line of Eq

269 becomes

$$f_1(BOS, MHT, BDL, \hat{A}) = d(BOS, \hat{A}) - d(MHT, \hat{A})$$
$$f_2(BOS, MHT, BDL, \hat{A}) = d(MHT, \hat{A}) - d(BDL, \hat{A}) \quad \text{Eq 340}$$

The Jacobian (Eq 276) is composed of the partial derivatives of the measurements with respect to the unknown variables — $\boldsymbol{L_A}$ and $\boldsymbol{\lambda_A}$ in this case. It is not necessary that the elements of the Jacobian used in LLS computations be exact derivatives of the measurement equation. Because the LLS technique is recursive, approximations of the derivatives are sufficient. Thus, the derivatives of slant-range with respect to $\boldsymbol{L_A}$ and $\boldsymbol{\lambda_A}$ are computed using the corresponding expressions for a spherical earth model (Eq 318).

The LLS process is initialized using values for $\bar{L}_A$ and $\bar{\lambda}_A$ found using the spherical earth model (Section 7.4 and Subsection 7.9.5). The perturbation corrections $\delta\hat{L}_A$ and $\delta\hat{\lambda}_A$ are found using Eq 279, since a weight matrix **W** is not used in the absence of redundant measurements.

Results — Carrying out the LLS process for five iterations for four airport locations yields a sequence of increasingly accurate position estimates. Their residual errors are shown in Table 13. "Iteration 0" corresponds to the solution based on a spherical-earth model, which is used to initialize the iteration — the table provides its ellipticity error. For these four locations, the average ellipticity error is 1,204 ft; the maximum (for BAF) is 2,122 ft.

Table 13 Gauss-Newton Residual Error for WAM Slant-Range Difference Measurements

Iter-ation	Westfield-Barnes Regional (BAF)		Dillant-Hopkins, Keene (EEN)	
	Lat Error* (deg)	Lon Error* (deg)	Lat Error* (deg)	Lon Error* (deg)
0	-0.001,301,968,265,58	0.007,647,699,521,99	-0.001,104,331,349,71	0.003,587,102,019,89
1	-0.000,023,346,121,51	-0.000,083,388,490,38	0.000,003,508,767,16	-0.000,020,825,500,81
2	0.000,000,023,629,92	0.000,000,077,274,69	-0.000,000,013,518,20	0.000,000,091,899,49
3	-0.000,000,000,019,79	-0.000,000,000,082,41	0.000,000,000,068,21	-0.000,000,000,412,05
4	0.000,000,000,000,03	0.000,000,000,000,08	-0.000,000,000,000,27	0.000,000,000,001,82
5	0.000,000,000,000,01	0.000,000,000,000,00	0.000,000,000,000,00	-0.000,000,000,000,01
Iter-ation	**Lawrence Municipal (LWM)**		**Hanscom Field, Bedford (BED)**	
	Lat Error* (deg)	**Lon Error* (deg)**	**Lat Error* (deg)**	**Lon Error* (deg)**
0	-0.001,215,745,248,65	-0.003,554,998,523,51	-0.001,341,677,997,11	-0.001,310,031,212,80
1	0.000,003,288,339,05	0.000,029,318,295,92	-0.000,003,587,543,95	0.000,008,337,514,17
2	0.000,000,018,603,13	-0.000,000,113,464,86	-0.000,000,004,694,52	-0.000,000,028,663,83
3	0.000,000,000,023,39	0.000,000,000,519,98	-0.000,000,000,019,15	0.000,000,000,097,83
4	0.000,000,000,000,22	-0.000,000,000,002,11	-0.000,000,000,000,02	-0.000,000,000,000,33
5	0.000,000,000,000,00	0.000,000,000,000,01	-0.000,000,000,000,01	0.000,000,000,000,00

* True minus estimated coordinate value

In this example, convergence of the LLS technique is rapid. Each of the first four iteration steps reduces the error by a minimum factor of 50; the average latitude or longitude error reduction by one iteration is a factor of 426. The fifth iteration appears to approach the limits of machine precision. This performance is consistent with that for pseudo spherical-range measurements addressed in Subsection 8.4.4.

Two iterations would be sufficient for virtually all real-world applications, as the survey error of most locations, including those of airports, exceeds 10^{-7} deg.

9. APPENDIX: RELATED SPECIALIZED TOPICS

9.1 Aircraft Altitude and Air Data Systems

9.1.1 Meanings of "Altitude"

This memorandum is primarily mathematical, and — except for application examples — the equations involve only one notion of altitude: geometric height above an assumed perfectly spherical earth, measured along a radial from the earth's center. However, when interpreting the results of calculations for applications, the analyst must be aware that there are multiple meanings of altitude. The differing meanings are of concern in aviation, because aircraft (a) utilize barometric altimeters, but (b) must also main a vertical geometric distance above terrain. Figure 49 illustrates several notions of vertical distance above the earth, or "altitude":

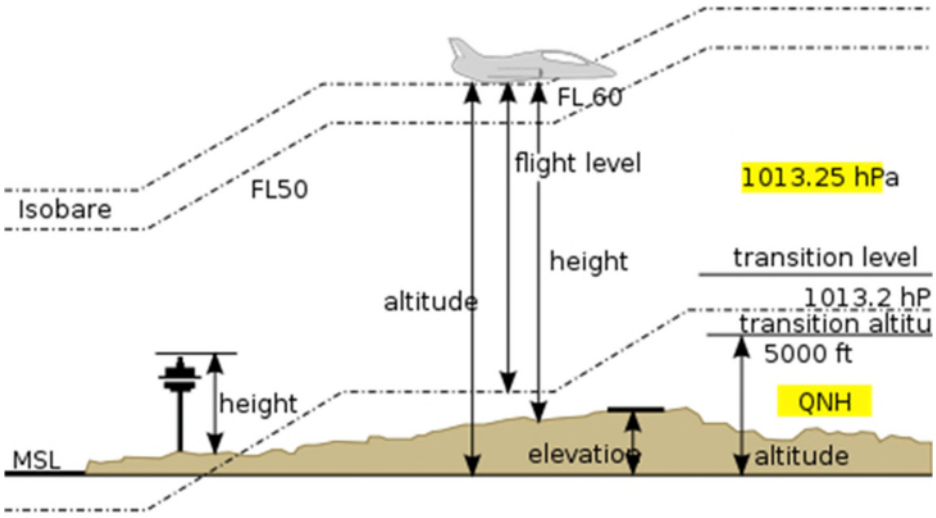

Figure 49 Different Notions of Altitude

- Height — or, better, Height Above Terrain (HAT) — is the vertical distance between an aircraft (or the top of a structure on the ground) and the terrain beneath it
- Altitude — or, better, Altitude MSL (above Mean Sea Level) — is the vertical distance between an aircraft and mean sea level. Generally, aircraft use altitude MSL in terminal areas/at low altitudes. To do so, the aircraft's altimeter is adjusted for the current local MSL pressure by applying the "QNH" correction†, which is broadcast by a local airport.
- Flight Level — Vertical distance between an aircraft and the point below where the sea-level standard day pressure occurs (29.92 inches of mercury). In the U.S., flight

† QNH is not an acronym. It is one of a collection of standardized three-letter message encodings, all of which start with the letter "Q". They were initially developed for commercial radiotelegraph communication, and were later adopted by other radio services, especially amateur radio. Although created when radio used Morse code exclusively, Q-codes continued to be employed after the introduction of voice transmissions.

levels are used above the transition altitude of 18,000 ft.[‡]

- Elevation — Height of the terrain above MSL.

These definitions are reasonably standard, but are not universally used. Documents related to aircraft procedures are particularly carefully to adhere to these definitions.

9.1.2 Aircraft Pitot-Static System

Aircraft certified under Federal Aviation Regulations[§] Parts 91, 121 and 135 are required to be equipped with a pitot-static system. A pitot-static system utilizes the static air pressure (collected at the static port), and the dynamic pressure due to the motion of the aircraft through the air (collected by the pitot tube) — illustrated in Figure 50, from Ref. 54. These combined pressures are utilized to provide the pilot with three indicators critical to operation of the aircraft:

- Airspeed indicator (ASI)
- Altimeter
- Vertical speed indicator (VSI).

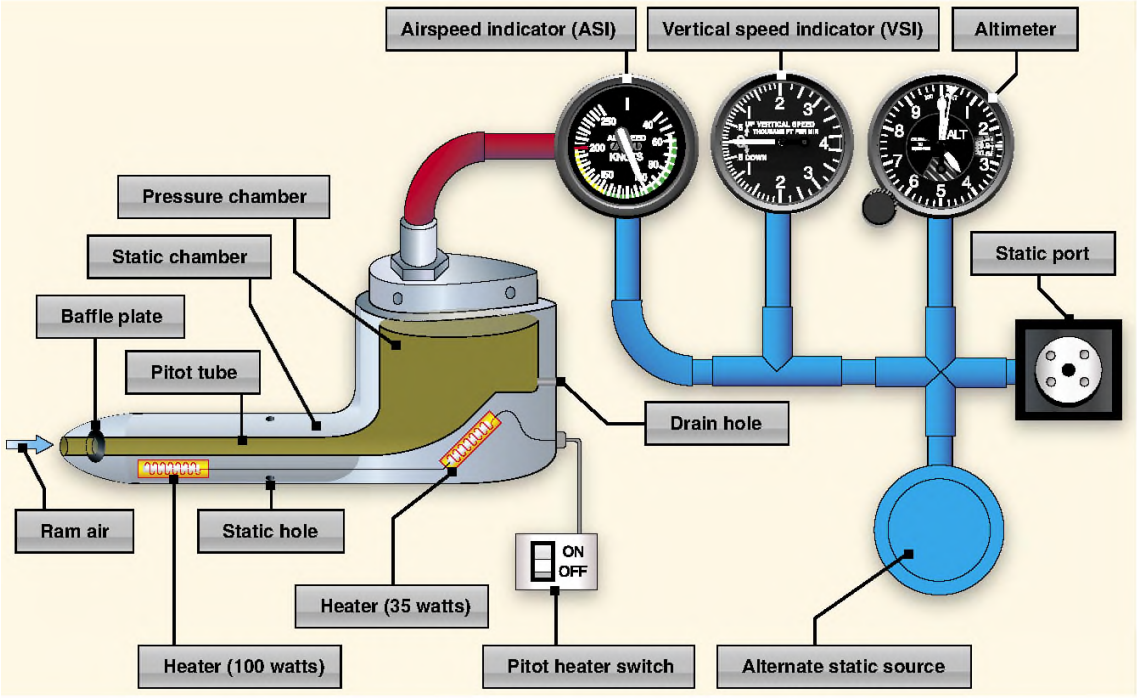

Figure 50 Basic Aircraft Pitot-Static System

[‡] The figure, from Wikipedia, was drawn from a European perspective. It has (a) a lower transition altitude, and (b) the QNH quantified in hectopascals (hPa) rather than inches of mercury.

[§] The Federal Aviation Regulations, or FARs, are rules governing all aviation activities in the United States. The FARs are part of Title 14 of the Code of Federal Regulations (CFR).

9.1.3 Barometric Altimeter Temperature Sensitivity

The basic design of aircraft barometric altimeters does not provide a means for compensating for deviations from the assumed standard day sea level temperature of 15 °C (59 °F)[**]. Such a deviation results in an uncompensated altitude error that: (a) is the same for all aircraft at the same altitude, and (b) does not fluctuate. Temperatures that are less than the standard 15 °C cause the altimetry system to report a higher altitude than is true. Conversely, temperatures that are greater than the standard cause the altimetry system to report a lower altitude than is true (Figure 51).

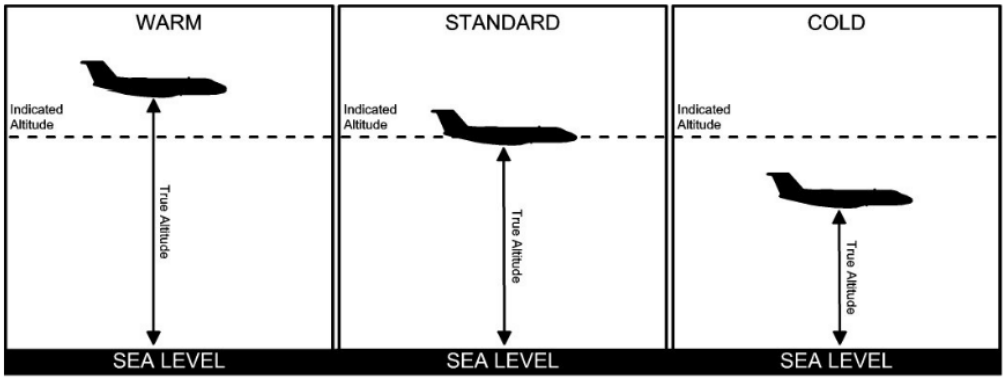

Figure 51 Effect of Non-Standard MSL Temperature on Barometric Altimeter Indication

Altitude errors due to uncompensated temperature deviations from the standard value are a particular concern for low-altitude operations. The amount is quantified by the ICAO Cold Temperature Error Table, which is reproduced in Ref. 55.

9.1.4 Vertical Speed Indicator Temperature Sensitivity

The Vertical Speed Indicator is subject to the same temperature sensitivity as the barometric altimeter. Most pertinent to VNAV approaches: Ref. 36 cautions: "Because of the pronounced effect of nonstandard temperature on baro-VNAV operations, VNAV approaches will contain a temperature restriction below which use of the approach is not authorized." For example, the RNAV (GPS) approach plate for Logan International Airport (BOS) runway 04R that was valid for 07 Feb 2013 to 07 March 2013 had this statement: "Uncompensated Baro-VNAV systems, LNAV/VNAV NA [Not Available] below -13 °C (9 °F) or above 43 °C (109 °F)".[††]

[**] The correction applied by a pilot in a terminal area, utilizing Automatic Terminal Information Service (ATIS) or Automated Weather Observation System (AWOS) information, only accounts for atmospheric deviations from the standard day pressure at sea level.

[††] The low-temperature restriction ensures that the actual vertical path flown is obstacle-free. The high-temperature restriction reduces the likelihood that at Decision Height, the aircraft will be above the minimum ceiling and/or have to execute a significant vertical flight correction.

The International Civil Aviation Organization (ICAO) has estimated the impact of temperature on VNAV approaches, and developed the following table (Ref. 56):

Table 14 Effect of Uncompensated Airport Temperature on VNAV Glide Path Angle

Airport Temperature	Actual Glide Path Angle
+30 ^{0}C (+86 ^{0}F)	3.2 deg
+15 ^{0}C (+59 ^{0}F)	3.0 deg
0 ^{0}C (+32 ^{0}F)	2.8 deg
-15 ^{0}C (+5 ^{0}F)	2.7 deg
-31 ^{0}C (-24 ^{0}F)	2.5 deg

For airport at MSL and a charted 3 deg glide path angle

Temperature compensation of the VNAV system is offered on many full-sized transport aircraft and some smaller aircraft, but is not often found in aircraft currently operating.

9.2 VNAV Constant Descent Angle Trajectory

9.2.1 Derivation of Equations

Barometric Vertical NAVigation (Baro VNAV) creates a descent path that is, absent instrumentation errors and incorrect assumptions, similar to, but slightly different from, an ILS glide slope. Whereas ILS navigation involves flying a constant vertical angle α with respect to the plane of the runway, VNAV involves flying a constant vertical descent angle α' with respect to the horizontal plane at the current aircraft location, and is defined by

$$\tan(\alpha') = \frac{vertical\ speed}{ground\ speed} \qquad \text{Eq 341}$$

Generally, vertical speed is derived from the aircraft's pitot-static system, and ground speed is found from one of (a) the combination of airspeed and headwind, (b) a GPS receiver, or (c) range measurements to a DME ground station on the airport.

Employing the notation of Chapters 1-3, the differential equation governing a vertical trajectory involving a constant vertical descent angle α' with respect to the local horizontal plane is

$$dh = \tan(\alpha')(R_e + h)\,d\theta$$
$$\frac{dh}{R_e + h} = \tan(\alpha')\,d\theta \qquad \text{Eq 342}$$

Integrating both sides of Eq 342 from the surface of the earth to altitude h yields the expression for the geocentric angle θ

$$\theta = \frac{\log\left(\frac{R_e + h}{R_e}\right)}{\tan(\alpha')} \qquad \text{Eq 343}$$

The natural logarithm is employed in Eq 343. This equation can be manipulated to find the altitude and descent angle as a function of the other two variables.

$$h = R_e\,(\exp\left[\theta\,\tan(\alpha')\right] - 1) = R_e\,\theta\,\tan(\alpha') + \tfrac{1}{2} R_e\,\theta^2\,\tan^2(\alpha') + \text{etc.} \qquad \text{Eq 344}$$

$$\tan(\alpha') = \frac{\log\left(\frac{R_e + h}{R_e}\right)}{\theta} = \frac{h}{\theta R_e} - \frac{h^2}{2\theta R_e^2} + \frac{h^3}{3\theta R_e^3} \pm \text{etc.} \qquad \text{Eq 345}$$

The correspondence between the preceding three equations for a VNAV approach and those for an ILS glide slope approach are: geocentric angle, Eq 343 ↔ Eq 27; altitude, Eq 344 ↔ Eq 51; vertical angle, Eq 345 ↔ Eq 38.

9.2.2 Typical Vertical Profiles

Figure 52 is a plot of aircraft altitude above MSL versus distance along the curved earth's surface from the runway threshold for (a) baro-VNAV guidance with a descent angle of 3.00 deg, (b) ILS guidance with a glide path angle of 3.00 deg, and (c) ILS guidance with a glide path angle of 2.90 deg. At the threshold, the baro-VNAV and ILS 3.00 deg curves coincide; at 5-7 NM from the threshold, the baro-VNAV curve is about halfway between the two curves for ILS guidance; at 14 NM, the baro-VNAV and ILS 2.90 deg curves essentially over lay each other.

9.2.3 Remarks

- References 2 and 3 require the use of Eq 343 to Eq 345 in the design of VNAV approach procedures.
- Requirements for aircraft implementation of VNAV are found in FAA Advisory Circulars AC 90-105 (Ref. 36) and AC 20-138C (Ref. 37). These documents specify the use of a flight director and vertical deviation indicator (VDI) and assume the use of a flight management system.

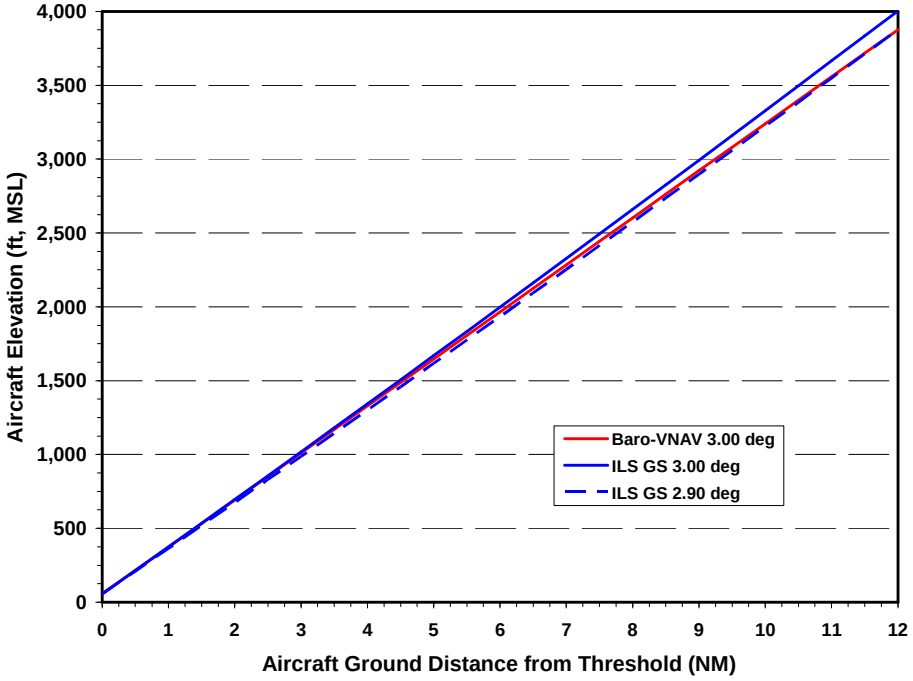

Figure 52 Aircraft Elevation vs. Distance along Ground, for Three Guidance Schemes

9.3 Ellipsoidal Earth Model and ECEF Coordinate Frame

This section presents coordinate frames and transformations associated with an ellipsoidal model for the earth. It draws on Section 2.2 (concerning ellipsoidal earth parameters) and Section 5.1 (concerning coordinate frames and transformations associated with a spherical earth model). In this document, the primary use of a model for an ellipsoidal relates to Chapter 8 — formulating analytic models for slant-range and slant-range difference measurements.

As in Section 5.1, the ellipsoidal earth-centered earth-fixed (ECEF) frame $\boldsymbol{e}$ is defined by:

- $\boldsymbol{x}^e$-axis: lies in the plane of the equator and points toward the Greenwich meridian
- $\boldsymbol{y}^e$-axis: completes the right-hand orthogonal system
- $\boldsymbol{z}^e$-axis: lies along the earth's spin axis.

For these axis, the ellipsoid model for the earth's surface is

$$\frac{(x^e)^2}{a^2}+\frac{(y^e)^2}{a^2}+\frac{(z^e)^2}{b^2}=1 \qquad \text{Eq 346}$$

As in Section 2.2, in this section, a denotes the earth's equatorial radius and b its polar radius. The WGS-84 values for a and b are given in Section 2.2. Figure 24, depicting a spherical earth — with slight flattening at the poles — is relevant here, as well.

Figure 53 is depicts an ellipsoidal model of the earth, employing a plane passing through the spin axis. The coordinate quantities of greatest interest are:

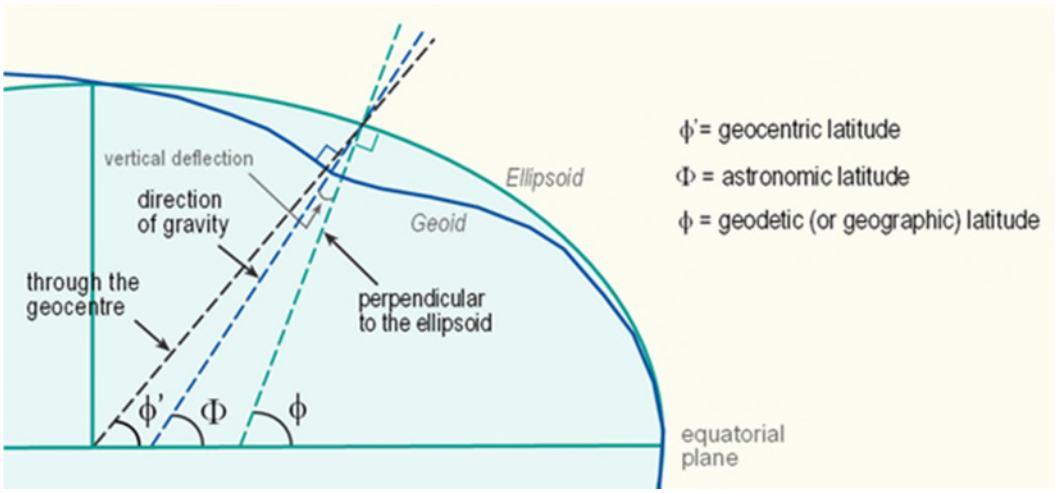

Figure 53 Ellipsoidal Earth Model for a Plane through the Spin Axis

- Geodetic latitude ***L*** (denoted by ϕ in Figure 53) — the angle that a normal to the ellipsoid surface makes with the plane of the equator. Geodetic latitude is generally used for navigation and surveying; other measures of latitude are used in mathematical analyses.
- Ellipsoid longitude λ — sometimes termed terrestrial longitude. Longitude for an ellipsoid earth model is conceptually the same as longitude for a spherical model.
- Several definitions of altitude are used. Height above the geoid, an equipotential gravitational surface that approximates mean sea level, is useful for some aspects of navigation. Height above the reference ellipsoid is more convenient for analysis. The two heights are related by the undulation of the geoid, which is published in the form of tables and/or formulas.

A user's height above the ellipsoid $h_{U,ellip}$, height above the geoid $h_{U,geoid}$ and undulation of the geoid at the user's location $\Delta h_{e\text{-}g}(L_U, \lambda_U)$ are related by

$$h_{U,ellip} = h_{U,geoid} + \Delta h_{e-g}(L_U, \lambda_U) \qquad \text{Eq 347}$$

Undulation of the geoid is usually computed as a harmonic expansion in latitude and longitude that's fit to measurements. Reference 57 is a source of data concerning undulation of the geoid relative to the WGS-84 reference ellipsoid. The order of the expansion used in Ref. 57 exceeds 2,000, which results in a resolution of 1 arc min. For the CONUS, the geoid is generally below the surface of the WGS-84 ellipsoid — more in the East and less in the West. For locations of interest — e.g., navigation and surveillance ground stations, runways, monuments, etc. — coordinates are generally provided in geodetic latitude and terrestrial longitude relative to the WGS-84 ellipsoid; their elevation is usually stated in relative to mean sea level.

To approximate an ellipsoidal earth at a location on its surface by a sphere, two radii of curvature (RoCs) are commonly defined —the RoC in the meridian (north-south orientation), R_{ns}, and the RoC in the prime vertical (east-west orientation), R_{ew}. These are given in Subsection 2.2.2 (Eq

20). The value for $\boldsymbol{R_{ew}}$ is repeated here, as it is needed below; again, $\boldsymbol{e^2}$ denotes the earth's eccentricity.

$$R_{ew} = \frac{a}{[1 - e^2 \sin^2(L)]^{1/2}} \qquad \text{Eq 348}$$

Given a user's geodetic latitude $\boldsymbol{L_U}$, terrestrial longitude $\boldsymbol{\lambda_U}$ and height above the ellipsoid $\boldsymbol{h_U}$, the location of the user **U** relative to the earth's center **O** in the *e*-frame is

$$\underline{\mathbf{r}}^{\mathbf{e}}_{\mathbf{OU}} = \begin{bmatrix} \underline{r}^{e}_{OU,x} \\ \underline{r}^{e}_{OU,y} \\ \underline{r}^{e}_{OU,z} \end{bmatrix} = \begin{bmatrix} (R_{ew} + h_U)\cos(L_U)\cos(\lambda_U) \\ (R_{ew} + h_U)\cos(L_U)\sin(\lambda_U) \\ \left[R_{ew}(1 - e^2) + h_U\right]\sin(L_U) \end{bmatrix} \qquad \text{Eq 349}$$

It is evident from Eq 349 that $\boldsymbol{R_{ew}}$ is the distance along the normal between the ellipsoid surface and the earth's spin axis, while $\boldsymbol{R_{ew}}$ $(\mathbf{1} - \boldsymbol{e^2})$ is the distance between the ellipsoid surface and the equatorial plane.

Given the components of $\underline{\mathbf{r}}^{\mathbf{e}}\mathbf{_{OU}}$ and those of ground station $\underline{\mathbf{r}}^{\mathbf{e}}\mathbf{_{OS}}$, the slant-range between the user and station is

$$d_{US} = \sqrt{\left(\underline{r}^{e}_{OU,x} - \underline{r}^{e}_{OS,x}\right)^2 + \left(\underline{r}^{e}_{OU,y} - \underline{r}^{e}_{OS,y}\right)^2 + \left(\underline{r}^{e}_{OU,z} - \underline{r}^{e}_{OS,z}\right)^2} \qquad \text{Eq 350}$$

Conversely, given the components of $\underline{\mathbf{r}}^{\mathbf{e}}\mathbf{_{OU}}$, the user's latitude, longitude and altitude can be found. User longitude is given by

$$\lambda_U = \arctan\left(\underline{r}^{e}_{OU,y}\,,\ \underline{r}^{e}_{OU,x}\right) \qquad \text{Eq 351}$$

The expressions for user latitude $\boldsymbol{L_U}$ and elevation above the ellipsoid $\boldsymbol{h_U}$ are in Eq 349 are not analytically invertible due to the presence of $\boldsymbol{R_{ew}}$. Thus an iterative solution is required. The three components of Eq 349 can be combined to eliminate elevation $\boldsymbol{h_U}$, yielding

$$\frac{\sqrt{(\underline{r}^{e}_{OU,x})^2 + (\underline{r}^{e}_{OU,y})^2}}{\cos(L_U)} = \frac{\underline{r}^{e}_{OU,z}}{\sin(L_U)} + e^2 R_{ew}(L_U) \qquad \text{Eq 352}$$

The geodetic latitude $\boldsymbol{L_U}$ can be found from Eq 352 iteration, using the geocentric latitude as the initial value

$$L_{U,init} = \arctan\left(\frac{\underline{r}^{e}_{OU,z}}{\sqrt{(\underline{r}^{e}_{OU,x})^2 + (\underline{r}^{e}_{OU,y})^2}}\right) \qquad \text{Eq 353}$$

Then $\boldsymbol{h_U}$ can be found from

$$h_U = \frac{r^e_{OU,z}}{\sin(L_U)} - (1-e^2)R_{ew}(L_U) \qquad \text{Eq 354}$$

In the methodology exposed herein, Eq 351 - Eq 354 are virtually never needed. When an ellipsoid earth model is employed in determining aircraft location, latitude, longitude and altitude are found by an iterative solution of the measurement equations (Subsection 8.1.2).

9.4 Rhumb Line Navigation

9.4.1 Background

The defining characteristic of rhumb[‡‡] line navigation is that the planned track over the ground has a constant azimuth angle with respect to North at each location along the track. That is,

$$\psi = \arctan(d\lambda\cos(L), dL) = \text{constant} \qquad \text{Eq 355}$$

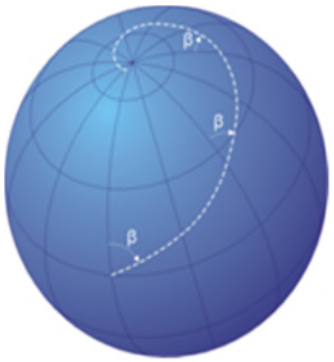

An example rhumb line course is shown to the right. Mathematically, such courses are loxodromes; they spiral toward, but do not reach, a pole. (The exception is a constant-latitude course; these are often treated separately.)

Rhumb line navigation has been used by mariners for hundreds of years.[§§] An advantage was that rhumb lines simplified the helmsman's task in an era when only the most rudimentary tools were available. Even when a great circle route was being implemented, the path was approximated by a series of waypoints and rhumb line navigation was employed between waypoints.

Another important advantage of rhumb line navigation is that, for a Mercator projection, a rhumb line course is a straight line on a chart. This greatly simplifies the planning process, and likely contributed to the popularity of the Mercator projection.

Today, great circle navigation has largely replace rhumb line navigation, particularly for aviation, since it provides shorter paths and air routes are less restricted than marine routes. Rhumb line navigation is still in use for applications lacking a flight computer (or the equivalent).

Three factors cause great circle and rhumb routes to be dissimilar and favor great circle navigation:

[‡‡] The word "rhumb" may come from Spanish/Portuguese *rumbo/rumo*, meaning course or direction (Wikipedia).

[§§] Rhumb lines were first discussed by the Portuguese mathematician Pedro Nunes in 1537, in (translated) *Treatise in Defense of the Marine Chart* (Wikipedia).

- Path length: The origin and destination (or end points of a navigation leg) are far apart (e.g., thousands of miles)
- Starting location: Route leg starts at mid- and/or high-latitude, and
- End location/route direction: The end point is at mid- and/or high-latitude on the same side of the equator.

Numerical examples illustrating the importance of these points are presented in Subsection 4.8.4.

Consistent with the intent of this document, the equations presented below are for rhumb line navigation with respect to a spherical earth (Refs. 26 and 58). More accurate equations applicable to an ellipsoidal earth may be found in Ref. 59.

9.4.2 Solution of the Indirect Problem

The indirect problem of geodesy / navigation is defined in Section 1.3 and its solution for great circle navigation is given in Section 4.2. Here the known quantities are the latitude/longitude of the starting point **U** ($\boldsymbol{L_U}$, $\boldsymbol{\lambda_U}$) and end point **S** ($\boldsymbol{L_S}$, $\boldsymbol{\lambda_S}$). The quantities to be found are the distance ***D*** between **U** and **S**; and the azimuth angles $\boldsymbol{\psi_{S/U}}$ at **U** and $\boldsymbol{\psi_{U/S}}$ at **S** of the trajectory connecting **U** and **S**.

If Eq 355 is rewritten with the latitude-related quantities on one side and the longitude related quantities on the other, then integrated from **U** to **S**, the result is

$$\psi_{S/U} = \arctan\left(\lambda_S - \lambda_U, \log[\tan(\tfrac{1}{2}L_S + \tfrac{\pi}{4})] - \log[\tan(\tfrac{1}{2}L_U + \tfrac{\pi}{4})]\right) \qquad \text{Eq 356}$$

The natural logarithm is used in Eq 356.

Since a constant azimuth angle is involved, it follows that

$$\psi_{U/S} = \arctan\left(\lambda_U - \lambda_S, \log[\tan(\tfrac{1}{2}L_U + \tfrac{\pi}{4})] - \log[\tan(\tfrac{1}{2}L_S + \tfrac{\pi}{4})] = \psi_{S/U} \pm \pi\right) \qquad \text{Eq 357}$$

Once the azimuth angle $\boldsymbol{\psi_{S/U}}$ is known, the distance ***D*** between **U** and **S** can be found using

$$D = R_e \int_{L_U}^{L_S} \frac{dL}{\cos(\psi_{S/U})} = R_e \frac{L_S - L_U}{\cos(\psi_{S/U})} = R_e \frac{L_U - L_S}{\cos(\psi_{U/S})} \qquad \text{when} \qquad L_S \neq L_U \qquad \text{Eq 358}$$

This equation fails for constant latitude paths, and must be replaced by

$$D = R_e \cos(L_S) = R_e \cos(L_U) \qquad \text{when} \qquad L_S = L_U \qquad \text{Eq 359}$$

An equation for the distance ***D*** between **U** and **S** that does not daisy-chain on the solution for $\boldsymbol{\psi_{S/U}}$ can be developed using the analyses associated with the Mercator projection. The results of

that analysis are quoted here. Define the stretched latitude difference by

$$\Delta L'_{US} = \log[\tan(\tfrac{1}{2} L_S + \tfrac{\pi}{4})] - \log[\tan(\tfrac{1}{2} L_U + \tfrac{\pi}{4})] \qquad \text{Eq 360}$$

Also, for convenience, let

$$\Delta L_{US} = L_S - L_U \quad \text{and} \quad \Delta\lambda_{US} = \lambda_S - \lambda_U \qquad \text{Eq 361}$$

Then the rhumb line distance ***D*** is given by

$$D = R_e \sqrt{(\Delta L_{US})^2 + \frac{(\Delta L_{US})^2}{(\Delta L'_{US})^2}(\Delta\lambda_{US})^2} \qquad \text{when} \qquad L_S \neq L_U \qquad \text{Eq 362}$$

With these definitions,

$$\psi_{S/U} = \arctan(\Delta\lambda_{US}, \Delta L'_{US}) \qquad \text{Eq 363}$$

9.4.3 Solution of the Direct Problem

The direct problem of geodesy / navigation is defined in Section 1.3 and its solution for great circle navigation is given in Section 4.3. Here the known quantities are: the latitude/longitude, (L_U, λ_U), of the starting point **U**; the distance, ***D***, between **U** and **S**; and the azimuth angle at **U**, $\psi_{S/U}$, of the trajectory connecting **U** and **S**. The quantities to be found are the latitude/longitude (L_S, λ_S), of the end point **S**.

From Eq 358 it follows that

$$L_S = L_U + \left(\frac{D}{R_e}\right)\cos(\psi_{S/U}) \qquad \text{Eq 364}$$

I am not aware of a solution for λ_S that does not utilize the solution for L_S. One option is to manipulate Eq 363 to obtain

$$\lambda_S = \lambda_U + \tan(\psi_{S/U})\log\left(\frac{\tan(\frac{1}{2} L_S + \frac{\pi}{4})}{\tan(\frac{1}{2} L_U + \frac{\pi}{4})}\right) \qquad \text{when} \qquad \psi_{S/U} \neq \pm\frac{\pi}{2} \qquad \text{Eq 365}$$

Substituting Eq 364 into Eq 365 yields the alternative form

$$\lambda_S = \lambda_U + \left(\frac{D}{R_e}\right)\sin(\psi_{S/U})\left[\log\left(\frac{\tan(\frac{1}{2} L_S + \frac{\pi}{4})}{\tan(\frac{1}{2} L_U + \frac{\pi}{4})}\right)/(L_S - L_U)\right] \quad \text{when} \quad \psi_{S/U} \neq \pm\frac{\pi}{2} \qquad \text{Eq 366}$$

When L_U is equal to L_S, then

$$\lambda_S = \lambda_U + \left(\frac{\text{sgn}(\psi_{S/U})\, D}{R_e \cos(L_U)} \right) = \lambda_U + \left(\frac{\text{sgn}(\psi_{S/U})\, D}{R_e \cos(L_S)} \right) \quad \text{when} \quad \psi_{S/U} = \pm \frac{\pi}{2} \qquad \text{Eq 367}$$

10. REFERENCES

1. Nathaniel Bowditch; *The American Practical Navigator*; National Imagery and Mapping Agency; 2002.

2. FAA Order 8260.3B: Change 25; *United States Standard for Terminal Instrument Procedures (TERPS)*; Flight Standards Service; March 9, 2012.

3. FAA Order 8260.58: *United States Standard for Performance Based Navigation (PBN) Instrument Procedure Design*; Flight Standards Service; September 21, 2012.

4. http://en.wikipedia.org/wiki/Inverse_trigonometric_functions

5. http://en.wikipedia.org/wiki/Newtons_method

6. Christopher Jekeli; *Geometric Reference Systems in Geodesy*; Ohio State University; July 2006.

7. Friedrich Robert Helmert: *Die mathematischen und physikalischen Theorieen der höheren Geodäsie*; Part I, 1880; Part II, 1884.

8. Friedrich Robert Helmert: *Mathematical and Physical Theories of Higher Geodesy*; Translation into English of Parts I and II of previous reference; Aeronautical Chart and Information Center; St. Louis; 1964.

9. Marie Henri Andoyer: “Formule donnant la longueur de la géodésique, joignant 2 points de l'ellipsoide donnes par leurs coordonnées geographiques”; *Bulletin Geodsique*; No. 34, 77-81, 1932.

10. Paul D. Thomas: *Mathematical Models for Navigation Systems*; U.S. Naval Oceanographic Office; TR- 182; October 1965.

11. P.B. Morris, et al: *Omega Navigation System Course Book*; TASC; July 1994.

12. Thaddeus Vincenty: “Direct and Inverse Solutions of Geodesics on the Ellipsoids with Applications of Nested Equations”, *Survey Review*; XXIII, Number 176; April 1975.

13. C. M. Thomas and W. E. Featherstone: “Validation of Vincenty’s Formulas for the Geodesic Using a New Fourth-Order Extension of Kivioja’s Formula”; *Journal of Surveying Engineering*; American Society of Civil Engineers; February 2005.

14. Emanuel M. Sodano: “A rigorous non-iterative procedure for rapid inverse solution of very long geodesics”; *Bulletin Géodésique*; vol 47/48, pp 13-25; 1958.

15. Emanuel M. Sodano: “General non-iterative solution of the inverse and direct geodetic problems”; *Bulletin Géodésique*; vol 75, pp 69-89; 1965.

16. Emanuel M. Sodano: “Supplement to inverse solution of long geodesics”; *Bulletin Géodésique*; vol 85: 233-236; 1967.

17. http://en.wikipedia.org/wiki/Non-line-of-sight_propagation

18. Armin W. Doerry: “Earth Curvature and Atmospheric Refraction Effects on Radar Signal Propagation”; Sandia National Laboratories; SAND2012-10690; January 2013.

19. http://www.radartutorial.eu/18.explanations/ex47.en.html

20. http://en.wikipedia.org/wiki/History_of_trigonometry

21. http://en.wikipedia.org/wiki/Mathematics_in_medieval_Islam

22. I. Todhunter: *Spherical Trigonometry*; MacMillan; 5th edition, 1886.

23. W.M. Smart and R.M. Green: *Spherical Astronomy*; Cambridge University Press; Sixth Edition, 1977.

24. http://en.wikipedia.org/wiki/Spherical_trigonometry

25. http://mathworld.wolfram.com/SphericalTrigonometry.html

26. http://williams.best.vwh.net/avform.htm

27. http://www.krysstal.com/sphertrig.html

28. http://en.wikipedia.org/wiki/File:Spherical_trigonometry_triangle_cases.svg

29. http://en.wikipedia.org/wiki/Versine

30. http://www.airnav.com/airport/KMCI

31. http://www.nstb.tc.faa.gov/index.htm

32. http://www3.sympatico.ca/craymer/geodesy/gps.html#matlab

33. A.S. Lenart: "Solutions of Direct Geodetic Problem in Navigational Applications"; *International Journal on Marine Navigation and Safety of Sea Transportation*; vol. 5, no. 4; December 2011.

34. FAA Advisory Circular AC 90-100A: *U.S. Terminal and En Route Area Navigation (RNAV) Operations*; Flight Standards Service (AFS-400); March 1, 2007.

35. FAA Advisory Circular AC 120-108: *Continuous Descent Final Approach*; Flight Standards Service (AFS-400); January 20, 2011.

36. FAA Advisory Circular AC 90-105: *Approval Guidance for RNP Operations and Barometric Vertical Navigation in the U.S. National Airspace System*; Flight Standards Service (AFS-400); January 23, 2009.

37. FAA Advisory Circular AC 20-138C, *Airworthiness Approval of Positioning and Navigation Systems*; Aircraft Certification Service (AIR-130); May 8, 2012.

38. Hugh Dibley: *Action to Reduce Continuing CFIT Accidents by Defining & Training Constant Angle Approaches*; 16th Annual World Aviation Training Conference & Tradeshow; April 2013.

39. David Carbaugh and Bryan Wyness: "Hazards of Erroneous Glide Slope Indications"; *Aero Magazine*; Boeing; v21, January 2003. http://www.boeing.com/commercial/aeromagazine/

40. Mitch Narins: "The Global Loran / eLoran Infrastructure Evolution"; FAA; presentation before U.S. Space-Based PNT Advisory Board; June 3, 2014.

41. S. Bancroft: "An Algebraic Solution of the GPS Pseudorange Equations"; *IEEE Transactions on Aerospace and Electronic Systems*; AES-21, November 1985, pp 56-59.

42. Bertrand T. Fang: “Simple Solutions for Hyperbolic and Related Position Fixes”; *IEEE Transactions on Aerospace and Electronic Systems*; September 1990, pp 748-753.

43. Sheldon Razin: “Explicit (Noniterative) Loran Solution”; *Navigation, Journal of the Institute of Navigation*; Vol. 14, No. 3, Fall 1967, pp. 265-269.

44. Michael Geyer and Anastasios Daskalakis: “Solving Passive Multilateration Equations Using Bancroft’s Algorithm”; *Digital Avionics Systems Conference (DASC)*; Seattle, WA; Oct. 31-Nov. 6, 1998.

45. Ming Yang and Kuo-Hwa Chen: “Performance Assessment of a Noniterative Algorithm for Global Positioning System (GPS) Absolute Positioning”; *Proc. Natl. Sci. Counc. ROC(A);* vol 25, no 2, pp 102-106; 2001.

46. Niilo Sirola: “Closed-form Algorithms in Mobile Positioning: Myths and Misconceptions”; *Proceedings of the 7th Workshop on Positioning, Navigation and Communication 2010 (WPNC'10)*; March 11, 2010.

47. Alfred Kleusberg: “Analytical GPS Navigation Solution”; *University of Stuttgart Research Compendium*; 1994.

48. Nicholas H.J. Stuifbergen: *Intersection of Hyperbolae on the Earth*; University of New Brunswick; Fredericton, New Brunswick, Canada; December 1980.

49. Paul Williams and David Last: “On Loran-C Time-Difference to Co-ordinate Converters”; *Proceedings - International Loran Association (ILA) - 32nd Annual Convention and Technical Symposium*; Boulder, Colorado; November 3-7, 2003.

50. *Minimum Performance Standards (MPS) Automatic Co-ordinate Conversion Systems*; Report of RTCM Special Committee No. 75; Radio Technical Commission for Marine Services; Washington, D.C; 1984.

51. Coast Guard Navigation Center: *POSAID2 ver 2.1a*; http://www.navcen.uscg.gov/.

52. Andrew Sage and James Melsa: *Estimation Theory with Applications to Communications and Control*; Robert Krieger Publishing Company; 1979.

53. http://en.wikipedia.org/wiki/Linear_least_squares_%28mathematics%29.

54. FAA: *Pilot's Handbook of Aeronautical Knowledge*; Chapter 7, “Flight Instruments”; http://www.faa.gov/regulations_policies/handbooks_manuals/aviation/pilot_handbook/; retrieved May 14, 2014.

55. FAA: *Aeronautical Information Manual*; April 3, 2014.

56. ICAO Doc 8168: *Flight Procedures*: International Civil Aviation Organization; Procedures for Air Navigation Services – Aircraft Operations (PANS-OPS).

57. U.S. National Geospatial-Intelligence Agency (NGA): *Earth Gravitational Model EGM2008*; http://earth-info.nga.mil/GandG/wgs84/gravitymod/egm2008/egm08_wgs84.html; retrieved Sept. 15, 2014.

58. http://www.titulosnauticos.net/astro/

59. G. G. Bennett, “Practical Rhumb Line Calculations on the Spheroid”, *Journal of Navigation*; The Royal Institute of Navigation; Vol. 49, No. 01, pp 112-119: January 1996.